BIO-SYSTEMS ENGINEERING FOR REGULATING NERVE REGENERATION

EDITED BY: Srinivas Madduri, Xavier Navarro and Antonio Salgado
PUBLISHED IN: Frontiers in Bioengineering and Biotechnology

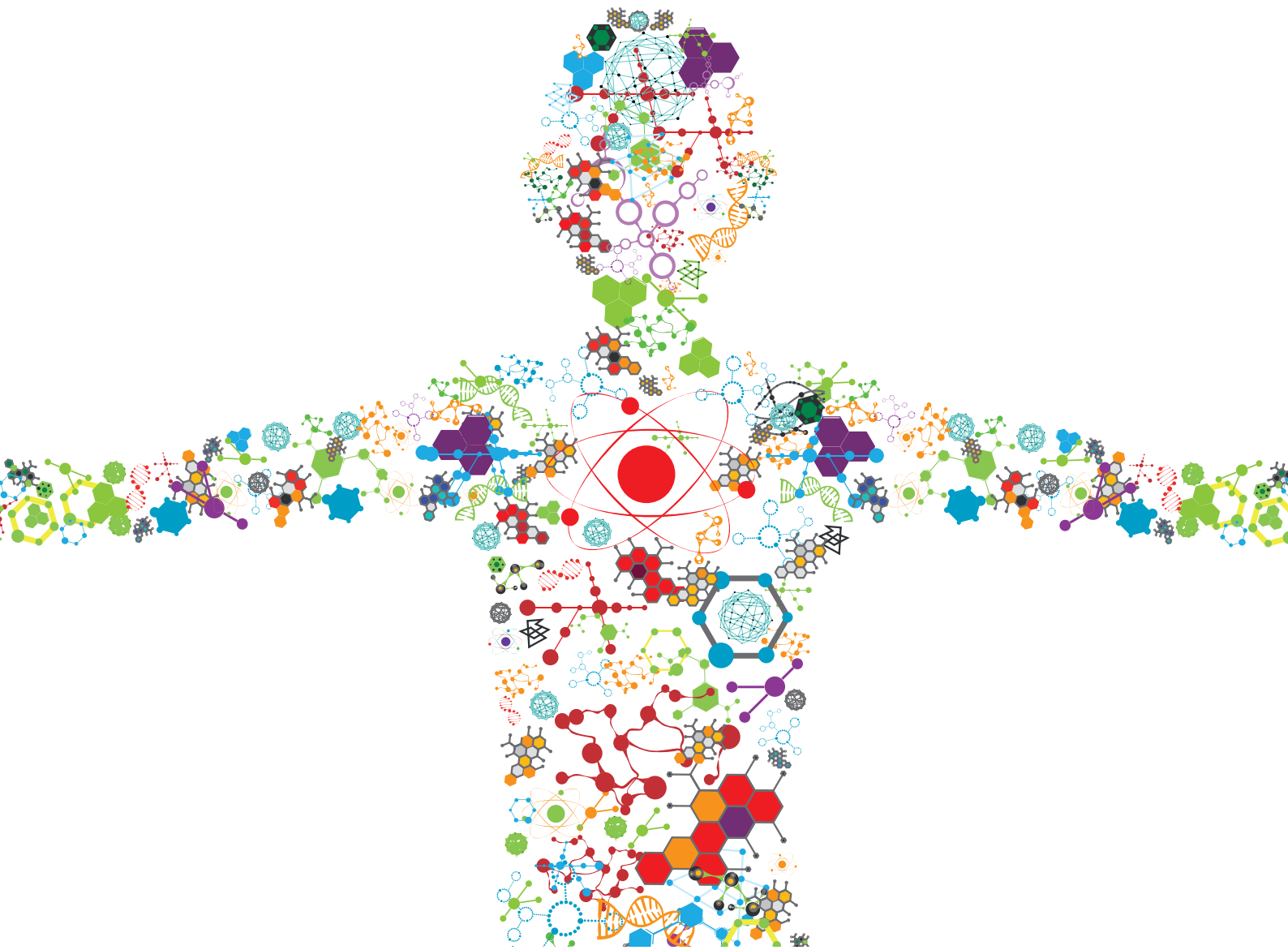

frontiers Research Topics

ISSN 1664-8714
ISBN 978-2-88974-983-6
DOI 10.3389/978-2-88974-983-6

About Frontiers

Frontiers is more than just an open-access publisher of scholarly articles: it is a pioneering approach to the world of academia, radically improving the way scholarly research is managed. The grand vision of Frontiers is a world where all people have an equal opportunity to seek, share and generate knowledge. Frontiers provides immediate and permanent online open access to all its publications, but this alone is not enough to realize our grand goals.

Frontiers Journal Series

The Frontiers Journal Series is a multi-tier and interdisciplinary set of open-access, online journals, promising a paradigm shift from the current review, selection and dissemination processes in academic publishing. All Frontiers journals are driven by researchers for researchers; therefore, they constitute a service to the scholarly community. At the same time, the Frontiers Journal Series operates on a revolutionary invention, the tiered publishing system, initially addressing specific communities of scholars, and gradually climbing up to broader public understanding, thus serving the interests of the lay society, too.

Dedication to Quality

Each Frontiers article is a landmark of the highest quality, thanks to genuinely collaborative interactions between authors and review editors, who include some of the world's best academicians. Research must be certified by peers before entering a stream of knowledge that may eventually reach the public - and shape society; therefore, Frontiers only applies the most rigorous and unbiased reviews.
Frontiers revolutionizes research publishing by freely delivering the most outstanding research, evaluated with no bias from both the academic and social point of view. By applying the most advanced information technologies, Frontiers is catapulting scholarly publishing into a new generation.

What are Frontiers Research Topics?

Frontiers Research Topics are very popular trademarks of the Frontiers Journals Series: they are collections of at least ten articles, all centered on a particular subject. With their unique mix of varied contributions from Original Research to Review Articles, Frontiers Research Topics unify the most influential researchers, the latest key findings and historical advances in a hot research area! Find out more on how to host your own Frontiers Research Topic or contribute to one as an author by contacting the Frontiers Editorial Office: frontiersin.org/about/contact

BIO-SYSTEMS ENGINEERING FOR REGULATING NERVE REGENERATION

Topic Editors:
Srinivas Madduri, University Hospital of Basel, Switzerland
Xavier Navarro, Universitat Autònoma de Barcelona, Spain
Antonio Salgado, University of Minho, Portugal

Citation: Madduri, S., Navarro, X., Salgado, A., eds. (2022). Bio-Systems Engineering for Regulating Nerve Regeneration. Lausanne: Frontiers Media SA. doi: 10.3389/978-2-88974-983-6

Table of Contents

frontiers in Bioengineering and Biotechnology

EDITORIAL
published: 31 March 2022
doi: 10.3389/fbioe.2022.891459

Editorial: Emerging Therapeutic Approaches for Repair and Regeneration of Injuries in the Peripheral Nervous System

Antonio Salgado[1], *Xavier Navarro*[2] *and Srinivas Madduri*[3,4]*

[1]School of Medicine, University of Minho, Braga, Portugal, [2]Department of Cell Biology, Universitat Autònoma de Barcelona, Barcelona, Spain, [3]Department of Biomedical Engineering, University of Basel, Basel, Switzerland, [4]Department of Surgery, University of Geneva, Geneva, Switzerland

Keywords: nerve injury, cell therapy, nerve bioengineering, neurotrophic factors, nerve guidance graft, nano materials, growth factors delivery

Editorial on the Research Topic

Bio-Systems Engineering for Regulating Nerve Regeneration

The research topic entitled "Bio-systems engineering for regulation of nerve regeneration" is focused on new and emerging approaches for promoting nerve regeneration.

Acute and chronic nerve injuries often result in the loss of sensory, motor and autonomic functions with variable pathological changes arising from traumatic or non-traumatic forms of injuries. Despite the severe consequences of such injuries for the patients, existing treatment options, i.e., surgical repair, often using autologous nerve grafting, and pharmacological compounds, such as corticosteroids, non-steroidal anti-inflammatory and analgesic drugs, are all associated with important drawbacks and are far from being optimal solutions. Consequently, the quality of patient's life is poor and the resulting socioeconomic impact is huge. Thus, there is a great need for further research to advance with new and innovative treatment strategies for improving functional recovery and patient wellbeing and to minimize the socioeconomic burden.

So far, research over the past 100 years has achieved remarkable achievements in the field of nerve regeneration, resulting in the advancement of micro-surgical nerve management, nerve cellular and molecular biology, nerve guidance scaffolds, cell therapy and nerve tissue engineering. Nevertheless, the existing knowledge and translational modalities still remain inadequate for clinical applications. Within this context, the collected research articles in this issue represent the work of 62 different authors in the form of three review articles and six original research reports, presenting new and emerging strategies involving interdisciplinary efforts ranging from cell and molecular biology, engineered nano-micromaterials, bio-active delivery, cell and gene therapy, tissue engineered grafts, and complex nerve conduit scaffolds. Taken together, the collected research reports strengthen existing knowledge in the field and provide further insights to move forward.

Immediately after traumatic nerve injury, Wallerian degeneration (WD) begins and Schwann cells play a key role in the subsequent cellular and molecular changes paving the way for axonal regrowth. However, there are no reported models for investigating the potential therapeutic interventions for regulating WD. Elsayed et al., report the establishment and characterization of an *in vitro* WD model, which would enable further research for basic as well as translational applications. Furthermore, their data revealed the beneficial effects of the adipose stem cells as evidenced by the upregulation of neurotrophic factors (NTFs) and CJUN, which are closely associated with the axonal growth program.

OPEN ACCESS

Edited and reviewed by:
Ranieri Cancedda,
Independent researcher, Genova, Italy

***Correspondence:**
Srinivas Madduri
srinivas.madduri@usb.ch

Specialty section:
This article was submitted to Tissue Engineering and Regenerative Medicine, a section of the journal Frontiers in Bioengineering and Biotechnology

Received: *07 March 2022*
Accepted: *14 March 2022*
Published: *31 March 2022*

Citation:
Salgado A, Navarro X and Madduri S (2022) Editorial: Emerging Therapeutic Approaches for Repair and Regeneration of Injuries in the Peripheral Nervous System. Front. Bioeng. Biotechnol. 10:891459. doi: 10.3389/fbioe.2022.891459

In continuation with WD, topographical guidance in the form of physical, biological and electrical signals guide the axonal growth and elongation towards the target organ. To address these requirements, Yu et al., Castano et al., and Ferrari et al. report on the beneficial effects of micro/nano-patterned functional surfaces and nerve cuff electrodes, respectively. Micropatterned poly (D,L-lactide-co-caprolactone) films functionalized with KHI peptide and nerve growth factor promoted axo-glial growth and *in vivo* nerve conduction to a significant level. Furthermore, PLA nanofiber with a 950 nm range size and SDF-1/CXCL 12 functionalities demonstrated the potential to overcome the inhibitory substrates and enhance the growth and migration of olfactory ensheathing cells. Interestingly, conductive polymer printed regenerative nerve cuff electrodes optimized with cost-effective fabrication technology resulted in enhanced motor axonal regeneration and function in rats after 3 months. In brief, materials engineered with micro/nano patterns and bio-chemical physical functions hold great promise for further developments aiming for the effective regulation of axonal elongation over long-gap (i.e., 30–60 mm) nerve injuries and for neuroprostheses.

In their work, Panzer et al. describe the fabrication of bands of Büngner in the form of tissue engineered micro-tissue. For this, hydrogel-based micro-columns with an inner diameter of 300 µm and an outer diameter of 700 µm were used for inducing the Schwan cells into dense and aligned cellular structures resembling bands of Bünger. Such a promising tissue-engineered approach will enable future developments towards off-the-shelf production of the aligned micro-tissue. Indeed, one of the major barriers for the production of off-the-shelf bio-based products is existing culture conditions, such as xenogeneic serum supplementation. As a potential solution to this problem, Guiotto et al. report on the use of human platelet lysate for the culture of adipose stem cell and further proved the synergistic function of platelet lysate in combination with extracellular matrix components for nerve tissue engineering applications. These results open up a viable and new option for the personalization of cell-based therapeutic product development.

Growth factors are widely accepted for their key role in regulating tissue growth and development. However, the current lack of appropriate delivery scaffolds and strategies has limited their therapeutic potential. In their review, Salvin et al. present the therapeutic potential of insulin-like growth factor-1, known for its trophic and protective effects on neuronal and non-neuronal glial cells. In addition, the review offers important insights on the most promising delivery routes and dosage forms for supporting nerve regeneration. Spinal root (ventral root) avulsion is critical and represents the most serious proximal nerve injury, given the fact that the distance between the lesion and target innervation site is too long and often results in a permanent loss of motor function. Among all the neurotrophic factors, glial cell line-derived neurotrophic factor (GDNF) is the most potent for the survival and growth of motor axons. In another review by Egger et al., recent advances in the field of GDNF gene therapy are presented, as well as future research directions emphasizing the importance of the spatio-temporal aspects of the therapeutic intervention, such as the location, timing, dose and duration of GDNF.

The extracellular matrix composition of nerve tissue is complex in nature and architecture. Biomaterials and bio-based research approaches are promising for recapitulating the key features and for instructing the sequence of cellular and molecular events of the axonal regeneration and nerve tissue formation. However, the detailed mechanisms underlying the interface regulation between engineered biomaterials and nerve tissue components are largely unclear. In a detailed review article, Powel et al. present such mechanisms with further information on the cell controllable micro-environment resulting from engineered bio-active biomaterials.

In summary, we consider that all the articles included in the current issue provide new and interesting data and important insights for further research in the field, particularly regarding the interdisciplinary aspects of nerve repair and regeneration approaches. The guest editors of this research topic thank all authors once again for their valuable contributions and hope that the readers in the field will be inspired by these significant research findings and expert opinions.

AUTHOR CONTRIBUTIONS

SM wrote the editorial and all the authors contributed to reading and corrections. SM conceived the idea and gathered all co-editors within the Editorial.

Conflict of Interest: The authors declare that the research was conducted in the absence of any commercial or financial relationships that could be construed as a potential conflict of interest.

frontiers in Bioengineering and Biotechnology

ORIGINAL RESEARCH
published: 10 July 2020
doi: 10.3389/fbioe.2020.00784

Development and Characterisation of an *in vitro* Model of Wallerian Degeneration

*Heba Elsayed[1,2], Alessandro Faroni[1], Mohammad R. Ashraf[1], Judith Osuji[1], Lydia Wunderley[3], Ling Zhang[4], Hesham Elsobky[2], Mohamed Mansour[2], Ashraf S. Zidan[2,5] and Adam J. Reid[1,6]**

[1] Blond McIndoe Laboratories, Division of Cell Matrix Biology and Regenerative Medicine, School of Biological Sciences, Faculty of Biology, Medicine and Health, The University of Manchester, Manchester Academic Health Science Centre, Manchester, United Kingdom, [2] Department of Neurosurgery, Mansoura University Hospitals, Mansoura, Egypt, [3] Division of Cellular and Molecular Function, School of Biological Sciences, Faculty of Biology, Medicine and Health, The University of Manchester, Manchester Academic Health Science Centre, Manchester, United Kingdom, [4] College of Polymer Science and Engineering, Sichuan University, Chengdu, China, [5] Mansoura University Hospital, Mansoura, Egypt, [6] Department of Plastic Surgery & Burns, Wythenshawe Hospital, Manchester University NHS Foundation Trust, Manchester Academic Health Science Centre, Manchester, United Kingdom

OPEN ACCESS

Edited by:
Srinivas Madduri, University Hospital of Basel, Switzerland

Reviewed by:
Petr Dubový, Masaryk University, Czechia
Jose Antonio Gomez-Sanchez, University College London, United Kingdom
Valerio Magnaghi, University of Milan, Italy

***Correspondence:**
Adam J. Reid
Adam.Reid@manchester.ac.uk

Specialty section:
This article was submitted to Tissue Engineering and Regenerative Medicine, a section of the journal Frontiers in Bioengineering and Biotechnology

Received: *07 May 2020*
Accepted: *22 June 2020*
Published: *10 July 2020*

Citation:
Elsayed H, Faroni A, Ashraf MR, Osuji J, Wunderley L, Zhang L, Elsobky H, Mansour M, Zidan AS and Reid AJ (2020) Development and Characterisation of an in vitro Model of Wallerian Degeneration. Front. Bioeng. Biotechnol. 8:784. doi: 10.3389/fbioe.2020.00784

Following peripheral nerve injury, a sequence of events termed Wallerian degeneration (WD) takes place at the distal stump in order to allow the regenerating axons to grow back toward the target organs. Schwann cells (SCs) play a lead role in this by initiating the inflammatory response attracting macrophages and immune cells, as well as producing neurotrophic signals that are essential for nerve regeneration. The majority of existing research has focused on tools to improve regeneration, overlooking the critical degeneration phase. This is also due to the lack of *in vitro* models recapitulating the features of *in vivo* WD. In particular, to understand the initial SC response following injury, and to investigate potential interventions, a model that isolates the nerve from other systemic influences is required. Stem cell intervention has been extensively studied as a potential therapeutic intervention to augment regeneration; however, data regarding their role in WD is lacking. Thus, in this study we describe an *in vitro* model using rat sciatic nerve explants degenerating up to 14 days. Characterisation of this model was performed by gene and protein expression for key markers of WD, in addition to immunohistochemical analysis and electron microscopy. We found changes in keeping with WD *in vivo*: upregulation of repair program protein CJUN, downregulation of myelin protein genes and subsequent disorganisation and breakdown of myelin structure. As a means of testing the effects of stem cell intervention on WD we established indirect co-cultures of human adipose-derived mesenchymal stem cells (AD-MSC) with the degenerating nerve explants. The stem cell intervention potentiated neurotrophic factors and C*jun* expression. We conclude that our *in vitro* model shares the main features of *in vivo* WD, and we provide proof of principle on its effectiveness to study experimental approaches for nerve regeneration focused on the events happening during WD.

Keywords: Wallerian degeneration, Schwann cells, nerve injury, myelin degradation, neurotrophic factors, *in vitro* model, adipose-derived mesenchymal stem cells

INTRODUCTION

Treatment options following peripheral nerve injuries are dependent on surgical interventions which have demonstrated that the perfect microsurgical repair of injured nerve stumps cannot alone restore prior function to the patient (Palispis and Gupta, 2017). A multitude of research has therefore focused on enhancing regeneration of peripheral nerves, perhaps neglecting the pre-requisite of distal stump degeneration to lay the groundwork for subsequent regeneration. WD is orchestrated by SC plasticity (Boerboom et al., 2017) with the ability to dedifferentiate from a myelinating phenotype to a repair phenotype. This process involves upregulation of genes such as *Cjun* and *P75* encoding proteins responsible for proliferation, migration, adhesion and systemic inflammatory response activation (Jessen and Arthur-Farraj, 2019). SCs initiate the inflammatory response to increase the number of macrophages and monocytes in the distal stump; moreover, both act to clear myelin debris in order to pave the way for the regenerating growth cone to navigate toward the distal stump (Dubovy, 2011). Therefore, it is logical that the degenerative phase of clearing axon-myelin debris could be targeted for therapeutic intervention in order to accelerate or improve efficiency of the process and ultimately promote regeneration.

Models of WD used in research are limited by poor characterisation, failure to isolate the critical SC response from the systemic response and lack of potential to translate into human tissue models. Recent insightful studies have used injured *ex vivo* nerve models of WD in genetic knockout mice to identify mechanisms underpinning autophagic action of SCs (Gomez-Sanchez et al., 2015; Jang et al., 2016). Furthermore, macrophages and SCs are known to act synergistically in the degradation and removal of myelin (myelinophagy) following injury (Gaudet et al., 2011; Rotshenker, 2011). In order to understand the capacity of the resident cells to regulate myelinophagy independent of the systemic response, it is necessary to characterise a model which isolates the injured nerve immediately following injury. This model would also permit investigation of interventions in the degenerative phase following nerve injury.

Perhaps the most promising experimental intervention for regeneration is the use of stem cells; however, nothing is known of their impact on WD (Dezawa et al., 2001; Kingham et al., 2007). AD-MSCs have been demonstrated to improve neuronal regeneration *in vitro* and *in vivo* models following chemical stimulation into a Schwann-like phenotype (dASC) (Faroni et al., 2013); however, survival *in vivo* after nerve injury has been demonstrated to be less than a few weeks, therefore their therapeutic window spans only the initial regenerative response (Faroni et al., 2016). As such, it stands to reason that AD-MSC and dASC may impact WD as well as the regenerative response and perhaps through a similar mechanism of growth factor (BDNF and NGF) production. In this work, we establish and characterise an *in vitro* model of WD to determine ultrastructural and histological morphology, alongside a timeline of important gene and protein expression changes over 14 days. We subsequently use this model to test the effect of AD-MSCs and dASC intervention on SC functions during WD.

Abbreviations: AD-MSCs, adipose derived mesenchymal stem cells; aMEM, alpha-modified minimum essential Eagle's medium; BDNF, brain derived neurotropic factor; DAPI, 4',6-diamidino-2-phenylindole; dASCs, differentiated adipose stem cells; DMEM, glucose Dulbecco's Modified Eagle's medium; FBS, foetal bovine serum; GAPDH, glyceraldehyde 3-phosphate dehydrogenase; GDNF, glial derived neurotropic factor; HBSS, Hanks balanced salt solution; IHC, immunohistochemistry; MBP, myelin basic protein; NGF, nerve growth factor; OCT, optimum cutting temperature; P0, myelin protein zero; PBS, phosphate-buffered saline; PCR, polymerase chain reaction; PFA, paraformaldehyde; PMP22, peripheral myelin protein 22; RNA, ribonucleotide acid; RT, room temperature; SCs, Schwann cells; SVF, stromal vascular fraction; TEM, transmission electron microscope; TLRs, toll like receptors; WD, Wallerian degeneration.

MATERIALS AND METHODS

Establishing an *in vitro* Explant Model

All the animal work was performed in accordance with the UK Animal Scientific Procedures Act 1986. Following CO_2 euthanasia and cervical dislocation (S1) the hind limbs of adult 200–300 g Sprague Dawley rats were carefully dissected in surgical planes to expose the whole course of sciatic nerve up to its origin. Blunt dissection freed the nerve from underlying fascia and muscle before being divided and placed into Hanks balanced salt solution (HBSS, Sigma-Aldrich). Four rats (eight sciatic nerves) were used per experiment. Nerves were de-sheathed (removal of the epineurium) unless otherwise specified under a microscope at 20× magnification, and subsequently divided into smaller pieces (nerve explants) of 5–10 mm size, using sharp micro-scissors. For all experiments, day 0 time points were processed first and frozen at −80°C or fixed immediately, whereas for days 1, 3, 5, 7, and 14, the nerve explants were placed in six well plates containing 2 ml of low glucose Dulbecco's Modified Eagle's Medium (DMEM; Sigma-Aldrich, United Kingdom) supplemented with 10% (v/v) of FBS (LabTech, Uckfield, United Kingdom), 1% (v/v) of penicillin–streptomycin solution (PS; Sigma-Aldrich, United Kingdom), and 2 mM L-glutamine (GE Healthcare UK, Little Chalfont, United Kingdom). No media change was performed in the first 7 days of culture; however, for explants to be collected at day 14, a single media change was performed at day 7. All explants were incubated in 5% CO_2 at 37°C, frozen or fixed at their respective time points, and stored at −80°C until further processing.

Transmission Electron Microscope (TEM)

For electron microscopy studies, nerve explants (not de-sheathed) at each time point were pinned to a plastic strip with sterile needles and fixed by immersing in a 2% (w/v) PFA and 2% (v/v) glutaraldehyde solution for 24 h, transferred into PBS, and refrigerated until all time points were collected. The samples were then processed by University of Manchester Electron Microscopy Facility as ultrathin nerve cross sections for TEM imaging. The nerve samples were fixed for an hour in 1% osmium tetroxide and 1.5% potassium ferrocyanide in 0.1 M cacodylate buffer, followed by another 24 h in 1% uranyl acetate in water. The sample was then dehydrated in an ethanol series with 812 resin (TAAB laboratories), before polymerization for 24 h at 60°C. Samples

were cut with the Reichert Ultracut Ultra-Microtome as ultra-thin sections. These were visualised with FEI Tecnai 12 Biotwin microscope at 100 kV accelerating voltage, and snapshots saved with Gatan Orius SC1000 CCD camera.

Immunohistochemistry (IHC)

In order to preserve the fine structure of the nerve, samples were not de-sheathed when processed for IHC, with the exception of the DAPI count experiment (**Figure 2B**). Nerve explants were pinned to a plastic strip to straighten up with minimal tension and were fixed for 24 h by immersing in 4% (w/v) PFA, followed by three serial changes with 15% (w/v) sucrose and 0.1% (w/v) sodium azide in PBS. Samples were refrigerated until embedding in optimal cutting temperature (OCT) cryo-compound (Klinipath), after which they were stored at −80°C. The blocks were then cut longitudinally at University of Manchester histology facility by using cryostat (Leica ASP300). Sections were cut at 5 um and caught in between the microtome blade and glass. The sections were transferred to pre-heated Superfrost Plus slides (VWR International) and then incubated overnight at 37°C. Slides were then stored at −80°C until staining procedure. On the staining day, the slides were submerged in 0.2% Triton X-100/PBS for 1 h at RT then a blocking serum containing normal goat or donkey serum solution (both 5:100; Sigma-Aldrich, Poole, United Kingdom) was added for 1 h at RT after 2 × PBS washes 5 min each. The slides were incubated with the primary antibody [P0 Abcam (ab183868) 1:200], [MBP Millipore (MAB384-1ML) 1:200] βIII Tubulin [βIIIT Sigma (ab6046) 1:200] and CD68 [AbD serotec (MCA1957GA) 1:200] overnight at 4°C followed by two PBS washes and secondary antibody incubation the following day for 1 h at RT [goat/monkey anti-rabbit and goat/monkey anti-mouse (488 for green and 568 for red) (Life Technologies, Thermo Fisher Scientific)] in dark.

In desheathed nerve segments, explants were treated as above with the addition of three PBS washes for 5 min before mounting with Vectashield (Vector Laboratories, United Kingdom) containing 4′,6-diamidino-2-phenylindole (DAPI) for nuclear staining. This permitted the quantification of cells which are presumed to be predominantly SCs.

For FluoroMyelin staining: the slides were washed with PBS for 20 min and stained with green FluoroMyelin dye [1:300 in PBS, Molecular Probes, United Kingdom (F34651)] for 20 min at RT. Sections were washed 3 × 5 min with PBS before mounting with aqueous media containing DAPI (Vector Laboratories, United Kingdom).

Images were acquired using a fluorescence microscope (Olympus BX60, Southend-on-Sea, United Kingdom), and processed with ImageJ imaging software (Version 1.52a, National Institutes of Health NIH, Bethesda, MD, United States).

RNA Extraction

The RNeasy Lipid Tissue Mini Kit (QIAGEN, United Kingdom) was used to extract purified RNA from the nerve samples according to the manufacturer's protocol. Briefly, each of the frozen nerve samples were placed in 5 ml Falcon Polypropylene Rounded-Bottom Tube containing 1 ml QIAzol Lysis Reagent (QIAGEN, United Kingdom). A TissueRupter tissue homogeniser (QIAGEN, United Kingdom) was used to homogenise the nerve explants on ice. After 5 min, the sample was transferred to a 1.5 ml Eppendorf tube to which 200 ul of chloroform was added (Sigma-Aldrich). The tube was then vortexed for a few seconds, allowed to sit for 2–3 min, before being centrifuged at 12,000 × *g* for 15 min at (4°C). The aqueous phase was isolated and one volume of 70% ethanol (Fisher Chemical) was added; following gentle pipetting, the resulting solution was transferred to RNeasy Mini spin column (QIAGEN) in 2 ml collection tube and centrifuged for 30 s at 13,000 rpm at RT. Columns were then washed with Buffer RW1, and twice with Buffer RPE. Finally, the column was placed into a 1.5 ml Eppendorf tube, and 30 ul of RNase free water (QIAGEN) was added directly to the column to elute RNA with a 1 min centrifugation at 13,000 rpm at RT.

The RNA concentration was determined by spectrophotometric analysis with a NanoDrop ND-100 (Thermo Fisher Scientific, Waltham, MA, United States).

Real Time qPCR (RT-qPCR)

1 μg of each sample was reverse transcribed using the RT2 First Strand Kit (Qiagen), according to the manufacturer's instructions. Briefly, 2 μl buffer GE (QIAGEN) was added to 1 μg of RNA diluted in 8 μl RNase free water and the resulting mixture was incubated for 5 min at 42°C to eliminate genomic DNA, before being cooled down to 4°C for 20 min. 10 μl of Reverse Transcription mix was added to the sample according to manufacturer's guide. Each sample was then incubated at 42°C for 15 min using the PTC-200 Peltier Thermal Cycler (MJ Research). The reaction was stopped by incubating the samples at (95°C) for 5 min, before being cooled down to 4°C for 20 min. 91 ul of RNase free water was finally added to the resulting reverse transcribed cDNA sample.

RT-qPCR was performed using a Corbett Rotor Gene 6000 (Qiagen) and RT2 SYBR Green qPCR Mastermix (Qiagen) as follows: hot start for 10 min at 95°C, followed by 40 cycles of 15 s at 95°C, annealing for 30 s at 55°C, and extension for 30 s at 72°C. Melting curve was obtained as follow: 95°C for 1 min, 65°C for 2 min, and a gradual temperature increase from 65°C to 95°C at 2°C/min. All of the primers for the genes of interest and for the housekeeping gene were obtained from Sigma-Aldrich (listed in **Table 1**). Data were normalised for the housekeeping gene (GAPDH or 18S) and the ΔΔCt method was used to determine the fold changes in gene expression. Data is presented as mean ± standard error of the mean (SEM, error bars) and analysed by one-way ANOVA (Tukey's multiple comparison test).

Western Blot

Nerve explants were homogenised using a TissueRuptor (QIAGEN) in radio-immunoprecipitation assay (RIPA Sigma, United Kingdom) buffer (800 μl each) supplemented with a cocktail of protease and phosphatase inhibitors (Thermo Scientific, Loughborough, United Kingdom), and left for 30 min on ice. Following centrifugation at 14,000 rpm for 20 min at (4°C), proteins were quantified using Pierce™ BCA Protein Assay Kit (Thermo Scientific, Waltham, MA, United States)

TABLE 1 | Primer sequences used in PCR studies.

Gene	Forward	Reverse
Sox10	TGCCTAGGGACCTGCTTCAA	GGGTGAAAGGATCAGAGTGTCC
Cjun	GACCTTCTACGACGATGC	CAGCGCCAGCTACTGAGGC
Oct6	TCCGACGACCTGGAGCAG	CGAAGCGGCAGATGGTGG
Krox20	ACTGCTACCCCCTACAATCCGC	GAACCTCCTGTCGCAACCCTCT
S100	TCCATCAGTATTCAGGGAGAGA	TCCATCACTTTGTCCACCACT
P75	CACGACCAGCAGACCCATA	GCCAGATGTCGCCAGGTAT
Nestin	CCGGGTCAAGACGCTAGAAGA	CTCCAGCTCTTCCGCAAGGTTGT
Ngf	AAGGACGCAGCTTTCTATCC	CTATCTGTGTACGGTTCTGCC
Bdnf	AAGTCTGCATTACATTCCTCGA	GTTTTCTGAAAGAGGGACAGTTTAT
Gdnf	CAGTGACTCCAATATGCCCGA	TCGTAGCCCAAACCCAAGTC
P0	CCTGCTCTTCTCTTCTTTG	CACAGCACCATAGACTTC
Mbp	CGCATCTTGTTAATCCGTTCTAAT	GAGGGTTTGTTTCTGGAAGTTTC
Pmp22	TCCTGTTCCTTCACATCG	TGCCAGAGATCAGTCCTG
Trka	CCCCATCCCTGACACTAACA	GAGCAGCGTAGAAAGGAAGAG
Gapdh	CCGTATCGGACGCCTGGTTA	CCGTGGGTAGAGTCATACTGGAAC
18S	GGATCCATTGGAGGGCAAGT	ACGAGCTTTTTAACTGCAGCAA

according to the manufacturer's instruction. Protein samples were boiled in RIPA buffer and Laemmli sample buffer (×6) for 5 min at 100°C. An equal amount of the protein of interest (listed in **Table 2**) was loaded and run in sodium dodecyl sulphate polyacrylamide gels (SDS-PAGE) using Tris-glycine running buffer [25 mM Tris, 190 mM glycine, 0,08% (w/v) SDS]. The proteins were then transferred onto a nitrocellulose membrane (GE Healthcare Life Science, Amersham, Germany) in transfer buffer [25 mM Tris-base; 192 nM glycine, 20% (v/v) methanol]. The membranes were blocked for 1 h in a Tris-buffer saline (TBS) - Tween Solution containing 5% non-fat dry milk. Membranes were incubated overnight with primary antibodies (details in **Table 2**) diluted in blocking buffer or 5% bovine serum albumin (BSA) (Sigma-Aldrich, United Kingdom). Washes were done using TBS-Tween followed by 1 h incubation of the secondary antibody horseradish peroxidase (HRP) conjugated against rabbit or mouse (Cell Signaling, Hitchin, United Kingdom) for chemiluminescence detection. For housekeeping protein (GAPDH) membranes were stripped with a glycine solution (100 mM, pH 2.9; Sigma-Aldrich, United Kingdom) for 15 min at RT and re-blocked again as before, prior to further blotting. Membranes were exposed to SuperSignal West Pico Chemiluminescent Substrate (Thermo Scientific, Waltham, MA, United States), and the signal was analysed by densitometry using ImageJ 64 imaging software (Version 1.52a, National Institutes of Health NIH, United States). Western blot densitometry data of all proteins were normalised for the levels of GAPDH for each time point and used as a loading control.

Harvest and Culture of Human AD-MSCs

Adipose tissue samples were collected from patients undergoing reconstructive breast surgery at Wythenshawe Hospital, Manchester University NHS Foundation Trust, Manchester, United Kingdom. Patients were fully consented and procedures approved by the National Research Ethics Committee (NRES 13/SC/0499). All the samples were derived from subcutaneous abdominal fat. All patients were females aged 45–65 years and otherwise fit and healthy. AD-MSCs were obtained according to previously described protocol (Kingham et al., 2007). The adipose tissue was cut into small pieces then minced with razor blade and digested enzymatically using 0.2% (w/v) collagenase (Life Technologies, Paisley, United Kingdom) at 37°C for 45 min under constant agitation. The resulting tissue was filtered through a vacuum-assisted 100 μm nylon mesh (Merck Millipore UK, Watford, United Kingdom), followed by the addition of an equal amount of alpha-modified Minimum Essential Eagle's medium (aMEM) (Sigma-Aldrich, Poole, United Kingdom) supplemented with, 10% (v/v) FBS (LabTech, Uckfield, United Kingdom), 2 mM L-glutamine (GE Healthcare UK, Little Chalfont, United Kingdom), and 1% (v/v) penicillin–streptomycin solution. After centrifugation at 400 × *g* for 10 min, the SVF was pelleted. 1 ml of Red Blood Cell Lysis Buffer (Sigma-Aldrich) was added for 1 min followed by the addition of 15 ml of fresh aMEM and further centrifugation at 400 × *g* for 10 min. The resulting SVF pellet was plated in T75 at 37°C and 5% CO_2 with media change twice to three times a week and split when confluent. Characterisation was done according to our previously published protocol (Faroni et al., 2016). Passage 2 cells were used for co-culture experiments involving AD-MSC.

Stimulation of AD-MSC to a Schwann-Like Phenotype dASC

As previously described (Kingham et al., 2007), passage 2 AD-MSC were plated at 20 to 30% confluency and treated with 1 mM b-mercaptoethanol (Sigma-Aldrich) for 24 h, prior to 72 h of exposure to 35 ng/mL all-*trans*-retinoic

TABLE 2 | Antibodies and experimental conditions used for Western Blot analyses.

Protein name	Company	Gel%	Amount	Transfer	1ry Ab	2ry Ab
BDNF Rabbit polyclonal	Alomone Labs (ANT-010)	15%	20 μg	1.5 h at RT 30 MV	1:200 in 3% BSA	1:2000 in 3% BSA
NGF Rabbit polyclonal	Alomone Labs (AN-240)	15%	20 μg	1.5 h at RT 30 MV	1:400 in 3% BSA	1:2000 in 3% BSA
CJUN Rabbit polyclonal	Abcam, United Kingdom (ab31419)	15%	20 μg	1.5 h at RT 30 MV	1:500 in 5% milk	1:2000 in 5% milk
MBP Mouse monoclonal	Millipore, United States (MAB384-1ML)	15%	10 μg	Overnight at 4°C 30 MA	1:500 in 5% milk	1:2000 in 5% milk
P0 Rabbit monoclonal	Abcam, United Kingdom (ab183868)	15%	5 μg	Overnight at 4°C 30 MA	1:5000 in 5% milk	1:10000 in 5% milk
P75 Rabbit monoclonal	Abcam, United Kingdom (ab52987)	10%	20 μg	1 h at 80 V	1:500 in 5% milk	1:2000 in 5% milk
KROX20 Rabbit Polyclonal	Proteintech, United States (13491-1-AP)	10%	20 μg	1 h at 80 V	1:500 in 5% milk	1:2000 in 5% milk
GAPDH Rabbit polyclonal	Proteintech, United States (10494-1-AP)				1:5000 in 5% milk	1:4000 in 5% milk

acid (Sigma-Aldrich). The differentiation media (d-aMEM) was then added ([aMEM) + 14 μM forskolin (Sigma-Aldrich) + 5 ng/mL platelet-derived growth factor (Peprotech EC, London, United Kingdom) + 192 ng/mL glial growth factor-2 (GGF-2) (Acorda Therapeutics, Ardsley, NY, United States) + 10 ng/mL basic fibroblast growth factor (Peprotech EC)]. Cells were split at the fourth and tenth days of differentiation, and cells were considered differentiated (dASCs) after 14 days, as previously reported (Kingham et al., 2007). Cells at passage 4 to 6 were used in co-culture experiment involving dASCs.

Co-culture Experiments

Twenty-four hours before nerve explants were harvested, both AD-MSC and dASCs cells from confluent flasks were collected and counted using a Scepter 2.0 (Merck-Millipore). 100,000 cell per well were plated in 24-well plates (three wells for each time point) and 500 μl of either aMEM or d-aMEM media was used for each well.

Nerve explants were collected from four Sprague Dawley rats as described above, with 15–20 nerve explants collected for each condition. All the nerves were de-sheathed under the microscope and cut into 5–10 mm length. Experimental groups were as follow: D0 healthy nerve explants (D0 c), D3 degenerated nerve explants cultured without cells (D3 c), D3 nerves co-cultured with AD-MSC (uASCs) and D3 nerve explants cultured with dASCs (dASCs).

Using an insert with a 0.4 um porous membrane (Greiner Bio-One), the nerve explants were inserted into the 24 well plate containing the plated cells after a media change and HBSS wash. 1200 μl of DMEM media was added to both the cells and the nerves (across the permeable membrane). The well insert ensured that no direct contact between AD-MSC and explants occurred. The co-cultures were kept in the incubator at 37°C at 5% CO_2 for 3 days without a media change. The nerve explants were collected at each time point and processed for either gene or protein expression as described above.

Statistical Analysis

Data analysis were performed using GraphPad Prism 5 (7.0, GraphPad Software Inc., La Jolla, CA, United States). PCR data were presented as mean ± standard error of the mean (SEM, error bars) by one-way ANOVA (Tukey's multiple comparison test) (*$p < 0.05$, **$p < 0.01$, ***$p < 0.001$, ****$p < 0.0001$).

RESULTS

TEM Highlights Morphological/Structural Features of Degenerating Nerves in the *in vitro* WD Model

In order to assess WD *in vitro*, we performed TEM analysis of degenerating explants at day 0, 2, 5, and 12 after transection and degeneration *in vitro*. Transmission electron micrographs showed degeneration of both axons and myelin with loss of nerve structure and disorganisation (**Figure 1**). Day 0 (D0) healthy non-injured sciatic nerve (**Figure 1A**) (left panel)

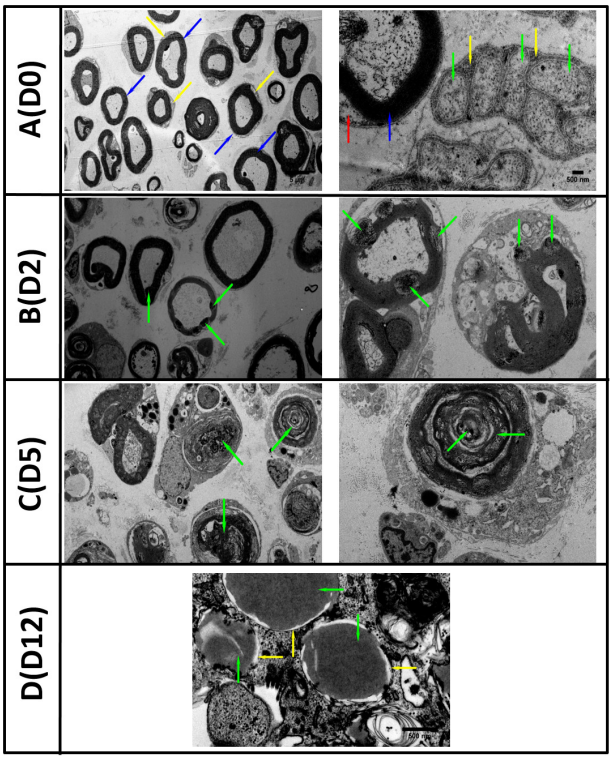

FIGURE 1 | TEM images of *in vitro* Wallerian degeneration model showing ongoing degeneration of the nerve axons and myelin. **(A)** (D0 left) Healthy rat sciatic nerve at day zero (D0) showed preserved myelin structures (blue arrows) and surrounded by Schwann cells cytoplasm (yellow arrow). **(A)** (D0 right) Nerve at higher magnification with regular myelin lamellae (blue arrow) and Schwann cell nucleus (red arrow). Multiple unmyelinated axons (green arrow) surrounded by Remak Schwann cell (yellow arrow) grouped in Remak bundles were also observed**. (B)** (D2 left) The second day (D2) post transection, the Wallerian Degeneration (WD) was evidenced by the appearance of multiple vacuoles within the myelin structures (green arrows) with the collapse of myelin evident at higher magnification **(B)** (D2 right). **(C)** Five days (D5) post *in vitro* WD we observed the disappearance of axonal structures and abundance of myelin debris within Schwann cell cytoplasm (green arrows). **(D)** Twelve days (D12) post transection and WD, the axons were replaced with amorphous material (green arrows) and myelin structures disappeared (yellow arrows) (Scale bars as in the top row are 5 μm on the right and 500 nm on the left).

showed preserved myelin structures (blue arrows) and cytoplasm of surrounding SCs was visible (yellow arrow). At higher magnification (right panel) we observed regular myelin lamellae (blue arrow) with SC nucleus (red arrow), alongside multiple unmyelinated axons (green arrow) surrounded by Remak SC (yellow arrow) to form Remak bundles. Two days after the *in vitro* degeneration (D2) the injured sciatic nerves contained multiple vacuoles within the myelin structure with evidence of early disorganisation and myelin collapse, accompanied by gradual loss of lamellar myelin structure (highlighted by green arrows at low (left) and high (right) magnification, **Figure 1B**). At day 5 (D5) post injury we observed the disappearance of some axons and the presence of multiple myelin debris within SC cytoplasm (green arrows), at low (left) and high (right) magnification

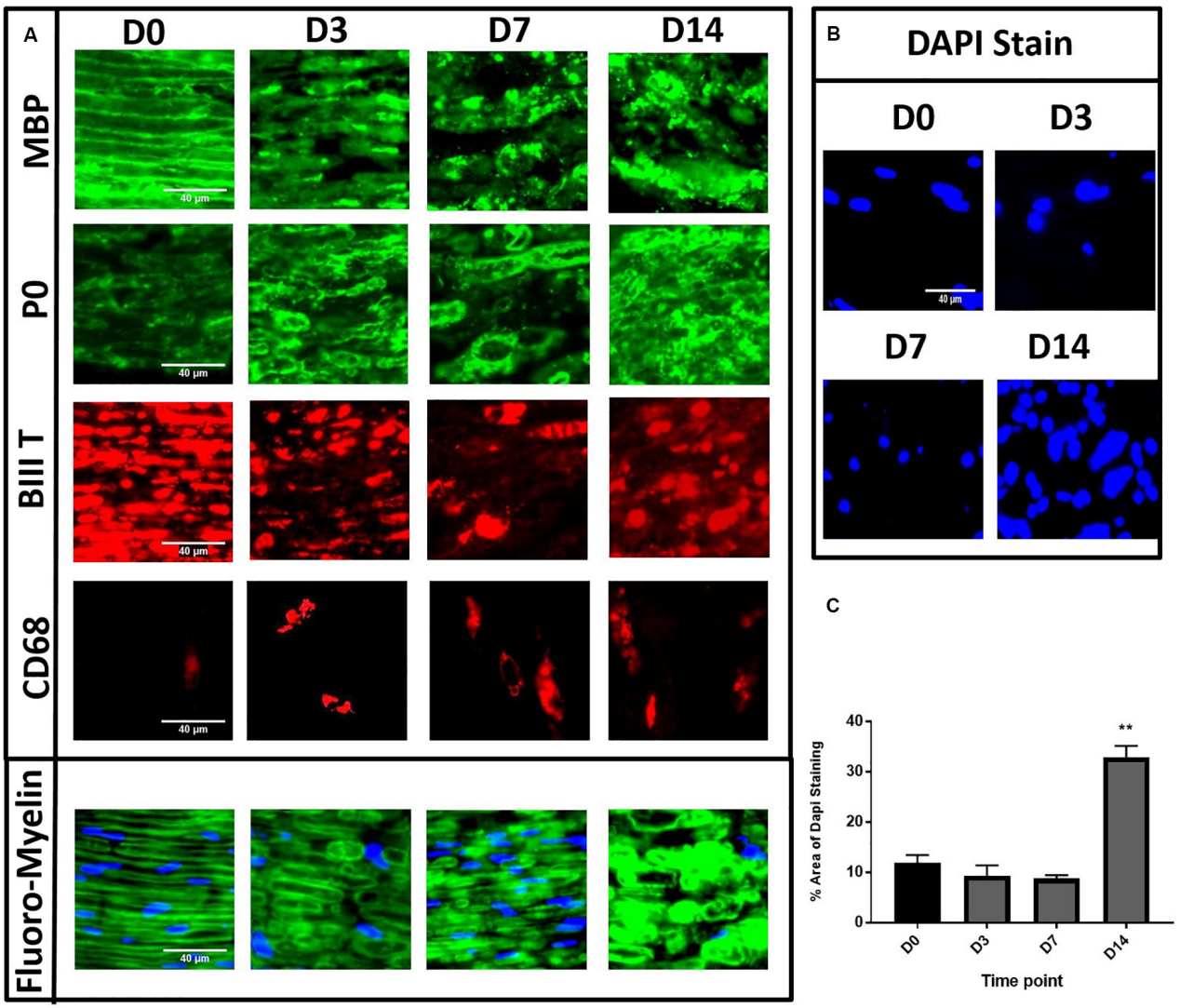

FIGURE 2 | Immunohistochemistry of *in vitro* model of degeneration showing degenerative changes to both myelin lipids, myelin proteins and axons. Panel **(A)** showed MBP/βIIIT/P0 staining with evident degeneration at D14 and Fluoro-Myelin staining with lipid degeneration. (D0) Compact homogenous organised myelin and axons resembling normal nerve. (D3) Loosening and disorganisation of myelin with multiple discontinuity. (D7) Continued loosening and disorganisation with greater disruption of myelin structure. (D14) Consolidated mass with loss of architecture. CD68 staining with gradual increase in numbers of cells after degeneration induction. **(B,C)** Gradual increase of % area of DAPI staining in desheathed explants at different time points showing significant increase at D14. (D0 is control.) (**$P < 0.001$) Scale bar for MBP, P0, βIIIT, Fluoro-Myelin and DAPI is 40 μm. Scale bar for CD68 is 200 μm.

(**Figure 1C**). After 12 days (D12) of WD induction *in vitro*, the nerve structure was compromised, myelin was unfolded or completely degenerated (yellow arrows), and axonal structure was replaced by amorphous material (green arrows) denoting the complete degeneration of the nerve sections (**Figure 1D**).

The *in vitro* Explant Model Shows Typical Immunohistochemical Features of WD

To further investigate the extent of WD in our *in vitro* model, we performed immunohistochemical analyses for myelin proteins, axonal structures and macrophage markers. The nerve explants were collected and fixed at different time points following *in vitro* WD (D0, 3, 7, and 14). Embedded nerves were cut in longitudinal sections and stained with myelin protein antibodies MBP and P0, FluoroMyelin (a non-specific stain for myelin lipids), axonal marker βIII tubulin as well as macrophage marker CD68. We observed consistent patterns of distribution of myelin and axonal structures at the different time points in three separate experiments. Healthy nerve at D0 (**Figure 2A**) showed compact myelin structures with complete homogeneity of the MBP and P0 staining (green), with lamellar organisation of myelin proteins and associated axons (βIII tubulin, red staining). At D3 post WD induction we observed early loosening and subtle disorganisation of both myelin lamellae (green) and corresponding axons (red) with appearance of multiple myelin discontinuity. With the

progression of degeneration at D7, we found further loosening of the myelin structures and disorganisation, which progressed to a complete loss of tissue architecture at D14 post-harvest (**Figure 2A**). Interestingly, we noticed a progressive increase in the number of CD68 positive cells from D0 to D14, a macrophage marker, in non-desheathed nerves (**Figure 2A**), compared to nearly complete absence in de-sheathed nerve sections (results not shown), suggesting that macrophages only migrate within the nerve after WD is induced. Finally, we quantified the number of nuclei present in the nerve sections, stained by DAPI as an indication of cell density within the explant. The area of DAPI staining (%) in desheathed nerves was calculated from three independent experiments and showed a significant three-fold increase in the number of cells at D14 in the *in vitro* model ($p < 0.01$) compared to D0 intact nerve (**Figures 2B,C**).

Gene Expression Level of WD Markers Indicate Progression of Degeneration in the *in vitro* Model

In order to assess the efficacy of the *in vitro* model to recapitulate WD, gene expression for key transcription factors, SC markers, neurotrophic markers and myelin genes was performed on D0 to 7 samples of degenerating nerves.

We analysed key transcription factors for SC function. We did not observe any change in *Sox10* gene expression levels after *in vitro* degeneration (**Figure 3A**). Conversely, there was significant upregulation of *Cjun* post WD induction, especially at D1 compared to D0 healthy nerve ($^{*}P < 0.05$), although levels returned at baseline levels by D7 (**Figure 3B**). *Oct6* and *Krox20* genes were significantly and progressively downregulated with *in vitro* degeneration, reaching minimal levels at D7 following injury ($^{****}P < 0.0001$ vs. D0) (**Figures 3C,D**).

Amongst the SC markers, we found significant downregulation of *S100* expression levels ($^{***}P < 0.001$ and $^{****}P < 0.0001$ at D1 and D3, 5, 7, respectively, vs. D0) (**Figure 3E**), and significant upregulation of *P75* (D0 vs. D1, 3, 5, 7, $^{****}P < 0.0001$) (**Figure 3F**) with progression of the degeneration. Neuronal marker and intermediate filament *Nestin*, showed transient significant upregulation at D1 post-harvest ($^{****}P < 0.0001$), followed by return to baseline levels at later time points (**Figure 3G**).

The analysis of neurotrophic factors expression in our model showed upregulation of the key neurotrophins such as *Ngf*, *Bdnf* and *Gdnf*. *Ngf* expression after *in vitro* WD was biphasic, with significant surge of *Ngf* expression at D1 and D5 ($^{****}P < 0.0001$) compared to D0 samples (**Figure 3H**). The upregulation of *Bdnf* was gradual during the progression of WD, and significantly higher at D3 ($^{*}P < 0.05$), D5 and D7 ($^{****}P < 0.0001$) post-harvest, compared to D0 healthy nerve (**Figure 3I**). Furthermore, *Gdnf* expression levels were significantly increased at the earliest time point (D1, $^{****}P < 0.0001$), and gradually declined at D3 and 5 ($^{**}P < 0.01$), to finally reach baseline levels at D7, all compared to D0 healthy nerve (**Figure 3J**). We also analysed at *Ngf* receptor *Trka* and noticed gradual downregulation of gene expression after WD induction, with levels significantly decreased at D5 ($^{***}P < 0.001$) and D7 ($^{****}P < 0.0001$) compared to D0 intact nerve (**Figure 3K**).

Finally, the gene expression of myelin proteins *P0*, *Pmp22* and *Mbp* was significantly downregulated following WD as early as the day after the harvest. Indeed, *P0* expression significantly decreased at D1 following degeneration ($^{***}P < 0.001$), and was almost absent at D3, 5 and 7 ($^{****}P < 0.0001$) (**Figure 3L**). Similarly, *Mbp* expression levels were significantly downregulated at D1 ($^{**}P < 0.01$), and nearly undetectable at D3, 5, and 7 ($^{****}P < 0.0001$) (**Figure 3M**). In addition, expression of *Pmp22* gene was significantly decreased at D1 ($^{****}P < 0.0001$) and completely abolished at later time points ($^{****}P < 0.0001$) (**Figure 3N**).

Expression Changes of Key Proteins Confirm Features of WD

To evaluate the extent to which our model recapitulates WD, we assessed the expression of some of these genes at the protein level.

We observed upregulation of both CJUN and P75 proteins after *in vitro* WD with levels reaching up to seven fold and six fold, respectively, at D7 compared to D0 healthy nerve (**Figures 4A,B**). MBP protein showed gradual downregulation resulting in approximately 50% of expression at D14, compared to D0 healthy nerve. Conversely, P0 protein expression remained constant throughout the 14 days of the *in vitro* WD model (**Figures 4C,D**). KROX 20 protein expression levels raised at D3 post-degeneration, reaching a plateau which remained constant until D14 post WD induction (**Figures 4E,F**). PRO-BDNF protein expression showed an opposite trend with the neurotrophin gradually downregulated starting from D3 post degeneration and reaching 60% expression at D14 compared to D0 controls (**Figures 4E,F**). In addition. PRO-NGF protein expression gradually decreased: interestingly, amongst the PRO-NGF isoforms, the 25 kDa variant showed the greatest decrease in expression levels at D14 post degeneration compared to D0 control (**Figures 4G,H**).

Assessing Novel Stem Cell Therapies With the *in vitro WD* Model: A Proof of Principle

To test the efficacy of our model to evaluate the potential of novel therapeutic approaches for nerve regeneration, we tested stem cell intervention with degenerating nerve explants. The nerve explants were co-cultured indirectly with AD-MSC or dASCs for 3 days; we then performed analysis of both gene and protein expression for the key markers of WD previously characterised (**Figure 5**).

We confirmed upregulation of P75 gene/protein following 3 days of WD ($^{****}P < 0.0001$), compared to D0 (control); nevertheless, AD-MSC and dASC intervention only marginally increased *P75* expression at the gene level compared to D3 control (**Figure 5B**), and did not seem to affect protein levels (**Figure 5A**). Expression of *Cjun* gene was also significantly upregulated at D3 of WD ($^{****}P < 0.0001$) compared to D0 (control); AD-MSC intervention further increased the gene expression of *Cjun* ($P < 0.0001$), whereas dASCs contributed

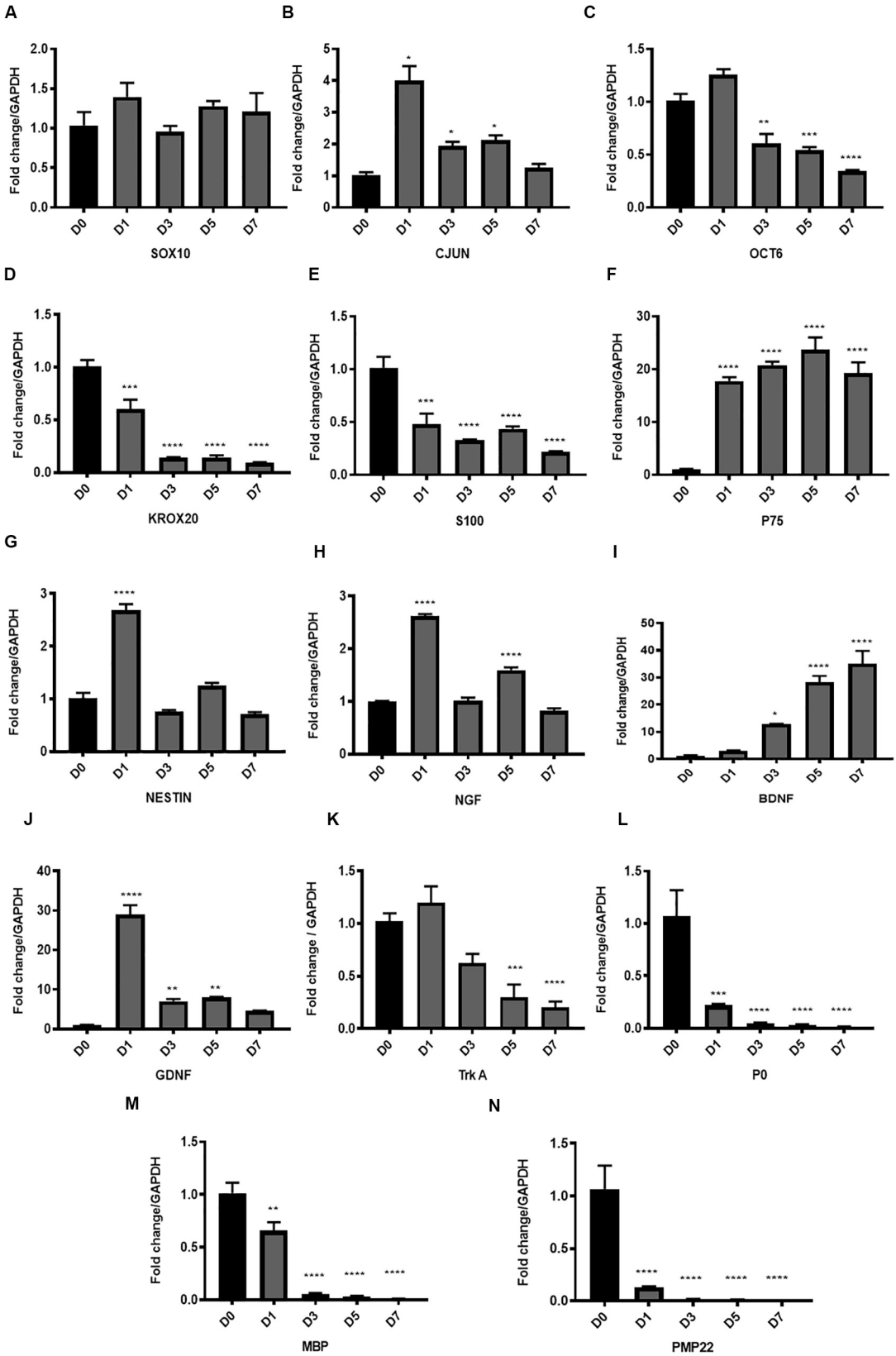

FIGURE 3 | Continued

FIGURE 3 | Gene expression of key transcription factors, Schwann cell markers, myelin proteins and neurotrophic factors in the *in vitro* model of Wallerian degeneration. **(A)** No significant change in *Sox10* gene expression levels after *in vitro* degeneration. **(B)** Significant upregulation of *Cjun* transcription factor after injury mostly at D1 compared to D0 healthy nerve with return to baseline levels at D7. **(C)** Transcription factor *Oct 6* expression after WD induction showed significant downregulation at D3, 5 and 7 post transection. **(D)** Transcription factor *Krox20* showed significant progressive downregulation in its expression levels with *in vitro* degeneration. **(E)** SC marker *S100* after *in vitro* WD showed significant downregulation relative to D0 (control healthy nerve). **(F)** *P75* after *in vitro* WD showed significant persistent upregulation. **(G)** Neuronal marker and intermediate filament *Nestin* showed transient significant upregulation at D1 post-harvest followed by return to baseline levels at later time points. **(H)** Expression of *Ngf* after *in vitro* WD was biphasic with significant surge of its expression at D1 and D5 compared to D0 healthy nerve. **(I)** Neurotrophic factor *Bdnf* showed significant continuous upregulation after *in vitro* WD in later time points. **(J)** Neurotrophic factor *Gdnf* showed significant early upregulation at D1 followed by gradual reduction at D3, 5 and D7 post-harvest. **(K)** The *Ngf* receptor *Trka* showed gradual downregulation of its gene expression in *in vitro* WD reaching significant reduction at D7 compared to D0 (control healthy nerve). **(L)** Gene expression of *P0* after WD induction showed early significant downregulation relative to D0 (control). **(M)** Gene expression of *Mbp* showed early significant downregulation relative to D0 (control). **(N)** Gene expression of *Pmp 22* after WD induction showed significant downregulation relative to D0 (control). Data are expressed as log2 fold change in D1, 3, 5 and 7 relative to D0 healthy nerve control sample. Data is presented as mean ± SEM (error bars) by one-way ANOVA (Tukey's multiple comparison test) (*$P < 0.05$, **$P < 0.01$, ***$P < 0.001$, ****$P < 0.0001$).

to a downregulation of the *Cjun* transcripts to D3 control levels (*$P < 0.05$, **Figure 5C**). At protein levels, we observed upregulation of CJUN in all D3 groups, with a 50% increase in the dASCs groups compared to D0 control (**Figure 5A**). Similarly, *Bdnf* gene expression is significantly increased following WD compared to D0 (****$P < 0.0001$), further upregulated by co-culture with AD-MSC (****$P < 0.0001$), but significantly decreased following dASCs intervention compared to D3 control (*$P < 0.05$, **Figure 5D**). On the other hand, the levels of expression of PRO-BDNF proteins were largely unaltered in all experimental groups (**Figure 5A**).

As shown during baseline characterisation of the *in vitro* model, we confirmed that *Krox20* gene expression is significantly downregulated following WD (****$P < 0.0001$), whereas protein levels are increased at D3 (**Figures 5A,E**). AD-MSC intervention caused a significant upregulation of *Krox20* transcript compared to D3 control (***$P < 0.001$) which did not translate to an increase in protein levels (**Figures 5A,E**). Conversely, co-culture to dASC did not significantly alter gene expression levels of *Krox20*, which was comparable to D3 control (**Figures 5A,E**). All myelin genes were found to be downregulated following the *in vitro* degeneration, and stem cell interventions did not alter the gene expression levels (**Figures 5F,G,J** for *P0*, *Mbp* and *Pmp22*, respectively). This was not the case at protein level, where expression of P0 and MBP was sustained despite *in vitro* WD and AD-MSC/dASCs intervention (**Figure 5A**). We confirmed the increase in *Gdnf* gene expression at D3 post WD (****$P < 0.0001$) with further significant upregulation in the AD-MSC co-culture group compared to D3 control (***$P < 0.001$, **Figure 5H**), but no effect was observed in the dASCs group. The gene expression levels of the SC marker *S100* showed significant decline at D3 control and no changes after AD-MSC/dASC intervention compared to D3 control (**Figure 5I**).

DISCUSSION

The vast majority of scientific endeavour in the field of peripheral nerve injury focuses on the regenerative response of nerves, including stem cell interventions. Given that efficient degeneration of the distal stump is a prerequisite for regeneration, it is an important target for interventions aimed at improving nerve regeneration outcomes. Studies on WD have predominantly been performed *in vivo* which incorporates the local response of SCs and resident macrophages with the more complex systemic pathophysiological immune response following injury. Establishing a model for WD, in which the immune response and other systemic influences are excluded is appealing because such a model would permit the exploration of novel therapies such as stem cell intervention, in higher throughput *in vitro* systems and focus on local effects which can otherwise be lost. Although the concept of using nerve segments *in vitro* as a representative of WD model was adopted previously, the cut nerve segments were allowed to degenerate *in vitro* for only 48 h without characterisation; moreover, the nerves were not de-sheathed, a condition that allows cells other than SCs to engage in the degenerative response and influences the cell population being characterised (Fex Svenningsen and Kanje, 1998). In this work, we have characterised an *in vitro* model of WD allowing better understanding of the biological changes that take place within the nerve without systemic influence. Our model clearly demonstrates histoarchitectural degeneration and gene/protein expressions in keeping with significant degeneration of the nerve and switching on of the SC regenerative response. In addition, as a proof of principle, we have used the model to study the effect of AD-MSC intervention in WD. Day 3 was selected for study of this intervention for two reasons: (i) many of the WD events are underway with morphological and molecular changes clearly evidenced in our model; and (ii) it is hypothesised that the impact of stem cell intervention is likely to be early before the onset of transplanted cell death.

Transcription Factors

Our *in vitro* model identified early and persistent upregulation of CJUN protein after injury. There is strong evidence that the transcription factor CJUN is a key reprogramming factor modulating the activity of repair SCs (Parkinson et al., 2008; Glenn and Talbot, 2013; Boerboom et al., 2017). CJUN drives increase in the expression levels of a multitude of trophic factors that are necessary for nerve regeneration acting both directly, such as GDNF and artemin, and indirectly, BDNF and NGF (Fontana et al., 2012). Gene ontology analyses have shown that *Cjun* modulates the expression of 172 genes, all involved in neuronal growth and regeneration (Arthur-Farraj et al., 2012). In our *in vitro* model of WD *Cjun* gene expression is upregulated at

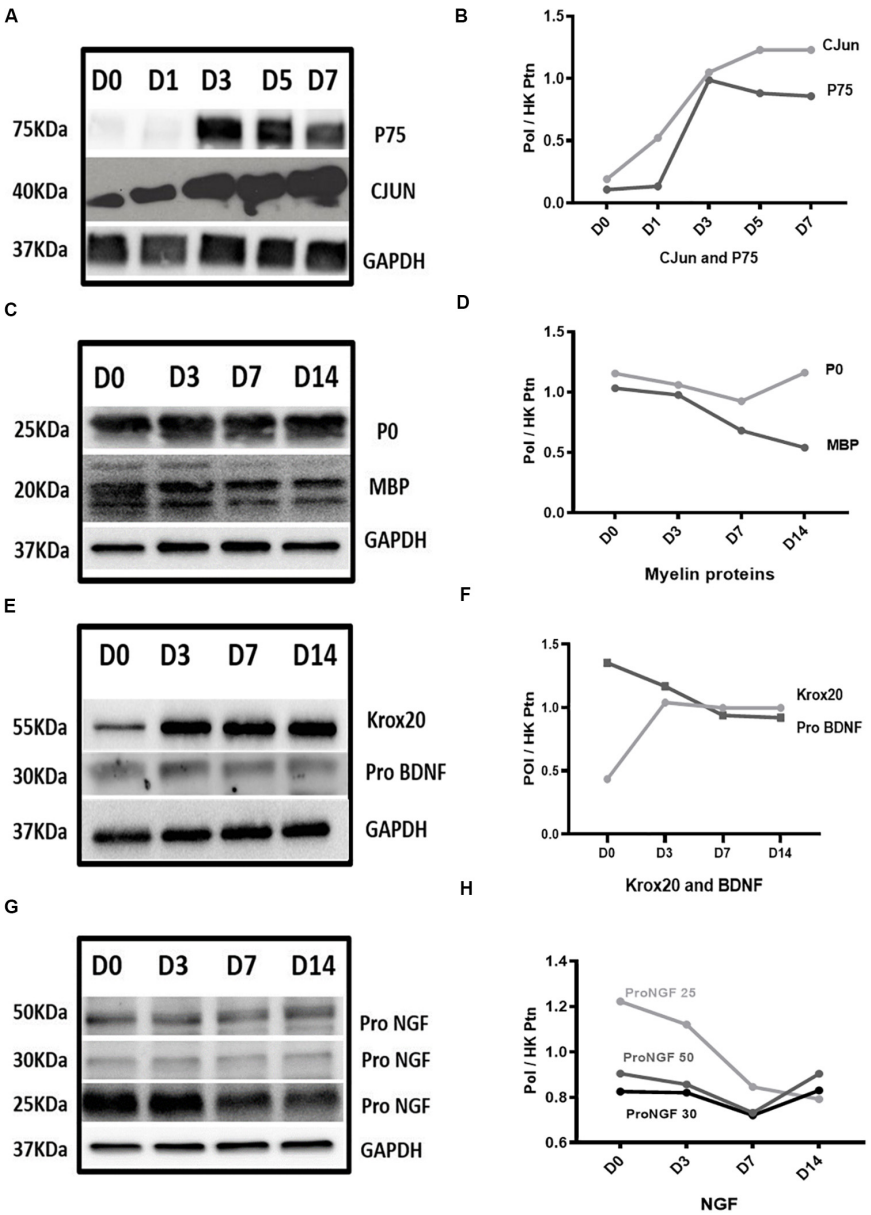

FIGURE 4 | Protein expression results in Wallerian degeneration *in vitro* model. **(A,B)** Western blot images and graph, respectively, showed persistent upregulation of CJUN and P75 proteins after WD induction. **(C,D)** Western blot images and graph, respectively, showed gradual downregulation of MBP protein reaching approximately 50% of its expression at D14 and P0 remained constant throughout the 14 days of *in vitro* WD compared to D0 healthy nerve. **(E,F)** Western blot images and graph, respectively, showed upregulation of KROX20 protein at D3 post-degeneration reaching a plateau which remained constant until D14 post-degeneration. PRO-BDNF protein expression showed gradual downregulation starting from D3 post-regeneration and reaching 60% of expression at D14 compared to D0 control. **(G,H)** Western blot graph and image of PRO-NGF, respectively, showed gradual reduction of different isoforms gradually reaching almost the same level at D14. Data is normalised by GAPDH for each time point. (Pol) is Protein of Interest. (HK ptn) is house-keeping protein.

day 1 post injury but returns to normal over the 7 day time course; however, its levels are sufficient to induce persistent elevation of its protein levels which is the ultimate goal to trigger its cascade of influence in particular negative regulation of myelination and upregulation of neurotrophic factors. It is worth mentioning that upregulation of CJUN after nerve injury has been recently observed in human degenerating nerves, an observation that is comparable to our rodent *in vitro* model (Wilcox et al., 2020).

Mature SCs constitutively express SOX10 (Britsch et al., 2001; Jessen and Mirsky, 2019) which maintains expression of ErbB3 receptors for NRG1 and regulates *Oct 6* and *Krox20* in controlling myelination (Pereira et al., 2012). Whilst *Sox10* gene expression levels are unchanged following injury, our *in vitro* model demonstrates that this regulatory pathway is interrupted after nerve injury leading to a dramatic decrease in the level of both *Oct6* and *Krox20* genes across all time points after nerve

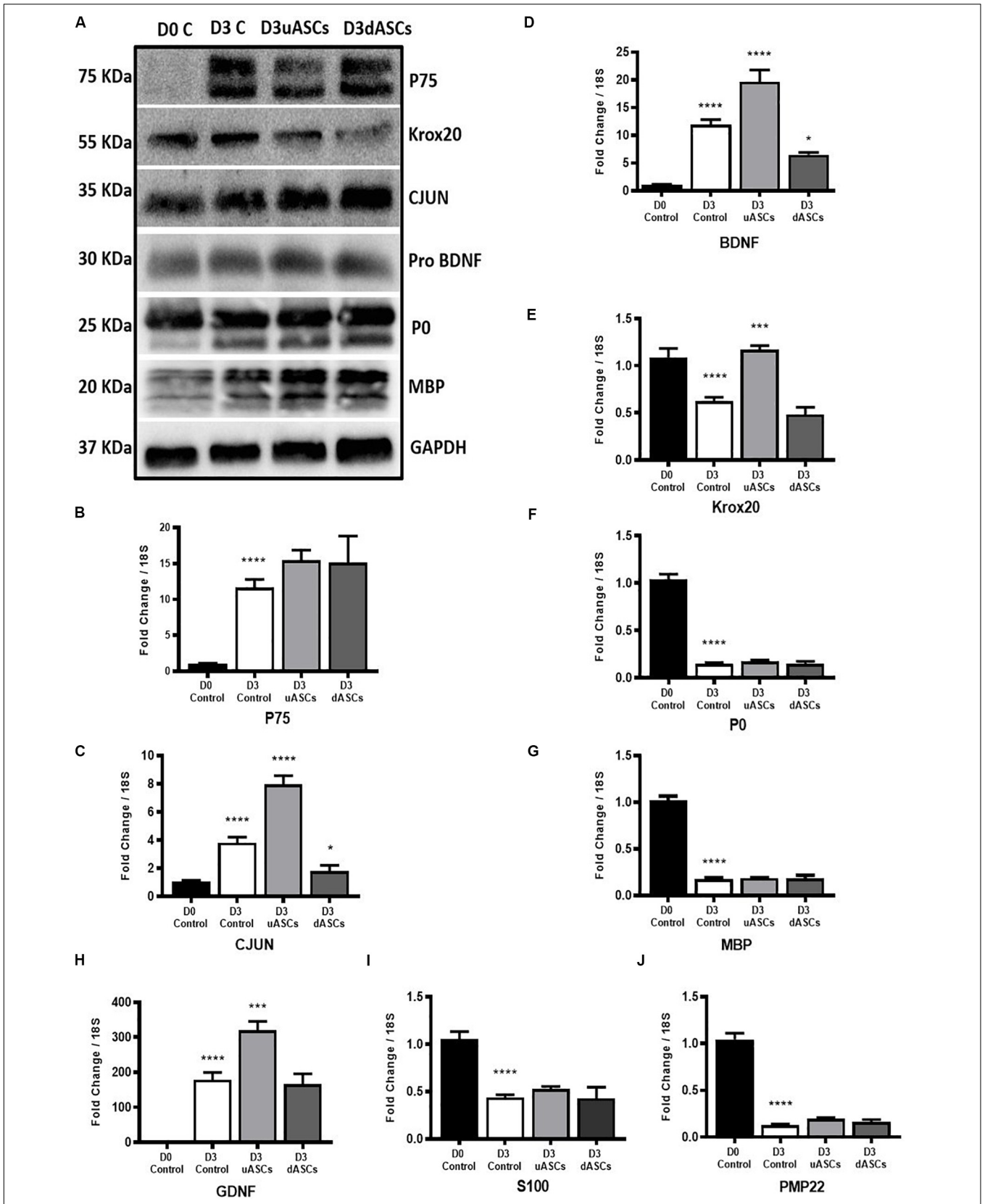

FIGURE 5 | Continued

FIGURE 5 | Gene and protein expression results of key transcription factors, Schwann cell markers, neurotrophic factors and myelin proteins of Wallerian degeneration model application. Indirect co-culture with both undifferentiated and differentiated adipose stem cells (uASCs, dASCs). **(A)** Protein expression of P75, KROX20, CJUN PRO-BDNF, P0 and MBP showing: an increase in the expression of P75 by five-fold at D3 without intervention and almost the same folds increase with AD-MSCs intervention compared to D0 control. An increase in expression of CJUN at D3 without intervention and continued upregulation by 30% for AD-MSCs and 50% fold for dASCs intervention compared to D0 control. Protein expression of KROX20 showing: upregulation of KROX20 at D3 without intervention with 30% and 50% downregulation at both AD-MSCs and dASCs intervention, respectively, compared to D0 control. No change in PRO-BDNF expression at D3 control, AD-MSCs and dASCs intervention compared to D0 control. Protein expression of myelin proteins showing: persistence of P0 and MBP proteins at D3 control and after stem cell intervention. **(B)** *P75* gene expression is upregulated in all D3 groups compered to D0 control that is further potentiated with both AD-MSCs and dASCs intervention. **(C)** *Cjun* gene expression is upregulated at D3 control group and AD-MSCs intervention markedly upregulates it gene expression in uASCs and dASCs were compared regarding D3c not D0 control whereas dASCs downregulates *Cjun* transcripts compared to D3 control levels **(D)** *Bdnf* gene expression is upregulated in all D3 groups compared to D0 control. AD-MSCs further potentiates this upregulation while dASCs intervention supresses it compared to D3 control group. **(E)** *Krox20* gene expression is downregulated at D3 non-interventional control group there is marginal downregulation with with dASCs intervention compared to D3 control; however, significant upregulation is noticed with AD-MSCs intervention compared to D3 control. **(F)** Significant downregulation of *P0* gene in all D3 groups compared to D0 control **(G)** Significant downregulation of *Mbp* gene in all D3 groups compared to D0 control. **(H)** The *Gdnf* gene is upregulated in all D3 groups compared to D0 control. Relative to D3 non-interventional control, AD-MSCs upregulates *Gdnf* levels but no effect is observed in the dASCs group. **(I)** *S100* gene expression is significantly downregulated to roughly about the same degree in nerves in all D3 groups compared to D0 control. **(J)** *Pmp22* gene expression is significantly downregulates in all D3 groups compared to D0 control. Gene data is presented as mean ± SEM (error bars) by one-way ANOVA (Tukey's multiple comparison test) (*$P < 0.05$, **$P < 0.01$, ***$P < 0.001$, ****$P < 0.0001$).

injury induction. Although KROX20 protein is present at D14, the changes in gene expression of these transcriptional factors are in line with *in vivo* models of WD (Jessen and Arthur-Farraj, 2019). The accumulated KROX20 protein in our model may be attributed to the lack of systemic inflammatory response that enhances the capability SCs to remove cell debris and non-functioning proteins. Furthermore, the expression of *S100,* a pan SC marker, is rapidly reduced and does not return for at least 7 days in our model and in previous *in vivo* models (Perez and Moore, 1968). Together, the expression patterns of these key SC mediators confirms the reliability of our model to be used as a simulator to the previously described *in vivo* models of WD.

With the intervention of human AD-MSC to the *in vitro* WD model system, we noticed a promising effect of human dASCs increasing the upregulation of CJUN protein to 1.5-fold increase at D3 compared to D3 control; and downregulation of both gene and protein expression of KROX20. This significant enhancement of transcriptional control could result in a rapid switch off of pro-myelinating pathways which may result in a more rapid deployment in greater scale of the 'repair' SCs in their critical roles in WD.

Neurotrophic Factors

Our *in vitro* WD model produces neurotrophic factor expression largely in keeping with that observed in *in vivo* models of injury. SCs upregulate neurotrophic factor expression and their cell surface receptors to prevent the death of injured neurons and stimulate axonal regeneration (Jessen and Arthur-Farraj, 2019).

In keeping with gene expression changes in our model, *Bdnf* expression has been demonstrated to increase up to 28 days post rat sciatic nerve transection (Meyer et al., 1992; Funakoshi et al., 1993); *Gdnf* upregulated progressively to day 7 post injury (Naveilhan et al., 1997); *Ngf* had a biphasic pattern of upregulation after nerve injury with a rapid surge within 6 h followed by sharp decrease and subsequent increase again by day 3 with persistent elevation up to 14 days post transection (Heumann et al., 1987a; Meyer et al., 1992); and upregulation of the neurotrophin receptor $P75^{ntr}$ (You et al., 1997; Boyd and Gordon, 2003). It is difficult to compare the temporal relationship of these models too precisely with our own given the nature of the injury differs from crush to single cut as opposed to our own double level transection; however, it is clear that the systemic immune response to injury will play an important role in neurotrophic factor expression, in particular *Ngf* via IL-1β. Macrophage invasion occurs 3 days after injury which is correlated with the second surge of *Ngf* levels in the *in vivo* model. This observation is further accredited *in vitro* by addition of macrophages or IL-1β (Heumann et al., 1987b). However, in our model SCs achieved a delayed second surge of *Ngf* gene expression at day 5 without the systemic inflammatory triggers.

Protein expression of the neurotrophic growth factors in our model decreases over time which is likely as a result of increased growth factor secretion, although we did not measure this directly. NGF protein has different isoforms with distinct molecular weights and is secreted as a PRO-NGF precursor biologically active on differing tissues (Fahnestock et al., 2004). PRO-NGF 25 protein expression was most significantly depleted in our model over 14 days post WD induction implying gradual secretion of this mature NGF. It is also notable that the P75 receptor increases by day 3 and remains at this level for at least 7 days.

AD-MSC have the ability to improve neurite outgrowth *in vitro* and *in vivo* which is likely as a result of neurotrophic factor expression (Faroni et al., 2014; Kingham et al., 2014). In our *in vitro* WD model, the upregulation of *Bdnf* and *Gdnf* in SCs was significantly greater after co-culture with AD-MSC than compared to control degenerated nerve explants at D3. This provides further evidence that AD-MSC can potentiate SCs into a regenerative phenotype. Interestingly, dASC failed to produce this response in SCs which may be attributable to the de-differentiation of dASC following growth factor withdrawal (Faroni et al., 2016).

Myelin Features in Our *in vitro* Model

Following peripheral nerve injury, the adaptive injury response triggered in SCs results in loss of axonal contact and myelin maintenance is switched to clearance initiated by SC myelinophagy (Gomez-Sanchez et al., 2015; Jang et al., 2016). In accordance with this, myelin protein gene (*P0, Mbp and Pmp22*) expression was switched off and there was

progressive morphological disorganisation and degradation of myelin protein and lipid structures following injury in our *in vitro* WD model.

Using TEM and immunohistochemistry on the injured nerve *in vitro* over 2 weeks, we noted the early appearance of multiple vacuoles and myelin lamellae collapse, followed by axonal degeneration and complete myelin disorganisation in keeping with previous findings (Johannessen, 1979; King, 1999; Kidd et al., 2013); however, myelin debris persisted in our model and this may be an important attribute to explore further because myelin debris inhibits pathways for axonal regeneration (Boerboom et al., 2017). SCs work in combination with resident and haematogenous macrophages toward myelinophagy, an active macro-autophagic process induced by SCs after injury (Gomez-Sanchez et al., 2015; Jang et al., 2016). In non-desheathed nerves, we noted an increase in CD68 staining for macrophages at days 7 and 14. These are presumed to be epineurium resident macrophages responding to the inflammatory process initiated by repair SCs although the systemic response describes invasion of macrophages by day 3 (Mueller et al., 2001). In our desheathed model, however, the epineurium is removed which likely removes the majority of resident macrophages although internal connective tissue structure is maintained. The persistence of myelin proteins at 14 days reveals one significant difference between our model and other systems either *in vivo* or the culture of dissociated SCs in which myelin degradation occurs (Gomez-Sanchez et al., 2015).

The importance of the systemic immune response in particular macrophages has been described as mandatory for complete and effective WD and myelin clearance (Scheidt et al., 1986). In a model of *in vivo* WD in which the mouse nerve explants were embedded in chambers with differential pore sizes to permit or exclude immune cells. Nerves exposed to macrophages and leucocytes permitted complete degeneration of myelin, whilst the lack of immune cells resulted in persistent myelin debris at 28 days. Furthermore, SCs secrete and activate pro-inflammatory markers after WD induction, such as TNFα and interleukin which lead to disturbance of the blood nerve barrier and allow monocytes and haematogenous macrophages to reach the field (Gaudet et al., 2011). Toll like receptors (TLRs) are expressed on the surface of SCs after injury and full knockout of TLRs in injured nerve leads to retardation in myelin clearance and macrophage recruitment (Chen et al., 2015). We can conclude that our *in vitro* model, in which there is no systemic inflammatory or immune response to aid SCs in myelinophagy, succeeded in early myelin collapse and breakdown but failed to achieve myelin clearance. There is promising pharmaceutical research targeting WD in many disorders of the central and peripheral nervous system (Coleman and Hoke, 2020). This leaves the *in vitro* WD model open to controlled manipulation of the key immune players in an *in vitro* system; in addition to the investigation of interventions such as pharmaceutical agents and stem cells to activate or inhibit autophagy machinery in SCs.

DATA AVAILABILITY STATEMENT

All datasets presented in this study are included in the article/supplementary material.

ETHICS STATEMENT

The studies involving human participants were reviewed and approved by National Research Ethics Committee (NRES 13/SC/0499). The patients/participants provided their written informed consent to participate in this study. Ethical review and approval was not required for the animal study because only *ex vivo* animal tissue was used. All the animal work was performed in accordance with the UK Animal Scientific Procedures Act 1986.

AUTHOR CONTRIBUTIONS

HbE, AF, MA, JO, and LW performed all studies and analysis. HbE, HsE, MM, AZ, and AR conceived of the study and drafted the manuscript. All authors read and approved the final manuscript.

FUNDING

HbE has been supported by a scholarship programme, under the Newton Mosharafa Fund partnership. The grant was funded by the UK Department for Business, Energy and Industrial Strategy and Central Department of Missions and delivered by the British Council. AF and AR are supported by the Hargreaves and Ball Trust and the Academy of Medical Sciences (AMS-SGCL7).

ACKNOWLEDGMENTS

Thank you to Mr. Jonathan Duncan, Miss Siobhan O'Ceallaigh (Consultant Plastic Surgeons) and their patients at Wythenshawe Hospital, Manchester University NHS Foundation Trust for donation of adipose tissue. The authors would like to thank Acorda Therapeutics for kindly supplying us with recombinant GGF-2 for use in this study.

REFERENCES

Arthur-Farraj, P. J., Latouche, M., Wilton, D. K., Quintes, S., Chabrol, E., Banerjee, A., et al. (2012). c-Jun reprograms schwann cells of injured nerves to generate a repair cell essential for regeneration. *Neuron* 75, 633–647. doi: 10.1016/j.neuron.2012.06.021

Boerboom, A., Dion, V., Chariot, A., and Franzen, R. (2017). Molecular mechanisms involved in schwann cell plasticity. *Front. Mol. Neurosci.* 10:38. doi: 10.3389/fnmol.2017.00038

Boyd, J. G., and Gordon, T. (2003). Neurotrophic factors and their receptors in axonal regeneration and functional recovery after peripheral nerve injury. *Mol. Neurobiol.* 27, 277–324. doi: 10.1385/mn:27:3:277

Britsch, S., Goerich, D. E., Riethmacher, D., Peirano, R. I., Rossner, M., Nave, K. A., et al. (2001). The transcription factor Sox10 is a key regulator of peripheral glial development. *Genes Dev.* 15, 66–78. doi: 10.1101/gad.186601

Chen, P., Piao, X., and Bonaldo, P. (2015). Role of macrophages in Wallerian degeneration and axonal regeneration after peripheral nerve injury. *Acta Neuropathol.* 130, 605–618. doi: 10.1007/s00401-015-1482-4

Coleman, M. P., and Hoke, A. (2020). Programmed axon degeneration: from mouse to mechanism to medicine. *Nat. Rev. Neurosci.* 21, 183–196. doi: 10.1038/s41583-020-0269-3

Dezawa, M., Takahashi, I., Esaki, M., Takano, M., and Sawada, H. (2001). Sciatic nerve regeneration in rats induced by transplantation of in vitro differentiated bone-marrow stromal cells. *Eur. J. Neurosci.* 14, 1771–1776. doi: 10.1046/j.0953-816x.2001.01814.x

Dubovy, P. (2011). Wallerian degeneration and peripheral nerve conditions for both axonal regeneration and neuropathic pain induction. *Ann. Anat. Anatomisch. Anzeig.* 193, 267–275. doi: 10.1016/j.aanat.2011.02.011

Fahnestock, M., Yu, G., and Coughlin, M. D. (2004). Prongf: a neurotrophic or an apoptotic molecule? *Prog. Brain Res.* 146, 101–110. doi: 10.1016/s0079-6123(03)46007-x

Faroni, A., Smith, R. J., Lu, L., and Reid, A. J. (2016). Human schwann-like cells derived from adipose-derived mesenchymal stem cells rapidly de-differentiate in the absence of stimulating medium. *Eur. J. Neurosci.* 43, 417–430. doi: 10.1111/ejn.13055

Faroni, A., Smith, R. J., and Reid, A. J. (2014). Adipose derived stem cells and nerve regeneration. *Neural Regen. Res.* 9, 1341–1346.

Faroni, A., Terenghi, G., and Reid, A. J. (2013). Adipose-derived stem cells and nerve regeneration: promises and pitfalls. *Int. Rev. Neurobiol.* 108, 121–136. doi: 10.1016/b978-0-12-410499-0.00005-8

Fex Svenningsen, A., and Kanje, M. (1998). Regulation of Schwann cell proliferation in cultured segments of the adult rat sciatic nerve. *J. Neurosci. Res.* 52, 530–537. doi: 10.1002/(sici)1097-4547(19980601)52:5<530::aid-jnr5>3.0.co;2-d

Fontana, X., Hristova, M., Da Costa, C., Patodia, S., Thei, L., Makwana, M., et al. (2012). c-Jun in Schwann cells promotes axonal regeneration and motoneuron survival via paracrine signaling. *J. Cell Biol.* 198, 127–141. doi: 10.1083/jcb.201205025

Funakoshi, H., Frisen, J., Barbany, G., Timmusk, T., Zachrisson, O., Verge, V. M., et al. (1993). Differential expression of mrnas for neurotrophins and their receptors after axotomy of the sciatic nerve. *J. Cell Biol.* 123, 455–465. doi: 10.1083/jcb.123.2.455

Gaudet, A. D., Popovich, P. G., and Ramer, M. S. (2011). Wallerian degeneration: gaining perspective on inflammatory events after peripheral nerve injury. *J. Neuroinflamm.* 8:110. doi: 10.1186/1742-2094-8-110

Glenn, T. D., and Talbot, W. S. (2013). Signals regulating myelination in peripheral nerves and the Schwann cell response to injury. *Curr. Opin. Neurobiol.* 23, 1041–1048. doi: 10.1016/j.conb.2013.06.010

Gomez-Sanchez, J. A., Carty, L., Iruarrizaga-Lejarreta, M., Palomo-Irigoyen, M., Varela-Rey, M., Griffith, M., et al. (2015). Schwann cell autophagy, myelinophagy, initiates myelin clearance from injured nerves. *J. Cell Biol.* 210, 153–168. doi: 10.1083/jcb.201503019

Heumann, R., Korsching, S., Bandtlow, C., and Thoenen, H. (1987a). Changes of nerve growth factor synthesis in nonneuronal cells in response to sciatic nerve transection. *J. Cell Biol.* 104, 1623–1631. doi: 10.1083/jcb.104.6.1623

Heumann, R., Lindholm, D., Bandtlow, C., Meyer, M., Radeke, M. J., Misko, T. P., et al. (1987b). Differential regulation of mrna encoding nerve growth factor and its receptor in rat sciatic nerve during development, degeneration, and regeneration: role of macrophages. *Proc. Natl. Acad. Sci. U.S.A.* 84, 8735–8739. doi: 10.1073/pnas.84.23.8735

Jang, S. Y., Shin, Y. K., Park, S. Y., Park, J. Y., Lee, H. J., Yoo, Y. H., et al. (2016). Autophagic myelin destruction by Schwann cells during wallerian degeneration and segmental demyelination. *Glia* 64, 730–742. doi: 10.1002/glia.22957

Jessen, K. R., and Arthur-Farraj, P. (2019). Repair Schwann cell update: adaptive reprogramming, Emt, and stemness in regenerating nerves. *Glia* 67, 421–437. doi: 10.1002/glia.23532

Jessen, K. R., and Mirsky, R. (2019). Schwann cell precursors; multipotent glial cells in embryonic nerves. *Front. Mol. Neurosci.* 12:69. doi: 10.3389/fnmol.2017.00069

Johannessen, J. V. (1979). Electron microscopy in human medicine. *J. Clin. Pathol.* 33:511.

Kidd, G. J., Ohno, N., and Trapp, B. D. (2013). Biology of Schwann cells. *Handb. Clin. Neurol.* 115, 55–79.

King, R. H. M. (1999). *Atlas of Peripheral Nerve Pathology*. London: Georgina Bentliff.

Kingham, P. J., Kalbermatten, D. F., Mahay, D., Armstrong, S. J., Wiberg, M., and Terenghi, G. (2007). Adipose-derived stem cells differentiate into a Schwann cell phenotype and promote neurite outgrowth in vitro. *Exper. Neurol.* 207, 267–274. doi: 10.1016/j.expneurol.2007.06.029

Kingham, P. J., Reid, A. J., and Wiberg, M. (2014). Adipose-derived stem cells for nerve repair: hype or reality? *Cells Tissues Organs.* 200, 23–30. doi: 10.1159/000369336

Meyer, M., Matsuoka, I., Wetmore, C., Olson, L., and Thoenen, H. (1992). Enhanced synthesis of brain-derived neurotrophic factor in the lesioned peripheral nerve: different mechanisms are responsible for the regulation of Bdnf and Ngf mrna. *J. Cell Biol.* 119, 45–54. doi: 10.1083/jcb.119.1.45

Mueller, M., Wacker, K., Ringelstein, E. B., Hickey, W. F., Imai, Y., and Kiefer, R. (2001). Rapid response of identified resident endoneurial macrophages to nerve injury. *Am. J. Pathol.* 159, 2187–2197. doi: 10.1016/s0002-9440(10)63070-2

Naveilhan, P., Elshamy, W. M., and Ernfors, P. (1997). Differential regulation of mrnas for Gdnf and its receptors Ret and Gdnfr alpha after sciatic nerve lesion in the mouse. *Eur. J. Neurosci.* 9, 1450–1460. doi: 10.1111/j.1460-9568.1997.tb01499.x

Palispis, W. A., and Gupta, R. (2017). Surgical repair in humans after traumatic nerve injury provides limited functional neural regeneration in adults. *Exp. Neurol.* 290, 106–114. doi: 10.1016/j.expneurol.2017.01.009

Parkinson, D. B., Bhaskaran, A., Arthur-Farraj, P., Noon, L. A., Woodhoo, A., Lloyd, A. C., et al. (2008). c-Jun is a negative regulator of myelination. *J. Cell Biol.* 181, 625–637. doi: 10.1083/jcb.200803013

Pereira, J. A., Lebrun-Julien, F., and Suter, U. (2012). Molecular mechanisms regulating myelination in the peripheral nervous system. *Trends Neurosci.* 35, 123–134. doi: 10.1016/j.tins.2011.11.006

Perez, V. J., and Moore, B. W. (1968). Wallerian degeneration in rabbit tibial nerve: changes in amounts of the S-100 protein. *J. Neurochem.* 15, 971–977. doi: 10.1111/j.1471-4159.1968.tb11640.x

Rotshenker, S. (2011). Wallerian degeneration: the innate-immune response to traumatic nerve injury. *J. Neuroinflamm.* 8:109. doi: 10.1186/1742-2094-8-109

Scheidt, P., Waehneldt, T. V., Beuche, W., and Friede, R. L. (1986). Changes of myelin proteins during Wallerian degeneration in situ and in millipore diffusion chambers preventing active phagocytosis. *Brain Res.* 379, 380–384. doi: 10.1016/0006-8993(86)90795-x

Wilcox, M. B., Laranjeira, S. G., Eriksson, T. M., Jessen, K. R., Mirsky, R., Quick, T. J., et al. (2020). Characterising cellular and molecular features of human peripheral nerve degeneration. *Acta Neuropathol. Commun.* 8:51.

You, S., Petrov, T., Chung, P. H., and Gordon, T. (1997). The expression of the low affinity nerve growth factor receptor in long-term denervated Schwann cells. *Glia* 20, 87–100. doi: 10.1002/(sici)1098-1136(199706)20:2<87::aid-glia1>3.0.co;2-1

Conflict of Interest: The authors declare that the research was conducted in the absence of any commercial or financial relationships that could be construed as a potential conflict of interest.

The reviewer VM declared a past co-authorship with one of the authors AF to the handling Editor.

frontiers in Bioengineering and Biotechnology

MINI REVIEW
published: 30 October 2020
doi: 10.3389/fbioe.2020.583184

GDNF Gene Therapy to Repair the Injured Peripheral Nerve

Ruben Eggers[1], Fred de Winter[1], Martijn R. Tannemaat[1,2], Martijn J. A. Malessy[1,3] and Joost Verhaagen[1,4]*

[1] Laboratory for Neuroregeneration, Netherlands Institute for Neuroscience, Institute of the Royal Academy of Arts and Sciences, Amsterdam, Netherlands, [2] Department of Neurology, Leiden University Medical Center, Leiden, Netherlands, [3] Department of Neurosurgery, Leiden University Medical Center, Leiden, Netherlands, [4] Department of Molecular and Cellular Neurobiology, Center for Neurogenomics and Cognition Research, Vrije Universiteit Amsterdam, Amsterdam, Netherlands

A spinal root avulsion is the most severe proximal peripheral nerve lesion possible. Avulsion of ventral root filaments disconnects spinal motoneurons from their target muscles, resulting in complete paralysis. In patients that undergo brachial plexus nerve repair, axonal regeneration is a slow process. It takes months or even years to bridge the distance from the lesion site to the distal targets located in the forearm. Following ventral root avulsion, without additional pharmacological or surgical treatments, progressive death of motoneurons occurs within 2 weeks (Koliatsos et al., 1994). Reimplantation of the avulsed ventral root or peripheral nerve graft can act as a conduit for regenerating axons and increases motoneuron survival (Chai et al., 2000). However, this beneficial effect is transient. Combined with protracted and poor long-distance axonal regeneration, this results in permanent function loss. To overcome motoneuron death and improve functional recovery, several promising intervention strategies are being developed. Here, we focus on GDNF gene-therapy. We first introduce the experimental ventral root avulsion model and discuss its value as a proxy to study clinical neurotmetic nerve lesions. Second, we discuss our recent studies showing that GDNF gene-therapy is a powerful strategy to promote long-term motoneuron survival and improve function when target muscle reinnervation occurs within a critical post-lesion period. Based upon these observations, we discuss the influence of timing of the intervention, and of the duration, concentration and location of GDNF delivery on functional outcome. Finally, we provide a perspective on future research directions to realize functional recovery using gene therapy.

Keywords: gene therapy, peripheral nerve injury, nerve regeneration, ventral root avulsion, axonal regeneration

OPEN ACCESS

Edited by:
Xavier Navarro, Autonomous University of Barcelona, Spain

Reviewed by:
Antal Nógrádi, University of Szeged, Hungary
Alexandre Leite Rodrigues Oliveira, Campinas State University, Brazil

****Correspondence:***
Ruben Eggers
r.eggers@nin.knaw.nl

Specialty section:
This article was submitted to Tissue Engineering and Regenerative Medicine, a section of the journal Frontiers in Bioengineering and Biotechnology

Received: *14 July 2020*
Accepted: *12 October 2020*
Published: *30 October 2020*

Citation:
Eggers R, de Winter F, Tannemaat MR, Malessy MJA and Verhaagen J (2020) GDNF Gene Therapy to Repair the Injured Peripheral Nerve. Front. Bioeng. Biotechnol. 8:583184. doi: 10.3389/fbioe.2020.583184

INTRODUCTION

Root avulsion lesions are typically part of a brachial plexus traction injury which occurs during traffic accidents and complicated childbirth. Following an avulsion lesion, the rupture of nerve root filaments from the surface of the spinal cord leads to a combined central and peripheral nervous system lesion. This lesion is often not limited to only one nerve root, but consists of the avulsion of multiple roots. Despite neurosurgical repair, the degree of recovery of function in patients suffering a brachial plexus lesion often remains poor and results in lifelong dysfunction and pain. Thus, in order to regain useful function following neurosurgical repair, multiple supplementary

regenerative treatment strategies are required. Here, we will focus on GDNF gene therapy while other intervention strategies have been discussed elsewhere (Chu and Wu, 2009; Carlstedt, 2010; Eggers et al., 2016).

THE VALUE OF THE VENTRAL ROOT AVULSION AS A MODEL TO STUDY NEUROTMETIC NERVE LESIONS AND TREATMENT STRATEGIES

A ventral root avulsion lesion is not frequently used as a lesion model to study axonal regeneration. This might partially be due to the complexity of the lesion model and surgical procedures. Additionally, from a clinical perspective, this type of lesion might be considered beyond repair (Seddon, 1942; Robotti et al., 1995). Most often, studies on experimental peripheral nerve regeneration in mouse or rat models use either a crush (axonotmesis) or transection (neurotmesis) of a mixed peripheral nerve such as the sciatic, femoral, median or ulnar nerve. These lesions are performed relatively close to the target organ, which requires only a relatively short follow-up period. Following these types of lesions, spontaneous axonal regeneration and recovery of function is quite robust. These studies have provided important insights in the pathophysiological understanding of the regenerative response mechanisms in an injured peripheral nerve. However, translation to the clinical situation with different anatomical dimensions appears unsatisfactory. In patients, proximal lesions lead to a prolonged denervation period associated with a limited degree of axon regeneration and poor recovery of function. In order to obtain translatable data, animal models that more closely mimic the clinical situation are required. Long denervation and regeneration time-periods have been achieved by delaying surgical repair (Fu and Gordon, 1995; Gordon et al., 2011; Jonsson et al., 2013; Ronchi et al., 2017) or creating large nerve defects (Saheb-Al-Zamani et al., 2013; Marquardt et al., 2015; Hoben et al., 2018). In agreement with clinical observations, in these models of protracted denervation, spontaneous recovery of function is extremely poor or even absent. The main cause for the limited functional recovery in these injury models is attributed to the failure of repair Schwann cells to continue to support axon regeneration after a critical post-lesion period of 6 to 8 weeks (Sulaiman and Gordon, 2000; Hoke et al., 2002). After this period, a state of chronic denervation develops and the process of supported regeneration comes to a halt.

Reimplantation of the avulsed ventral root has been pioneered by the Carlstedt laboratory and in patients has resulted in recovery in the proximal limb similar to that achieved by conventional nerve grafts (Carlstedt et al., 1986, 1995, 2000; Htut et al., 2007). Reimplantation has since been used by several laboratories worldwide (Wu et al., 2003; Bergerot et al., 2004; Haninec et al., 2004; Hoang and Havton, 2006; Penas et al., 2011; Barbizan et al., 2013; Pajenda et al., 2014). Directly following avulsion progressive death of motoneurons occurs within 2 weeks (Koliatsos et al., 1994). Acute reimplantation of a peripheral nerve graft or avulsed ventral root enhances motoneuron survival and acts as a conduit for regenerating axons (Wu et al., 1994; Hoang and Havton, 2006; Ohlsson et al., 2006). However, a spatio-temporal analysis following the trajectory between the spinal motoneurons and distal target muscle after experimental lumbar ventral root avulsion and reimplantation, revealed that the beneficial effect of ventral root reimplantation on motoneuron survival is not maintained beyond 4 weeks (**Figure 1A**; Eggers et al., 2010). The initial axonal outgrowth response is robust, but includes aberrant growth to ectopic sites while the number of axons able to regenerate over a long distance is low. The failure to regenerate over long distances is associated with a loss of endogenous peripheral neurotrophic support, including decreasing levels of glial cell line-derived neurotrophic factor (GDNF) protein. Similar to chronic denervation models, after a ventral root avulsion lesion, the pro-regenerative period is limited to 6 to 8 weeks, after which the ability for long distance axon regeneration becomes increasingly poor (Eggers et al., 2010, 2019a; Torres-Espin et al., 2013).

The regeneration distance of 12 cm which is created with a lumbar ventral root avulsion in the rat is the longest peripheral nerve regeneration distance possible in small animal research. Performing a spinal root avulsion in larger species such as rabbit (Lang et al., 2005; Reichert et al., 2015), cat (Cullheim et al., 1989; Rafuse et al., 1992; Hoffmann et al., 1996), or macaque (Hallin et al., 1999; Ohlsson et al., 2013; Nieto et al., 2019) inherently results in longer regeneration distances. The proof of concept studies in these larger animals mainly focused on axonal regeneration into the reimplanted root, showing the feasibility of ventral root reimplantation as a clinical treatment option. Functionally, signs of reinnervation on electromyography and co-contractions due to axonal misrouting are primarily observed in the proximal musculature. Considering our and others' observed degree of long-distance axonal regeneration and functional recovery following lumbar ventral root avulsion in the rat, in our view, performing regenerative gene therapy studies in larger animals is not warranted before meaningful functional recovery in the rat is achieved.

A ventral root avulsion lesion has several unique characteristics, which are distinct from most peripheral nerve regeneration models. *First,* avulsion is an extensive proximal nerve lesion, which combines a longitudinal spinal cord lesion with denervation of the complete peripheral nerve (Carlstedt and Havton, 2012). *Second*, axotomy close to the motoneuron cell body results in progressive degeneration and death of spinal motoneurons, which does not occur if axotomy is performed more than 4 mm distal from the cell body (Gu et al., 1997). *Third*, ventral root avulsion is a selective motor axon lesion, while the afferent sensory axons remain intact. *Fourth*, in delayed surgical repair models, a chronically denervated distal nerve is achieved by halting regeneration until a second additional repair surgery is performed allowing regeneration to proceed. This contrasts with acute root avulsion and reimplantation, which allows for uninterrupted axonal regeneration, while the required long regeneration distance leads to a prolonged period of distal Schwann cell denervation. Clinically, brachial plexus lesions can be variable consisting of a combined axonotmetic and neurotmetic nerve lesion of multiple adjacent motor and sensory nerve roots (Narakas, 1985). Although our selective

ventral root avulsion and acute reimplantation does not reflect this heterogeneity, by performing a complete motor nerve lesion, this methodology provides us with a highly reproducible and predictable model for long-distance motor axon regeneration accompanied with chronic denervation. Compared to chronic peripheral nerve lesion models, an avulsion lesion more closely represents the severe pathogenesis as observed in the clinic after a proximal nerve lesion such as a brachial plexus injury.

GDNF GENE THERAPY AS A POWERFUL TREATMENT STRATEGY

To improve recovery of function, supplementary regenerative treatment strategies are required. We and others have shown that Glial cell line-derived neurotrophic factor (GDNF) is a compelling treatment candidate due to its role in neuronal differentiation and identification as a potent motoneuron survival and axon outgrowth factor (Henderson et al., 1994; Li et al., 1995). Furthermore, in motoneurons following axotomy, the GDNF receptors c-RET and GFRα-1 are strongly upregulated (Hammarberg et al., 2000). In Schwann cells, GDNF-mediated signaling cascades play an important role in myelination, proliferation and migration (Iwase et al., 2005).

However, GDNF and other neurotrophic factors have a short half-life, exhibit poor tissue penetration and systemic or topical delivery of GDNF results in unwanted side effects in non-targeted tissues. Here, the advantage of gene therapy is the sustained production of GDNF protein by viral vector transduced cells, resulting in the constant availability of biologically active therapeutic protein restricted to the site of viral vector application. Despite these advantages, persistent high local levels of GDNF expression lead to impaired axon regeneration by inducing coil formation at the site of GDNF expression (Blits et al., 2004; Love et al., 2005; Eggers et al., 2008, 2013; Tannemaat et al., 2008; Santosa et al., 2013; Shakhbazau et al., 2013; Marquardt et al., 2015; Ee et al., 2017; Wang et al., 2018). Application of a 4 cm long increasing proximo-distal GDNF gradient in a lesioned peripheral nerve, demonstrated that an increasing GDNF concentration enhanced distal axonal sprouting and axon numbers (Eggers et al., 2013). However, coil formation was observed already at relatively low GDNF concentrations (**Figure 1B**) and the degree of coil formation strongly correlates to the level of expression. These observations indicate that it is important to control the timing, dose and location of neurotrophic factor expression in order to achieve successful long-distance axonal regeneration (Harvey et al., 2015).

In recent proof of concept studies, transplantation of engineered Schwann cells in the peripheral nerve allowed for doxycycline-inducible GDNF expression (Shakhbazau et al., 2013; Marquardt et al., 2015). In contrast to the disrupted axonal regeneration following persistent GDNF expression, time restricted GDNF expression was beneficial for axonal growth. These findings are in agreement with studies showing the paramount importance of achieving control over neurotrophic factor delivery (Kemp et al., 2011; Pajenda et al., 2014; Marquardt et al., 2015; Santos et al., 2016; Tajdaran et al., 2016). Although the doxycycline-inducible system is a robust platform for therapeutic gene regulation *in vivo*, in rodents and non-human primates long-term therapeutic gene regulation is hampered due to an immune response directed against the foreign rtTA transactivator, resulting in an immune-mediated removal of transduced cells (Favre et al., 2002; Ginhoux et al., 2004; Le Guiner et al., 2014). This compromises the experimental *in vivo* use and clinical translation.

To obtain sustained control over GDNF expression, an immune-evasive doxycycline-inducible GDNF gene switch (dox-i-GDNF) has been previously developed (Hoyng et al., 2014; Eggers et al., 2019b). Using this dox-i-GDNF system, we investigated whether time-restricted GDNF expression improves motoneuron survival and attenuates coil formation following a ventral root avulsion lesion. Injection into the reimplanted lumbar ventral root close to the motoneuron pool and a 4 week timed GDNF expression was sufficient to enhance motoneuron survival up to 45 weeks (**Figures 1C–E**). This achievement is clinically relevant because increased motoneuron survival significantly augments the chance of axonal outgrowth and extends the time window for long-distance regeneration. In contrast to persistent GDNF expression, time-restricted GDNF expression attenuated coil formation and leads to a two-fold increase in axonal outgrowth over a distance of 10 cm. This increased outgrowth facilitated an earlier and enhanced muscle reinnervation as shown by the improved electromyographical recovery in the distal denervated musculature (**Figure 1C**; Eggers et al., 2019b). Despite these promising results, the degree of recovery remained insufficient to enable voluntary hind paw function. The regenerating axons present in the distal sciatic nerve originate from only 8 to 10% of the surviving motoneurons, whereas the remaining surviving motoneurons were unable to project an axon toward and beyond a 10 cm distance from the spinal cord. Although it remains difficult to determine the threshold that needs to be overcome to obtain functional recovery, it has been suggested that more than 25% of the motoneurons need to regenerate an axon and successfully innervate a target muscle (Rafuse et al., 1992; Gordon and Tyreman, 2010). A possible mechanism limiting long distance regeneration is the development of a chronically denervated distal nerve after a critical period of 6 to 8 weeks post-lesion. During the protracted long distance regeneration period, denervated Schwann cells gradually fail to support axon regeneration and a non-permissive environment develops.

To investigate the influence of prolonged regeneration time, an identical dox-i-GDNF treatment was performed following avulsion and re-implantation of cervical ventral roots. By performing a root avulsion in the brachial plexus instead of the lumbar plexus, the regeneration distance toward the distal muscles was reduced by half and thus the deleterious effects of chronic denervation were diminished (**Figure 1D**). We replicated previous observations that timed dox-i-GDNF treatment leads to sustained motoneuron survival and a twofold increase in motor axon regeneration. In addition, timed GDNF treatment leads to enhanced reinnervation of the forelimb paw musculature and recovery of voluntary grip function (Eggers et al., 2019a). The first

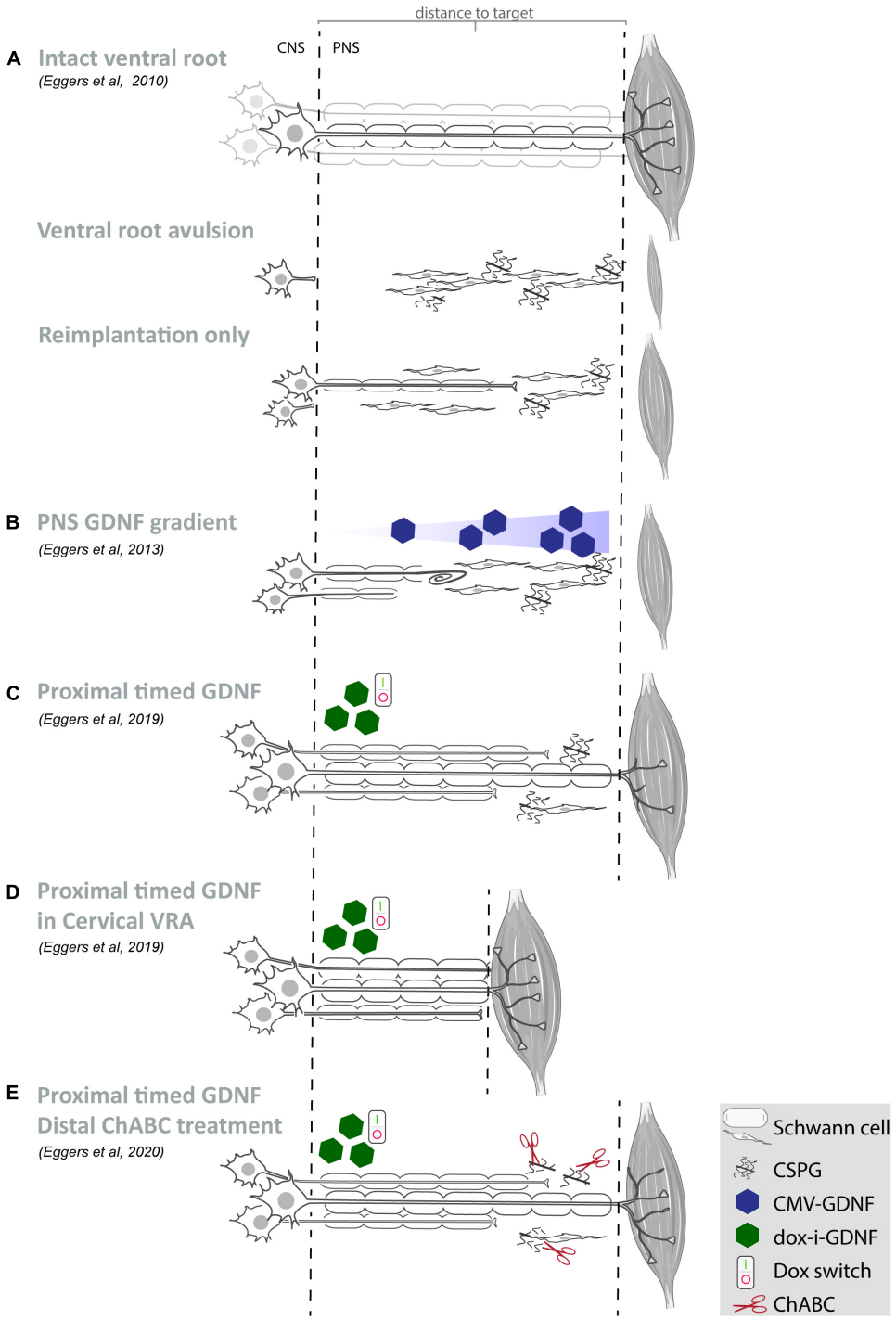

FIGURE 1 | Summary of our recent GDNF treatment strategies. **(A–E)** Schematic overview of motoneurons located in the spinal ventral horn and axonal projections toward the distal target muscle. For each study, the experimental strategy and primary experimental outcomes are shown. Depicted are schematic representations of the degree of motoneuron loss, axonal outgrowth, muscle atrophy and target reinnervation based upon histological or electrophysiological observations. **(A)** Ventral root avulsion or reimplantation only leads to severe motoneuron loss and poor axonal regeneration. **(B)** An increasing GDNF gradient in the peripheral nerve resulted in coil formation already at relatively low GDNF concentrations and the degree of coil formation strongly correlates to the level of expression. Proximal timed GDNF treatment inside the reimplanted ventral root using a regulatable gene switch in a lumbar ventral root avulsion **(C)** or cervical ventral root avulsion **(D)** results in enhanced motoneuron survival and axonal outgrowth. The degree of muscle reinnervation and functional recovery is enhanced following short-distance **(D)** axonal regeneration. **(E)** As a first step toward improving distal axonal regeneration we combined proximal timed GDNF treatment and peripheral ChABC mediated CSPG digestion to overcome the inhibitory chronically denervated peripheral nerve environment. (VRA, ventral root avulsion; CNS, central nervous system; PNS, peripheral nervous system; CSPG, chondroitin sulfate proteoglycan; ChABC, chondroitinase ABC; GDNF, glial cell line-derived neurotrophic factor).

signs of improved muscle reinnervation were observed before the critical state of chronic denervation has fully developed, demonstrating that beneficial effects of timed GDNF-gene therapy are more robust if target muscle reinnervation can occur within a relatively short time window post-lesion. This further suggests it is erroneous to assume that interventions that were shown to be successful in short distance regeneration models will also be effective in long distance regeneration or in human patients. These observations support the value and the necessity of chronic denervation and long-distance regeneration models in studies on nerve regeneration.

As a first step toward improving distal axonal outgrowth, combined proximal timed dox-i-GDNF gene therapy with a chondroitinase-ABC (ChABC) expression treatment in the distal peripheral nerve (**Figure 1E**) was performed. Inhibitory chondroitin sulfate proteoglycans (CSPG) accumulate throughout the extracellular matrix of the chronically denervated peripheral nerve and form a major obstacle for regenerating axons. Successful digestion of the inhibitory CSPG sidechains occurs in the distal stump using LV-ChABC (Eggers et al., 2020). Despite successful CSPG digestion and a modest electrophysiological improvement after 45 weeks, distal regeneration was not significantly improved after ChABC treatment and GDNF and ChABC do not display synergistic effects. These results showed that the proximal application of dox-i-GDNF treatment leads to an earlier enhanced electrophysiological response, whereas the distal ChABC treatment effect is modest and occurs during the later stages of the regeneration process.

In summary, the beneficial effect of GDNF gene therapy on motoneuron survival, attenuating motoneuron death up to 1 year is robust and reproducible. Despite increased distal axonal outgrowth, remaining factors that obstruct regeneration and functional recovery still need to be addressed. Here, the chronically denervated Schwann cells and axonal misrouting are considered the primary obstructing factors (Brushart, 1991; Fu and Gordon, 1995; Hoke et al., 2002; Sulaiman and Gordon, 2002; English, 2005; de Ruiter et al., 2008; Sulaiman and Gordon, 2009; O'Daly et al., 2016; Ronchi et al., 2017). A combined treatment strategy aimed at improving motoneuron survival and limiting the deleterious effect of chronic denervation could provide essential support to achieve functional recovery. In the next two sections we discuss the influence of GDNF treatment timing, duration, concentration and location and provide a perspective on future steps to accomplish improved recovery of function.

INFLUENCE OF INTERVENTION TIMING, DURATION, CONCENTRATION AND LOCATION

Based on the results obtained with different gene therapy strategies (**Figure 1**), we propose that there is a relationship between the experimental outcome: (i) GDNF treatment duration and timing, (ii) GDNF concentration, and (iii) location of GDNF delivery. To aid in this discussion, a graphical representation of the proposed relation between GDNF treatment duration, concentration and experimental outcome is depicted in **Figure 2**.

GDNF Treatment Timing and Duration

In patients, the lesion severity and possibility of spontaneous recovery needs to be assessed first, which is a challenging task, requires time and delays the decision for surgical repair. Although in experimental studies, delayed surgical repair or GDNF treatment still leads to some motoneuron survival and axonal regeneration, delayed treatment greatly diminishes the degree of motoneuron survival (Wu et al., 2004; Zhou and Wu, 2006). The effect of delayed treatment strongly supports strategies that aim at early neurosurgical repair and GDNF treatment in order for patients to benefit from a maximal degree of axonal outgrowth (Pondaag et al., 2018). Until surgical repair can be performed, bridging the post-lesion period with a systemic pharmacological treatment that delays the acute motoneuron death could result in a more favorable final functional outcome (Nogradi and Vrbova, 2001; Zhang et al., 2005; Hoang et al., 2008; Romeo-Guitart et al., 2017).

In addition to *timing*, the *duration* of GDNF delivery affects the experimental outcome. Delivery of GDNF for a short period results in poor axonal regeneration, whereas prolonged GDNF treatment results in axonal trapping (Marquardt et al., 2015). Our studies extend previous observations where treatment using GDNF protein improved motoneuron survival up to 12 weeks (Li et al., 1995; Yuan et al., 2000; Wu et al., 2003; Bergerot et al., 2004; Zhou and Wu, 2006; Chu et al., 2009, 2012; Pajenda et al., 2014; Ruven et al., 2018). Due to the method used to apply GDNF protein in these studies, the exposure of motoneurons to biologically active GDNF was limited to 2 to 14 days. In these studies, a single topical GDNF protein application, however, is less beneficial for motoneuron survival compared to continued

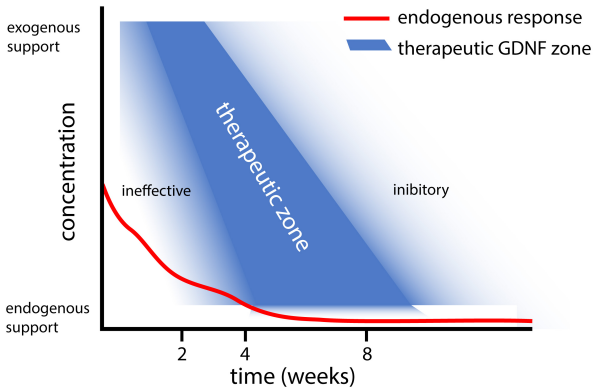

FIGURE 2 | Graphical representation of the proposed relation between GDNF treatment duration and concentration. This graph summarizes our observations that (i) Short and low levels of *endogenous* GDNF expression (red line) is ineffective in achieving motoneuron survival (Eggers et al., 2010), whereas prolonged low dose GDNF results in coil formation (Eggers et al., 2013). (ii) Moderate 4 week timed GDNF expression enhanced motoneuron survival and attenuates coil formation (Eggers et al., 2019a,b). (iii) This contrasts higher GDNF expression levels for 4 weeks, which leads to coil formation (Eggers et al., 2020).

local infusion therapy (Li et al., 1995; Wu et al., 2003; Chu et al., 2009), suggesting a relationship exists between the duration of GDNF treatment and the degree of motoneuron survival. Following 2 weeks of local GDNF protein infusion, the degree of motoneuron survival is identical to our 4 week viral vector-based treatment period (Wu et al., 2003; Eggers et al., 2019b). It is possible that our 4 week timed dox-i-GDNF treatment could be reduced to 2 weeks and still achieve robust motoneuron survival. Based upon our hypothesis of factors influencing the GDNF treatment outcome, however (**Figure 2**), reducing the treatment duration without adjusting the local GDNF treatment concentration could result in a gradual loss of motoneurons.

GDNF Treatment Concentration and Motoneuron Survival

Endogenous GDNF expression following ventral root avulsion is elevated for a period of 2 to 4 weeks (Eggers et al., 2010). This is a similar duration compared to above mentioned GDNF protein delivery studies, where frequently a strong reduction of exogenously applied GDNF is observed after 2 weeks (Pajenda et al., 2014). However, only the exogenous application leads to increased motoneuron survival, whereas reimplantation of a ventral root expressing endogenous GDNF prevents motoneuron death for a limited period of 2 weeks (Eggers et al., 2010). An important difference between endogenous and exogenous applied GDNF, is the high local GDNF concentrations that are obtained following local protein application or viral expression. This suggests supraphysiological local GDNF concentrations are essential to achieve successful and prolonged motoneuron survival (**Figure 2**).

GDNF Treatment Concentration and Axonal Coil Formation

Regulating the duration of GDNF expression, could potentially overcome axonal coil formation. Although coil formation was attenuated significantly in our first study, with only incidental small isolated coils observed (Eggers et al., 2019b), in a second study increased coil formation was observed in 34% of the dox-i-GDNF treated animals (Eggers et al., 2020). Between these studies, two differences exist which could underlie the observed coil development in the second study. In the study where only small incidental coils were observed, GDNF expression levels were increased 3-fold compared to controls and animals were followed up to 25 weeks post-reimplantation. In contrast, during the first 4 weeks GDNF expression levels were increased 5 fold in the second study where larger coil formation was observed and animals were followed up to 45 weeks post reimplantation.

Axonal outgrowth and coil formation is influenced by the local GDNF concentration (Eggers et al., 2013; Santos et al., 2016; Wang et al., 2018), showing that endogenous or moderate supraphysiological GDNF expression levels for an appropriate period do not result in large axon coils. If, in contrast to moderate GDNF expression, further increasing GDNF concentration during the first 4 weeks stimulates an earlier or advanced state of coil formation, it could be possible that these structures remain present throughout the experiment. Alternatively, it is known that the rtTA transactivator retains some degree of affinity for its DNA binding site, which in the absence of the dox inducer results in low levels of "leaky" expression (Urlinger et al., 2000; Loew et al., 2010; Roney et al., 2016). If local coil formation is the result of continuous GDNF secretion from a leaky vector, based upon **Figure 2**, there might be a higher chance for the development and observation of coils after a period of 45 weeks rather than after 25 weeks. Although both mechanisms individually or combined could underlie local coil formation, the creation of an immune-evasive rtTA transactivator by fusing with a GlyAla-repeat greatly reduced the leak expression (Hoyng et al., 2014). We were unable to detect leaky expression above endogenous GDNF concentrations using ELISA and immunohistochemical staining, suggesting that leak expression is a less likely cause for residual coil formation.

Our proposed relation between the GDNF concentration, treatment duration and experimental outcome as depicted in **Figure 2**, suggests that a delicate balance exists to achieve therapeutic GDNF levels for motoneuron survival and axonal outgrowth. Low levels of GDNF appear to not support prolonged motoneuron survival (Eggers et al., 2010), whereas sustained high or low levels of GDNF leads to axonal coil formation (Eggers et al., 2008, 2013). To determine the precise causal mechanism for coil development, more research needs to be performed focusing on GDNF treatment concentration and duration (Santos et al., 2016; Wang et al., 2018).

Gene Therapy Treatment Location

To support regenerating axons, GDNF treatment in the distal chronically denervated peripheral nerve following ventral root avulsion was unsuccessful in significantly advancing axonal growth and function recovery (Eggers et al., 2013). It is possible that the distal treatment location explains the limited beneficial effect. Distal GDNF expression did not lead to enhanced motoneuron survival, which contrasts proximal GDNF treatment (Eggers et al., 2008, 2019b). A spatially distinct effect of GDNF treatment *in vitro* at the cell body or axon has been shown previously (Zahavi et al., 2015), revealing axon growth and innervation occurred only when GDNF was applied to the axons. As discussed above, increased loss of motoneurons greatly limits the degree of distal axonal outgrowth.

Similarly, although ChABC treatment does not enhance motoneuron survival, our distal ChABC treatment might have been more beneficial when applied more proximally at the reimplantation site (**Figure 1E**; Eggers et al., 2020). This was shown recently in a study delivering a peptide inhibiting CSPG signaling near the reimplanted nerve root (Li et al., 2015). Increased axonal outgrowth following ChABC treatment is only observed following a transection lesion and not following a crush lesion (Zuo et al., 2002; Muir, 2010; Graham and Muir, 2016). Inhibitory CSPGs are present in the endoneurium surrounding the basal lamina tubes, while the tube itself is relatively permissive. At a transection site, axons will exit the basal lamina tube and are exposed to CSPGs, whereas following a nerve crush axons remain within the pro-regenerative tube. Thus, it is possible that in our avulsion model, most axons enter a basal lamina tube at the implantation site and will not be in close

proximity to the distal inhibitory environment, explaining why distal CSPG digestion only has a limited additional effect.

PERSPECTIVE ON FUTURE STEPS TO ACCOMPLISH RECOVERY OF FUNCTION

In future studies, keeping the distal nerve in a pro-regenerative state should be the next priority. The key factors responsible for obstructed axonal regeneration in the peripheral nerve are the loss of neurotrophic support (Funakoshi et al., 1993; Hoke et al., 2002; Eggers et al., 2010), fragmentation of the Schwann cell basal lamina (Brushart et al., 2013) and increased deposits of inhibitory matrix molecules such as CSPGs in the nerve fascicle (Zuo et al., 1998, 2002; Muir, 2010; Graham and Muir, 2016). The unifying component between these growth-promoting and inhibitory factors is the loss of repair Schwann cells. Keeping these cells in a repair phenotype state could therefore be an effective strategy to promote axonal outgrowth (Jessen and Arthur-Farraj, 2019). This requires the ability to specifically target all denervated Schwann cells and to introduce one or multiple factors that are able to achieve this.

Overexpression of a transcription factor could result in a wide range of downstream pro-regenerative molecular changes. As an important regulator in the Schwann cell injury response, the transcription factor c-Jun is such a promising candidate for targeted therapeutic intervention (Parkinson et al., 2008; Arthur-Farraj et al., 2012; Jessen and Mirsky, 2016; Huang et al., 2019). C-Jun has a central role in to promoting expression of the repair program and absence of c-Jun results in the failure of axon growth, functional recovery and neural death (Arthur-Farraj et al., 2012). Recent findings show that moderate c-Jun overexpression levels are beneficial, but supraphysiological levels of c-Jun perturbs myelination (Fazal et al., 2017). Similar to our GDNF treatments, we therefore expect that c-Jun application for therapeutic purposes requires a tightly controlled treatment approach (Huang et al., 2019). We have shown the advantages and potency of viral vector mediated gene therapy and the ability to regulate gene expression. With the development of our immune-evasive stealth gene switch, the gene therapy system was further improved, rendering it even safer. For future research in which factors such as GDNF or C-Jun are applied, it remains to be determined whether the potential low levels of leak expression are detrimental for the treatment strategy or whether the required level of control is sufficient.

To prevent unwanted side effects, gene therapy provides us with the ability to target specific areas or cells with a high degree of precision. LV vectors outperform AAV vectors in transducing Schwann cells in the rat peripheral nerve (Hoyng et al., 2015). However, LV vectors integrate their genetic material in the host cell genome and this could potentially interfere with the function of cellular genes. Adeno-associated viral vectors are increasingly regarded as safe and are well-tolerated following application to the human brain. AAV2 and 8 transduce primate and rat Schwann cells (Girard et al., 2005; Homs et al., 2011). As a first step toward optimizing AAV-mediated gene transfer to Schwann cells we performed a screen of all 9 common serotypes and showed that AAV2 vectors outperform other serotypes in transducing Schwann cells in human peripheral nerve explants, whereas several AAV serotypes efficiently transduced rat Schwann cells (Hoyng et al., 2015). In future studies we will build on these findings and investigate the use of AAV vectors in peripheral nerve repair paradigms.

To keep the peripheral nerve in a pro-regenerative state, ideally, all denervated Schwann cells between the motoneuron and denervated muscle are precisely and equally targeted. This poses a technical challenge, as surgically injecting the entire nerve length including all its thin terminal branches is highly invasive, leads to unwanted additional nerve damage, whereas small diameter nerves are impossible to inject. The recent generation of vector capsids that following intravenous administration can selectively pass the blood brain barrier and transduce neurons located in the brain, spinal cord and DRG is a promising new development (Chan et al., 2017). It is conceivable that comparable viral vectors will be developed that are able to selectively transduce all Schwann cells along an injured peripheral nerve using non-invasive intravenous delivery. When combined with a promotor specific for denervated Schwann cells, this would create the ultimate viral vector, which allows for non-invasive, cell specific, precise control of therapeutic gene expression along the entire denervated peripheral nerve.

CONCLUSION

Gene therapy is a powerful tool to improve motoneuron survival and axonal regeneration, and advancements are being made to bring this treatment strategy closer to clinical application. To achieve long distance axonal regeneration, control over treatment location, timing and dose is, however, required. Combined, our data provide a basis to better understand this delicate balance. Although all treatment strategies will need to be tailored to individual patients, ultimately, this and future research could lead to a guiding template which aids the nerve surgeon in selecting the additional gene therapy treatment strategy.

AUTHOR CONTRIBUTIONS

RE, FW, MT, MM, and JV wrote this manuscript, conceived, designed, performed, and analyzed the studies on which **Figures 1**, **2** are based. All authors contributed to the article and approved the submitted version.

FUNDING

This work was supported by grants from the Wings for Life Spinal Cord Research Foundation (WFL-NL-17-16 and WFL-NL-25/20 to JV) and the International Spinal Research Trust (TRI004_3 to JV).

REFERENCES

Arthur-Farraj, P. J., Latouche, M., Wilton, D. K., Quintes, S., Chabrol, E., Banerjee, A., et al. (2012). c-Jun reprograms Schwann cells of injured nerves to generate a repair cell essential for regeneration. *Neuron* 75, 633-647.

Barbizan, R., Castro, M. V., Rodrigues, A. C., Barraviera, B., Ferreira, R. S., and Oliveira, A. L. (2013). Motor recovery and synaptic preservation after ventral root avulsion and repair with a fibrin sealant derived from snake venom. *PLoS One* 8:e63260. doi: 10.1371/journal.pone.0063260

Bergerot, A., Shortland, P. J., Anand, P., Hunt, S. P., and Carlstedt, T. (2004). Co-treatment with riluzole and GDNF is necessary for functional recovery after ventral root avulsion injury. *Exp. Neurol* 187, 359-366.

Blits, B., Carlstedt, T. P., Ruitenberg, M. J., de Winter, F., Hermens, W. T., Dijkhuizen, P. A., et al. (2004). Rescue and sprouting of motoneurons following ventral root avulsion and reimplantation combined with intraspinal adeno-associated viral vector-mediated expression of glial cell line-derived neurotrophic factor or brain-derived neurotrophic factor. *Exp. Neurol.* 189, 303-316.

Brushart, T. M. (1991). Central course of digital axons within the median nerve of *Macaca mulatta*. *J. Comp. Neurol.* 311, 197-209. doi: 10.1002/cne.903110203

Brushart, T. M., Aspalter, M., Griffin, J. W., Redett, R., Hameed, H., Zhou, C., et al. (2013). Schwann cell phenotype is regulated by axon modality and central-peripheral location, and persists in vitro. *Exp. Neurol.* 247, 272-281.

Carlstedt, T. (2010). Perspectives on the treatment of the longitudinal spinal cord injury. *Front. Neurol.* 1:11. doi: 10.3389/fneur.2010.00011

Carlstedt, T., Anand, P., Hallin, R., Misra, P. V., Noren, G. and Seferlis, T. (2000). Spinal nerve root repair and reimplantation of avulsed ventral roots into the spinal cord after brachial plexus injury. *J. Neurosurg.* 93, 237-247.

Carlstedt, T., Grane, P., Hallin, R.G. and Noren, G. (1995). Return of function after spinal cord implantation of avulsed spinal nerve roots. *Lancet* 346, 1323-1325.

Carlstedt, T., Linda, H., Cullheim, S. and Risling, M. (1986). Reinnervation of hind limb muscles after ventral root avulsion and implantation in the lumbar spinal cord of the adult rat. *Acta Physiol. Scand.* 128, 645-646.

Carlstedt, T. and Havton, L. (2012). The longitudinal spinal cord injury: lessons from intraspinal plexus, cauda equina and medullary conus lesions. *Handb. Clin. Neurol.* 109, 337-354.

Chai, H., Wu, W., So, K. F. and Yip, H. K. (2000). Survival and regeneration of motoneurons in adult rats by reimplantation of ventral root following spinal root avulsion. *Neuroreport* 11, 1249-1252.

Chan, K. Y., Jang, M. J., Yoo, B. B., Greenbaum, A., Ravi, N., Wu, W. L., et al. (2017). Engineered AAVs for efficient noninvasive gene delivery to the central and peripheral nervous systems. *Nat. Neurosci.* 20, 1172-1179.

Chu, T. H., Li, S. Y., Guo, A., Wong, W. M., Yuan, Q. and Wu, W. (2009). Implantation of neurotrophic factor-treated sensory nerve graft enhances survival and axonal regeneration of motoneurons after spinal root avulsion. *J.Neuropathol.Exp.Neurol.* 68, 94-101.

Chu, T. H., Wang, L., Guo, A., Chan, V. W., Wong, C. W. and Wu, W. (2012). GDNF-treated acellular nerve graft promotes motoneuron axon regeneration after implantation into cervical root avulsed spinal cord. *Neuropathol. Appl. Neurobiol.* 38, 681-695.

Chu, T. H. and Wu, W. (2009). Neurotrophic factor treatment after spinal root avulsion injury. *Cent. Nerv. Syst. Agents Med. Chem.* 9, 40-55.

Cullheim, S., Carlstedt, T., Linda, H., Risling, M. and Ulfhake, B. (1989). Motoneurons reinnervate skeletal muscle after ventral root implantation into the spinal cord of the cat. *Neuroscience* 29, 725-733.

de Ruiter, G. C., Malessy, M. J., Alaid, A. O., Spinner, R. J., Engelstad, J. K., Sorenson, E. J., et al. (2008). Misdirection of regenerating motor axons after nerve injury and repair in the rat sciatic nerve model. *Exp. Neurol.* 211, 339-350.

Ee, X., Yan, Y., Hunter, D. A., Schellhardt, L., Sakiyama-Elbert, S. E., Mackinnon, S. E., et al. (2017). Transgenic SCs expressing GDNF-IRES-DsRed impair nerve regeneration within acellular nerve allografts. *Biotechnol. Bioeng.* 114, 2121-2130.

Eggers, R., de Winter, F., Arkenaar, C., Tannemaat, M. R., and Verhaagen, J. (2019a). Enhanced regeneration and reinnervation following timed GDNF gene therapy in a cervical ventral root avulsion. *Exp. Neurol.* 321:113037. doi: 10.1016/j.expneurol.2019.113037

Eggers, R., de Winter, F., Hoyng, S. A., Hoeben, R. C., Malessy, M. J. A., Tannemaat, M. R., et al. (2019b). Timed GDNF gene therapy using an immune-evasive gene switch promotes long distance axon regeneration. *Brain* 142, 295-311.

Eggers, R., de Winter, F., Hoyng, S. A., Roet, K. C., Ehlert, E. M., Malessy, M. J., et al. (2013). Lentiviral vector-mediated gradients of GDNF in the injured peripheral nerve: effects on nerve coil formation, Schwann cell maturation and myelination. *PLoS One* 8:e71076. doi: 10.1371/journal.pone.0071076

Eggers, R., de Winter, F., Smit, L., Luimens, M., Muir, E. M., Bradbury, E. J., et al. (2020). Combining timed GDNF and ChABC gene therapy to promote long-distance regeneration following ventral root avulsion and repair. *FASEB J.* 34, 10605–10622. doi: 10.1096/fj.202000559R

Eggers, R., Hendriks, W. T., Tannemaat, M. R., van Heerikhuize, J. J., Pool, C. W., Carlstedt, T. P., et al. (2008). Neuroregenerative effects of lentiviral vector-mediated GDNF expression in reimplanted ventral roots. *Mol.Cell Neurosci.* 39, 105-117.

Eggers, R., Tannemaat, M. R., De Winter, F., Malessy, M. J., and Verhaagen, J. (2016). Clinical and neurobiological advances in promoting regeneration of the ventral root avulsion lesion. *Eur. J. Neurosci.* 43, 318-335.

Eggers, R., Tannemaat, M. R., Ehlert, E. M., and Verhaagen, J. (2010). A spatio-temporal analysis of motoneuron survival, axonal regeneration and neurotrophic factor expression after lumbar ventral root avulsion and implantation. *Exp. Neurol.* 223, 207-220.

English, A. W. (2005). Enhancing axon regeneration in peripheral nerves also increases functionally inappropriate reinnervation of targets. *J. Comp. Neurol.* 490, 427-441. doi: 10.1002/cne.20678

Favre, D., Blouin, V., Provost, N., Spisek, R., Porrot, F., Bohl, D., et al. (2002). Lack of an immune response against the tetracycline-dependent transactivator correlates with long-term doxycycline-regulated transgene expression in nonhuman primates after intramuscular injection of recombinant adeno-associated virus. *J. Virol.* 76, 11605-11611.

Fazal, S. V., Gomez-Sanchez, J. A., Wagstaff, L. J., Musner, N., Otto, G., Janz, M., et al. (2017). Graded elevation of c-jun in schwann cells in vivo: gene dosage determines effects on development, remyelination, tumorigenesis, and hypomyelination. *J. Neurosci.* 37, 12297-12313.

Fu, S. Y., and Gordon, T. (1995). Contributing factors to poor functional recovery after delayed nerve repair: prolonged denervation. *J. Neurosci.* 15, 3886-3895. doi: 10.1523/JNEUROSCI.15-05-03886.1995

Funakoshi, H., Frisen, J., Barbany, G., Timmusk, T., Zachrisson, O., Verge, V. M., et al. (1993). Differential expression of mRNAs for neurotrophins and their receptors after axotomy of the sciatic nerve. *J.Cell Biol.* 123, 455-465.

Ginhoux, F., Turbant, S., Gross, D. A., Poupiot, J., Marais, T., Lone, Y., et al. (2004). HLA-A*0201-restricted cytolytic responses to the rtTA transactivator dominant and cryptic epitopes compromise transgene expression induced by the tetracycline on system. *Mol. Ther.* 10, 279-289.

Girard, C., Tenenbaum, L., Chtarto, A., Attali, B., Salvetti, A., Bachelin, C., et al. (2005). Efficiency of adeno-associated virus type-2 vectors in non-human primate Schwann cells. *Neuroreport* 16, 1757-1762.

Gordon, T., Tyreman, N., and Raji, M. A. (2011). The basis for diminished functional recovery after delayed peripheral nerve repair. *J. Neurosci.*, 31, 5325-5334.

Gordon, T., and Tyreman, N. (2010). Sprouting capacity of lumbar motoneurons in normal and hemisected spinal cords of the rat. *J. Physiol.* 588, 2745-2768. doi: 10.1113/jphysiol.2010.190389

Graham, J. B., and Muir, D. (2016). Chondroitinase C selectively degrades chondroitin sulfate glycosaminoglycans that inhibit axonal growth within the endoneurium of peripheral nerve. *PLoS One* 11:e0167682. doi: 10.1371/journal.pone.0167682 doi: 10.1371/journal.pone.0167682

Gu, Y., Spasic, Z., and Wu, W. (1997). The effects of remaining axons on motoneuron survival and NOS expression following axotomy in the adult rat. *Dev.Neurosci.* 19, 255-259.

Hallin, R.G., Carlstedt, T., Nilsson-Remahl, I., and Risling, M. (1999). Spinal cord implantation of avulsed ventral roots in primates; correlation between restored motor function and morphology. *Exp.Brain Res.* 124, 304-310.

Hammarberg, H., Piehl, F., Risling, M., and Cullheim, S. (2000). Differential regulation of trophic factor receptor mRNAs in spinal motoneurons after sciatic nerve transection and ventral root avulsion in the rat. *J.Comp Neurol.* 426, 587-601.

Haninec, P., Dubovy, P., Samal, F., Houstava, L., and Stejskal, L. (2004). Reinnervation of the rat musculocutaneous nerve stump after its direct reconnection with the C5 spinal cord segment by the nerve graft following avulsion of the ventral spinal roots: a comparison of intrathecal administration of brain-derived neurotrophic factor and Cerebrolysin. *Exp. Brain Res.* 159, 425–432. doi: 10.1007/s00221-004-1969-z

Harvey, A. R., Lovett, S. J., Majda, B. T., Yoon, J. H., Wheeler, L. P., and Hodgetts, S. I. (2015). Neurotrophic factors for spinal cord repair: which, where, how and when to apply, and for what period of time? *Brain Res.* 1619, 36-71.

Henderson, C. E., Phillips, H. S., Pollock, R. A., Davies, A. M., Lemeulle, C., Armanini, M., et al. (1994). GDNF: a potent survival factor for motoneurons present in peripheral nerve and muscle. *Science* 266, 1062-1064.

Hoang, T. X., Akhavan, M., Wu, J. and Havton, L. A. (2008). Minocycline protects motor but not autonomic neurons after cauda equina injury. *Exp. Brain Res.* 189, 71-77.

Hoang, T. X. and Havton, L. A. (2006). A single re-implanted ventral root exerts neurotropic effects over multiple spinal cord segments in the adult rat. *Exp. Brain Res.* 169, 208-217. doi: 10.1007/s00221-005-0137-4

Hoben, G. M., Ee, X., Schellhardt, L., Yan, Y., Hunter, D. A., Moore, A. M., et al. (2018). Increasing nerve autograft length increases senescence and reduces regeneration. *Plast. Reconstr. Surg.* 142, 952-961.

Hoffmann, C. F., Marani, E., van Dijk, J. G., vd Kamp, W. and Thomeer, R. T. (1996). Reinnervation of avulsed and reimplanted ventral rootlets in the cervical spinal cord of the cat. *J. Neurosurg.* 84, 234-243.

Hoke, A., Gordon, T., Zochodne, D. W. and Sulaiman, O. A. (2002). A decline in glial cell-line-derived neurotrophic factor expression is associated with impaired regeneration after long-term Schwann cell denervation. *Exp. Neurol.* 173, 77-85.

Homs, J., Ariza, L., Pages, G., Udina, E., Navarro, X., Chillon, M., et al. (2011). Schwann cell targeting via intrasciatic injection of AAV8 as gene therapy strategy for peripheral nerve regeneration. *Gene Ther.* 18, 622-630.

Hoyng, S. A., De Winter, F., Gnavi, S., van Egmond, L., Attwell, C. L., Tannemaat, M. R., et al. (2015). Gene delivery to rat and human Schwann cells and nerve segments: a comparison of AAV 1-9 and lentiviral vectors. *Gene Ther.* 22, 767-780.

Hoyng, S. A., Gnavi, S., de Winter, F., Eggers, R., Ozawa, T., Zaldumbide, A., et al. (2014). Developing a potentially immunologically inert tetracycline-regulatable viral vector for gene therapy in the peripheral nerve. *Gene Ther.* 21, 549-557.

Htut, M., Misra, V. P., Anand, P., Birch, R., and Carlstedt, T. (2007). Motor recovery and the breathing arm after brachial plexus surgical repairs, including re-implantation of avulsed spinal roots into the spinal cord. *J. Hand Surg. Eur.* 32, 170-178.

Huang, L., Xia, B., Shi, X., Gao, J., Yang, Y., Xu, F., et al. (2019). Time-restricted release of multiple neurotrophic factors promotes axonal regeneration and functional recovery after peripheral nerve injury. *FASEB J.* 33, 8600-8613.

Iwase, T., Jung, C. G., Bae, H., Zhang, M., and Soliven, B. (2005). Glial cell line-derived neurotrophic factor-induced signaling in Schwann cells. *J. Neurochem.* 94, 1488-1499.

Jessen, K. R., and Arthur-Farraj, P. (2019). Repair Schwann cell update: adaptive reprogramming, EMT, and stemness in regenerating nerves. *Glia* 67, 421-437. doi: 10.1002/glia.23532

Jessen, K. R. and Mirsky, R. (2016). The repair Schwann cell and its function in regenerating nerves. *J. Physiol.* 594, 3521-3531. doi: 10.1113/JP270874

Jonsson, S., Wiberg, R., McGrath, A. M., Novikov, L. N., Wiberg, M., Novikova, L. N., et al. (2013). Effect of delayed peripheral nerve repair on nerve regeneration, Schwann cell function and target muscle recovery. *PLoS One* 8:e56484. doi: 10.1371/journal.pone.0056484.g002

Kemp, S. W., Webb, A. A., Dhaliwal, S., Syed, S., Walsh, S. K., and Midha, R. (2011). Dose and duration of nerve growth factor (NGF) administration determine the extent of behavioral recovery following peripheral nerve injury in the rat. *Exp. Neurol.* 229, 460-470.

Koliatsos, V. E., Price, W. L., Pardo, C. A., and Price, D. L. (1994). Ventral root avulsion: an experimental model of death of adult motor neurons. *J.Comp. Neurol.* 342, 35-44.

Lang, E. M., Schlegel, N., Sendtner, M., and Asan, E. (2005). Effects of root replantation and neurotrophic factor treatment on long-term motoneuron survival and axonal regeneration after C7 spinal root avulsion. *Exp. Neurol.* 194, 341-354.

Le Guiner, C., Stieger, K., Toromanoff, A., Guilbaud, M., Mendes-Madeira, A., Devaux, M., et al. (2014). Transgene regulation using the tetracycline-inducible TetR-KRAB system after AAV-mediated gene transfer in rodents and nonhuman primates. *PLoS One* 9:e102538. doi: 10.1371/journal.pone.0102538

Li, H., Wong, C., Li, W., Ruven, C., He, L., Wu, X., et al. (2015). Enhanced regeneration and functional recovery after spinal root avulsion by manipulation of the proteoglycan receptor PTPsigma. *Sci. Rep.* 5:14923.

Li, L., Wu, W., Lin, L. F., Lei, M., Oppenheim, R. W. and Houenou, L. J. (1995). Rescue of adult mouse motoneurons from injury-induced cell death by glial cell line-derived neurotrophic factor. *Proc. Natl. Acad. Sci. U.S.A.* 92, 9771-9775.

Loew, R., Heinz, N., Hampf, M., Bujard, H., and Gossen, M. (2010). Improved Tet-responsive promoters with minimized background expression. *BMC Biotechnol.*, 10:81. doi: 10.1186/1472-6750-10-81

Love, S., Plaha, P., Patel, N. K., Hotton, G. R., Brooks, D. J., and Gill, S. S. (2005). Glial cell line-derived neurotrophic factor induces neuronal sprouting in human brain. *Nat. Med.* 11, 703-704.

Marquardt, L. M., Ee, X., Iyer, N., Hunter, D., Mackinnon, S. E., Wood, M. D. et al. (2015). Finely tuned temporal and spatial delivery of GDNF promotes enhanced nerve regeneration in a long nerve defect model. *Tissue Eng. Part A* 21, 2852-2864.

Muir, D. (2010). The potentiation of peripheral nerve sheaths in regeneration and repair. *Exp. Neurol.* 223, 102-111. doi: 10.1016/j.expneurol.2009.05.038

Narakas, A.O. (1985). The treatment of brachial plexus injuries. *Int. Orthop.* 9, 29-36. doi: 10.1007/BF00267034

Nieto, J. H., Chang, H. H., Ohlsson, M., Lee, U., Villablanca, J. P., Christe, K.L., et al. (2019). Surgical Replantation of Avulsed Lumbosacral Ventral Roots and Urodynamic Studies in a Rhesus Macaque (*Macaca mulatta*) Model of Cauda Equina/Conus Medullaris Injury and Repair *Animal Models of Neurotrauma*. Berlin: Springer, 207-220.

Nogradi, A. and Vrbova, G. (2001). The effect of riluzole treatment in rats on the survival of injured adult and grafted embryonic motoneurons. *Eur. J. Neurosci.* 13, 113-118. doi: 10.1046/j.0953-816X.2000.01362.x

O'Daly, A., Rohde, C., and Brushart, T. (2016). The topographic specificity of muscle reinnervation predicts function. *Eur. J. Neurosci.* 43, 443-450.

Ohlsson, M., Hoang, T. X., Wu, J. and Havton, L. A. (2006). Glial reactions in a rodent cauda equina injury and repair model. *Exp. Brain Res.* 170, 52-60.

Ohlsson, M., Nieto, J. H., Christe, K. L., and Havton, L. A. (2013). Long-term effects of a lumbosacral ventral root avulsion injury on axotomized motor neurons and avulsed ventral roots in a non-human primate model of cauda equina injury. *Neuroscience* 250, 129-139. doi: 10.1016/j.neuroscience.2013.06.054

Pajenda, G., Hercher, D., Marton, G., Pajer, K., Feichtinger, G. A., Maleth, J., et al. (2014). Spatiotemporally limited BDNF and GDNF overexpression rescues motoneurons destined to die and induces elongative axon growth. *Exp. Neurol.* 261, 367-376. doi: 10.1016/j.expneurol.2014.05.019

Parkinson, D. B., Bhaskaran, A., Arthur-Farraj, P., Noon, L.A., Woodhoo, A., Lloyd, A.C., et al. (2008). c-Jun is a negative regulator of myelination. *J. Cell Biol.* 181, 625-637.

Penas, C., Pascual-Font, A., Mancuso, R., Fores, J., Casas, C., and Navarro, X. (2011). Sigma receptor agonist 2-(4-morpholinethyl)1 phenylcyclohexanecarboxylate (Pre084) increases GDNF and BiP expression and promotes neuroprotection after root avulsion injury. *J. Neurotrauma* 28, 831–840. doi: 10.1089/neu.2010.1674

Pondaag, W., van Driest, F. Y., Groen, J. L. and Malessy, M. J. A. (2018). Early nerve repair in traumatic brachial plexus injuries in adults: treatment algorithm and first experiences. *J. Neurosurg.* 130, 172-178.

Rafuse, V. F., Gordon, T., and Orozco, R. (1992). Proportional enlargement of motor units after partial denervation of cat triceps surae muscles. *J. Neurophysiol.* 68, 1261-1276. doi: 10.1152/jn.1992.68.4.1261

Reichert, P., Kielbowicz, Z., DziEgiel, P., Pula, B., Kuryszko, J., Gosk, J., et al. (2015). The rabbit brachial plexus as a model for nerve repair surgery–histomorphometric analysis. *Anat. Rec.* 298, 444-454.

Robotti, E., Longhi, P., Verna, G., and Bocchiotti, G. (1995). Brachial plexus surgery, An historical perspective. *Hand Clin.* 11, 517-533.

Romeo-Guitart, D., Fores, J., Navarro, X., and Casas, C. (2017). Boosted regeneration and reduced denervated muscle atrophy by neuroheal in a

pre-clinical model of lumbar root avulsion with delayed reimplantation. *Sci. Rep.* 7:12028.

Ronchi, G., Cillino, M., Gambarotta, G., Fornasari, B. E., Raimondo, S., Pugliese, P., et al. (2017). Irreversible changes occurring in long-term denervated Schwann cells affect delayed nerve repair. *J. Neurosurg.* 127, 843-856.

Roney, I. J., Rudner, A. D., Couture, J. F., and Kaern, M. (2016). Improvement of the reverse tetracycline transactivator by single amino acid substitutions that reduce leaky target gene expression to undetectable levels. *Sci. Rep.* 6:27697.

Ruven, C., Badea, S. R., Wong, W. M., and Wu, W. (2018). Combination Treatment With Exogenous GDNF and fetal spinal cord cells results in better motoneuron survival and functional recovery after avulsion injury with delayed root reimplantation. *J. Neuropathol. Exp. Neurol.* 77, 325-343.

Saheb-Al-Zamani, M., Yan, Y., Farber, S. J., Hunter, D. A., Newton, P., Wood, M. D., et al. (2013). Limited regeneration in long acellular nerve allografts is associated with increased Schwann cell senescence. *Exp. Neurol.* 247, 165-177.

Santos, D., Gonzalez-Perez, F., Navarro, X. and Del Valle, J. (2016). Dose-dependent differential effect of neurotrophic factors on in vitro and in vivo regeneration of motor and sensory neurons. *Neural Plast.* 2016:4969523.

Santosa, K. B., Jesuraj, N. J., Viader, A., MacEwan, M., Newton, P., Hunter, D. A., et al. (2013). Nerve allografts supplemented with schwann cells overexpressing glial-cell-line-derived neurotrophic factor. *Muscle Nerve* 47, 213-223.

Seddon, H. J. (1942). A Classification of Nerve Injuries. *Br. Med. J.* 2, 237-239. doi: 10.1136/bmj.2.4260.237

Shakhbazau, A., Mohanty, C., Shcharbin, D., Bryszewska, M., Caminade, A. M., Majoral, J. P., et al. (2013). Doxycycline-regulated GDNF expression promotes axonal regeneration and functional recovery in transected peripheral nerve. *J. Cont. Rel.* 172, 841-851.

Sulaiman, O. A., and Gordon, T. (2000). Effects of short- and long-term Schwann cell denervation on peripheral nerve regeneration, myelination, and size. *Glia* 32, 234-246. doi: 10.1002/1098-1136(200012)32:3<234::AID-GLIA40>3.0.CO;2-3

Sulaiman, O. A., and Gordon, T. (2002). Transforming growth factor-beta and forskolin attenuate the adverse effects of long-term Schwann cell denervation on peripheral nerve regeneration in vivo. *Glia* 37, 206-218. doi: 10.1002/glia.10022

Sulaiman, O. A., and Gordon, T. (2009). Role of chronic Schwann cell denervation in poor functional recovery after nerve injuries and experimental strategies to combat it. *Neurosurgery* 65, A105-A114. doi: 10.1227/01.NEU.0000358537.30354.63

Tajdaran, K., Gordon, T., Wood, M. D., Shoichet, M. S., and Borschel, G. H. (2016). A glial cell line-derived neurotrophic factor delivery system enhances nerve regeneration across acellular nerve allografts. *Acta Biomater.* 29, 62-70.

Tannemaat, M. R., Eggers, R., Hendriks, W. T., de Ruiter, G. C., van Heerikhuize, J. J., Pool, C. W., et al. (2008). Differential effects of lentiviral vector-mediated overexpression of nerve growth factor and glial cell line-derived neurotrophic factor on regenerating sensory and motor axons in the transected peripheral nerve. *Eur. J. Neurosci.* 28, 1467-1479.

Torres-Espin, A., Corona-Quintanilla, D. L., Fores, J., Allodi, I., Gonzalez, F., Udina, E., et al. (2013). Neuroprotection and axonal regeneration after lumbar ventral root avulsion by re-implantation and mesenchymal stem cells transplant combined therapy. *Neurotherapeutics* 10, 354-368.

Urlinger, S., Baron, U., Thellmann, M., Hasan, M.T., Bujard, H. and Hillen, W. (2000). Exploring the sequence space for tetracycline-dependent transcriptional activators: novel mutations yield expanded range and sensitivity. *Proc. Natl. Acad. Sci. U.S.A.* 97, 7963-7968.

Wang, Z. Z., Wood, M. D., Mackinnon, S. E., and Sakiyama-Elbert, S. E. (2018). A microfluidic platform to study the effects of GDNF on neuronal axon entrapment. *J. Neurosci. Methods* 308, 183-191.

Wu, W., Chai, H., Zhang, J., Gu, H., Xie, Y., and Zhou, L. (2004). Delayed implantation of a peripheral nerve graft reduces motoneuron survival but does not affect regeneration following spinal root avulsion in adult rats. *J. Neurotr.* 21, 1050-1058.

Wu, W., Han, K., Li, L. and Schinco, F. P. (1994). Implantation of PNS graft inhibits the induction of neuronal nitric oxide synthase and enhances the survival of spinal motoneurons following root avulsion. *Exp.Neurol.* 129, 335-339.

Wu, W., Li, L., Yick, L. W., Chai, H., Xie, Y., Yang, Y., Prevette, D. M. and Oppenheim, R. W. (2003). GDNF and BDNF alter the expression of neuronal NOS, c-Jun, and p75 and prevent motoneuron death following spinal root avulsion in adult rats. *J. Neurotr.* 20, 603-612.

Yuan, Q., Wu, W., So, K. F., Cheung, A. L., Prevette, D. M., and Oppenheim, R. W. (2000). Effects of neurotrophic factors on motoneuron survival following axonal injury in newborn rats. *Neuroreport* 11, 2237-2241.

Zahavi, E. E., Ionescu, A., Gluska, S., Gradus, T., Ben-Yaakov, K., and Perlson, E. (2015). A compartmentalized microfluidic neuromuscular co-culture system reveals spatial aspects of GDNF functions. *J. Cell Sci.* 128, 1241-1252.

Zhang, C. G., Welin, D., Novikov, L., Kellerth, J. O., Wiberg, M., and Hart, A. M. (2005). Motorneuron protection by N-acetyl-cysteine after ventral root avulsion and ventral rhizotomy. *Br. J. Plast. Surg.* 58, 765-773.

Zhou, L. H., and Wu, W. (2006). Survival of injured spinal motoneurons in adult rat upon treatment with glial cell line-derived neurotrophic factor at 2 weeks but not at 4 weeks after root avulsion. *J. Neurotrauma* 23, 920-927. doi: 10.1089/neu.2006.23.920

Zuo, J., Hernandez, Y. J., and Muir, D. (1998). Chondroitin sulfate proteoglycan with neurite-inhibiting activity is up-regulated following peripheral nerve injury. *J. Neurobiol.* 34, 41-54.

Zuo, J., Neubauer, D., Graham, J., Krekoski, C. A., Ferguson, T. A., and Muir, D. (2002). Regeneration of axons after nerve transection repair is enhanced by degradation of chondroitin sulfate proteoglycan. *Exp. Neurol.* 176, 221-228.

Conflict of Interest: The authors declare that the research was conducted in the absence of any commercial or financial relationships that could be construed as a potential conflict of interest.

frontiers in Bioengineering and Biotechnology

ORIGINAL RESEARCH
published: 20 November 2020
doi: 10.3389/fbioe.2020.580654

Tissue Engineered Bands of Büngner for Accelerated Motor and Sensory Axonal Outgrowth

Kate V. Panzer[1,2,3†], Justin C. Burrell[1,2,3†], Kaila V. T. Helm[1,2], Erin M. Purvis[1,2,4], Qunzhou Zhang[5,6], Anh D. Le[5,6], John C. O'Donnell[1,2] and D. Kacy Cullen[1,2,3]*

[1] Center for Brain Injury and Repair, Department of Neurosurgery, Perelman School of Medicine, University of Pennsylvania, Philadelphia, PA, United States, [2] Center for Neurotrauma, Neurodegeneration and Restoration, Corporal Michael J. Crescenz Veterans Affairs Medical Center, Philadelphia, PA, United States, [3] Department of Bioengineering, School of Engineering and Applied Science, University of Pennsylvania, Philadelphia, PA, United States, [4] Department of Neuroscience, Perelman School of Medicine, University of Pennsylvania, Philadelphia, PA, United States, [5] Department of Oral and Maxillofacial Surgery, School of Dental Medicine, University of Pennsylvania, Philadelphia, PA, United States, [6] Department of Oral and Maxillofacial Surgery, Penn Medicine Hospital of University of Pennsylvania, Philadelphia, PA, United States

OPEN ACCESS

Edited by:
Xavier Navarro, Autonomous University of Barcelona, Spain

Reviewed by:
Jose Antonio Gomez-Sanchez, University College London, United Kingdom
Lorenza Draghi, Politecnico di Milano, Italy

***Correspondence:**
D. Kacy Cullen
dkacy@pennmedicine.upenn.edu

† These authors have contributed equally to this work

Specialty section:
This article was submitted to Tissue Engineering and Regenerative Medicine, a section of the journal Frontiers in Bioengineering and Biotechnology

Received: *06 July 2020*
Accepted: *28 September 2020*
Published: *20 November 2020*

Citation:
Panzer KV, Burrell JC, Helm KVT, Purvis EM, Zhang Q, Le AD, O'Donnell JC and Cullen DK (2020) Tissue Engineered Bands of Büngner for Accelerated Motor and Sensory Axonal Outgrowth. Front. Bioeng. Biotechnol. 8:580654. doi: 10.3389/fbioe.2020.580654

Following peripheral nerve injury comprising a segmental defect, the extent of axon regeneration decreases precipitously with increasing gap length. Schwann cells play a key role in driving axon re-growth by forming aligned tubular guidance structures called bands of Büngner, which readily occurs in distal nerve segments as well as within autografts – currently the most reliable clinically-available bridging strategy. However, host Schwann cells generally fail to infiltrate large-gap acellular scaffolds, resulting in markedly inferior outcomes and motivating the development of next-generation bridging strategies capable of fully exploiting the inherent pro-regenerative capability of Schwann cells. We sought to create preformed, implantable Schwann cell-laden microtissue that emulates the anisotropic structure and function of naturally-occurring bands of Büngner. Accordingly, we developed a biofabrication scheme leveraging biomaterial-induced self-assembly of dissociated rat primary Schwann cells into dense, fiber-like three-dimensional bundles of Schwann cells and extracellular matrix within hydrogel micro-columns. This engineered microtissue was found to be biomimetic of morphological and phenotypic features of endogenous bands of Büngner, and also demonstrated 8 and 2× faster rates of axonal extension *in vitro* from primary rat spinal motor neurons and dorsal root ganglion sensory neurons, respectively, compared to 3D matrix-only controls or planar Schwann cells. To our knowledge, this is the first report of accelerated motor axon outgrowth using aligned Schwann cell constructs. For translational considerations, this microtissue was also fabricated using human gingiva-derived Schwann cells as an easily accessible autologous cell source. These results demonstrate the first tissue engineered bands of Büngner (TE-BoBs) comprised of dense three-dimensional bundles of longitudinally aligned Schwann cells that are readily scalable as implantable grafts to accelerate axon regeneration across long segmental nerve defects.

Keywords: tissue engineering, peripheral nervous system, Schwann cells, axon guidance, stem cells

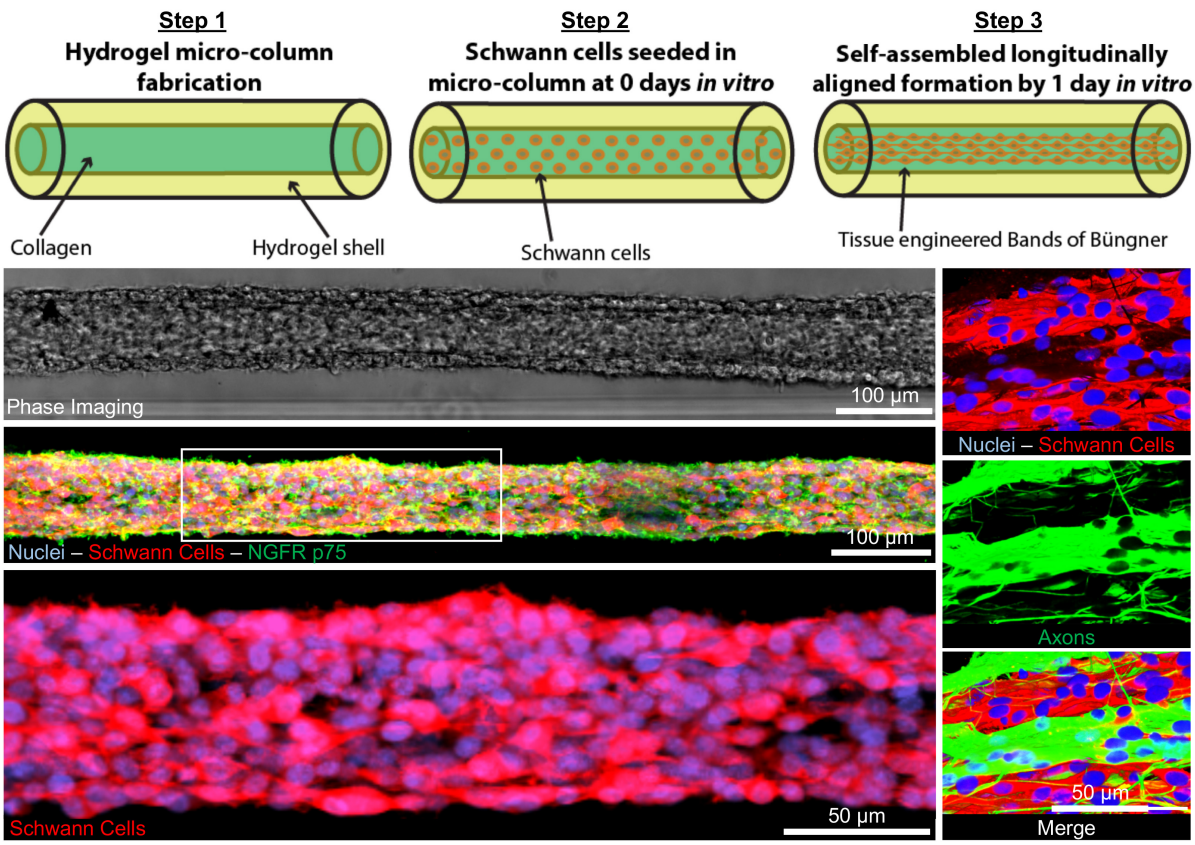

GRAPHICAL ABSTRACT 1 | Tissue Engineered Bands of Büngner (TE-BoB) are comprised of longitudinally-aligned Schwann cells within a hydrogel micro-column. By 1 day *in vitro*, the Schwann cells rapidly self-assemble into the longitudinal organization. By 4 days *in vitro*, the Schwann cells form a dense bundle as seen using phase microscopy. High-resolution confocal imaging enabled visualization of longitudinally-aligned Schwann cell processes. Notably, when co-cultured with a neuronal population plated on one end of the construct, axons rapidly accelerated through the TE-BoB construct along the aligned Schwann cells mimicking a key feature found in the naturally-occurring bands of Büngner necessary for regeneration after injury.

INTRODUCTION

Peripheral nerve injury (PNI) presents in 2–5% of all trauma cases, such as sports-related injuries, vehicle accidents, combat situations, or iatrogenic damage (Robinson, 2000; Pfister et al., 2011; Wang et al., 2017). PNIs are often associated with poor functional recovery due to inherently slow axonal regeneration (∼1 mm/day) and prolonged periods of denervation that decrease the capacity for axon regeneration (Ruijs et al., 2005; Gordon et al., 2011). Nerve injuries are primarily classified based on the extent of damage to the overall nerve structure, ranging from a mild crush or stretch injury to a complete disconnection requiring surgical reconstruction to reconnect the proximal and distal nerve stumps (Ruijs et al., 2005; Ali et al., 2014, 2015; Zager, 2014). The most severe nerve injuries are disconnections with a segmental defect that require implantation of grafting material, such as a biological or synthetic nerve conduit, to guide regeneration (Pfister et al., 2011). Poor regeneration is often associated with severe nerve injury, especially with long segmental defects and/or long total regenerative distances.

After nerve injury, axons in the distal nerve segment undergo Wallerian degeneration—the rapid degradation of axons disconnected from the proximal neuronal cell body in or near the spinal cord. Schwann cells distal to the injury dedifferentiate and align with the basal lamina forming highly longitudinally-oriented parallel tubular structures called the bands of Büngner (Salzer, 2015). These pro-regenerative micro-structures serve as a natural living scaffold that facilitates targeted reinnervation of the denervated end-target(s) (Gordon and Stein, 1982; Jessen and Mirsky, 2016).

In cases of segmental nerve defects, grafting is often required to replace the lost nervous tissue with a permissive scaffold that bridges the gap between the nerve stumps (Ray and Mackinnon, 2010). Despite recent advancements in biomaterial development and tissue engineering, autografts remain the most common bridging strategy for long segmental nerve defects. In contrast to alternative commercially-available strategies, such as nerve guidance conduits or acellular nerve allografts, autografts are natural living scaffolds that provide anisotropic structural support as well as neurotrophic support and a myriad of other signaling molecules actively secreted by cells residing in the

scaffold (Zhang et al., 2019). Similar to the pro-regenerative response in the distal nerve segment, the Schwann cells found within the donor nerve of the autograft dedifferentiate and form bands of Büngner along the basal lamina (Pfister et al., 2011). Autografts likely promote functional recovery and enable rapid axonal extension across segmental defects by providing endogenous structural support as well as a rich supply of growth factors from the resident Schwann cells (**Figure 1**).

In contrast, for nerve guidance conduits and acellular nerve grafts, infiltration of host Schwann cells from both nerve stumps is necessary to enable axon re-growth from the proximal stump and across the defect (Kaplan et al., 2015). This process – involving Schwann cell proliferation, migration, and alignment – occurs relatively slowly, likely contributing to reduced rates of axon regeneration across acellular bridging strategies as compared to autografts (Katiyar et al., 2020; Maggiore et al., 2020). In addition, acellular bridging strategies are generally inadequate in enabling axon regeneration across long segmental defects (e.g., >3 cm), which is believed to be due to an inability of host Schwann cells to fully infiltrate the grafts. While not completely understood, this failure may be due to limitations in Schwann cell migratory capacity and/or an insufficient number of proliferative cycles to meet requirements for spanning the graft zone (Saheb-Al-Zamani et al., 2013; Poppler et al., 2016). Moreover, decreased rates and quantity of regenerating axons across acellular grafts also results in prolonged periods of distal nerve and muscle denervation. In these cases, Schwann cells are unable to sustain the bands of Büngner phenotype for prolonged periods without direct axonal contact (Pfister et al., 2011). Thus, prolonged denervation of the distal Schwann cells ultimately results in diminished regenerative capacity and decreased targeted reinnervation (Jessen and Mirsky, 2019). Therefore, greater functional recovery can be achieved by increasing the rate of axon regeneration across a segmental defect to best leverage the regenerative capacity of the bands of Büngner across the full length of the distal nerve segment.

While the use of autografts in peripheral nerve repair surgery most consistently results in positive outcomes, this strategy is far from an ideal solution. Indeed, the procedure of autograft harvest inherently involves the deliberate creation of an additional functional nerve deficit, as well as having limited donor nerve availability for long gap nerve repair and/or polytrauma, and often presenting diameter mismatch at the interface between the injured nerve and the donor nerve. As an alternative, the development of a tissue engineered living scaffold containing Schwann cells may recapitulate pro-regenerative architecture and accelerate host axon regeneration (**Figure 1**). Various approaches have been pursued to increase Schwann cell alignment and enhance neurite extension *in vitro* (Bozkurt et al., 2007, 2009). For use *in vivo*, the fabrication of cell-laden nerve guidance conduits is intended to induce Schwann cell organization into the bands of Büngner *in situ* and subsequently enable rapid axonal regeneration (Das et al., 2015, 2017). Indeed, transplantation of Schwann cells, mesenchymal stem cells, or Schwann cell-like cells encased in hydrogel matrices have been investigated as a potential therapeutic strategy for more challenging nerve repair; however, previous approaches have yet to directly recreate the intra- and inter-cellular morphology and phenotype of the bands of Büngner prior to implant (Daud et al., 2012; Georgiou et al., 2013; Weightman et al., 2014; Kornfeld et al., 2016).

We have previously utilized microtissue engineering strategies to develop various living scaffolds as advanced approaches for regenerative medicine (Struzyna et al., 2015, 2017; Winter et al., 2016; Katiyar et al., 2018; O'Donnell et al., 2018). Here, we report the development of the first miniaturized, transplantable, preformed tissue engineered bands of Büngner (TE-BoB). Specifically, we demonstrate the facile biofabrication of TE-BoBs exploiting principles of material-guided cell self-assembly, as well as characterization of the resulting cellular structure, phenotype, and functional capacity to accelerate motor and sensory axonal outgrowth *in vitro*. TE-BoBs are comprised of self-assembled longitudinally-aligned Schwann cells that can facilitate axon outgrowth and bundling *in vitro*. Remarkably, we found that TE-BoBs achieved motor axon and sensory axon growth rates that were at least 10.7 and 4.3× faster, respectively, than rates achieved by alternative previously published Schwann cell-mediated strategies (Phillips et al., 2005; Gingras et al., 2008; Daud et al., 2012; Georgiou et al., 2013; Hyung et al., 2015). For translational consideration, we demonstrate proof-of-concept of TE-BoB fabrication using human gingiva stem cell-derived Schwann cells. TE-BoBs are a novel living scaffold suitable for use in follow-on studies to assess their ability to accelerate axon regeneration across segmental defects in an *in vivo* model of PNI.

MATERIALS AND METHODS

All procedures were approved by the Institutional Animal Care and Use Committees at the University of Pennsylvania and the Michael J. Crescenz Veterans Affairs Medical Center and adhered to the guidelines set forth in the NIH Public Health Service Policy on Humane Care and Use of Laboratory Animals (2015).

Hydrogel Micro-Column Fabrication

Three-dimensional hollow hydrogel micro-columns were formed to promote alignment and bundling of Schwann cells throughout the lumen. This protocol was adapted from our previous studies utilizing a similar microtissue engineering technique to align astrocytes for a tissue engineered rostral migratory stream (Winter et al., 2016; Katiyar et al., 2018; O'Donnell et al., 2018). All hollow micro-columns were fabricated with an inner diameter (ID) of 300 μm, an outer diameter (OD) of 701 μm, a length of 5 mm, and an agarose concentration of 3%. Agarose is a biocompatible, optically transparent, and relatively inert biomaterial that lacks adhesive ligands, which allows for specific investigation of the relationship between the cells and the collagen extracellular matrix (ECM) coating the inner lumen. Approximately 2.0 μL of collagen (1 mg/ml) was microinjected into each lumen. A polymerization/dehydration time of 3 h allowed collagen to coat the inner lumen of the micro-columns, creating an outer agarose shell, inner collagen coating, and hollow core. Corresponding 2D controls were prepared in 10-mm petri dishes, pretreated with poly-L-lysine overnight, and then rinsed three times. Approximately 2.0 μL of collagen (1 mg/ml) was

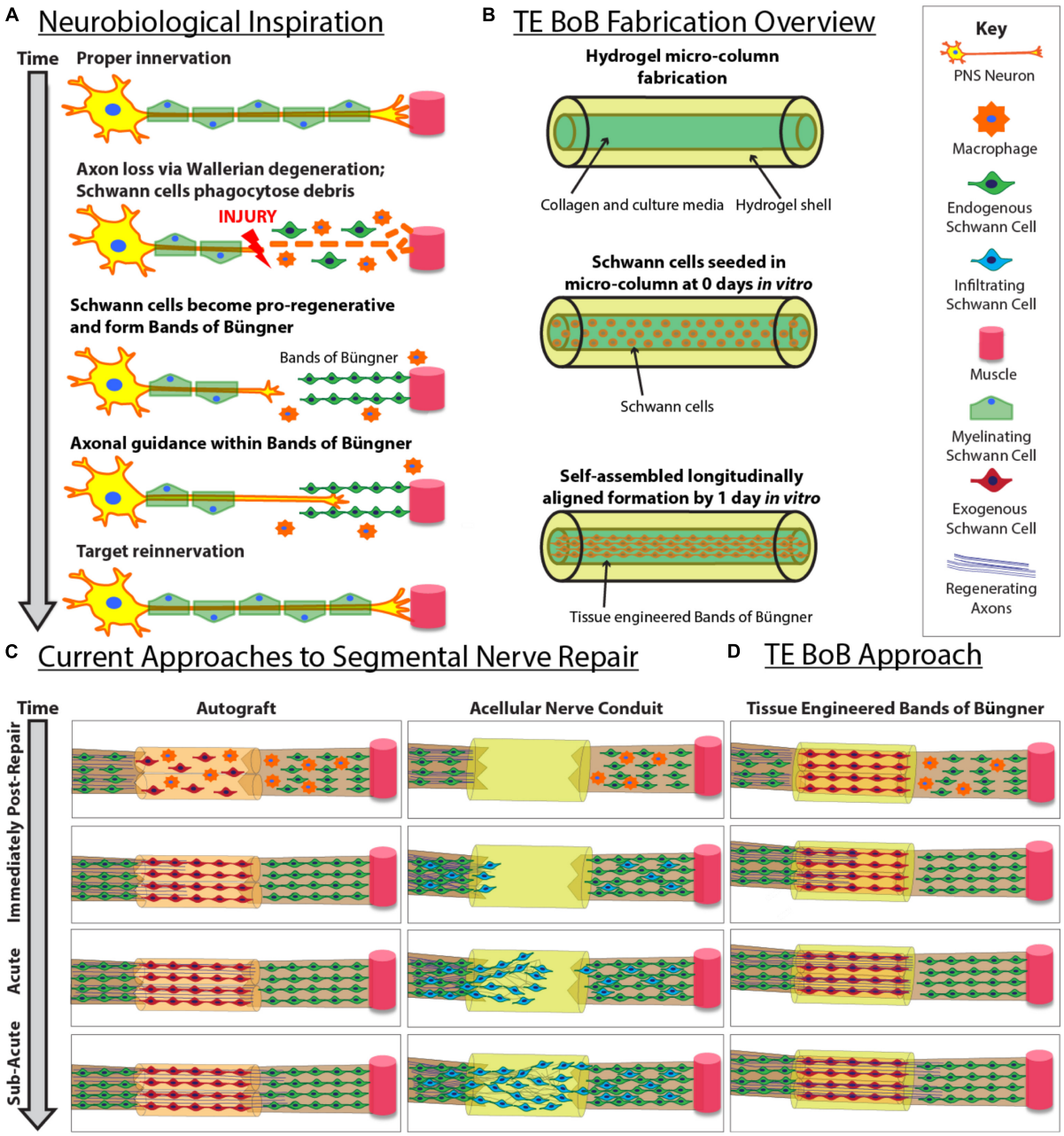

FIGURE 1 | Inspiration, fabrication protocol, and proposed applications for TE-BoBs. This diagram illustrates **(A)** features of endogenous peripheral nerve regeneration that inspired TE-BoB design, **(B)** TE-BoB general fabrication process, **(C)** current techniques to guide injured axons from the proximal nerve to the distal nerve closing the nerve gap, and **(D)** application of the TE-BoB for nerve regeneration and reinnervation.

added to the center of the dish. The 2D controls were returned to the incubator to polymerize for 3 h similar to the micro-columns.

Primary Schwann Cell Culture

Primary Schwann cells were obtained from the Salzer Lab (NYU) and subsequently passaged every 7 days during the duration of this study. Schwann cells were cultured in minimum essential media (Thermo Fisher Scientific, Gibco 11095072), 10% fetal bovine serum (FBS), 10 ng/mL recombinant human neuregulin-1-β1 EGF domain (R&D, 396-HB-050), 2.5 μM forskolin (Sigma, F-6886), and 1% Penicillin/Streptomycin (Kim and Maurel, 2009). The resulting cell suspension was split to maintain the cell line and to seed the constructs. Collagen-coated micro-columns were seeded with approximately 2 μL of cell suspension (1.1×10^5–1.3×10^7 cells/mL). Additional cell suspension was plated onto 2D polymerized collagen with identical cell suspension concentration and volume. For TE-BoB fabrication and 2D controls, Schwann cells were incubated for

30 min to allow for adhesion before carefully submerging them in 2 mL Schwann cell growth medium. A total number of $n = 35$ TE-BoBs and control cultures were generated for this study.

Primary Dorsal Root Ganglion (DRG) and Spinal Motor Neuron (MN) Isolation and Co-culture

Dorsal root ganglion (DRG) explants and spinal cords were isolated from embryonic day 16 Sprague-Dawley rats (Charles River, Wilmington, MA, United States). DRG explants were stored overnight in Hibernate-E. MN aggregates were formed from dissociated spinal MNs isolated from embryonic spinal cords using an Optiprep density gradient and subsequent forced-aggregation as previously described (Katiyar et al., 2019). Briefly, dissociated MNs were plated in a "reverse pyramid" well comprised of polydimethyl siloxane. Each well received 12 μL of 100,000 dissociated MNs, and centrifuged at 1500 RPM for 5 min. Motor neuron aggregates were incubated overnight in media.

At 1 day *in vitro*, MN aggregates or DRG explants comprised of sensory neurons (SNs) were plated under stereoscopic magnification using fine forceps on one end of a TE-BoB or acellular collagen-coated micro-column, or on top of Schwann cells seeded on planar collagen. Cultures were allowed to adhere at 37°C and 5% CO_2.

Media was changed on the next day and then every other day. For these co-culture studies, the media was Neurobasal media and 10% FBS first conditioned in a flask of astrocytes overnight, and then supplemented the next day with 37 ng/mL hydrocortisone, 2.2 μg/mL isobutylmethylxanthine, 10 ng/mL brain-derived neurotrophic factor, 10 ng/mL ciliary neurotrophic factor, 10 ng/mL cardiotrophin-1, 10 ng/mL glial cell line-derived neurotrophic factor, 2% B-27, 20 ng/mL nerve growth factor, 4 μM uridine, 4 μM 5-FdU, 2 mM L-glutamine, 417 ng/mL forskolin, 1 mM sodium pyruvate, 0.1 mM β-mercaptoethanol, 2.5 g/L glucose, and 10 ng/ml recombinant human neuregulin-1-β1 epidermal growth factor domain (Katiyar et al., 2019).

Immunocytochemistry

All samples were fixed at 4 days *in vitro*. Immunocytochemistry was completed to evaluate Schwann cell and neuronal phenotype, assess the presence of collagen, and characterize the cytoarchitecture within the micro-column and 2D cultures. Briefly, cultures were fixed in 4% formaldehyde for 30 min, washed in phosphate buffered saline (PBS), and permeabilized in 0.3% Triton X100 plus 4% normal horse serum (NHS) for 1 h. Cultures were incubated with primary antibodies in PBS + 4% serum solution) at 4°C for 12 h. To label Schwann cells, guinea pig anti-S100β (Synaptic Systems 287004; 1:500; intracellular calcium-binding protein) and rabbit anti-p-75 (Sigma N3908; 1:500; nerve growth factor receptor) were used. To evaluate neurite outgrowth, cultures were stained with mouse anti-beta tubulin III (Tuj1) (Sigma T8578; 1:500) to label all axons and neurons. To assess the distribution of collagen ECM, rabbit anti-collagen I (Abcam ab34710; 1:500) was used. After rinsing, appropriate secondary antibodies (1:500 in PBS + 4% NHS; anti-mouse 488, Invitrogen, A21202; anti-rabbit 488, Life Technology, A21206; anti-guinea pig 568, Sigma SAD4600038; and/or anti-rabbit 647, Invitrogen, A31573) were applied at room temperature for 2 h and Hoechst (Invitrogen H3570; 1:10,000) was then added to label all nuclei.

Microscopy and Data Acquisition

Schwann cell cultures and constructs were imaged using phase contrast microscopy at 1 and 4 days *in vitro* with a Nikon Inverted Eclipse Ti-S microscope with digital image acquisition using a QiClick camera interfaced with Nikon Elements Basic Research software (4.10.01). Confocal images were taken at 4 days *in vitro* using a Nikon A1RSI laser scanning confocal microscope.

All images acquired for comparative analyses were captured with identical acquisition settings. Samples were fluorescently imaged using a Nikon A1Rsi Laser Scanning Confocal microscope with a 10× (CFI Plan Apo Lambda 10×; n.a. 0.45) or 16x objective (CFI75 LWD 16× W; n.a. 0.8).

Image post-processing and quantification was completed using FIJI (Fiji Is Just ImageJ) software platform (Schindelin et al., 2012). Nikon image files were imported into FIJI via the Bioformats function and each channel was split into individual channels. To minimize potential bias, trained researchers were given only the axonal channel containing a randomly-coded ID. Images were rotated to align the horizontal axis with the inner lumen. Schwann cell orientation was measured relative to the horizontal axis from 150 individual S100+ cells evenly distributed across TE-BoBs at 4 days *in vitro*. Neurite length was quantified by measuring the distance from the edge of the neuronal bodies. Neurite directionality was analyzed qualitatively.

To compare the degree of axon fasciculation, a macro for automated image processing analyses was designed to minimize any potential bias. Background subtraction was applied to all images using the rolling ball method with a diameter of 100 pixels (O'Donnell et al., 2016). Images were rotated to ensure constructs were parallel to the horizontal axis. A 5,000 μm × 300 μm (length × width) region of interest (ROI) was placed starting from the edge of the neuronal-axonal interface. Axonal segments were isolated from the Tuj1 channel using MaxEntropy thresholding and subsequently quantified using the "Analyze Particles" function on features with an area greater than 10 μm^2 to minimize noisy particles and circularity between 0 and 0.3 to eliminate circular artifacts. The total bundle area of the segmented regions, average size of each bundle, and area percent covered were calculated per construct. Mean values were obtained by averaging across constructs for further statistical analyses.

To compare neuronal density within the aggregate region, Tuj1 expression was measured using an automated image processing macro to minimize any potential bias. The neuron region was isolated from the axonal region by placing a 500 μm × 300 μm (length × width) in a representative area in the middle of the neuronal population. Three representative ROIs (100 μm × 100 μm) were selected for further analysis. Background subtraction was applied to all images using the rolling ball method with a diameter of 50 pixels, which appeared to remove smaller and more diffuse axonal staining

(O'Donnell et al., 2016). Neurons were isolated from the Tuj1 channel using MaxEntropy thresholding and subsequently quantified using the "Analyze Particles" function on features with an area greater than 10 μm^2 to minimize noisy signal. The percent area covered was calculated for each ROI and averaged per construct. Therefore, in this study, the percentage of the Tuj1 expression within the aggregate may be considered as a surrogate marker for neuronal health. Mean values were obtained by averaging across constructs for further statistical analyses.

Study Design and Statistical Analysis

Initial TE-BoB characterization was completed using phase imaging and immunocytochemistry ($n = 7$). Various conditions were studied to quantify the effects of aligned Schwann cell bundles on sensory and motor axon outgrowth *in vitro*. The independent variables included Schwann cell configuration (2D culture vs. 3D bundling) and aligned Schwann cell presence (Schwann cell/collagen vs. collagen-only constructs), while the dependent variables included neurite length and directionality. These variables were selected to assess the regenerative promotion and directional guidance provided by TE-BoBs.

Experimental groups included hydrogel micro-column constructs with bundles of collagen and aligned Schwann cells (TE-BoBs), plated with either one SN explant ($n = 4$) or one MN aggregate ($n = 6$). The 3D control groups contained collagen-coated hydrogel micro-columns plated with one SN explant ($n = 5$) or one MN aggregate ($n = 5$) in the absence of Schwann cells. The 2D control groups consisted of Schwann cell cultures on a planar bed of collagen, each plated with either one SN explant ($n = 3$) or one MN aggregate ($n = 5$).

At 4 days *in vitro*, the length of neurite outgrowth was measured linearly from the nearest soma aggregate edge to the axon terminal of the longest neurite. Neurite outgrowth was measured for each culture from confocal z-stack maximum projections and analyzed using FIJI software (Schindelin et al., 2012). Mean neurite length was determined for each group and statistically analyzed using one-way ANOVA followed by Tukey's multiple comparison test to determine statistical significance ($p < 0.05$ required for significance). For the axon fasciculation assay, mean values were compared between TE-BoBs and constructs lacking Schwann cells by two-tailed unpaired Student's *t*-tests ($\alpha = 0.05$). Values are reported as mean ± SEM, unless otherwise noted. Statistical testing was performed in GraphPad Prism 8 for Windows 64 bit.

Human Gingiva-Derived TE-BoB Fabrication

In a separate proof-of-concept experiment, TE-BoBs were fabricated using Schwann cell-like cells induced from human gingiva-derived mesenchymal stem cell (GMSC) source using a previously established derivation protocol (Zhang et al., 2018a,b). Human gingival tissues were obtained as remnants of discarded tissues from healthy human subjects aged from 20 to 40 years old, who underwent routine dental procedures. Informed consents were obtained from all subjects and all procedures were performed under the approved Institutional Review Board (IRB) protocol at University of Pennsylvania. Primary GMSCs were cultured and maintained in complete alpha-minimum essential medium (α-MEM) supplemented with 1% L-glutamine, 10% FBS (Zen Bio) and 1% penicillin/streptomycin at 37°C with 5% CO_2 as describe previously (Zhang et al., 2009). Cells less than 8 passages were used for experiments.

For induction of GMSC-derived neural crest stem-like cells (NCSCs) (Zhang et al., 2018b), GMSCs were plated in poly-L-ornithine pre-coated culture dishes and cultured in media consisting of 50% DMEM/F12 (Life Technologies, 11330-032) and 50% Neurobasal medium (Life Technologies, 21103-049) supplemented with 20 ng/mL human basic fibroblast growth factor (PeproTech, 100-18C), 20 ng/mL human epidermal growth factor (PeproTech, AF-100-15), 55 μM β-mercaptomethanol (Life Technologies, 21985-023), 1% N2 (Life Technologies, 17-502-048), 1% B27 (Life Technologies, 17-502-044), and 100 units penicillin, 100 μg/mL streptomycin (Life Technologies, 15140-122). Six days later, cells were harvested for Schwann cell induction (Zhang et al., 2018a,b). Briefly, GMSC-derived NCSCs were cultured Schwann cell differentiation media consisting of α-minimal essential media (Life Technologies, 12561-056) supplemented with 10% fetal bovine serum (Zenbio Inc., SER-500), 35 ng/mL all *trans*-retinoic acid (Sigma, R2625), 5 μM forskolin (Cayman Chemical, 11018), 10 ng/mL human basic fibroblast growth factor (PeproTech, 100-18C), 5 ng/mL platelet-derived growth factor-AA (PeproTech, 100-13A), 200 ng/mL β-heregulin (PeproTech, 100-03), 100 units penicillin, 100 μg/mL streptomycin (Life Technologies, 15140-122).

Following induction for 7 days, GMSC-derived Schwann cell-like cells were dissociated and plated in micro-columns as described above (2.5×10^5–3.0×10^6 cells/mL). Immunocytochemistry was performed on planar cultures at 3 days *in vitro* to label for nuclei (DAPI) and Schwann cells (S100β) as described above. Phase microscopy was performed at 3 days after TE-BoB fabrication.

RESULTS

Schwann Cell Seeding, Process Extension, and Bundling

To biofabricate TE-BoBs, Schwann cells were seeded in an agarose hydrogel micro-column 5 mm long with OD of 701 μm, ID of 300 μm, and collagen-coated inner lumen. By 1 day *in vitro*, Schwann cells that were seeded in the agarose micro-columns had adhered to the collagen ECM coating the inner lumen, began to exhibit a process-bearing morphology, and eventually self-assembled into a dense network along the inner lumen of the micro-column (**Figure 2A**). By 4 days *in vitro*, as the Schwann cells continued to remodel the collagen ECM, the density of the Schwann cells rapidly increased, forming a singular dense bundle in the lumen several millimeters long and, in most cases, spanning the entire 5 mm lumen of the micro-column (**Figure 2B**). At 4 days *in vitro*, the bundled Schwann cells exhibiting a bipolar morphology aligned along the lumen of the micro-column (−1.2° ± 10.1° relative to longitudinal

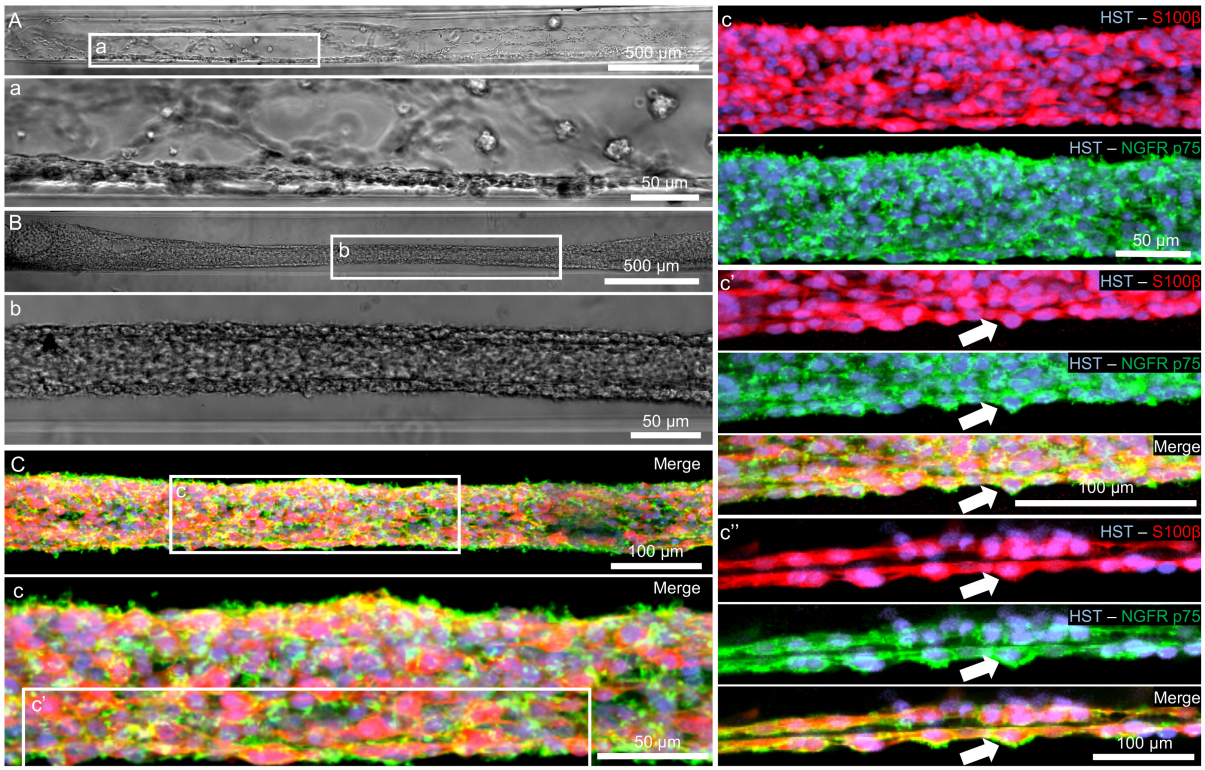

FIGURE 2 | Characterization of Schwann cell constructs following self-assembly fabrication process using phase-imaging, immunocytochemistry, and confocal microscopy. **(A,B)** Phase microscopy was utilized to visualize Schwann cells seeded in a 300 μm ID agarose hydrogel micro-column. **(A)** At 1 day *in vitro*, Schwann cells were found adhering to the collagen ECM coating the inner lumen of the micro-column. **(a)** Higher magnification revealed the cells begun to self-assemble into cables and exhibit process-bearing morphology. **(B)** By 4 days *in vitro*, the Schwann cells formed dense bundles within the inner lumen of the agarose micro-column. **(b)** These bundles appeared highly organized comprised of Schwann cells with longitudinally-aligned processes. **(C)** Morphometric assessment of the dense bundles at 4 days *in vitro* revealed Hoechst (HST)-positive cells with elevated expression of S100b and NGFR p75, common Schwann cell markers. **(c)** Under higher magnification, most of the Schwann cells co-localized with NGFR p75R and exhibited bipolar morphologies with elongated processes, a common phenotype during nervous system development and regeneration. **(c′)** Max projection image showing a high density of aligned Schwann cells denoted by arrows. **(c″)** Single z-plane frame from the same image illustrating NGFR p75 expression on the membrane of highly aligned S100β positive Schwann cells denoted by arrows. Scale bars: **(A,B)** 500 μm, **(a,b)** 50 μm, **(C)** 100 μm, **(c)** 50 μm, **(c″)** 100 μm.

axis; mean ± standard deviation) and demonstrated consistent co-expression of both S100β and nerve growth factor receptor (NGFR p75) (**Figure 2C**).

Longitudinally-Aligned Schwann Cells Accelerate Neurite Outgrowth

To evaluate the effect of TE-BoBs on motor and sensory neurite outgrowth, we compared axonal extension within TE-BoB micro-columns containing aligned Schwann cells to 3D control micro-columns containing only collagen and 2D controls containing Schwann cells on collagen in planar culture. Here, we added either MN or SN aggregates to one end of micro-columns at 1 day *in vitro*, which were then returned to culture until 4 days *in vitro* (**Figures 3A–D**). Although there was some S100β positivity within the MN and SN aggregates and at the interface with Tuj1 positive axons, the absence of S100β positivity within the collagen micro-columns lacking Schwann cells suggested that there was no Schwann cells migration into the micro-column. In this study, Tuj1 expression within the aggregate region was measured to provide an indirect measurement of neuron density and serve as a surrogate marker for neuronal health. Greater area of Tuj1 expression was found in MN aggregates containing aligned Schwann cells (mean: 49.5% ± 12.6%; range: 37.2 – 65.8%; $n = 6$) compared to the control collagen micro-column ($p < 0.05$; mean: 33.3% ± 10.5%; range: 20.2–44.5%; $n = 5$) (**Figure 3E**). No significant differences were found between SNs co-cultured with aligned Schwann cells (mean: 39.4% ± 22.9%; range: 10.2–65.8%; $n = 4$) and the control collagen micro-column (mean: 46.1% ± 23.2%; range: 13.2–63.2%; $n = 5$) (**Figure 3F**). The presence of longitudinally-aligned Schwann cells resulted in the longest axonal outgrowth for both sensory and motor neurite assays. Increased neurite outgrowth was observed in TE-BoBs containing a MN aggregate (mean: 2614.6 μm ± 249.9; range: 2093.6–3652.8 μm; $n = 6$) compared to control collagen micro-columns ($p < 0.0001$; mean: 341.8 μm ± 145.7 μm; range: 0–742.3 μm; $n = 5$), and 2D Schwann cell co-culture ($p < 0.0001$; mean: 756.5 μm ± 67.4 μm; range: 582.5–950.0 μm; $n = 5$) (**Figure 4**). Similarly, greater sensory axon outgrowth was observed in TE-BoBs with a SN

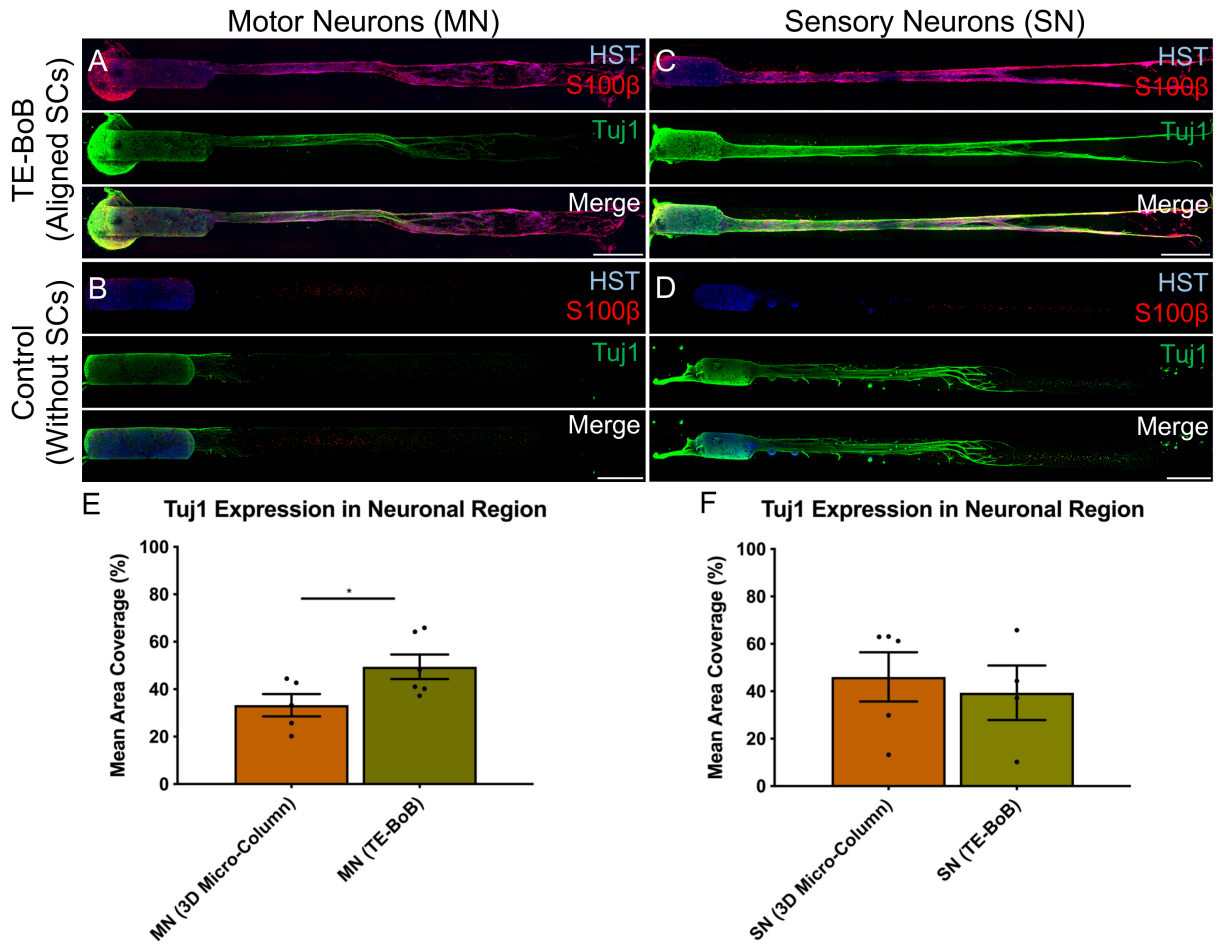

FIGURE 3 | Comparison of three-dimensional neurite outgrowth in TE-BoBs and collagen-only constructs. A neurite outgrowth assay was performed to elucidate the effect of longitudinally aligned Schwann cells (SCs) on axonal extension by carefully plating a population of motor neurons **(A,B)** or sensory neurons **(C,D)** on one end of a TE-BoB containing aligned Schwann cells or collagen-only micro-column at 1 day *in vitro* following fabrication. Constructs were fixed at 4 days *in vitro* and stained for nuclei (HST), Schwann cells (S100β) and axons (Tuj1). Highly aligned motor and sensory neurites were visualized extending from the neurons and spanning the Schwann cell constructs **(A,C)**. Axon outgrowth appeared more disorganized in collagen control constructs lacking Schwann cells **(B,D)**. In contrast, axonal outgrowth within the cellular constructs appeared to closely follow the dense bundles of longitudinally-aligned Schwann cells. **(E)** Detailed image analysis of the neuronal population revealed greater Tuj1 expression in motor neurons co-cultured with Schwann cells compared to motor neurons cultures lacking Schwann cells. **(F)** No significant differences in Tuj1 expression were found in sensory neurons with or without co-cultured Schwann cells. Scale bar: 500 μm. *$p < 0.05$.

explant (mean: 4665.1 μm ± 355.4; range: 3605.2–5118.3 μm; $n = 4$) compared to control collagen columns ($p < 0.05$; mean: 2122.2 μm ± 728.1 μm; range: 522.9–4226.1 μm; $n = 5$). No significant difference was found compared to SN explants plated on 2D Schwann cell control cultures (mean: 2883.1 μm ± 272.3 μm; range: 2449.6–3385.4 μm; $n = 3$) (**Figure 5**).

TE-BoBs Enhance Axon Area and Fasciculation

Detailed image analysis was performed on TE-BoBs and constructs lacking Schwann cells using automated image analysis across a 5000 μm × 300 μm ROI. Percent axon area coverage, total bundle area, average bundle size, and average bundle count were analyzed.

The presence of longitudinally-aligned Schwann cells in TE-BoBs resulted in large MN bundles within the lumen compared to control constructs lacking Schwann cells (**Figure 6A**). The percent area covered by MN bundles in TE-BoBs (mean: 19.1% ± 1.7%; range: 12.1–23.7%) was greater than the control constructs lacking Schwann cells ($p < 0.0001$; mean: 2.7% ± 0.8%; range: 0.4–5.0%). The total area covered by MN bundles in TE-BoBs (mean: 258,947 μm^2 ± 28,318 μm^2; range: 170,591–375,707 μm^2) was greater than control constructs lacking Schwann cells ($p < 0.001$; mean: 40,042 μm^2 ± 12,506 μm^2; range: 5778–75,356 μm^2). The average size of the MN bundles in TE-BoBs (mean: 29,939 μm^2 ± 9328 μm^2; range: 6768 μm^2–62,185 μm^2) was greater than control constructs lacking Schwann cells ($p < 0.05$; mean: 2933 μm^2 ± 1708 μm^2; range: 577.8–9131 μm^2). Therefore, dense motor axonal bundles were

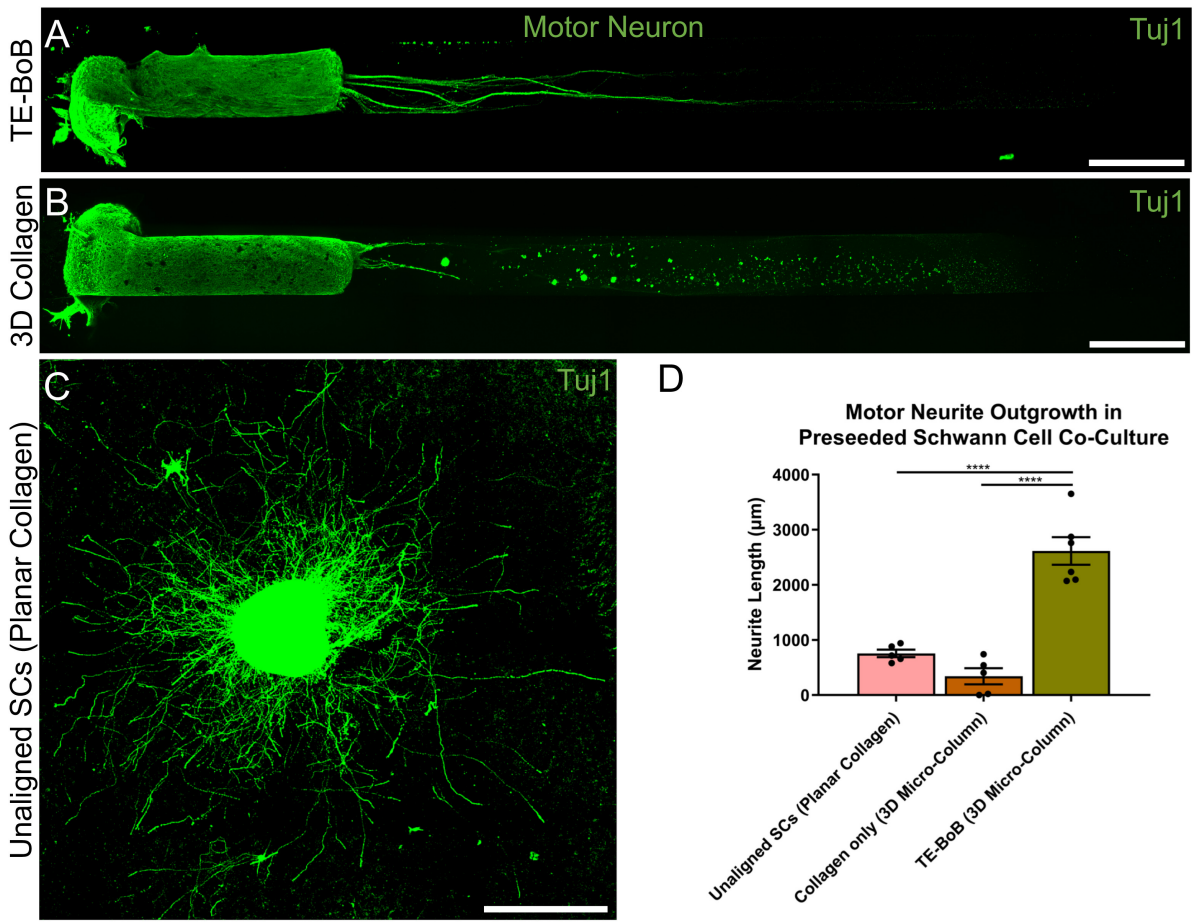

FIGURE 4 | Quantification of motor neuron outgrowth in TE-BoBs. Neurite outgrowth was measured at 4 days *in vitro* after plating a motor neuronal aggregate in a micro-column containing aligned Schwann cells **(A)** or collagen only control **(B)**, or on a bed of Schwann cells in 2D **(C)**. **(D)** Greater neurite outgrowth was found in TE-BoBs (i.e., aligned Schwann cells in a 3D micro-column) compared to the collagen only control and the 2D planar Schwann cell control. Error bars represent standard error of mean. Scale bar: 500 μm. ****$p < 0.0001$.

formed in the presence of longitudinally-aligned Schwann cells compared to small bundles with less dense axons within control micro-columns containing only collagen.

Similar to these findings with MNs, the presence of longitudinally-aligned Schwann cells in TE-BoBs also resulted in large SN bundles within the lumen compared to control constructs lacking Schwann cells (**Figure 6B**). The percent area covered by SN bundles in TE-BoBs (mean: 29.2% ± 3.8%; range: 17.8–34.7%) was greater than the control constructs lacking Schwann cells ($p < 0.05$; mean: 12.1% ± 4.6%; range: 2.4–24.3%). The total area covered by SN bundles in TE-BoBs (mean: 437,991 μm^2 ± 56,875 μm^2; range: 270,358 μm^2–521,157 μm^2) was greater than control constructs lacking Schwann cells ($p < 0.05$; mean: 179,987 μm^2 ± 69,323 μm^2; range: 35,625–366,309 μm^2). The average size of the SN bundles in TE-BoBs (mean: 113,539 μm^2 ± 42,174 μm^2; range: 45,060 μm^2–234,720 μm^2) was greater than control constructs lacking Schwann cells ($p < 0.05$; mean: 20,890 μm^2 ± 7761 μm^2; range: 7125–43,473 μm^2). Overall, the presence aligned Schwann cells resulted in the formation of dense sensory axonal bundles, as compared to small bundles with more diffuse axons within control micro-columns containing only collagen.

Axon-Schwann Cell Interactions Within TE-BoBs Mimic Natural Bands of Büngner and Provide Longitudinal Directionality

As TE-BoBs present longitudinally-aligned Schwann cells in a tight, bundled formation, we also ascertained the structural relationships and directivity of axonal outgrowth on these structures in comparison to growth within 3D micro-columns alone and on 2D control cultures. We found that axonal outgrowth from both MNs and SNs were in direct contact and longitudinally-aligned with the Schwann cell bundles comprising the TE-BoBs (see **Figures 4**, **5**). Axonal extension from the MNs and SNs in the 3D micro-columns primarily occurred within the collagen ECM and was not as bundled as that in the TE-BoBs, although outgrowth was physically constrained by the inner walls of the micro-column. In contrast to these cases, motor

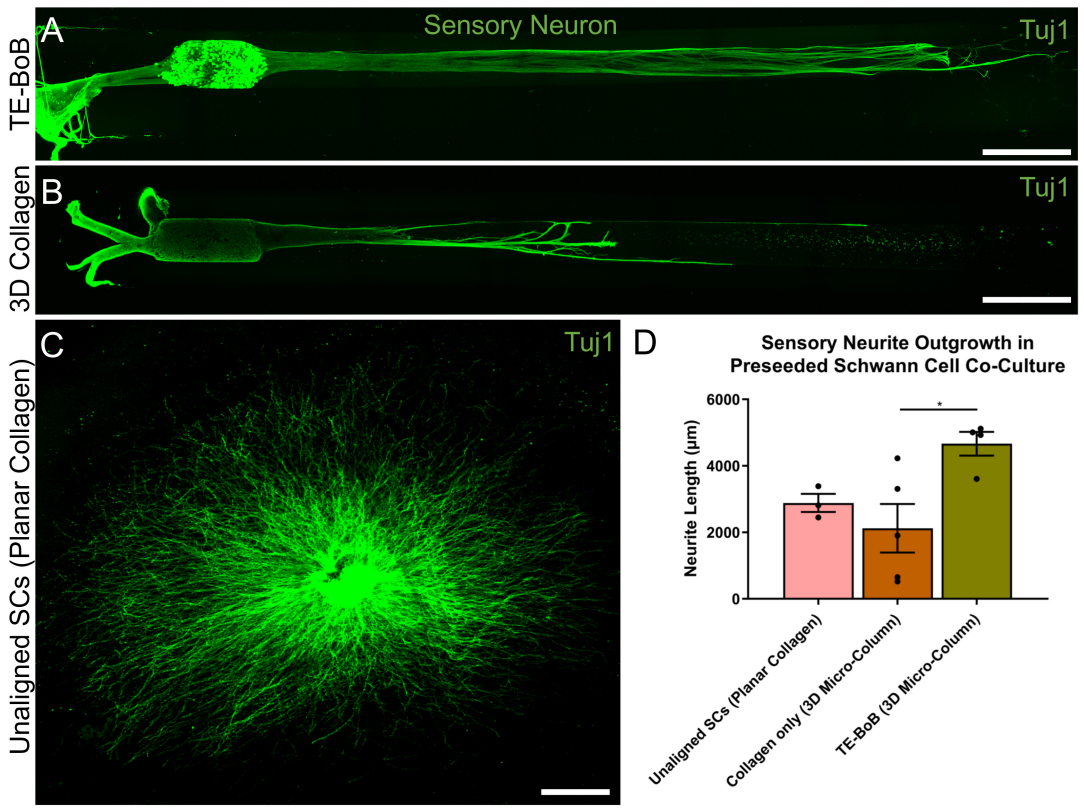

FIGURE 5 | Quantification of sensory neuron outgrowth in TE-BoBs. Neurite outgrowth was measured at 4 days *in vitro* after plating sensory neurons (DRG explant) in a micro-column containing aligned Schwann cells **(A)** or collagen only control **(B)**, or on a bed of Schwann cells in 2D **(C)**. **(D)** Greater neurite outgrowth was found in TE-BoBs (i.e., aligned Schwann cells in a 3D micro-column) compared to the collagen only control. Error bars represent standard error of mean. Scale bar: 500 μm. $^*p < 0.05$.

and sensory axons extended from the 2D control populations in all directions. At a finer level, axonal outgrowth had a "frayed" appearance in the case of growth within acellular micro-columns as compared to tighter, directed outgrowth along the aligned Schwann cells in TE-BoBs (**Figure 6**). This frayed outgrowth pattern may be due to axonal growth cones "searching" for guiding signals in acellular constructs, as compared to precisely presented longitudinal cues presented by the bundled Schwann cells in TE-BoBs. Building on this observation, high resolution confocal imaging further revealed a familiar spatial relationship between the growing axons and longitudinally-aligned Schwann cells. Axons extending from both MN aggregates (**Figure 7**) and SN explants (**Figure 8**) grew along and through these dense bands of aligned Schwann cells comprising the TE-BoBs in a manner reminiscent of *in vivo* axon regeneration within bands of Büngner.

Human GMSC-Derived Schwann Cell-Like Cells Self-Assemble Into Longitudinally-Aligned Morphology Within TE-BoBs

Human Schwann cell-like cells were induced from human GMSC-derive neural crest stem-like cells (Zhang et al., 2018a,b). Prior to TE-BoB fabrication, immunocytochemistry characterization was performed in planar cultures at 3 days *in vitro*. Greater S100β expression was found in human GMSC-derived Schwann cell-like cells compared to the undifferentiated GMSC control culture. The presence of S100β within GMSC-derived Schwann cell-like cell planar culture indicated that these cells expressed a protein commonly found in Schwann cells similar to previous studies (Zhang et al., 2018a,b). Therefore, TE-BoBs were fabricated using these Schwann cell-like cells. By 3 days *in vitro* following fabrication, GMSC-derived Schwann cell-like cells within the TE-BoB self-assembled into a tightly bundled formation that resembled the rodent TE-BoB constructs (**Figure 9**). These findings demonstrate that the self-assembly mechanisms described for rat Schwann cells are conserved in human Schwann cells, and bode well for the potential of fabricating large-scale human TE-BoBs for future efficacy testing.

DISCUSSION

Following nerve injury, Schwann cells form bands of Büngner that provide axonal guidance to distal targets for functional reinnervation. To date, autografts remain the gold standard

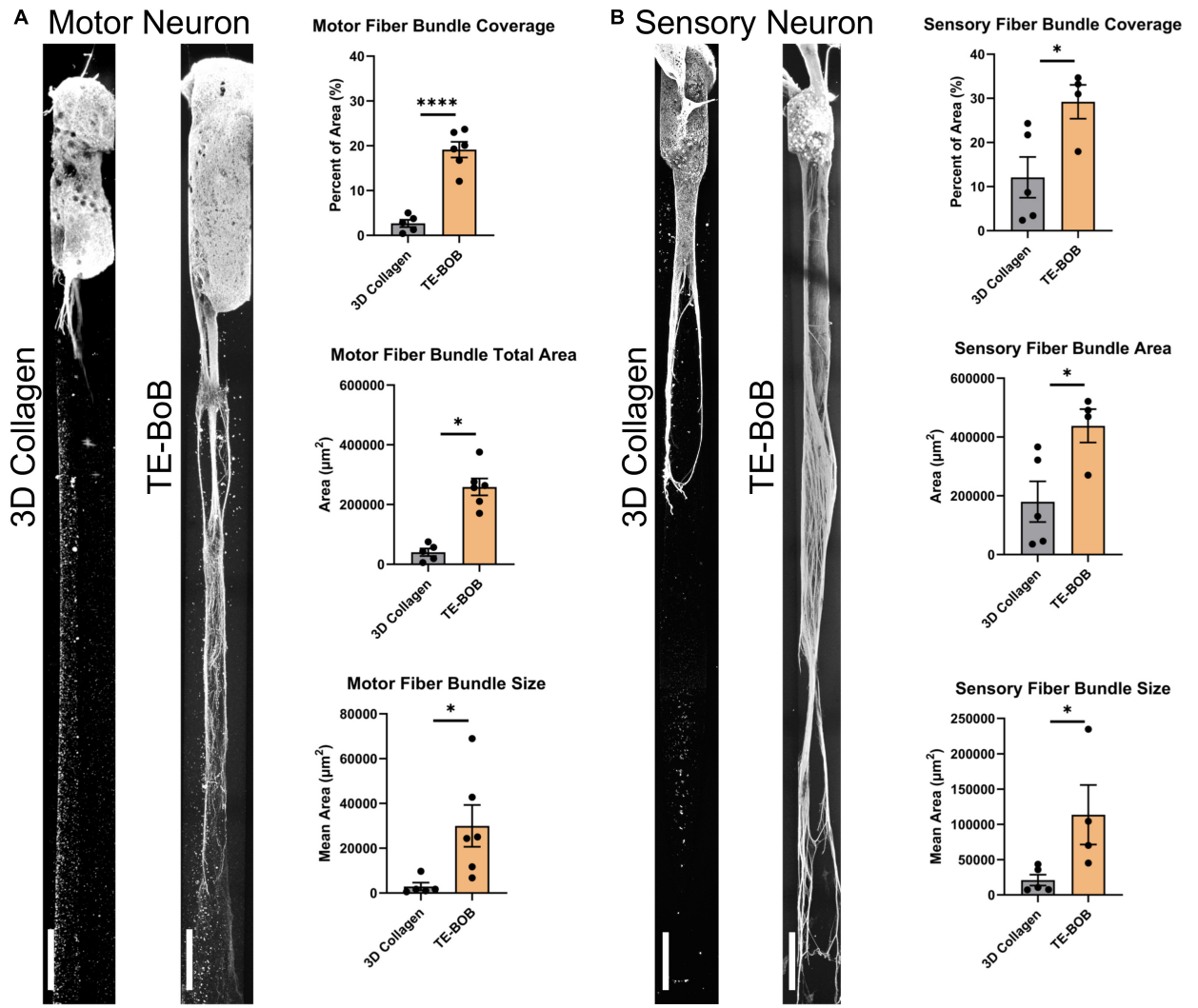

FIGURE 6 | Assessment of motor and sensory axon bundling in TE-BoBs. Axon bundling was measured at 4 days *in vitro* after plating either a **(A)** spinal cord motor neuron aggregate or **(B)** DRG explant containing sensory neurons on the end of a 3D micro-column comprised of 3D collagen ECM (control) or aligned Schwann cells (TE-BoB). Fluorescent images were gray-scaled and a 5,000 μm × 300 μm ROI was drawn starting at the edge of the neuronal-axonal interface. An automated macro was applied over each ROI to identify regions of bundled axons after excluding small debris and/or artifact. The presence of longitudinally-aligned Schwann cells resulted in the formation of large axon bundles covering the lumen of the micro-column. Error bars represent standard error of mean. Scale bar: 250 μm. $^{*}p < 0.05$, $^{****}p < 0.0001$.

for challenging clinical scenarios, serving as naturally-occurring living scaffolds that facilitate regeneration by providing a permissive substrate with anisotropic structural and neurotrophic support due to indwelling cells. Indeed, resident Schwann cells found in the donor nerve undergo similar phenotypic alterations as denervated Schwann cells found in the distal nerve, and facilitate regeneration by enabling the rapid growth across the defect (Pfister et al., 2011). However, over time, prolonged denervation results in the degradation of the pro-regenerative bands of Büngner, leading to diminished regenerative capacity.

Alternative bridging strategies are generally acellular (i.e., non-living), such as the use of decellularized nerve allografts or biological/synthetic conduits, and unable to consistently support axonal regeneration across defects greater than the critical length of 3 cm (Kornfeld et al., 2019). This is likely due to slow axon regeneration across the defect—which is reliant upon host Schwann cell infiltration and organization across the entire length of the graft region—resulting in prolonged denervation of the Schwann cells in the distal nerve as well as the motor end targets. Indeed, a major challenge for axon regeneration following long gap nerve repair using acellular strategies has been suggested to be senescence of host Schwann cells needed to fill the graft, whereby endogenous Schwann cells lack sufficient proliferative capacity to create enough progeny to fill graft zones more than a few centimeters. Several studies have shown that the expression of senescence markers in Schwann cells is associated with poor regeneration

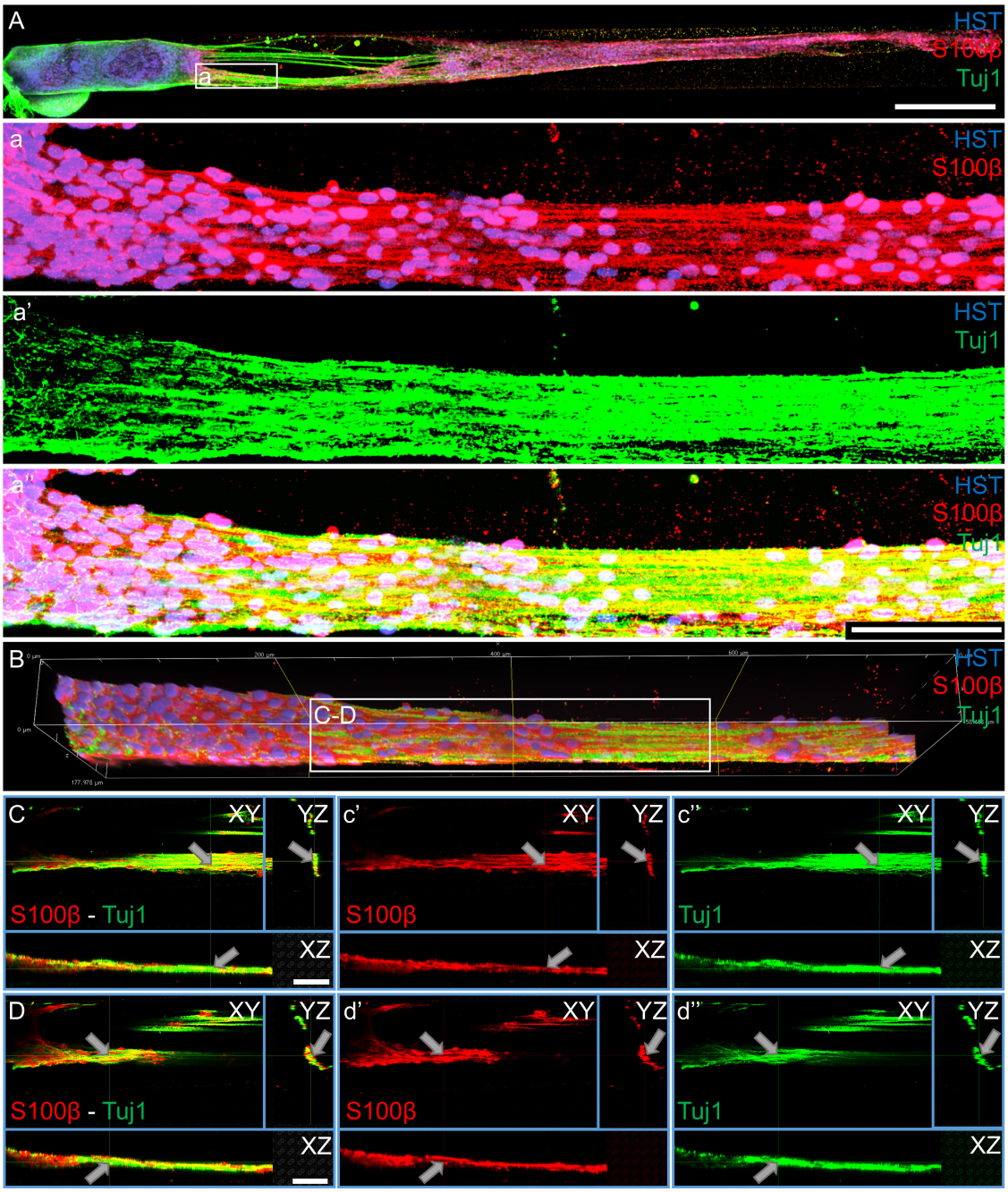

FIGURE 7 | Motor axons extending through longitudinally-aligned Schwann cells in TE-BoBs. **(A)** Motor axons extending from the neuronal aggregate (Tuj1) appear to interact closely with the highly aligned Schwann cells with bipolar morphology (S100β). **(a)** At higher magnification, highly bundled axons were visualized extending parallel to the longitudinally-aligned Schwann cells. **(B)** Volumetric reconstruction of high resolution confocal z-stack images demonstrating the relationship between the motor axons and longitudinally-aligned Schwann cells in the TE-BoB construct, which resembles the arrangement found between axons and Schwann cells in the pro-regenerative bands of Büngner *in vivo*. **(C,D)** Individual z-planes and orthogonal perspective views from **(B)** are shown to highlight that the axons are extending parallel to the longitudinally-aligned Schwann cells. Arrows denote same area across different perspectives further illustrating the relationship between the motor axons and Schwann cells within the TE-BoB. Scale bars: **(A)** 500 μm, **(a)** 100 μm, **(C,D)** 50 μm.

following long gap nerve repair using acellular nerve allografts (Saheb-Al-Zamani et al., 2013; Poppler et al., 2016; Hoben et al., 2018). However, in a recent review of the state-of-the-art for acellular approaches, the authors concluded that while they showed some potential, non-cellular constructs would likely need to incorporate a "recellularization step" to achieve comparable efficacy with the gold-standard autografts (Lovati et al., 2018).

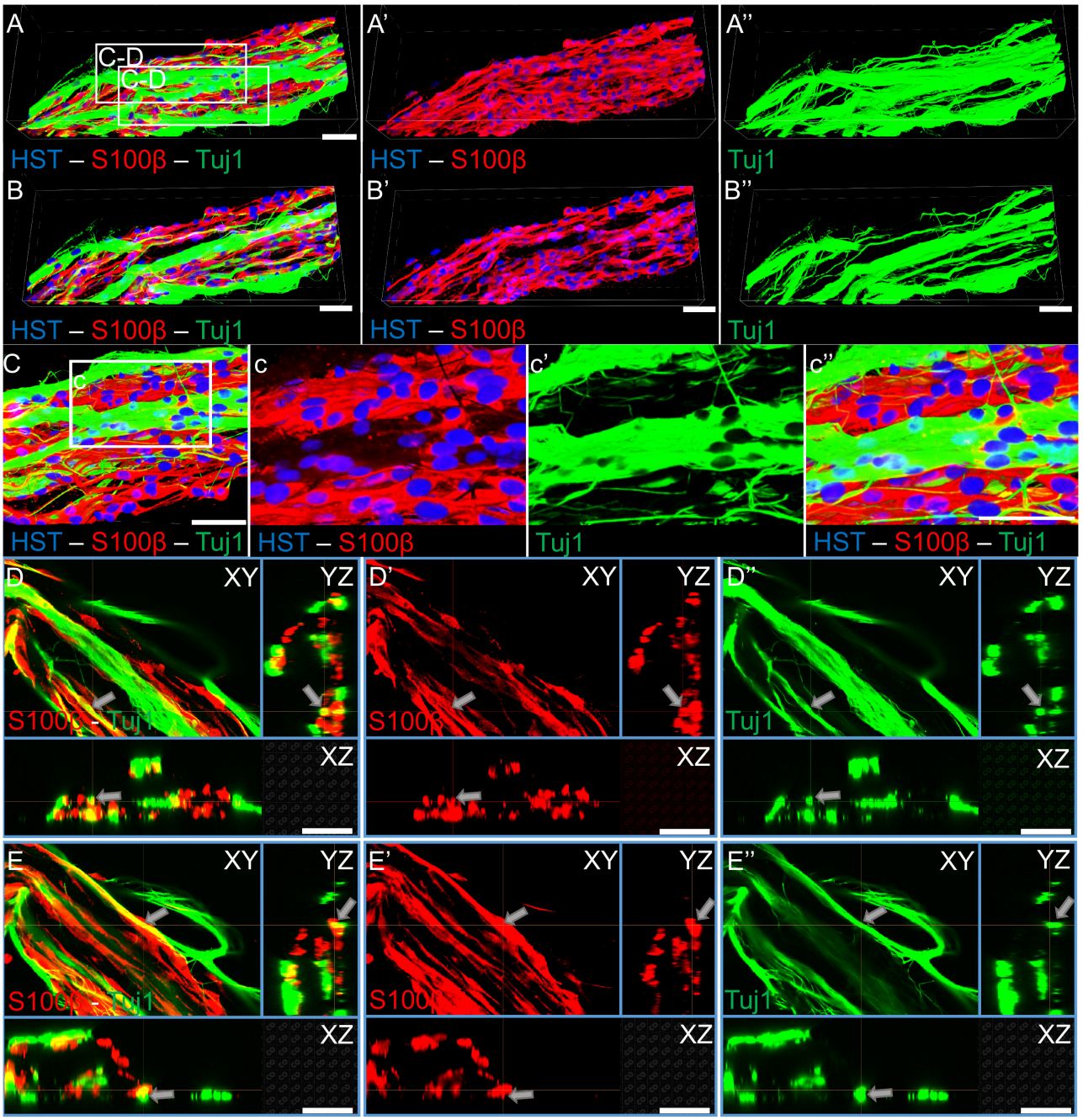

FIGURE 8 | Sensory axons extending through longitudinally-aligned Schwann cells in TE-BoBs. **(A)** Volumetric reconstruction of high resolution confocal z-stack images revealing the close interaction between the sensory axons extending from the DRG explant (Tuj1) and the longitudinally-aligned Schwann cells (S100β). **(B)** By examining specific z-planes within the volumetric reconstruction, axons can be clearly visualized closely following Schwann cells in a columnar organization with bipolar morphology. **(C)** Higher magnification reveals the relationship between the axons and the aligned Schwann cells resembling the arrangement found *in vivo* between axons and Schwann cells within the pro-regenerative bands of Büngner **(D,E)** Individual z-planes and orthogonal perspective views from **(C)** are shown to highlight that the axons are extending parallel to the longitudinally-aligned Schwann cells. Arrows denote same area across different perspectives further illustrating the relationship between the sensory axons and Schwann cells within the TE-BoB. Scale bars: Scale bars: **(A–E)** 50 μm.

In the current study, we aimed to develop a microtissue engineered living scaffold comprised of longitudinally-aligned Schwann cells as an alternative bridging strategy for peripheral nerve repair. The TE-BoB biofabrication protocol presented here would allow for the creation of a nerve graft that mimics the bundling of natural bands of Büngner that endogenously supports peripheral neuroregeneration. Similar to our previously reported microtissue engineered living scaffolds

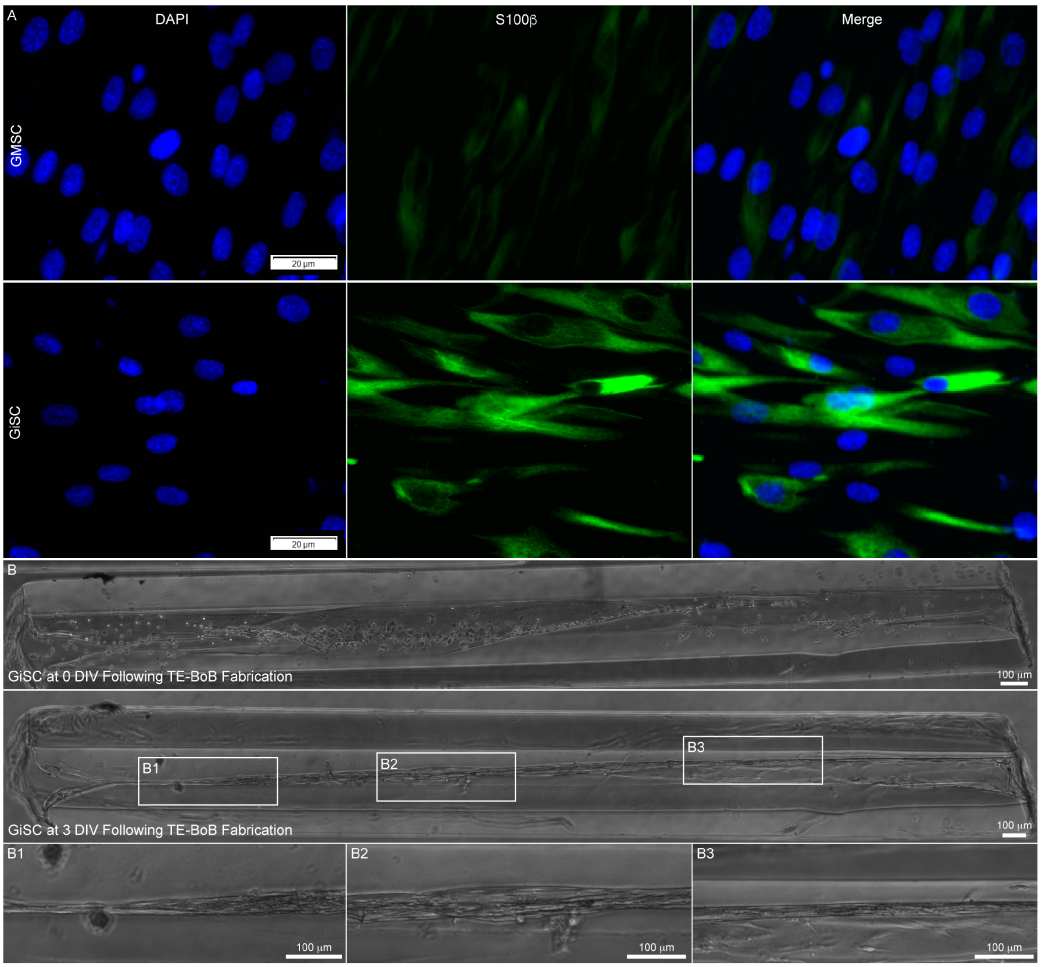

FIGURE 9 | Proof-of-concept fabrication of human gingiva-derived TE-BoBs. In a proof-of-concept demonstration using a potential clinical cell source, TE-BoBs were fabricated using human gingiva-derived mesenchymal stem cells (GMSC) that were induced into a Schwann cell-like phenotype (GiSC). **(A)** Immunocytochemistry was performed on planar cultures at 3 days *in vitro* to label for nuclei (DAPI) and Schwann cells (S100β). Greater S100β expression was found in the GiSC culture, indicating the protein commonly found in Schwann cells was upregulated and expressed in these cells. **(B)** GiSCs were seeded in micro-columns to fabricate human gingiva-derived TE-BoBs and were imaged with phase microscopy over time. At 3 days *in vitro* post TE-BoB fabrication, the cells self-assembled into a longitudinally aligned formation, similar to the rodent derived TE-BoBs. **(B1–B3)** Higher magnification imaging revealed tight bundles of cells with a bipolar morphology within the collagen matrix.

(Struzyna et al., 2015, 2017; Winter et al., 2016; Katiyar et al., 2018; O'Donnell et al., 2018), these Schwann cell constructs were constructed within a protective agarose hydrogel outer encasement with a collagen ECM inner core. Agarose was selected as the hydrogel for the micro-column due to several favorable biomaterial properties, such as biocompatibility, optical transparency, mass transport properties, relative inertness, and lack of adhesive ligands. In this application, the lack of adhesive ligands results in a hydrogel micro-column that provides geometric structure without inhibiting 3D cell/microtissue-mediated remodeling processes. During TE-BoB fabrication, Schwann cells extended processes and aligned longitudinally within the collagen substrate throughout the micro-column resulting in structural and phenotypic emulation of the bands of Büngner. For future translation, we demonstrated TE-BoBs fabrication a using clinically-applicable cell source, human Schwann cell-like cells derived from human gingiva-derived mesenchymal stem cells (GMSCs). These human TE-BoBs may present a clinically relevant solution to the morbidity associated with the commonly-used autograft and the limited efficacy of acellular bridging conduits/scaffolds.

After optimizing TE-BoB fabrication to produce longitudinally-aligned bundles of Schwann cells that emulate the structure and phenotype of bands of Büngner, we sought to test whether the TE-BoBs provided superior guidance of regenerating axons compared to Schwann cells in planar 2D culture or acellular agarose micro-columns containing only a collagenous matrix. Regenerating axons from MN and SN aggregates were found to precisely follow the dense longitudinal bundle of Schwann cells in the TE-BoBs, growing along and within the bundle itself. In contrast, the 2D controls revealed axonal extension from the aggregate in all directions.

Additionally, acellular collagen-coated micro-column controls revealed limited longitudinal directionality, indicating some contribution of the angle of curvature of the micro-column itself to the directional guidance of axon growth, as we reported previously (Struzyna et al., 2015, 2018).

Axonal outgrowth length was also quantified to determine the regenerative potential of TE-BoBs relative to 2D and 3D controls. Neuron aggregates plated in aligned Schwann cell constructs resulted in extensive axonal outgrowth for both MNs and SNs. Faster SN axonal growth was found compared to MNs, supporting intrinsic differences in regenerative capacity between these neuronal subtypes (Cheah et al., 2017). Substantial sensory axon outgrowth was found within TE-BoBs, often spanning the entire length of the 5 mm construct by 4 days *in vitro*. Thus, the length of the micro-columns limited the maximum axonal outgrowth in this study. TE-BoBs resulted in 2× greater SN outgrowth compared to acellular control counterparts. For MN aggregates, the effects of TE-BoBs were more striking. Here, TE-BoBs also enhanced MN axonal outgrowth, and resulted in a remarkable 8x greater motor axon outgrowth relative to acellular collagen control micro-columns. These results indicate that the extensive growth is due to the presence of Schwann cells rather than the agarose micro-column and collagen ECM. The extent of axonal bundling was also assessed to determine the effect of longitudinally-aligned Schwann cells in TE-BoBs compared to constructs lacking Schwann cells. SN and MN axon bundles in TE-BoBs both were larger and covered a significantly greater portion of the lumen compared to bundles in the respective control constructs. This effect also varied based on neuronal subtype, as the average size and percent coverage of the axon bundles were approximately 3.8 and 1.5 times greater, respectively, for SN than MN bundles. Interestingly, a strong predictor for eventual motor recovery after nerve repair is early sensory reinnervation, suggesting that rapid sensory axon regeneration occurs first followed by motor axon regeneration (Jaquet et al., 2001). Our findings corroborate the clinical observations by showing sensory axons grow faster than motor neurons in our model of aligned Schwann cells, which likely recapitulate elements of pro-regenerative Schwann cells present after nerve injury.

Schwann cells also have a crucial role following nerve injury and during regeneration to preserve the proximal neuron health and regenerative capacity by providing multi-faceted neurotrophic support (Gordon, 2009). In the current study, Tuj1 protein expression within the aggregate region was assessed as a surrogate marker for neuronal health. Greater Tuj1 protein expression was found in MNs co-cultured with longitudinally-aligned Schwann cells compared to the collagen only control; whereas no differences were found in SNs co-cultured with longitudinally-aligned Schwann cells compared to the collagen only control. These findings suggest there may be preferential preservation of the MNs within the explant region in the presence of aligned Schwann cells. Interestingly, these findings corroborate other work suggesting SNs may be more resilient to extrinsic microenvironmental factors at acute time points following injury (Cheah et al., 2017; Maggiore et al., 2020).

Several biomaterial approaches have been proposed as potential replacements for autografts by mimicking structural guidance and/or neurotrophic support of aligned Schwann cells. These acellular approaches may act by mimicking features of aligned Schwann cells by selecting bioactive materials (e.g., spider silk) or by fabricating scaffolds from electrospun fibers or microgrooved polymer substrates to provide anisotropic cues (Sun et al., 2010; Daud et al., 2012; Kornfeld et al., 2016). While acellular approaches may enhance infiltration and regenerative capacity of host Schwann cells, TE-BoBs are designed to better represent autografts by serving as a preformed living scaffold for regenerating axons. Indeed, TE-BoBs are comprised of Schwann cells with similar morphology, protein expression, and function as native the bands of Büngner found in autografts and the distal nerve after injury. Similar to other preformed tissue engineered neural constructs, the longitudinally-aligned Schwann cells are densely bundled within a protective tubular hydrogel outer encasement that can be easily placed in a commercially-available nerve conduit for transplantation across nerve defects.

We selected both primary SN and MN aggregates for use in our *in vitro* neurite outgrowth assay to ascertain the potential of TE-BoBs to facilitate axon regeneration following nerve injury. Previous studies have demonstrated that aligned Schwann cell constructs improve neurite outgrowth *in vitro*, and this prior work provides a useful basis of comparison for our current findings. For example, the neurite growth rate from SNs within aligned Schwann cells has been reported to be 270 μm/day on electrospun polycaprolactone fiber scaffolds (Daud et al., 2012) and range from 178 to 270 μm/day on tethered aligned collagen (Phillips et al., 2005; Georgiou et al., 2013). In comparison, TE-BoBs achieved an average sensory neurite growth rate of 1,166 μm/day, indicating that the sensory growth rate achieved within our constructs is 4.3–6.5× faster than that achieved by alternative approaches. In addition, to the best of our knowledge, the current study is the first report demonstrating accelerated axonal outgrowth from MNs using aligned Schwann cell constructs. However, MN neurite outgrowth in non-aligned Schwann cell-seeded biomaterials has been reported to be 50 μm/day on 3 mm thick Matrigel (Hyung et al., 2015) and 61 μm/day on a collagen sponge co-cultured with fibroblasts (Gingras et al., 2008). In contrast, our study using 3D aligned Schwann cell constructs found MN outgrowth in TE-BoBs to be 653 μm/day, suggesting that TE-BoBs achieved axon growth rates that are 10.7–13.1× greater than these previous reports. Additionally, several studies using the NG108-15 cell line have reported increased neurite outgrowth in aligned constructs (35–334 μm/day) (Armstrong et al., 2007; Kingham et al., 2007; Sun et al., 2010; Daud et al., 2012); however, while not providing an ideal comparison as these are only "neuron-like" cells (Kowtha et al., 1993; Molnar and Hickman, 2007), these axon outgrowth rates are still below those achieved in TE-BoBs. Collectively, these stark improvements in axon growth rates for both sensory and motor neurons support the potential for improved PNS regeneration using TE-BoBs.

The accelerated axonal outgrowth induced by TE-BoBs may be partially due to the presence of NGFR p75 in the

aligned Schwann cell constructs, which has been shown to facilitate axon pathfinding and regeneration in mice (Bentley and Lee, 2000; Tomita et al., 2007). However, regeneration is exponentially more complex than the signaling cascade of a single receptor. Relying on a single growth factor or receptor to promote regeneration is like trying to provide a solution to a complex problem with a one-word vocabulary. Tissue engineered constructs comprised of living cells are fluent in the language of cells. In contrast, acellular constructs may speak the equivalent of one word for each structural and/or soluble factor they contain, and acellular constructs are not "listening" to provide appropriately timed responses as is possible with living scaffolds. Indeed, TE-BoBs may be considered part of a broader class of living scaffolds that we have developed, which are designed to structurally and functionally mimic endogenous repair mechanisms relying on dynamic cell-to-cell interactions. For instance, we have engineered another glial-based construct comprised of aligned astrocytes that are designed to serve as a living scaffold for sustained neuronal replacement in the brain (Winter et al., 2016). By emulating the architecture and function of the endogenous glial tube in the rostral migratory stream, these constructs, described as a "tissue engineered rostral migratory stream" (TE-RMS) may redirect neuroblast migration and facilitate neuronal maturation (O'Donnell et al., 2018). Although both TE-BoBs and TE-RMS contain aligned glial cells fabricated using similar methodology, they interact with neurons very differently, promoting either axonal outgrowth or neuronal migration, respectively.

In addition to their therapeutic potential, TE-BoBs could also serve as an *in vitro* testbed for rapid, high throughput screening of mechanisms and efficacy of pro-regenerative strategies in a physiologically-relevant, 3D model of nerve regeneration. There is a growing demand across all science disciplines for tissue engineered 3D models which more closely mimic complex *in vivo* mechanisms, ultimately increasing translatable drug discovery and reducing the need for *in vivo* animal models (Nam et al., 2015; Vanderburgh et al., 2017; Rayner et al., 2018). Thus, the structural and phenotypical similarities between TE-BoBs and natural bands of Büngner suggest potential for future applications which require an anatomically- and physiologically-inspired pro-regenerative testing environment *in vitro*. For example, TE-BoBs may be useful to study various regenerative mechanisms, such as the role of c-Jun, a transcription factor that is considered the master regulator of the PNI response by governing the Schwann cell repair program, and the impact on neurite outgrowth following changes to pro-repair Schwann cell protein expression (e.g., GDNF, BDNF, NGF, or shh) (Arthur-Farraj et al., 2012).

There are several areas of TE-BoB optimization that will be explored in future studies. For instance, we were surprised to find that SNs extended neurites through the full length of the TE-BoBs used in the current experiments; since we can fabricate significantly longer TE-BoBs, future studies will investigate the maximal limits of axon growth facilitated by TE-BoBs. In addition, further optimization studies may be warranted to fabricate TE-BoBs specifically designed to accelerate motor or sensory axon outgrowth. Moreover, although agarose is a relatively inert biomaterial which would likely result in minimal *in vivo* host response, it exhibits slow rates of degradation and resorption *in vivo*. The modular fabrication methodology readily allows for the use of alternative hydrogel micro-columns and ECM constituents depending on the scientific question or the specific application. Therefore, it may be useful to investigate alternative encapsulation strategies, such as agarose composite hydrogels, such as agarose and gelatin, to further enhance degradation, resorption, biocompatibility, provide complimentary release of drugs or neurotrophic supplements, or to fine-tune other physical properties.

In this study, Schwann cells plated in the micro-column rapidly self-assembled into a longitudinal orientation. By tuning these physical properties, it may be possible to inhibit the self-assembly process and further investigate whether unaligned Schwann cells in a 3D micro-column increase neurite length/outgrowth. Notably, a previous study using genetic lineage tracing in a mouse model has shown that aligned Schwann cells are able to remyelinate regenerating axons *in vivo* (Gomez-Sanchez et al., 2017). Indeed, previous studies have reported myelination occurs around neurons co-cultured with primary rodent Schwann cells at later time points, often around 28 days *in vitro*, with the addition of ascorbic acid (Callizot et al., 2011). Therefore, it is possible that the axons extending within the aligned Schwann cell constructs may eventually undergo myelination.

Also, the current study generated TE-BoBs using both primary rodent Schwann cells and human GMSC-derived Schwann cells, however, future work will focus on these Schwann cells derived from easily accessible human GMSCs that are available throughout adulthood in humans (Zhang et al., 2018a,b). Additional investigation of TE-BoB fabrication using these human stem cells as well as neurite outgrowth and eventual myelination using human neurons – from allogeneic or even autologous sources – may provide mechanistic insights into the translational potential of TE-BoBs. Lastly, this biofabrication process is readily scalable, enabling the creation of longer lengths for testing in long gap PNI models that are greater than the critical nerve gap length of rats (2 cm) and humans (5 cm). These modifications would further advance TE-BoBs as an effective peripheral nerve repair strategy that mimics key advantages of the gold standard autograft repair, yet eliminates several of the shortcomings of current repair strategies.

The ultimate TE-BoB repair strategy for PNI may involve implanting several aligned Schwann cell constructs within a larger nerve conduit—for instance, one TE-BoB per fascicle—to provide living bridges spanning a segmental nerve defect. Indeed, it would be trivial to build multi-lumen constructs for TE-BoB fabrication, or even to stack multiple versions of the current TE-BoBs within a nerve guidance wrap, for testing in larger caliber nerves. We postulate that these TE-BoBs would augment endogenous mechanisms of regeneration by providing preformed bands of Büngner in cases where the gap lengths are too great for host Schwann cells to infiltrate and fill. Direct contact with the proximal side of the nerve defect will enable axons to extend through the engineered aligned Schwann cells and efficiently transverse the gap to ultimately reach the endogenous bands of Büngner within the distal nerve sheath that

provide targeted axon guidance to appropriate sensory and/or muscle targets. Given the promising results of this *in vitro* study, we will proceed to test the efficacy of the TE-BoB repair strategy using appropriate *in vivo* models of PNI.

CONCLUSION

We demonstrated the development and validation of the first tissue engineered bands of Büngner (TE-BoBs) comprised of three-dimensional, longitudinally aligned bundles of pro-regenerative Schwann cells. TE-BoBs were biofabricated based on a biomaterial guided cell self-assembly scheme using either rat primary Schwann cells or human stem cell derived Schwann cells. Functional testing using *in vitro* neurite outgrowth assays revealed that TE-BoBs directly facilitated and accelerated longitudinal axonal outgrowth from both primary motor and sensory neurons as compared to that measured in 2D and 3D control groups. Moreover, TE-BoBs achieved motor axon and sensory axon growth rates that were at least 10.7× and 4.3× faster, respectively, than rates achieved by alternative Schwann cell-mediated strategies. These self-assembled, aligned glial constructs represent a novel approach utilizing microtissue engineering strategies that specifically recapitulate 3D biological "living scaffolds" found *in vivo* to direct axonal outgrowth. Furthermore, given that long gap PNIs often result in insufficient axonal growth leading to failed muscle innervation, future repair strategies that can overcome this barrier have significant clinical relevance. With further development, these TE-BoBs may serve as implantable microtissue that can supplement or replace the use of autograft techniques to accelerate axon outgrowth across segmental defects and thereby enhance peripheral nerve regeneration and functional recovery.

DATA AVAILABILITY STATEMENT

The raw data supporting the conclusions of this article will be made available by the authors, without undue reservation.

ETHICS STATEMENT

Human gingival tissues were obtained as remnants of discarded tissues from healthy human subjects aged from 20 to 40 years old, who underwent routine dental procedures. Informed consents were obtained from all subjects and all procedures were performed under the approved Institutional Review Board (IRB) protocol at the University of Pennsylvania.

AUTHOR CONTRIBUTIONS

DKC conceived the study and provided the experimental design. KP and KH fabricated TE-BoBs and completed *in vitro* assays. KP and JB conducted the *in vitro* histological assessments and statistical analyses. KH, EP, and JO provided technical assistance with fabrication and quantification, and assisted with figure preparation. QZ and AL provided the human gingiva-derived Schwann cell-like cells. KP, JB, and DKC prepared the final manuscript. All authors provided critical feedback on the manuscript.

FUNDING

The authors would like to thank the Salzer lab for generously providing Schwann cells for use in these studies (New York University, New York, NY, United States). Financial support provided by the United States Department of Defense [CDMRP/JPC8-CRMRP W81XWH-16-1-0796 (Cullen) and MRMC W81XWH-15-1-0466 (Cullen)], the Department of Veterans Affairs [BLR&D Merit Review I01-BX003748 (Cullen)], the National Institutes of Health [NRSA Graduate Research Fellowship F31-NS103253 (O'Donnell)], and the Center for Undergraduate Research and Fellowships at the University of Pennsylvania [Panzer and Helm]. Opinions, interpretations, conclusions and recommendations are those of the author(s) and are not necessarily endorsed by the Department of Defense, the Department of Veterans Affairs, or the National Institutes of Health.

REFERENCES

Ali, Z. S., Bakar, D., Li, Y. R., Judd, A., Patel, H., Zager, E. L., et al. (2014). Utility of delayed surgical repair of neonatal brachial plexus palsy. *J. Neurosurg. Pediatr.* 13, 462–470. doi: 10.3171/2013.12.peds13382

Ali, Z. S., Heuer, G. G., Faught, R. W., Kaneriya, S. H., Sheikh, U. A., Syed, I. S., et al. (2015). Upper brachial plexus injury in adults: comparative effectiveness of different repair techniques. *J. Neurosurg.* 122, 195–201. doi: 10.3171/2014.9.jns132823

Armstrong, S. J., Wiberg, M., Terenghi, G., and Kingham, P. J. (2007). ECM molecules mediate both Schwann cell proliferation and activation to enhance neurite outgrowth. *Tissue Eng.* 13, 2863–2870. doi: 10.1089/ten.2007.0055

Arthur-Farraj, P. J., Latouche, M., Wilton, D. K., Quintes, S., Chabrol, E., Banerjee, A., et al. (2012). c-Jun reprograms Schwann cells of injured nerves to generate a repair cell essential for regeneration. *Neuron* 75, 633–647. doi: 10.1016/j.neuron.2012.06.021

Bentley, C. A., and Lee, K. F. (2000). p75 is important for axon growth and schwann cell migration during development. *J. Neurosci.* 20, 7706–7715. doi: 10.1523/jneurosci.20-20-07706.2000

Bozkurt, A., Brook, G. A., Moellers, S., Lassner, F., Sellhaus, B., Weis, J., et al. (2007). In vitro assessment of axonal growth using dorsal root ganglia explants in a novel three-dimensional collagen matrix. *Tissue Eng.* 13, 2971–2979. doi: 10.1089/ten.2007.0116

Bozkurt, A., Deumens, R., Beckmann, C., Olde Damink, L., Schugner, F., Heschel, I., et al. (2009). In vitro cell alignment obtained with a Schwann cell enriched microstructured nerve guide with longitudinal guidance channels. *Biomaterials* 30, 169–179. doi: 10.1016/j.biomaterials.2008.09.017

Callizot, N., Combes, M., Steinschneider, R., and Poindron, P. (2011). A new long term in vitro model of myelination. *Exp. Cell Res.* 317, 2374–2383. doi: 10.1016/j.yexcr.2011.07.002

Cheah, M., Fawcett, J. W., and Haenzi, B. (2017). Differential regenerative ability of sensory and motor neurons. *Neurosci. Lett.* 652, 35–40. doi: 10.1016/j.neulet.2016.11.004

Das, S., Sharma, M., Saharia, D., Sarma, K. K., Muir, E. M., and Bora, U. (2017). Electrospun silk-polyaniline conduits for functional nerve regeneration in rat sciatic nerve injury model. *Biomed. Mater.* 12:045025. doi: 10.1088/1748-605x/aa7802

Das, S., Sharma, M., Saharia, D., Sarma, K. K., Sarma, M. G., Borthakur, B. B., et al. (2015). In vivo studies of silk based gold nano-composite conduits for functional peripheral nerve regeneration. *Biomaterials* 62, 66–75. doi: 10.1016/j.biomaterials.2015.04.047

Daud, M. F., Pawar, K. C., Claeyssens, F., Ryan, A. J., and Haycock, J. W. (2012). An aligned 3D neuronal-glial co-culture model for peripheral nerve studies. *Biomaterials* 33, 5901–5913. doi: 10.1016/j.biomaterials.2012.05.008

Georgiou, M., Bunting, S. C., Davies, H. A., Loughlin, A. J., Golding, J. P., and Phillips, J. B. (2013). Engineered neural tissue for peripheral nerve repair. *Biomaterials* 34, 7335–7343. doi: 10.1016/j.biomaterials.2013.06.025

Gingras, M., Beaulieu, M. M., Gagnon, V., Durham, H. D., and Berthod, F. (2008). In vitro study of axonal migration and myelination of motor neurons in a three-dimensional tissue-engineered model. *Glia* 56, 354–364. doi: 10.1002/glia.20617

Gomez-Sanchez, J. A., Pilch, K. S., van der Lans, M., Fazal, S. V., Benito, C., Wagstaff, L. J., et al. (2017). After nerve injury, lineage tracing shows that myelin and remak schwann cells elongate extensively and branch to form repair schwann cells, which shorten radically on remyelination. *J. Neurosci.* 37, 9086–9099. doi: 10.1523/jneurosci.1453-17.2017

Gordon, T. (2009). The role of neurotrophic factors in nerve regeneration. *Neurosurg. Focus* 26:E3.

Gordon, T., and Stein, R. B. (1982). Reorganization of motor-unit properties in reinnervated muscles of the cat. *J. Neurophysiol.* 48, 1175–1190. doi: 10.1152/jn.1982.48.5.1175

Gordon, T., Tyreman, N., and Raji, M. A. (2011). The basis for diminished functional recovery after delayed peripheral nerve repair. *J. Neurosci.* 31, 5325–5334. doi: 10.1523/jneurosci.6156-10.2011

Hoben, G. M., Ee, X., Schellhardt, L., Yan, Y., Hunter, D. A., Moore, A. M., et al. (2018). Increasing nerve autograft length increases senescence and reduces regeneration. *Plast Reconstr. Surg.* 142, 952–961. doi: 10.1097/prs.0000000000004759

Hyung, S., Yoon Lee, B., Park, J. C., Kim, J., Hur, E. M., and Francis Suh, J. K. (2015). Coculture of primary motor neurons and schwann cells as a model for in vitro myelination. *Sci. Rep.* 5:15122.

Jaquet, J. B., Luijsterburg, A. J., Kalmijn, S., Kuypers, P. D., Hofman, A., and Hovius, S. E. (2001). Median, ulnar, and combined median-ulnar nerve injuries: functional outcome and return to productivity. *J. Trauma* 51, 687–692. doi: 10.1097/00005373-200110000-00011

Jessen, K. R., and Mirsky, R. (2016). The repair Schwann cell and its function in regenerating nerves. *J. Physiol.* 594, 3521–3531. doi: 10.1113/jp270874

Jessen, K. R., and Mirsky, R. (2019). The success and failure of the schwann cell response to nerve injury. *Front. Cell Neurosci.* 13:33. doi: 10.3389/fncel.2019.00033

Kaplan, H. M., Mishra, P., and Kohn, J. (2015). The overwhelming use of rat models in nerve regeneration research may compromise designs of nerve guidance conduits for humans. *J. Mater. Sci. Mater. Med.* 26:226.

Katiyar, K. S., Struzyna, L. A., Das, S., and Cullen, D. K. (2019). Stretch growth of motor axons in custom mechanobioreactors to generate long-projecting axonal constructs. *J. Tissue Eng. Regen. Med.* 13, 2040–2054. doi: 10.1002/term.2955

Katiyar, K. S., Struzyna, L. A., Morand, J. P., Burrell, J. C., Clements, B., Laimo, F. A., et al. (2020). Tissue engineered axon tracts serve as living scaffolds to accelerate axonal regeneration and functional recovery following peripheral nerve injury in rats. *Front. Bioeng. Biotechnol.* 8:492. doi: 10.3389/fbioe.2020.00492

Katiyar, K. S., Winter, C. C., Gordian-Velez, W. J., O'Donnell, J. C., Song, Y. J., Hernandez, N. S., et al. (2018). Three-dimensional tissue engineered aligned astrocyte networks to recapitulate developmental mechanisms and facilitate nervous system regeneration. *J. Vis. Exp.* 10:55848.

Kim, H. A., and Maurel, P. (2009). "Primary Schwann Cell Cultures," in *Protocols for Neural Cell Culture*, ed. L. C. Doering (Totowa, NJ: Humana Press), 253–268. doi: 10.1007/978-1-60761-292-6_15

Kingham, P. J., Kalbermatten, D. F., and Experimental, M.-D. (2007). Adipose-derived stem cells differentiate into a Schwann cell phenotype and promote neurite outgrowth in vitro. *Experimental* 207, 267–274. doi: 10.1016/j.expneurol.2007.06.029

Kornfeld, T., Vogt, P. M., Bucan, V., Peck, C. T., Reimers, K., and Radtke, C. (2016). Characterization and schwann cell seeding of up to 15.0 cm long spider silk nerve conduits for reconstruction of peripheral nerve defects. *J. Funct, Biomater.* 7:30. doi: 10.3390/jfb7040030

Kornfeld, T., Vogt, P. M., and Radtke, C. (2019). Nerve grafting for peripheral nerve injuries with extended defect sizes. *Wien Med. Wochenschr.* 169, 240–251. doi: 10.1007/s10354-018-0675-6

Kowtha, V. C., Quong, J. N., Bryant, H. J., and Stenger, D. A. (1993). Comparative electrophysiological properties of NG108-15 cells in serum-containing and serum-free media. *Neurosci. Lett.* 164, 129–133. doi: 10.1016/0304-3940(93)90874-k

Lovati, A. B., D'Arrigo, D., Odella, S., Tos, P., Geuna, S., and Raimondo, S. (2018). Nerve repair using decellularized nerve grafts in rat models. a review of the literature. *Front. Cell Neurosci.* 12:427. doi: 10.3389/fncel.2018.00427

Maggiore, J. C., Burrell, J. C., Browne, K. D., Katiyar, K. S., Laimo, F. A., Ali, Z., et al. (2020). Peripheral nerve repair using tissue engineered "Living Scaffolds" comprised of stretch-grown aligned axonal tracts promotes survival of spinal cord motor neurons. *bioRxiv* [Preprint]. doi: 10.1101/847988

Molnar, P., and Hickman, J. J. (2007). Modeling of action potential generation in NG108-15 cells. *Methods Mol. Biol.* 403, 175–184. doi: 10.1007/978-1-60327-090-8_11

Nam, K. H., Smith, A. S., Lone, S., Kwon, S., and Kim, D. H. (2015). Biomimetic 3D tissue models for advanced high-throughput drug screening. *J. Lab Autom.* 20, 201–215. doi: 10.1177/2211068214557813

O'Donnell, J. C., Jackson, J. G., and Robinson, M. B. (2016). Transient Oxygen/Glucose deprivation causes a delayed loss of mitochondria and increases spontaneous calcium signaling in astrocytic processes. *J. Neurosci.* 36, 7109–7127. doi: 10.1523/jneurosci.4518-15.2016

O'Donnell, J. C., Katiyar, K. S., Panzer, K. V., and Cullen, D. K. (2018). A tissue-engineered rostral migratory stream for directed neuronal replacement. *Neural Regen. Res.* 13, 1327–1331. doi: 10.4103/1673-5374.235215

Pfister, B. J., Gordon, T., Loverde, J. R., Kochar, A. S., Mackinnon, S. E., and Cullen, D. K. (2011). Biomedical engineering strategies for peripheral nerve repair: surgical applications, state of the art, and future challenges. *Crit. Rev. Biomed. Eng.* 39, 81–124. doi: 10.1615/critrevbiomedeng.v39.i2.20

Phillips, J. B., Bunting, S. C., Hall, S. M., and Brown, R. A. (2005). Neural tissue engineering: a self-organizing collagen guidance conduit. *Tissue Eng.* 11, 1611–1617. doi: 10.1089/ten.2005.11.1611

Poppler, L. H., Ee, X., Schellhardt, L., Hoben, G. M., Pan, D., Hunter, D. A., et al. (2016). Axonal growth arrests after an increased accumulation of schwann cells expressing senescence markers and stromal cells in acellular nerve allografts. *Tissue Eng. Part A* 22, 949–961. doi: 10.1089/ten.tea.2016.0003

Ray, W. Z., and Mackinnon, S. E. (2010). Management of nerve gaps: autografts, allografts, nerve transfers, and end-to-side neurorrhaphy. *Exp. Neurol.* 223, 77–85. doi: 10.1016/j.expneurol.2009.03.031

Rayner, M. L. D., Laranjeira, S., Evans, R. E., Shipley, R. J., Healy, J., and Phillips, J. B. (2018). Developing an in vitro model to screen drugs for nerve regeneration. *Anat. Rec.* 301, 1628–1637. doi: 10.1002/ar.23918

Robinson, L. R. (2000). Traumatic injury to peripheral nerves. *Muscle Nerve* 23, 863–873. doi: 10.1002/(sici)1097-4598(200006)23:6<863::aid-mus4>3.0.co;2-0

Ruijs, A. C., Jaquet, J. B., Kalmijn, S., Giele, H., and Hovius, S. E. (2005). Median and ulnar nerve injuries: a meta-analysis of predictors of motor and sensory recovery after modern microsurgical nerve repair. *Plast Reconstr. Surg.* 116, 484–494. discussion 495-6 doi: 10.1097/01.prs.0000172896.86594.07

Saheb-Al-Zamani, M., Yan, Y., Farber, S. J., Hunter, D. A., Newton, P., Wood, M. D., et al. (2013). Limited regeneration in long acellular nerve allografts is associated with increased Schwann cell senescence. *Exp. Neurol.* 247, 165–177. doi: 10.1016/j.expneurol.2013.04.011

Salzer, J. L. (2015). Schwann cell myelination. *Cold Spring Harb. Perspect. Biol.* 7:a020529.

Schindelin, J., Arganda-Carreras, I., Frise, E., Kaynig, V., Longair, M., Pietzsch, T., et al. (2012). Fiji: an open-source platform for biological-image analysis. *Nat. Methods* 9, 676–682. doi: 10.1038/nmeth.2019

Struzyna, L. A., Adewole, D. O., Gordian-Velez, W. J., Grovola, M. R., Burrell, J. C., Katiyar, K. S., et al. (2017). Anatomically inspired three-dimensional

micro-tissue engineered neural networks for nervous system reconstruction, modulation, and modeling. *J. Vis. Exp.* 10:55609.

Struzyna, L. A., Browne, K. D., Brodnik, Z. D., Burrell, J. C., Harris, J. P., Chen, H. I., et al. (2018). Tissue engineered nigrostriatal pathway for treatment of Parkinson's disease. *J. Tissue Eng. Regen. Med.* 12, 1702–1716. doi: 10.1002/term.2698

Struzyna, L. A., Harris, J. P., Katiyar, K. S., Chen, H. I., and Cullen, D. K. (2015). Restoring nervous system structure and function using tissue engineered living scaffolds. *Neural Regen. Res.* 10, 679–685. doi: 10.4103/1673-5374.156943

Sun, M., McGowan, M., Kingham, P. J., Terenghi, G., and Downes, S. (2010). Novel thin-walled nerve conduit with microgrooved surface patterns for enhanced peripheral nerve repair. *J. Mater. Sci Mater. Med.* 21, 2765–2774. doi: 10.1007/s10856-010-4120-7

Tomita, K., Kubo, T., Matsuda, K., Fujiwara, T., Yano, K., Winograd, J. M., et al. (2007). The neurotrophin receptor p75NTR in Schwann cells is implicated in remyelination and motor recovery after peripheral nerve injury. *Glia* 55, 1199–1208. doi: 10.1002/glia.20533

Vanderburgh, J., Sterling, J. A., and Guelcher, S. A. (2017). 3D printing of tissue engineered constructs for in vitro modeling of disease progression and drug screening. *Ann. Biomed. Eng.* 45, 164–179. doi: 10.1007/s10439-016-1640-4

Wang, E., Inaba, K., Byerly, S., Escamilla, D., Cho, J., Carey, J., et al. (2017). Optimal timing for repair of peripheral nerve injuries. *J. Trauma Acute Care Surg.* 83, 875–881. doi: 10.1097/ta.0000000000001570

Weightman, A., Jenkins, S., Pickard, M., Chari, D., and Yang, Y. (2014). Alignment of multiple glial cell populations in 3D nanofiber scaffolds: toward the development of multicellular implantable scaffolds for repair of neural injury. *Nanomedicine* 10, 291–295. doi: 10.1016/j.nano.2013.09.001

Winter, C. C., Katiyar, K. S., Hernandez, N. S., Song, Y. J., Struzyna, L. A., Harris, J. P., et al. (2016). Transplantable living scaffolds comprised of micro-tissue engineered aligned astrocyte networks to facilitate central nervous system regeneration. *Acta Biomater.* 38, 44–58. doi: 10.1016/j.actbio.2016.04.021

Zager, E. L. (2014). For this peripheral nerve lesion, it is best to avoid the knife. *World Neurosurg.* 82, 333–334. doi: 10.1016/j.wneu.2013.10.054

Zhang, P. X., Han, N., Kou, Y. H., Zhu, Q. T., Liu, X. L., Quan, D. P., et al. (2019). Tissue engineering for the repair of peripheral nerve injury. *Neural Regen. Res.* 14, 51–58.

Zhang, Q., Nguyen, P. D., Shi, S., Burrell, J. C., Cullen, D. K., and Le, A. D. (2018a). 3D bio-printed scaffold-free nerve constructs with human gingiva-derived mesenchymal stem cells promote rat facial nerve regeneration. *Sci. Rep.* 8:6634.

Zhang, Q., Nguyen, P. D., Shi, S., Burrell, J. C., Xu, Q., Cullen, D. K., et al. (2018b). Neural crest stem-like cells non-genetically induced from human gingiva-derived mesenchymal stem cells promote facial nerve regeneration in rats. *Mol. Neurobiol.* 55, 6965–6983. doi: 10.1007/s12035-018-0913-3

Zhang, Q., Shi, S., Liu, Y., Uyanne, J., Shi, Y., Shi, S., et al. (2009). Mesenchymal stem cells derived from human gingiva are capable of immunomodulatory functions and ameliorate inflammation-related tissue destruction in experimental colitis. *J. Immunol.* 183, 7787–7798. doi: 10.4049/jimmunol.0902318

Conflict of Interest: The authors declare that the research was conducted in the absence of any commercial or financial relationships that could be construed as a potential conflict of interest.

frontiers in Bioengineering and Biotechnology

ORIGINAL RESEARCH
published: 10 February 2021
doi: 10.3389/fbioe.2021.615218

All-Polymer Printed Low-Cost Regenerative Nerve Cuff Electrodes

Laura M. Ferrari [1,2,3†], Bruno Rodríguez-Meana [4†], Alberto Bonisoli [1,2†], Annarita Cutrone [2], Silvestro Micera [2,5], Xavier Navarro [4], Francesco Greco [1,6,7] and Jaume del Valle [4*]*

[1] Center for Micro-BioRobotics @SSSA, Istituto Italiano di Tecnologia, Pontedera, Italy, [2] The BioRobotics Institute and Department of Excellence in Robotics and AI, Scuola Superiore Sant'Anna, Pontedera, Italy, [3] Université Côte d'Azur, INRIA, Sophia Antipolis, France, [4] Department of Cell Biology, Physiology and Immunology, Institute of Neurosciences, Universitat Autònoma de Barcelona, and CIBERNED, Bellaterra, Spain, [5] Bertarelli Foundation Chair in Translational NeuroEngineering, Center for Neuroprosthetics and Institute of Bioengineering, Ecole Polytechnique Federale de Lausanne, Lausanne, Switzerland, [6] Institute of Solid State Physics, NAWI Graz, Graz University of Technology, Graz, Austria, [7] Department of Life Science and Medical Bioscience, Graduate School of Advanced Science and Engineering, Waseda University, Tokyo, Japan

OPEN ACCESS

Edited by:
Diego Mantovani, Laval University, Canada

Reviewed by:
Tzu-Wei Wang, National Tsing Hua University, Taiwan
Lorenza Draghi, Politecnico di Milano, Italy

****Correspondence:***
Francesco Greco
francesco.greco@tugraz.at
Jaume del Valle
jaume.delvalle@uab.cat

† These authors have contributed equally to this work

Specialty section:
This article was submitted to Tissue Engineering and Regenerative Medicine, a section of the journal Frontiers in Bioengineering and Biotechnology

Received: *08 October 2020*
Accepted: *11 January 2021*
Published: *10 February 2021*

Citation:
Ferrari LM, Rodríguez-Meana B, Bonisoli A, Cutrone A, Micera S, Navarro X, Greco F and del Valle J (2021) All-Polymer Printed Low-Cost Regenerative Nerve Cuff Electrodes. Front. Bioeng. Biotechnol. 9:615218. doi: 10.3389/fbioe.2021.615218

Neural regeneration after lesions is still limited by several factors and new technologies are developed to address this issue. Here, we present and test in animal models a new regenerative nerve cuff electrode (RnCE). It is based on a novel low-cost fabrication strategy, called "Print and Shrink", which combines the inkjet printing of a conducting polymer with a heat-shrinkable polymer substrate for the development of a bioelectronic interface. This method allows to produce miniaturized regenerative cuff electrodes without the use of cleanroom facilities and vacuum based deposition methods, thus highly reducing the production costs. To fully proof the electrodes performance *in vivo* we assessed functional recovery and adequacy to support axonal regeneration after section of rat sciatic nerves and repair with RnCE. We investigated the possibility to stimulate the nerve to activate different muscles, both in acute and chronic scenarios. Three months after implantation, RnCEs were able to stimulate regenerated motor axons and induce a muscular response. The capability to produce fully-transparent nerve interfaces provided with polymeric microelectrodes through a cost-effective manufacturing process is an unexplored approach in neuroprosthesis field. Our findings pave the way to the development of new and more usable technologies for nerve regeneration and neuromodulation.

Keywords: regenerative cuff electrodes, low-cost fabrication, inkjet printing, wrinkling, organic bioelectronics, PEDOT:PSS, peripheral nerve interfaces

INTRODUCTION

Injuries to the peripheral nervous system (PNS) result in the partial or total loss of the motor, sensory and autonomic functions of the body part innervated by the lesioned nerve. The quality of life of people who suffer from these conditions is significantly reduced and major social consequences are payed in terms of health-care (Rosberg et al., 2005). When the whole nerve is transected and the two nerve ends cannot be surgically rejoined, an autologous nerve graft is commonly interposed in clinical practice to support axons regeneration. Nerve conduits have been extensively reported as a clinical alternative to the autograft repair (Deumens et al., 2010). However, even with surgical repair, axonal regeneration may fail or be insufficient to allow

functional reinnervation of targets and recovery of all motor and sensory functions. Prostheses and exoskeletons are therapeutic strategies used to improve patients' quality of life after severe nerve injuries or limb amputations. For the application of neuroprosthesis, peripheral nerve interfaces (PNIs) are a key element as they provide a link between the nervous system and the mechanical device (del Valle and Navarro, 2013).

Typically, PNIs are produced through state-of-the-art microfabrication and micromachining processes. Standard lithographic techniques, characterized by expensive high vacuum and high temperature processes, are commonly and efficiently used for the last 20 years (Stieglitz and Meyer, 1999; Boretius et al., 2010). Together with the drawbacks of cleanroom processes, some of the traditional metallic materials adopted (e.g., Au, Pt) have limitations in interfacing the soft biological tissues (Bellamkonda et al., 2012). In the last decade, organic electronic materials (mainly conducting polymers and semiconductors) have shown their potential in applications where electronics interfaces biology. Given their soft mechanical properties and mixed conductivity (ionic and electronic) (Rivnay et al., 2013), they proved to be an optimal bioelectronic interface, as already demonstrated in a variety of applications (Berggren and Richter-Dahlfors, 2007; Khodagholy et al., 2013; Simon et al., 2016). Organic materials represent the new frontier for PNIs development, since they can enhance signal quality, biocompatibility and chronic reliability (Bettinger, 2018). Particularly, organic materials have shown an increased charge injection capacity compared to standard metallic materials (Green et al., 2013), thus enabling the miniaturization of electrode arrays (Bettinger, 2018).

One of the benefits of adopting organic electronic materials is that they can be suited for printing. Inkjet printing is a large-scale and low-cost production process. It is a non-contact additive manufacturing method that operates in ambient conditions, at low temperatures. This allows the adoption of flexible substrates, with limited stability at high temperature, such as thermoplastic foils often exploited in flexible/printed electronics (Wong and Salleo, 2009; Caironi and Noh, 2015). The technique is suited for the deposition of various functional materials, as conductive polymers (CPs), organic semiconductors, polymers used for dielectric/passivation, which are solution processable (Berggren et al., 2007; Elschner et al., 2010). However, because of intrinsic limitations in resolution, inkjet printing cannot reach the miniaturization level required in some applications and addressable by cleanroom processing. Typically inkjet printing of features with lateral size smaller than $\sim$100 μm can be challenging, at least with commercially available facilities. On the other hand, there is a growing interest in adopting self-assembling methods for surface patterning, especially on a large area. Surface wrinkling is a self-assembling phenomenon which has been proposed as a rapid and convenient method for surface patterning (Genzer and Groenewold, 2006; Rodríguez-Hernández, 2015). It allows for tunable texturing with quasi periodic topographic motifs (with features size ranging from tens-hundreds of nm up to mm scale) over very large area (up to several m^2). Wrinkled surfaces of various materials have been successfully tested in various applications, such as stretchable electronics, sensors and cell cultures, among others (Chen et al., 2011; Greco et al., 2012). One of the possible approaches to obtain surface wrinkling relies on the use of heat-shrink thermoplastic substrates for the 3D patterning of thin films deposited onto them. By thermally inducing the in-plane shrinkage of the substrate, the top-deposited thin film buckles, resulting in a conformal wrinkled skin (Greco et al., 2013; Bonisoli et al., 2017). Concurrently, the heat-shrinking provides a suitable method for miniaturization (down to e.g., 10% of original size) of any pattern (i.e., circuit, electrode), while retaining the pristine large surface area (Gabardo et al., 2017; Chan et al., 2018). In this way, the charge injection capacity of the electrode per unit area can be increased, which is an attractive feature especially for stimulating electrodes (Green and Abidian, 2015). Moreover, electrodes miniaturization has positive effects on improving signal resolution during neural recording (Lacour et al., 2016).

Here we propose a novel non-conventional microfabrication technique to produce low-cost all-polymer PNIs. The produced design, named regenerative nerve cuff electrode (RnCE), consists in a flexible plastic tube embedding conducting polymer microelectrodes facing the lumen. Miniaturized 3D textured electrodes are produced by the combination of inkjet printing and shrink-induced surface wrinkling (Print and Shrink). To this aim, a heat-shrinkable polyolefin (PO) wrap film is used as low-cost, optically transparent and flexible substrate. Heat-shrink PO films are commonly adopted in food packaging and have been proposed as biocompatible substrates for cell culturing (Chen et al., 2011; Lew et al., 2011; Sharma et al., 2011), as well as molds for PDMS substrates in similar applications (Nguyen et al., 2009; Chen et al., 2014; Shum et al., 2017). The materials here adopted for the electrodes patterning are poly(3,4-ethylenedioxythiophene):poly(styrene sulfonate) (PEDOT:PSS) and SU-8. PEDOT:PSS, the most used conducting polymer in bioelectronics, is commercially available as waterborne dispersion and it has shown excellent chemical-physical stability and biocompatibility (Groenendaal et al., 2000; Bernards et al., 2008; Malhotra and Ali, 2017). Biocompatibility and stability of various printable PEDOT:PSS formulations have been investigated, revealing the crucial role of thermal annealing and additives (Stríteský et al., 2018). In implantable devices, PEDOT:PSS has shown to induce lower foreign body reaction (FBR) over other polymers (Cellot et al., 2016). Moreover, the use of CPs as coatings for neural electrodes was reported to lower the impedance at the electrode-tissue interface as compared to the bare metal electrode (Asplund et al., 2010), thus enhancing the charge transfer and downplaying the electrical insulation effect due to the encapsulation of the implant. SU-8, an epoxy resin-based dielectric, is used for electrical passivation, given its biocompatibility (Nemani et al., 2013) and the widespread use in neural probes applications (Cho et al., 2008; Altuna et al., 2013; Márton et al., 2020).

One of the main challenges for regenerative PNIs is the production of non-obtrusive interfaces, defined as transparent interfaces, still retaining a good degree of stimulation selectivity. Previous works remarked the effort in the assessment of transparent electrodes, as the regenerative multielectrode interface (REMI) (Garde et al., 2009), the regenerative scaffold

electrode (RSE) (Clements et al., 2012) and more recently the double-aisle regenerative electrode (Delgado-Martínez et al., 2017), comprising a silicone tube with a polyimide foil interposed in between and gold microelectrodes located on the two opposing sides of the foil. The latter was developed by exploiting the same manufacturing process used for intraneural PNIs, such as the thin film longitudinal intrafascicular electrode (tf-LIFE) (Lago et al., 2007) or the transversal intrafascicular multielectrode (TIME) (Boretius et al., 2010), and its design allowed unobstructed nerve regeneration, further enabling an interfacing with the axons. Despite the plurality of advantages of the design, the techniques used for the manufacturing of the above-mentioned devices are very expensive and require a cleanroom environment.

In this article we describe the RnCEs low-cost fabrication process and their performance as a regenerative nerve guide and PNI *in vivo*. Firstly, we assessed the RnCEs design as permissive for axonal regeneration across a nerve gap by using passive (i.e., without polymeric microelectrodes) PEDOT:PSS coated PO tubes (PPP tubes). Once the adequacy for axonal regeneration has been confirmed, the active RnCEs, with patterned polymeric microelectrodes, was implanted and tested *in vivo* for nerve stimulation. Functional analysis, comprising electrophysiological tests and sensory recovery, was performed. After 90 days, the implanted RnCEs were tested for their ability to stimulate the regenerated nerve axons and their selectivity assessed in relation to transparency.

MATERIALS AND METHODS

Regenerative Nerve Cuff Electrode (RnCE) Fabrication

The Print and Shrink fabrication started with the printing process, which entailed multiple layers deposition (**Figure 1**) with a lab-scale inkjet printer (DMP-2800; Fujifilm). Heat-shrink PO wrap films (Cryovac D-940; Shrink Packaging Sealed Air, 18 μm thickness) were used as substrates. PO films adopted here had a nominal free shrink of 70–75% upon heating at 120°C. The conductive materials used for printing were a PEDOT:PSS-based ink (PJET700; Clevios) mixed with 10% (w/w) glycerol (Farmalabor), and an Ag-precursor ink (Reactive silver ink; Sigma-Aldrich). As dielectric material, a solution of SU-8 (SU-8 2002; MicroChem Corp.), an epoxy resin-based dielectric, was used. The pristine SU-8 2002 (SU-8 29%) is characterized by 29% solid content in cyclopentanone solution. A less viscous SU-8 formulation (SU-8 10%), characterized by 10% solid content, was obtained by adding cyclopentanone (Sigma-Aldrich) to the SU-8 2002. For each step, a single layer was printed, at room temperature, using 1 jetting nozzle and a specific drop spacing (ds). The ds, which corresponds to the distance between centers of two contiguous jetted drops, was tuned in order to deposit the thinnest uniform layer possible. Before the deposition, polyimide (PI) adhesive tape (Kapton®) and metal clips (Double clips 25 mm; Lebez) were used to fix the PO film (70 mm x 40 mm) to a glass support slide (75 × 50 mm). Air plasma (Colibrì plasma system; Gambetti) was performed to activate the PO surface before each printing step with the following settings: 50 s, 10 W before printing of PEDOT:PSS and Ag ink; 100 s, 10 W before SU-8 printing.

The deposition started with the patterning of the electrodes, the feed lines and the contact pads by printing of the PEDOT:PSS-based ink with 30 μm ds (**Figure 1A**). Ag ink was then deposited with 40 μm ds onto the PEDOT:PSS terminal pads (**Figure 1B**). After drying overnight at room temperature, the dielectric layer was printed. Firstly, the SU-8 10% was printed with 70 μm ds [SU-8 (1), **Figure 1C**], dried by heating (95°C, 60 s), cured for cross-linking by UV exposure (365 nm, 410 mW cm-2, 30 s) with a spot light source (Lightningcure LC8; Hamamatsu) and then heated again (95°C, 60 s). During the thermal processes, in order to avoid its shrinkage, the substrate was accurately fixed to the glass slide by using extra Kapton tape and metal clips, three clips for long sides, one clip for short sides. A layer of SU-8 29% was then printed, with 50 μm ds, to efficiently insulate the conductive traces [SU-8 (2), **Figure 1D**]. Shortly after the deposition, the tape was removed and the PO was fixed to the glass slide only by clamping the short sides with metal clips (one clip for each). Then, by heating at 110°C for 4 min, the PO film uniaxially shrunk, along the direction parallel to the clamped sides (**Figures 1E–G**). After shrinkage, the PO was fixed to the glass slide by using Kapton tape and clips on each side (to avoid further shrinkage), and the SU-8 29% layer was cured for cross-linking by UV exposure (30 s) followed by heating (70°C, 4 min). In order to produce the proper final tube's dimension (10 mm length, 2.5 mm lumen) the PO film (≈30 μm final thickness, after shrinkage) was cut as shown in **Figure 2A**. The "tubing area", 10 mm square, was rolled up by wrapping it around a cylindrical metal mold with diameter 2.5 mm. The overlapping "binding areas" were bonded by pressing them together with a flat scalpel heated with a hot gun. A thin layer of poly(dimethyl siloxane) (PDMS; Sylgard 184) was added on the closure of the tubes to ensure the sealing. The PDMS was finely brushed onto the closure of the tubes, supported by silanized glass pipettes. The silanization process, adopted to prevent the tubes from sticking to the support, was performed by exposing the glass pipette to 30 min chlorotrimethylsilane (99%, Sigma Aldrich) vapor created in an airtight plastic container by putting a small quantity of solution in a vial (Bernardeschi et al., 2015). The sealed tubes were then left to dry in open air for 1 day.

The final RnCE is depicted in **Figure 2B**. A custom PCB (CadLine) (**Figure 2C**) was connected to the RnCE pads area with conductive epoxy (Ag/epoxy adhesive; Chemtronics). Connections were then insulated with UV-curable glue (Bondic; 365 nm, 410 mW cm-2, 60 s). A suture flap (**Figure 2B**) was left near the pads area to allow the anchoring of the RnCE at one of the nerve ends during the surgical procedure for implantation.

RnCE Surface and Electrical Characterization

The thickness of each printed layer was evaluated by printing the inks on a silicon wafer and measuring with a stylus profiler (P-6 stylus profiler; KLA Tencor). The inner wall surface topography was analyzed by means of atomic force

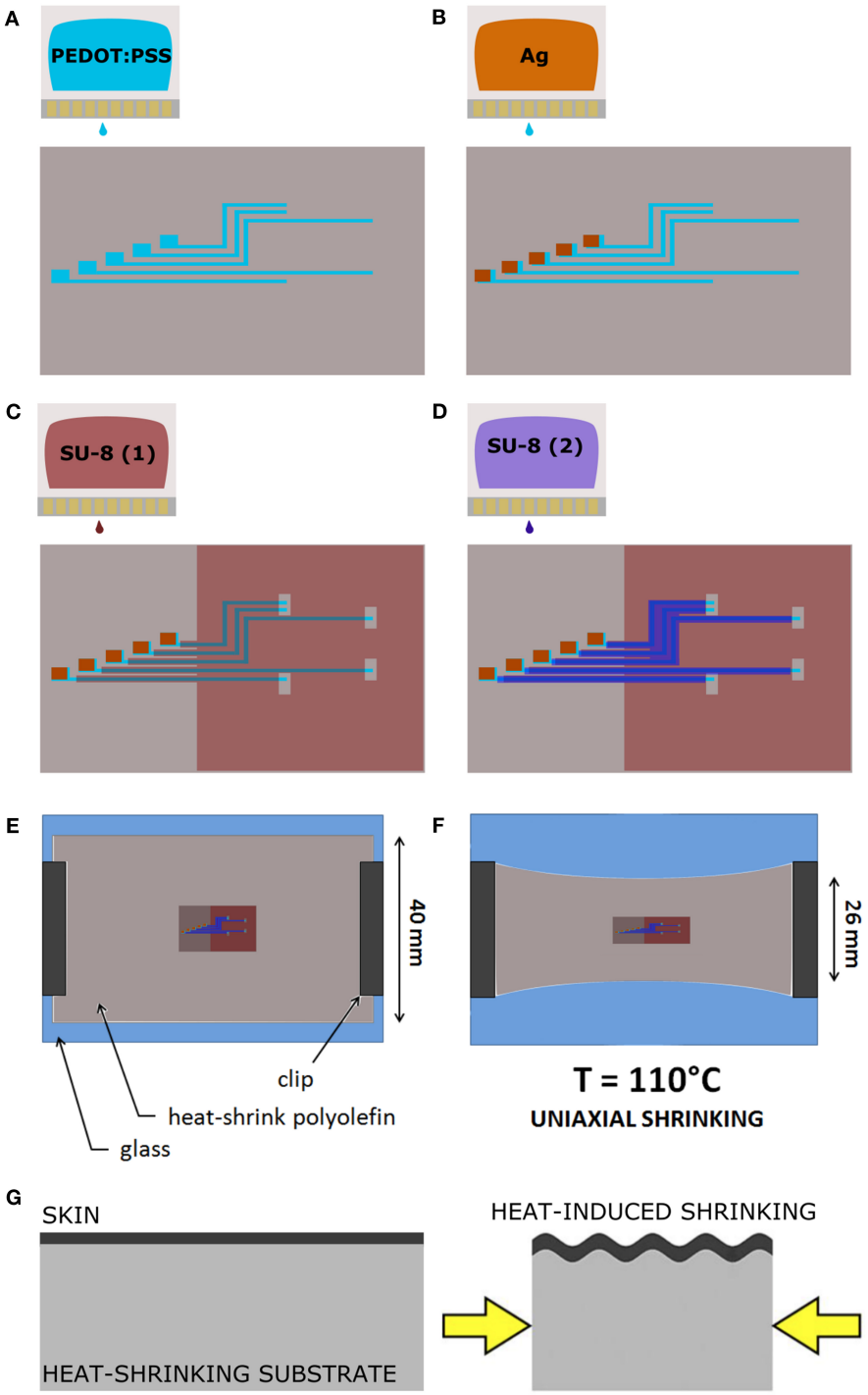

FIGURE 1 | The Print and Shrink fabrication process. **(A)** Inkjet printing of the conductive ink based on PEDOT:PSS. **(B)** Inkjet printing of the Ag ink. **(C)** Inkjet printing of the first SU-8 10% layer. **(D)** Inkjet printing of the SU-8 29% layer. **(E)** PO film clamped onto the glass slide. **(F)** Thermally-induced uniaxial shrinking. **(G)** Schematics of surface wrinkling induced by heat-shrinking.

microscopy (AFM) in order to have an insight on the spatial periodicity and the height of wrinkles. AFM images were acquired with a Veeco Innova Scanning Probe Microscope operating in tapping mode with a silicon probe (NSG01; NT-MDT), and scanning in the direction perpendicular to the wrinkle axis. The images were then analyzed with a free and

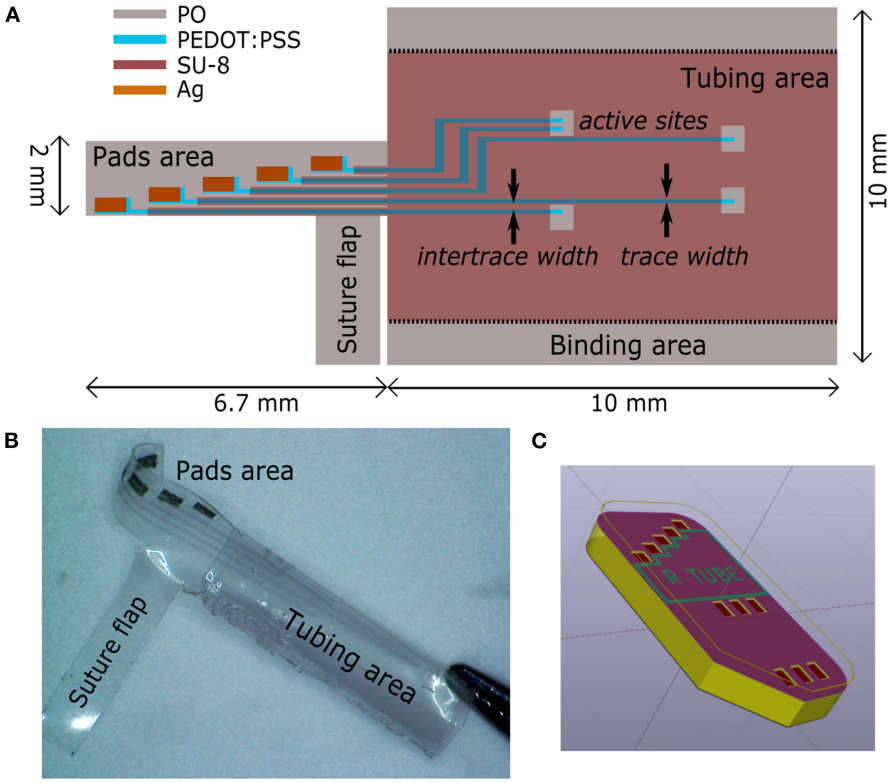

FIGURE 2 | Regenerative nerve Cuff Electrodes (RnCEs). **(A)** Planar view of the final device, with the design of the tube lumen and geometrical references before the rolling up. **(B)** Picture of the final RnCE. **(C)** Rendering of the device with an inset of the custom PCB.

open source software (Gwyddion[1]) by extracting the sequences of peaks (x-z profiles) along the direction perpendicular to the wrinkles (x axis). To describe the spatial periodicity, the wrinkle wavelength (λ) was defined as the average distance between first-neighboring peaks along the x axis. The wrinkle height (h), i.e., the average of the peak heights, was found by averaging the z axis distances between each peak and the first-neighboring left and right valleys along the profile. Scanning electron micrographs were acquired by using a EVO MA10 SEM (Zeiss), operating at 5 kV accelerating voltage. The electrical characterization of the printed PEDOT:PSS traces was performed with a four point probe tester (Cascade PM5), averaged over four samples.

In vivo Implantation

First, we tested the main features of the RnCEs, their design and the active materials, producing the PPP tubes (**Supplementary Material**, PEDOT:PSS coated PO tubes fabrication and **Supplementary Figure 1**). In order to assess whether PPP tubes are able to support nerve regeneration, they were implanted as nerve conduit to bridge a gap in the transected sciatic nerve of rats (Valero-Cabré et al., 2001) and compared with standard silicone tubes. For the implant, female Sprague–Dawley rats (250–300 g) were anesthetized with ketamine/xylacine (90/10 mg/kg i.p.). Then, the sciatic nerve was exposed at the midthigh following a muscle splitting incision. The sciatic nerve was transected 90 mm proximal to the third toe, a portion of 5 mm was resected, and the proximal and distal stumps were sutured to both ends of a silicone tube (10 mm long, 2.5 mm i.d., 0.5 mm thick, $n = 5$) or a PPP tube (10 mm long, 2.5 mm i.d., 30 μm thick, $n = 6$) leaving a 8 mm gap between nerve ends (**Figure 4**). All implanted tubes were filled with saline. After the nerve repair, the wound was closed with silk sutures and anesthesia was reversed with atipamezole hydrochloride (0.2 mg/kg s.c.).

The active RnCEs ($n = 6$) were implanted following a similar procedure (**Figure 4C**). First, the sciatic nerve was dissected and transected, and the distal nerve was introduced in the tube to test the functionality of the electrode for stimulation (section Electrophysiological Tests). After the tests, a 5 mm portion of the nerve was resected, and the distal and proximal stumps of the nerve were sutured to the tube of the electrode leaving an 8 mm gap. The tubes were filled with saline, the wounds were closed and animals were left to recover. Although six animals received the RnCE, one RnCE was not functional once implanted so the electrode was left to assess regeneration but the animal was not included in the functional evaluation of RnCEs. Then, also in this group, one of the animals died due

[1]https://www.gwyddion.net

to anesthesia-associated complications during nerve conduction test after 45 days of implantation.

The experimental procedures were approved by the ethical committee of the Universitat Autònoma de Barcelona in accordance with the European Communities Council Directive 2010/63/EU. Animals were kept on standard laboratory conditions with a light-dark cycle of 12:12 h and *ad libitum* access to food and tap water. All efforts were made to minimize pain and animal discomfort during surgery and treatments.

Evaluation of Axonal Regeneration

Assessment of Motor Reinnervation

Functional reinnervation of target muscles was assessed at 30, 45, 60, and 90 days post-injury (dpi) by motor nerve conduction tests. Briefly, animals were anesthetized and subdermal needle electrodes were placed transcutaneously at the sciatic notch for electrical stimulation using single electrical pulses (Synergy Medelec, Viasys HealthCare). The compound muscle action potentials (CMAPs) of tibialis anterior (TA) and plantar interosseus (PL) muscles were recorded using thin needles placed in the muscle belly in monopolar configuration. The reference electrode was placed at the fourth toe and a ground electrode was placed at the knee. The amplitude and latency of the CMAP was measured, and contralateral intact limbs ($n = 10$) were used as control. The rat body temperature was maintained throughout the test with a thermostatic warming flat coil.

Assessment of Skin Sensory Reinnervation

The progression of nociceptive reinnervation of the hind paw was assessed by means of pinprick test at 30, 45, 60, and 90 dpi. Animals were gently kept in a cloth with the sole of the injured paw facing upward, and the skin was stimulated with a needle. Five sites of the lateral side of the paw were tested, being each site stimulated three times, and responses were recorded as positive only when clear reaction (as fast withdrawal and vocalization) was triggered by the stimulation (Navarro et al., 1994). The percentage of positive areas per animal was calculated, and contralateral paws were tested as controls.

Histology of Regenerated Sciatic Nerve

At the end of functional evaluation (90 dpi), animals were euthanized by an intraperitoneal injection of pentobarbital, perfused with 4% paraformaldehyde in PBS for 30 min and the sciatic nerves were collected. The nerve guides were clipped and sciatic nerves divided in two parts. Proximal halves were stored in cryoprotected solution of PBS-sucrose 30% with azide 0.1% at 4°C before cryosectioning and immunofluorecent processing. Distal halves were post-fixed in 3% glutaraldehyde−3% paraformaldehyde in cacodylate-buffer solution (0.1 m, pH 7.4) at 4°C for epon embedding.

Proximal segments were embedded in OCT gel (Tissue Tek) before cryosectioning. A cryostat (Leica Microsystems, Germany) was used to collect 15 µm thick cross sections. For immunostaining, sections were first hydrated with TBS, blocked for endogenous biotins (E21390, ThermoFisher), and incubated for 90 min at room temperature in a blocking solution (BS, 1% BSA in TBS) containing 0.1% Tween. Sections were then incubated overnight at 4°C in a mixture in BS of NF200 (AB5539, 1:500 Millipore) and S100 (22520, 1:100 DiaSorin) primary antibodies for staining axons and Schwann cells, respectively. Samples were then washed and incubated again for 2 h at room temperature for biotin amplification of the S100 antibody (BA-1000, 1:200 Vector). Samples were washed again and incubated with secondary antibodies Alexa Fluor 594 Goat anti-Chicken (A11042 1:200 Thermofisher) and Alexa Fluor 488 Streptavidin (S11223, 1:200 Thermofisher) diluted in TBS. Finally, sections were washed and cover-slipped with Mowiol containing DAPI (1:10,000, Sigma) for nuclear counterstain. Sections were visualized with an epifluorescence microscope (Eclipse Ni, Nikon) attached to a digital camera (DS-Ri2, Nikon).

To evaluate the microstructure of the nerve, distal segments were post-fixed with osmium tetroxide (2%, 2 h) and dehydrated through ethanol series prior to embedding in epon resin. Semithin 0.5 µm thick sections were stained with toluidine blue. Microscope (Olympus BX51) images were taken and measurement of cross-section area of the distal segment of the sciatic nerve and quantification of the number of myelinated nerve fibers was carried out using Image J software (Del Valle et al., 2018).

Electrophysiological Tests

Functional evaluation of RnCEs was performed just after implantation (0 dpi) and after 90 dpi. As indicated above, at 0 dpi, the sciatic nerve was sectioned and introduced in the tube portion of the RnCE, and stimulated as with common cuff electrode implants. Afterwards, proximal and distal nerve stumps were sutured to the ends of the RnCE for allowing nerve regeneration. At 90 dpi, electrical stimulation was applied with the RnCE to the regenerated sciatic nerve to assess the stimulation performance of the implanted electrodes. At both timepoints, biphasic current pulses were delivered through each one of the electrodes against a small needle reference electrode placed proximally near the nerve. Increasing current pulses with a width of 10–100 µs and an intensity up to 8 mA (max charge 800 nC) were delivered by a Digitimer DS4 stimulator. The CMAP was recorded from gastrocnemius medialis (GM), TA and PL muscles using small needle electrodes placed in each muscle (Badia et al., 2011). The CMAPs were amplified (P511AC, Grass), band-pass filtered (3 Hz to 3 kHz) and digitized with a Powerlab recording system (PowerLab16SP, ADInstruments) at 20 kHz. The amplitude of each CMAP was measured baseline to peak and normalized to the maximum CMAP amplitude obtained in each experiment by stimulation of the sciatic nerve with a needle electrode. For each electrode, the threshold current of stimulation that elicited 5, 30, and 95% of the maximum CMAP was determined. The electrode with the lowest threshold value in each RnCE (best AS) was used for data analysis. Finally, the selectivity index (SI) was calculated to quantify the specific activation of a single muscle among the set of three muscles (GM, PL, TA) when stimulating from each electrode, as previously described (Veraart et al., 1993) and the maximum SI (SImax) from each electrode for each muscle was used.

Data Analysis

Data are presented as mean ± standard error of the mean (SEM). Results have been statistically analyzed by using GraphPad Prism 8 (GraphPad Software, USA). Statistical significance for comparison between groups has been analyzed using one-way ANOVA, or mixed effect models followed by Tukey's *post-hoc* tests when required. Statistical significance is considered when P-value was < 0.05.

RESULTS

RnCEs Fabrication Strategy

The Print and Shrink process consists of four steps: (1) the direct patterning of materials by means of inkjet printing on PO foil, (2) the heat-shrink induced self-assembly miniaturization, (3) the rolling-up of the foil into a tube and (4) the PCB packaging.

The printing process, depicted in **Figures 1A–D**, defines the microelectrode array (**Figure 2A**), which consists of 5 electrodes, with pre-shrink size of 200 × 130 μm^2, and the feed lines. The PEDOT:PSS-based ink, adopted as main conductive material, was formulated with 10% glycerol, enabling an increased conductivity and facilitating the printing process (Garma et al., 2019). A printed Ag pattern is added on top of the PEDOT:PSS terminal pads (i.e., at the external connection interface) to improve the electrical junction with the PCB. SU-8 is used as dielectrics, in two different formulations. SU-8 10% is used to define the electrodes and SU-8 29% to provide the full insulation of the feed lines (SU-8 29%). SU-8 29% was not used for the whole coverage since it tends to delaminate and crack upon PO shrinking, due to its stiffness. The less viscous SU-8 10% ink was therefore adopted to obtain a thin and flexible coverage. Insights on the SU-8 printing and shrinking are provided in **Supplementary Material** (SU-8 printing process, **Supplementary Figure 2**).

After printing, the heat-shrinking is performed. By heating above PO glass transition temperature the shrink-wrap film softened and irreversibly shrunk in-plane, as a result of relaxation of pre-stretched polymer chains. As a consequence, the skin layers (PEDOT:PSS and SU-8) were induced to be buckled, upon the compressive planar forces exerted by the substrate (**Figures 1E,F**). In the actual setup, the printed PO film uniaxially shrunk to 65% of its original lateral size (≈26 mm final width, **Figures 1E,F**). The final geometrical area of the electrodes is therefore 130 × 130 μm^2. Notably, after shrinking the PO wrap film remains flexible, optically transparent, puncture resistant and it can be wrapped and rolled-up in tubular conduits resulting in a flexible PNI (**Figure 2B**). A custom PCB is finally connected to the RnCE pads through a miniaturized package (**Figure 2C**).

RnCEs Surface and Electrical Characterization

Surface characterization allowed to analyze the 3D topography of the RnCE lumen. We found two different textures, a wrinkled one and a smooth one, which are essentially related to the composition of printed materials, the printing parameters and the curing processes.

The first texture, which is found on the electrodes and the major dielectric, is related to the wrinkling of PEDOT:PSS and SU-8 10%. Notably, both materials are well adherent to the PO wrap film, since they interlocked with the substrate during its softening. The process ensures the development of compliant interfaces (**Supplementary Material**, **Supplementary Figures 2**, **3**) without signs of delamination, even after prolonged incubation periods in cell culture medium, as demonstrated in previous studies with a similar heat-shrink substrate (Bonisoli et al., 2017). The PEDOT:PSS film is characterized by an anisotropic (i.e., uniaxial) wrinkled texture, uniform over the whole surface of the electrodes (**Figures 3A,B**). An average spacing between wrinkles (wrinkle wavelength, λ) of 1.1 ± 0.4 μm, and an average wrinkle height (h) of 0.4 ± 0.2 μm were found (**Figure 3C**). The SU-8 10% film defined a topography with wrinkled micro-grooves in a periodic pattern with a pitch of around 40 μm (**Figure 3D**), while the wrinkled areas (**Figures 3E,F**) showed characteristics very similar to the PEDOT:PSS wrinkled electrodes. Average SU-8 10% wrinkle wavelength was found to be $\lambda = 1.0 \pm 0.4\,\mu m$ and average wrinkle height $h = 0.3 \pm 0.2\,\mu m$. The 40 μm pitch grooves are the result of the self-assembly process in the SU-8 10% layer, where printed lines did not coalesce in a uniform layer. The wrinkling is here confined in the central region of each line, whereas a smooth surface is observed at the edges. The smooth areas did not undergo wrinkling probably because they were too thick due to the so-called coffee ring effect (Hu and Larson, 2006). Nevertheless, nor delamination or cracks were observed in the whole surface. A different texture is observed in the SU-8 29% layer, deposited only on top of the conductive traces. Such dielectric has not been dried neither UV-cured before shrinking. As a consequence, upon PO shrinking, it resulted in a uniform flat coating insulating the underlying bilayer. The coating thickness was 2.7 μm, two orders of magnitude larger than the thickness of the PEDOT:PSS patterns (40 nm). The SU-8 29% cover ensured an adherent interface with PEDOT:PSS wrinkled electrodes (**Supplementary Figure 2F**).

The electrical resistance of the PEDOT:PSS traces ranged from 144 ± 9 to 249 ± 23 kΩ (average ± standard deviation, averaged over four samples), depending on the length of each trace. Detailed electrical resistance data with respect to traces length are reported in **Table 1** (**Supplementary Figure 4** for traces reference).

Regeneration After Nerve Section and Repair

Silicone tubes, PPP tubes and RnCEs were compared as conduits to support sciatic nerve regeneration along a 8 mm gap in rats. In all cases, we found a regenerated nerve cable inside the tubes (**Figures 4D–F**) at 90 dpi. Nerve histological evaluation showed a centered nerve containing a dense core of regenerative units with myelinated and unmyelinated axons and small blood vessels. The immunolabeling of regenerated nerves showed in the three groups a wide distribution of axons surrounded by Schwann cells (**Figures 5A–C**). Histological sections showed high amount of regenerated nerve fibers without signs of axonal damage, such as no or very thin myelin sheath, or signs of Wallerian degeneration (**Figures 5D,E**).

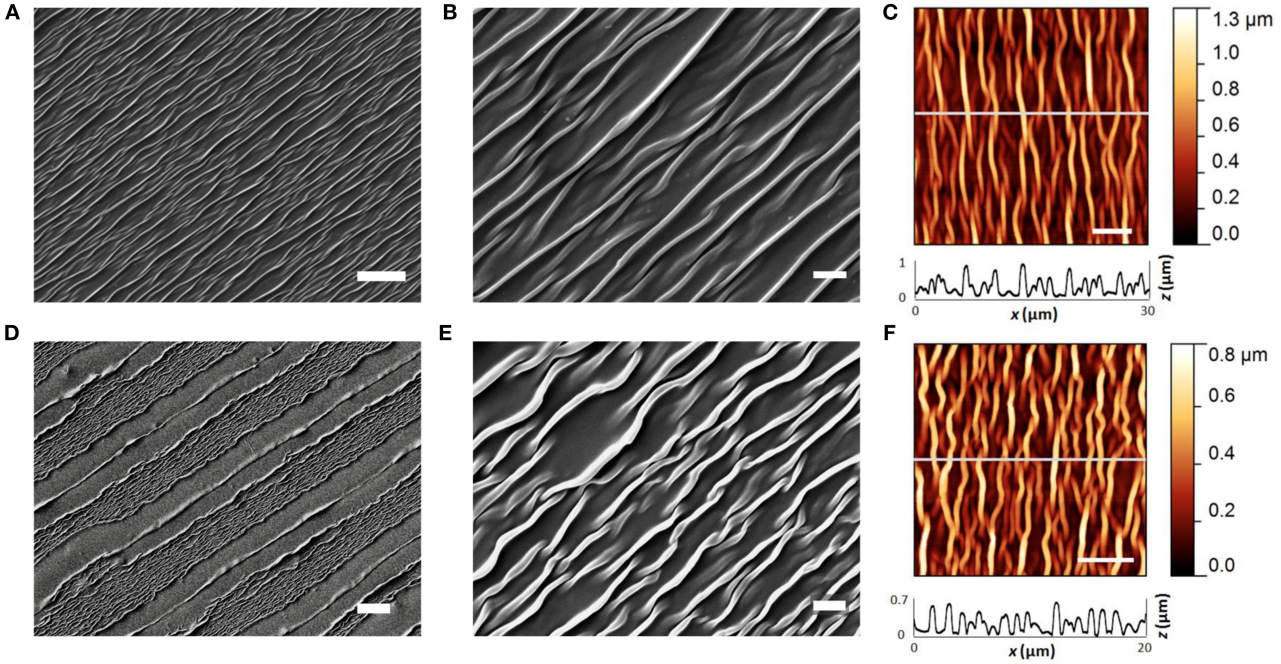

FIGURE 3 | PEDOT:PSS and SU-8 wrinkles. **(A,B)** SEM images of PEDOT:PSS wrinkled active site. Scale bar: 10 and 2 µm. **(C)** AFM image of wrinkled PEDOT:PSS (scale bar: 5 µm), and extracted x-z profile (gray line scan). **(D,E)** SEM images of SU-8 10% wrinkled micro-grooves. Scale bar: 20 and 2 µm. **(F)** AFM image of wrinkled SU-8 10% (scale bar: 5 µm), and extracted x-z profile (gray line scan).

TABLE 1 | Electrical characterization of PEDOT:PSS traces, averaged over 4 samples.

PEDOT:PSS traces	Length (mm)	Resistance (kΩ)
1	6.4	144 ± 9
2	7.6	164 ± 26
3	12.6	249 ± 23
4	12.2	214 ± 22
5	9.6	176 ± 28

*See **Supplementary Figure 4** for traces reference.*

Quantification of myelinated axons showed no differences ($p > 0.05$, one-way ANOVA) between the three tested tubes (**Figure 5H**).

We also carried out functional evaluation tests to assess muscle and skin reinnervation following nerve regeneration. Motor nerve conduction tests showed complete denervation of the hindlimb muscles after injury. At 45 dpi, CMAPs of very small amplitude and long latency were recorded from the TA muscle, while responses from the PL muscle, more distal in the paw, started to appear at 60 dpi. All animals showed evidence of reinnervation of TA and PL muscles at 90 dpi. The CMAP amplitude of both TA and PL muscles was significantly lower in the injured side than in the contralateral paw ($p < 0.05$) in all the groups during follow-up, indicating partial reinnervation. Regarding the implanted nerves, the group with a silicone tube had slightly higher CMAP amplitudes of both TA and PL muscles than the other two groups but differences were not significant ($p > 0.05$) at any time point (**Figure 5F**). The pinprick test on the plantar skin showed that pain sensation returned to the paw from 45 dpi, without differences ($p > 0.05$) between the three groups (**Figure 5G**). In summary, functional results indicated motor and sensory reinnervation in animals implanted with RnCEs, comparable to levels obtained with a standard silicone tube.

In vivo Assessment of RnCE Functionality

The RnCEs were used to stimulate the sectioned but still functional sciatic nerve at the implant time (0 dpi), and then following the same stimulation protocol at 90 dpi on the regenerated nerve (**Figure 6**). All the RnCEs were able to efficiently stimulate regenerated axons and induce a CMAP in the three tested muscles at 90 dpi. Recruitment curves of muscle activity were plotted for each muscle and compared between 0 and 90 dpi (**Figures 6A,B**). The thresholds of charge needed to reach a 5, 30, and 95% of the maximal CMAP amplitude significantly increased up to six times after 90 dpi ($p < 0.05$, Mixed-effects) in comparison with values needed at day 0 (**Figure 6C**). Finally, the capability of the RnCE to selectively stimulate different groups of axons leading to selective recruitment of different muscles was maintained over time, and the SImax showed no significant differences between the acute and chronic implant time-points ($p > 0.05$) (**Figure 6D**).

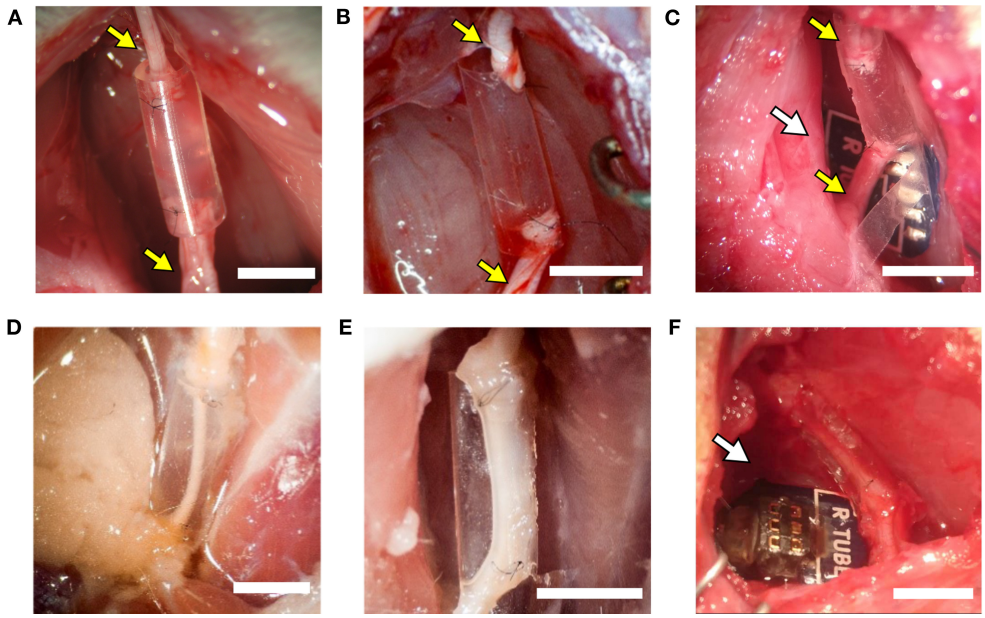

FIGURE 4 | The implanted regenerative cuff electrode. Representative images of: **(A)** silicone tube, **(B)** PEDOT:PSS coated PO tube (PPP tube), and **(C)** Regenerative nerve Cuff Electrode (RnCE) at the time of implant (0 dpi) bridging a 8 mm gap in the rat sciatic nerve, and of **(D)** silicone tube, **(E)** PPP tube and **(F)** RnCE at 90 dpi, showing the regenerated nerve cable inside. Yellow arrows point proximal and distal sciatic stumps sutured to each device. White arrows point the PCB. Scale bar: 5 mm.

DISCUSSION

In this study we present a novel regenerative PNI, the RnCE, fabricated through a non-conventional low-cost approach, the Print and Shrink strategy. RnCEs connect the microfabrication of CPs, the new frontier in PNIs material, with the development of non-obtrusive regenerative interfaces, the challenge of the next generation PNIs. To the best of our knowledge RnCE is the first fully transparent all-polymer regenerative PNIs.

The Print and Shrink entails low-cost substrate material and cost-effective fabrication techniques. We have already reported inkjet printing as an affordable technique for fabricating all-polymer PEDOT:PSS based multi-electrode arrays on flexible substrates, with application in *in vitro* electrophysiology (Garma et al., 2019). Since inkjet printing does not require any kind of masking, the process enables to save materials and quickly customize the design of the electrodes. Moreover, the optimized printing method here reported allowed the deposition of thin layers, with all the materials adopted, which is crucial to ensure a conformal wrinkling. Indeed, neither cracks nor delamination of all the printed layers were observed after shrinking and the inkjet printed films were stable upon bending of the flexible substrate and remained stable after *in vivo* tests. The wrinkling manufacturing process here reported is an expansion of a previous work on smart multifunctional biointerfaces for muscle and neuronal cells (Greco et al., 2013; Bonisoli et al., 2017). In those cases the self-assembled anisotropic topography and the conductive properties of PEDOT:PSS were found to promote and orient cell growth and differentiation. Here, the texturing of electrodes is meant to increase their surface area while minimizing the electrode size. This strategy has been indeed already reported to enhance charge injection capacity in PNIs (Cogan, 2008). Regarding the biocompatibility of the active material, *in vitro* studies already demonstrated the non-cytotoxicity of PEDOT:PSS coatings in neuronal cells (Charkhkar et al., 2014) and its *in vivo* stability in acute to early-chronic studies (Kozai et al., 2015). Although an exhaustive long-term *in vivo* analysis has not been performed yet, recent studies showed stability of PEDOT:PSS in *in vitro* long-term experiments [one or 3 weeks (Cellot et al., 2016) up to 4 months (Dijk et al., 2020)]. Hence, the facts that our results show a similar amount of axons between standard silicone tubes and the PEDOT:PSS tubes and also that the degree of functional recovery is similar, suggest that this material should be suitable for *in vivo* neural applications.

Remarkably, the here reported low-cost fabrication strategy enables a facile tailorability of the electrodes design. The ease of customization, in terms of electrodes sizing and overall device dimensions, opens for multiple applications with diverse animal models up to personalized peripheral interfaces in case of human lesions. Moreover, the developed technique allows reliable adhesion of the patterned materials, enabling to overcome mechanical instability, as cracks or delamination reported in multiple implants and limiting the neuroprostheses outcome (Barrese et al., 2016; Ganji et al., 2018).

Given their flexibility, RnCEs are suitable for soft interfacing with biological tissues. Nevertheless, the polymeric microelectrode array arranged on the PNI lumen and the whole design do not impair the natural process of nerve regrowth.

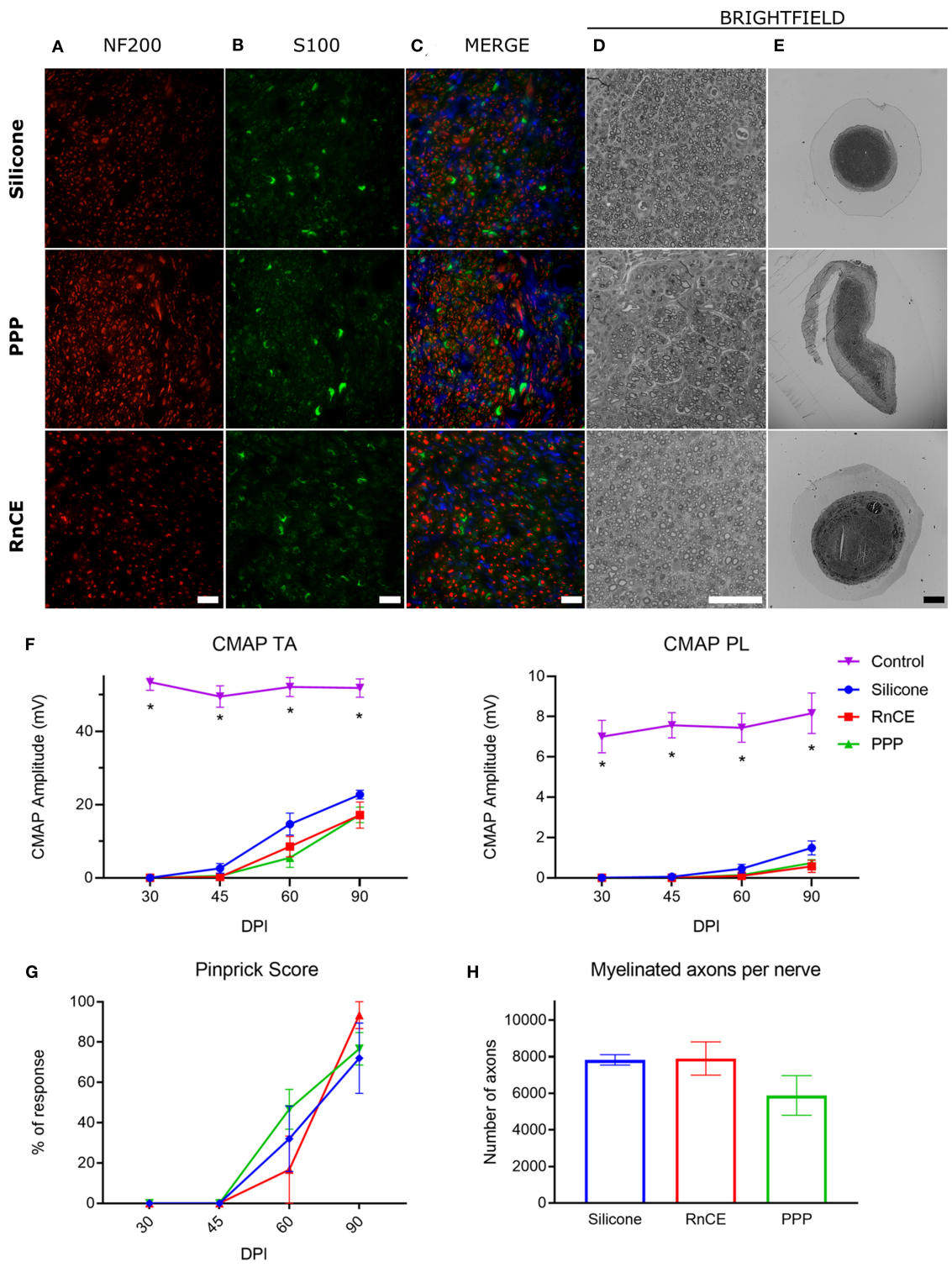

FIGURE 5 | Histological and electrophysiological evaluation of nerve regeneration. **(A–E)** Representative images of cross sectioned nerves repaired with silicone, PEDOT:PSS coated PO tube (PPP) and Regenerative nerve Cuff Electrode (RnCE) at 90 dpi. **(A)** NF200 (red) for axons; **(B)** S100 (green) for Schwann cells; **(C)** Merge of A and B with nuclear staining (DAPI, blue); **(D,E)** Brightfield images of regenerated nerves stained with toluidine blue labeling myelin sheaths at high **(D)** and low **(E)** magnification. Scale bar: 50 μm in **(A–D)**, 200 μm in **(E)**. **(F)** Amplitude of the CMAP of tibialis anterior (TA) and plantar interossei (PL) muscles along the 90 days follow-up after sciatic nerve section and repair. **(G)** Skin paw reinnervation tests by pinprick test. **(H)** Quantification of myelinated fibers in the sciatic nerve distal to the tube in the three tested groups. *$p < 0.05$ vs. other groups.

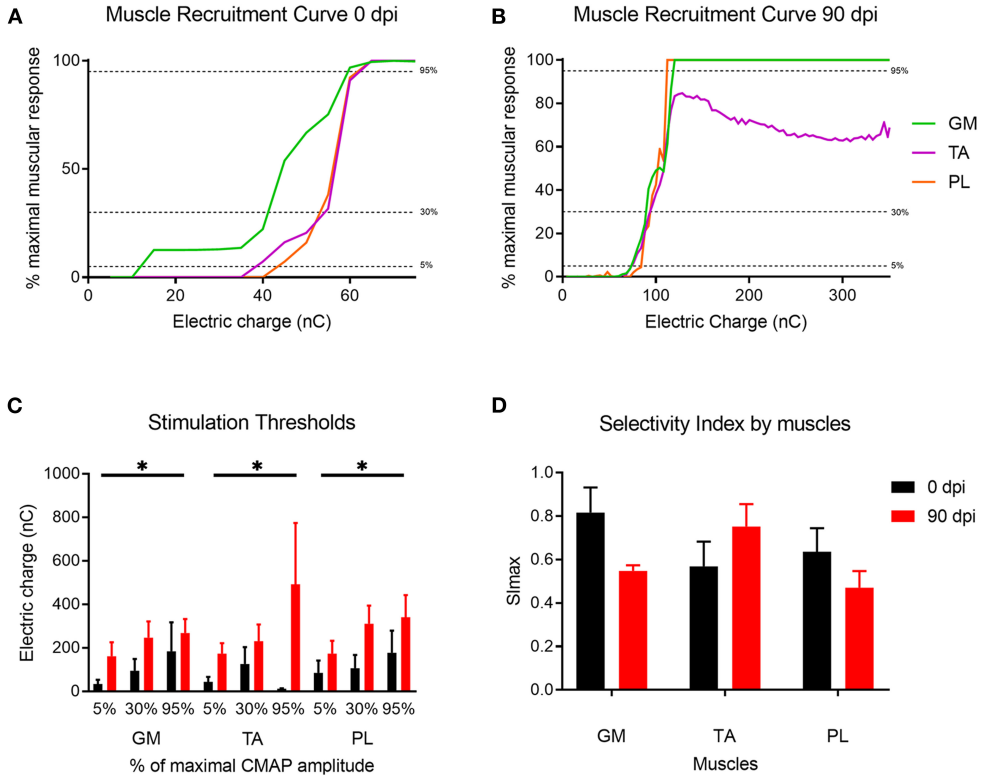

FIGURE 6 | Muscle recruitment curves. **(A,B)** Representative muscle recruitment curves from selected active sites at **(A)** 0 dpi and **(B)** 90 dpi. The increase of the electrical charge delivered through the device elicited recruitment of more muscular fibers thus increasing the CMAP amplitude. **(C)** Values of the electrical charge needed to elicit 5, 30, and 95% of the maximum CMAP amplitude of gastrocnemius (GM), tibialis anterior (TA) and plantar interossei muscles (PL). **(D)** Maximal selectivity index (SImax) for GM, TA, and PL muscles over time. *$p < 0.05$ vs. time.

In this sense, the RnCEs allowed axons to grow through a gap of 8 mm between nerve stumps (**Figure 4**), a longer distance than used in previous studies with other regenerative interfaces, such as sieve (Lago et al., 2005), microchannel (Srinivasan et al., 2015) or double-aisle (Delgado-Martínez et al., 2017) electrodes. The 8 mm gap chosen is a relatively long distance, but still below the critical length that can be repaired with standard polymer conduits (Lundborg et al., 1982; Valero-Cabré et al., 2001; Yannas and Hill, 2004). We chose the 8 mm gap to prove that both the PPP tube and the RnCE do not hinder regeneration and this material behaves similarly as other plastics such as Teflon (Navarro and Kennedy, 1991) or silicone (Deumens et al., 2010). Moreover, motor and sensory reinnervation outcomes were similar between the silicone, the PPP tube and the RnCE; and the number of myelinated axons did not differ between the three groups. Therefore, our results indicate that the RnCE device (which includes also the PCB that can induce traction forces which could affect regeneration) and the PPP tube alone are as good as conventional silicone tubes in terms of supporting peripheral nerve regeneration. However, the three groups did not reach complete functional recovery after 90 days of implantations, as expected. As with other regenerative electrodes, the RnCE cannot be considered as a better regenerative strategy than other tubulization techniques such as the use of porous materials (Meyer et al., 2016), or fillers with neurotrophic factors (Del Valle et al., 2018) or cells (Allodi et al., 2014), nor better also than the current gold standard as the autograft (Dietzmeyer et al., 2020). Finally, tube or cuff electrodes, such as the RnCE, should be flexible, self-sizing, have a larger diameter than the nerve to be implanted and with the thinnest wall without compromising their stability (Rodri et al., 2000). While potential damage to the regenerated nerve induced by the chronically implanted RnCE is a possibility, the small thickness of the device and the enhanced flexibility of the materials give the tube of the RnCE a soft interface with the nerve.

The RnCE exploits the PNS regeneration capabilities to directly interface the nervous system. In this way the RnCEs overcome the issues related to nerve compression and impaired nerve regeneration, known to affect the interface viability reported for sieve and microchannel devices (Navarro et al., 1996; Wallman et al., 2001; FitzGerald, 2016). RnCEs are able to stimulate regenerated axons, although a higher electrical charge is needed in comparison to axons that had been recently cut. This is attributable to the physiopathological changes of regenerated axons, which are considerable thinner in caliber and with thinner myelin sheaths than normal, for long time after injury (Gómez et al., 1996), and thus have a higher stimulation

threshold (Blair and Erlanger, 1933; McNeal, 1976). Moreover, resting membrane hyperpolarization is increased in regenerated motor axons (Moldovan and Krarup, 2004), contributing to the observed lower excitability.

We have characterized the RnCEs in terms of stimulation selectivity, that in PNIs is usually inversely related to the invasiveness of the device implantation (del Valle and Navarro, 2013). Compared with previous studies in the literature, the RnCEs showed a selectivity similar than non-regenerative cuff electrodes (Badia et al., 2011), but lower compared to the double-aisle regenerative electrodes which separated the regenerated nerve fascicles (Delgado-Martínez et al., 2017), or the TIME intrafascicular electrodes applied to the intact rat sciatic nerve (Badia et al., 2011). Hence, RnCEs may not be the best approach for implants in a large nerve trunk, such as the sciatic nerve, but it may be more efficient for implants in smaller nerves, that innervate a limited target. The combination of the technology developed for the RnCE with other regenerative interface designs, such as the double-aisle regenerative (Delgado-Martínez et al., 2017) or the REMI (Garde et al., 2009) electrodes, in which the tube lumen is divided in separate sections by a septum where electrodes can be also located, may be a favorable option to reach higher interface selectivity. In addition, innovative multiple aisle regenerative devices, may allow guidance by molecular cues for sorting the regeneration of specific axonal populations (Del Valle et al., 2018) directing motor or different types of sensory fibers to specific areas of the regenerative interface. RnCEs may also be suitable to be used in cases where nerve transections are surgically repaired with nerve conduits. Interestingly, nerve electrical stimulation with RnCEs might be further exploited to promote axonal regeneration and treat neuropathic pain within the rehabilitation program after nerve repair (Asensio-Pinilla et al., 2009; Cobianchi et al., 2013).

In conclusion, we report here a new fabrication method that can produce a fully transparent regenerative nerve electrode, the RnCE. This electrode can be adjusted in size to house different nerve calibers with a fast and cheap manufacturing process. Future studies will determine whether it has the potential advantages of regenerative interfaces, such as the possibility to record the signals of early regenerating fibers, to generate electrical field to improve regeneration (Gordon, 2016) or to interface axons that have regenerated to bidirectionally connect the subject with an external device (del Valle and Navarro, 2013). Future and more prolonged studies will be aimed at determining whether the RnCE could cause discomfort in the regenerated nerves after more than 3 months, or the materials cause any specific damage in the surrounding tissue. Moreover, it will be investigated the capability of the Print and Shrink strategy to produce microelectrode arrays at higher resolution with increased electrodes density. A significant reduction in electrode size can be obtained by fully exploiting the heat shrinking of the PO substrate. Nominally a bi-dimensional free shrinkage of 70–75% at 120°C can be reached, much higher than the 35% uniaxial shrinkage here obtained. Such improvement will require the setting of a dedicated fabrication methodology to ensure accuracy and repeatability in pattern miniaturization. By maintaining the maximal transparency of the PNI and increasing the microelectrodes array resolution, next generation RnCEs will combine the benefit of good support for axonal regeneration without obstacle or compression with improved selective stimulation and recording capabilities. Finally, the cost-effective Print and Shrink strategy would be useful for the manufacturing of neural interfaces wherein the optical transparency of the device plays a pivotal role, as in the case of optogenetics.

DATA AVAILABILITY STATEMENT

The datasets presented in this study can be provided by the authors under reasonable request.

ETHICS STATEMENT

The animal study was reviewed and approved by Comissió d'Ètica en l'Experimentació Animal i Humana de la Universitat Autònoma de Barcelona.

AUTHOR CONTRIBUTIONS

LMF and AB developed the fabrication strategy (Print and Shrink) under the supervision of FG. AC helped in the design of the electrodes array, developed the PCB, and the electrical interconnections. SM, FG, and XN conceived the study. BR-M and JV performed the *in vivo* experiments under the guide of XN. LMF, AC, AB, BR-M, JV, FG, and XN contributed to the analyses and discussion of the results. All authors contributed to writing and correcting the manuscript.

FUNDING

This work was partially supported by FLAG-ERA JTC 2017 project GRAFIN, grant PCI2018-093029 from Ministerio de Ciencia, Innovación y Universidades of Spain, co-funded by European Union (ERDF/ESF, Investing in your future), TERCEL (RD16/0011/0014) and CIBERNED (CB06/05/1105) funds from Instituto de Salud Carlos III of Spain. FG acknowledges partial financial support from Top Global University Project at Waseda University, Tokyo from MEXT Japan.

ACKNOWLEDGMENTS

The authors thank Monica Espejo and Jessica Jaramillo for their technical help.

SUPPLEMENTARY MATERIAL

The Supplementary Material for this article can be found online at: https://www.frontiersin.org/articles/10.3389/fbioe.2021.615218/full#supplementary-material

REFERENCES

Allodi, I., Mecollari, V., González-Pérez, F., Eggers, R., Hoyng, S., Verhaagen, J., et al. (2014). Schwann cells transduced with a lentiviral vector encoding Fgf-2 promote motor neuron regeneration following sciatic nerve injury. *Glia* 62, 1736–1746. doi: 10.1002/glia.22712

Altuna, A., Bellistri, E., Cid, E., Aivar, P., Gal, B., Berganzo, J., et al. (2013). SU-8 based microprobes for simultaneous neural depth recording and drug delivery in the brain. *Lab Chip*. 13, 1422–1430. doi: 10.1039/c3lc41364k

Asensio-Pinilla, E., Udina, E., Jaramillo, J., and Navarro, X. (2009). Electrical stimulation combined with exercise increase axonal regeneration after peripheral nerve injury. *Exp. Neurol*. 219, 258–265. doi: 10.1016/j.expneurol.2009.05.034

Asplund, M., Nyberg, T., and Inganäs, O. (2010). Electroactive polymers for neural interfaces. *Polym. Chem*. 1, 1374–1391. doi: 10.1039/c0py00077a

Badia, J., Boretius, T., Andreu, D., Azevedo-Coste, C., Stieglitz, T., and Navarro, X. (2011). Comparative analysis of transverse intrafascicular multichannel, longitudinal intrafascicular and multipolar cuff electrodes for the selective stimulation of nerve fascicles. *J. Neural Eng*. 8:036023. doi: 10.1088/1741-2560/8/3/036023

Barrese, J. C., Aceros, J., and Donoghue, J. P. (2016). Scanning electron microscopy of chronically implanted intracortical microelectrode arrays in non-human primates. *J. Neural Eng*. 13:026003. doi: 10.1088/1741-2560/13/2/026003

Bellamkonda, R. V., Pai, S. B., and Renaud, P. (2012). Materials for neural interfaces. *MRS Bull*. 37, 557–561. doi: 10.1557/mrs.2012.122

Berggren, M., Nilsson, D., and Robinson, N. D. (2007). Organic materials for printed electronics. *Nat. Mater*. 6:3. doi: 10.1038/nmat1817

Berggren, M., and Richter-Dahlfors, A. (2007). Organic bioelectronics. *Adv. Mater*. 19, 3201–3213. doi: 10.1002/adma.200700419

Bernardeschi, I., Greco, F., Ciofani, G., Marino, A., Mattoli, V., Mazzolai, B., et al. (2015). A soft, stretchable and conductive biointerface for cell mechanobiology. *Biomed. Microdevices*. 17:46. doi: 10.1007/s10544-015-9950-0

Bernards, D. A., Owens, R. M., and Malliaras, G. G. (2008). *Organic Semiconductors in Sensor Applications*. Berlin Heidelberg: Springer. doi: 10.1007/978-3-540-76314-7

Bettinger, C. J. (2018). Recent advances in materials and flexible electronics for peripheral nerve interfaces. *Bioelectron. Med*. 4:6. doi: 10.1186/s42234-018-0007-6

Blair, E. A., and Erlanger, J. (1933). Comparison of properties of individual axons in the frog. *Proc. Soc. Exp. Biol. Med*. 30, 728–729. doi: 10.3181/00379727-30-6647

Bonisoli, A., Marino, A., Ciofani, G., and Greco, F. (2017). Topographical and electrical stimulation of neuronal cells through microwrinkled conducting polymer biointerfaces. *Macromol. Biosci*. 17:1700128. doi: 10.1002/mabi.201700128

Boretius, T., Badia, J., Pascual-Font, A., Schuettler, M., Navarro, X., Yoshida, K., et al. (2010). A transverse intrafascicular multichannel electrode (TIME) to interface with the peripheral nerve. *Biosens. Bioelectron*. 26, 62–69. doi: 10.1016/j.bios.2010.05.010

Caironi, M., and Noh, Y. Y. (2015). *Large Area and Flexible Electronics*. Weinheim: Wiley-VCH Verlag GmbH & Co. doi: 10.1002/9783527679973

Cellot, G., Lagonegro, P., Tarabella, G., Scaini, D., Fabbri, F., Iannotta, S., et al. (2016). PEDOT: PSS interfaces support the development of neuronal synaptic networks with reduced neuroglia response *in vitro*. *Front. Neurosci*. 9:521. doi: 10.3389/fnins.2015.00521

Chan, Y., Skreta, M., McPhee, H., Saha, S., Deus, R., and Soleymani, L. (2018). Solution-processed wrinkled electrodes enable the development of stretchable electrochemical biosensors. *Analyst* 144, 172–179. doi: 10.1039/C8AN01637B

Charkhkar, H., Frewin, C., Nezafati, M., Knaack, G. L., Peixoto, N., Saddow, S. E., et al. (2014). Use of cortical neuronal networks for *in vitro* material biocompatibility testing. *Biosens. Bioelectron*. 53, 316–323. doi: 10.1016/j.bios.2013.10.002

Chen, A., Lee, E., Tu, R., Santiago, K., Grosberg, A., Fowlkes, C., et al. (2014). Integrated platform for functional monitoring of biomimetic heart sheets derived from human pluripotent stem cells. *Biomaterials* 35, 675–683. doi: 10.1016/j.biomaterials.2013.10.007

Chen, A., Lieu, D. K., Freschauf, L., Lew, V., Sharma, H., Wang, J., et al. (2011). Shrink-film configurable multiscale wrinkles for functional alignment of human embryonic stem cells and their cardiac derivatives. *Adv. Mater*. 23, 5785–5791. doi: 10.1002/adma.201103463

Cho, S.-H., Lu, H. M., Cauller, L., Romero-Ortega, M. I., J.-,Lee, B., and Hughes, G. A. (2008). Biocompatible SU-8-based microprobes for recording neural spike signals from regenerated peripheral nerve fibers. *IEEE Sens. J*. 8, 1830–1836. doi: 10.1109/JSEN.2008.2006261

Clements, I. P., Mukhatyar, V. J., Srinivasan, A., Bentley, J. T., Andreasen, D. S., and Bellamkonda, R. V. (2012). Regenerative scaffold electrodes for peripheral nerve interfacing. *IEEE Trans. Neural Syst. Rehabil. Eng*. 21, 554–566. doi: 10.1109/TNSRE.2012.2217352

Cobianchi, S., Casals-Diaz, L., Jaramillo, J., and Navarro, X. (2013). Differential effects of activity dependent treatments on axonal regeneration and neuropathic pain after peripheral nerve injury. *Exp. Neurol*. 240, 157–167. doi: 10.1016/j.expneurol.2012.11.023

Cogan, S. F. (2008). Neural stimulation and recording electrodes. *Annu. Rev. Biomed. Eng*. 10, 275–309. doi: 10.1146/annurev.bioeng.10.061807.160518

del Valle, J., and Navarro, X. (2013). Interfaces with the peripheral nerve for the control of neuroprostheses. *Int. Rev. Neurobiol*. 109: 63–83. doi: 10.1016/B978-0-12-420045-6.00002-X

Del Valle, J., Santos, D., Delgado-Martínez, I., de la Oliva, N., Giudetti, G., Micera, S., et al. (2018). Segregation of motor and sensory axons regenerating through bicompartmental tubes by combining extracellular matrix components with neurotrophic factors. *J. Tissue Eng. Regen. Med*. 12, e1991–e2000. doi: 10.1002/term.2629

Delgado-Martínez, I., Righi, M., Santos, D., Cutrone, A., Bossi, S., D'Amico, S., et al. (2017). Fascicular nerve stimulation and recording using a novel double-aisle regenerative electrode. *J. Neural Eng*. 14:046003. doi: 10.1088/1741-2552/aa6bac

Deumens, R., Bozkurt, A., Meek, M. F., Marcus, M. A. E., Joosten, E. A. J., Weis, J., et al. (2010). Repairing injured peripheral nerves: bridging the gap. *Prog. Neurobiol*. 92, 245–276. doi: 10.1016/j.pneurobio.2010.10.002

Dietzmeyer, N., Förthmann, M., Grothe, C., and Haastert-Talini, K. (2020). Modification of tubular chitosan-based peripheral nerve implants: applications for simple or more complex approaches. *Neural Regen. Res*. 15, 1421. doi: 10.4103/1673-5374.271668

Dijk, G., Rutz, A. L., and Malliaras, G. G. (2020). Stability of PEDOT: PSS-coated gold electrodes in cell culture conditions. *Adv. Mater. Technol*. 5:1900662. doi: 10.1002/admt.201900662

Elschner, A., Kirchmeyer, S., Lovenich, W., Merker, U., and Reuter, K. (2010). *PEDOT: Principles and Applications of an Intrinsically Conductive Polymer*. Boca Raton, FL: CRC Press. doi: 10.1201/b10318

FitzGerald, J. J. (2016). Suppression of scarring in peripheral nerve implants by drug elution. *J. Neural Eng*. 13:026006. doi: 10.1088/1741-2560/13/2/026006

Gabardo, C. M., Adams-McGavin, R. C., Fung, B. C., Mahoney, E. J., Fang, Q., and Soleymani, L. (2017). Rapid prototyping of all-solution-processed multi-lengthscale electrodes using polymer-induced thin film wrinkling. *Sci. Rep*. 7, 1–9. doi: 10.1038/srep42543

Ganji, M., Hossain, L., Tanaka, A., Thunemann, M., Halgren, E., Gilja, V., et al. (2018). Monolithic and scalable Au nanorod substrates improve PEDOT–metal adhesion and stability in neural electrodes. *Adv. Healthc. Mater*. 7:1800923. doi: 10.1002/adhm.201800923

Garde, K., Keefer, E., Botterman, B., Galvan, P., and Romero-Ortega, M. I. (2009). Early interfaced neural activity from chronic amputated nerves. *Front. Neuroeng*. 2:5. doi: 10.3389/neuro.16.005.2009

Garma, L. D., Ferrari, L. M., Scognamiglio, P., Greco, F., and Santoro, F. (2019). Inkjet-printed PEDOT: PSS multi-electrode arrays for low-cost *in vitro* electrophysiology. *Lab Chip*. 19, 3776–3786. doi: 10.1039/C9LC00636B

Genzer, J., and Groenewold, J. (2006). Soft matter with hard skin: From skin wrinkles to templating and material characterization. *Soft Matter*. 2, 310–323. doi: 10.1039/b516741h

Gómez, N., Cuadras, J., Butí, M., and Navarro, X. (1996). Histologic assessment of sciatic nerve regeneration following resection and graft or tube repair in the mouse. *Restor. Neurol. Neurosci*. 10, 187–196.

Gordon, T. (2016). Electrical stimulation to enhance axon regeneration after peripheral nerve injuries in animal models and humans. *Neurotherapeutics* 13, 295–310. doi: 10.1007/s13311-015-0415-1

Greco, F., Fujie, T., Ricotti, L., Taccola, S., Mazzolai, B., and Mattoli, V. (2013). Microwrinkled conducting polymer interface for anisotropic multicellular

alignment. *ACS Appl. Mater. Interfaces* 5, 573–584. doi: 10.1021/am3 01908w

Greco, F., Ventrelli, L., Dario, P., Mazzolai, B., and Mattoli, V. (2012). Micro-wrinkled palladium surface for hydrogen sensing and switched detection of lower flammability limit. *Int. J. Hydrogen Energy* 37, 17529–17539. doi: 10.1016/j.ijhydene.2012.04.145

Green, R., and Abidian, M. R. (2015). Conducting polymers for neural prosthetic and neural interface applications. *Adv. Mater.* 27, 7620–7637. doi: 10.1002/adma.201501810

Green, R. A., Matteucci, P. B., Hassarati, R. T., Giraud, B., Dodds, C. W. D., Chen, S., et al. (2013). Performance of conducting polymer electrodes for stimulating neuroprosthetics. *J. Neural Eng.* 10:016009. doi: 10.1088/1741-2560/10/1/016009

Groenendaal, L., Jonas, F., Freitag, D., Pielartzik, H., and Reynolds, J. R. (2000). Poly (3, 4-ethylenedioxythiophene) and its derivatives: past, present, and future. *Adv. Mater.* 12, 481–494. doi: 10.1002/(SICI)1521-4095(200004)12:7<481::AID-ADMA481>3.0.CO;2-C

Hu, H., and Larson, R. G. (2006). Marangoni effect reverses coffee-ring depositions. *J. Phys. Chem. B* 110, 7090–7094. doi: 10.1021/jp0609232

Khodagholy, D., Doublet, T., Quilichini, P., Gurfinkel, M., Leleux, P., Ghestem, A., et al. (2013). *In vivo* recordings of brain activity using organic transistors. *Nat. Commun.* 4, 1–7. doi: 10.1038/ncomms2573

Kozai, T. D. Y., Catt, K., Du, Z., Na, K., Srivannavit, O., Razi-ul, M. H., et al. (2015). Chronic *in vivo* evaluation of PEDOT/CNT for stable neural recordings. *IEEE Trans. Biomed. Eng.* 63, 111–119. doi: 10.1109/TBME.2015.2445713

Lacour, S. P., Courtine, G., and Guck, J. (2016). Materials and technologies for soft implantable neuroprostheses. *Nat. Rev. Mater.* 1, 1–14. doi: 10.1038/natrevmats.2016.63

Lago, N., Ceballos, D. F. J., Rodriguez, Stieglitz, T., and Navarro, X. (2005). Long term assessment of axonal regeneration through polyimide regenerative electrodes to interface the peripheral nerve. *Biomaterials* 26, 2021–2031. doi: 10.1016/j.biomaterials.2004.06.025

Lago, N., Yoshida, K., Koch, K. P., and Navarro, X. (2007). Assessment of biocompatibility of chronically implanted polyimide and platinum intrafascicular electrodes. *IEEE Trans. Biomed. Eng.* 54, 281–290. doi: 10.1109/TBME.2006.886617

Lew, V., Nguyen, D., and Khine, M. (2011). Shrink-induced single-cell plastic microwell array. *JALA* 16, 450–456. doi: 10.1016/j.jala.2011.06.003

Lundborg, G., Dahlin, L. B., Danielsen, N., Gelberman, R. H., Longo, F. M., Powell, H. C., et al. (1982). Nerve regeneration in silicone chambers: influence of gap length and of distal stump components. *Exp. Neurol.* 76, 361–375. doi: 10.1016/0014-4886(82)90215-1

Malhotra, B. D., and Ali, M. A. (2017). *Nanomaterials for Biosensors: Fundamentals and Applications*. Amsterdam: William Andrew.

Márton, G., Tóth, E. Z., Wittner, L., Fiáth, R., Pinke, D., Orbán, G., et al. (2020). The neural tissue around SU-8 implants: a quantitative *in vivo* biocompatibility study. *Mater. Sci. Eng. C Mater. Biol. Appl.* 112:110870. doi: 10.1016/j.msec.2020.110870

McNeal, D. R. (1976). Analysis of a model for excitation of myelinated nerve. *IEEE Trans. Biomed. Eng.* BME-23, 329–337. doi: 10.1109/TBME.1976.324593

Meyer, C., Stenberg, L., Gonzalez-Perez, F., Wrobel, S., Ronchi, G., Udina, E., et al. (2016). Chitosan-film enhanced chitosan nerve guides for long-distance regeneration of peripheral nerves. *Biomaterials* 76, 33–51. doi: 10.1016/j.biomaterials.2015.10.040

Moldovan, M., and Krarup, C. (2004). Mechanisms of hyperpolarization in regenerated mature motor axons in cat. *J. Physiol.* 560, 807–819. doi: 10.1113/jphysiol.2004.069443

Navarro, X., Calvet, S., Butí, M., Gómez, N., Cabruja, E., Garrido, P., et al. (1996). Peripheral nerve regeneration through microelectrode arrays based on silicon technology. *Restor. Neurol. Neurosci.* 9, 151–160. doi: 10.3233/RNN-1996-9303

Navarro, X., and Kennedy, W. R. (1991). The effects of autologous nerve transplants on motor and sudomotor reinnervation by regenerative axons. *Brain Res.* 565, 181–187. doi: 10.1016/0006-8993(91)91648-K

Navarro, X., Verdú, E., and Buti, M. (1994). Comparison of regenerative and reinnervating capabilities of different functional types of nerve fibers. *Exp. Neurol.* 129, 217–224. doi: 10.1006/exnr.1994.1163

Nemani, K. V., Moodie, K. L., Brennick, J. B., Su, A., and Gimi, B. (2013). *In vitro* and *in vivo* evaluation of SU-8 biocompatibility. *Mater. Sci. Eng. C* 33, 4453–4459. doi: 10.1016/j.msec.2013.07.001

Nguyen, D., Sa, S., Pegan, J. D., Rich, B., Xiang, G., McCloskey, K. E., et al. (2009). Tunable shrink-induced honeycomb microwell arrays for uniform embryoid bodies. *Lab Chip*. 9, 3338–3344. doi: 10.1039/b914091c

Rivnay, J., Owens, R. M., and Malliaras, G. G. (2013). The rise of organic bioelectronics. *Chem. Mater.* 26, 679–685. doi: 10.1021/cm4022003

Rodri, F. J., Ceballos, D., Schu, M., Valero, A., Valderrama, E., Stieglitz, T., et al. (2000). Polyimide cuff electrodes for peripheral nerve stimulation. *J. Neurosci. Methods* 98, 105–118. doi: 10.1016/S0165-0270(00)00192-8

Rodríguez-Hernández, J. (2015). Wrinkled interfaces: taking advantage of surface instabilities to pattern polymer surfaces. *Prog. Polym. Sci.* 42, 1–41. doi: 10.1016/j.progpolymsci.2014.07.008

Rosberg, H.-E., Carlsson, K. S., and Dahlin, L. B. (2005). Prospective study of patients with injuries to the hand and forearm: costs, function, and general health. *Scand. J. Plast. Reconstr. Surg. Hand Surg.* 39, 360–369. doi: 10.1080/02844310500340046

Sharma, H., Nguyen, D., Chen, A., Lew, V., and Khine, M. (2011). Unconventional low-cost fabrication and patterning techniques for point of care diagnostics. *Ann. Biomed. Eng.* 39, 1313–1327. doi: 10.1007/s10439-010-0213-1

Shum, A. M. Y., Che, H., Wong, A. O. T., Zhang, C., Wu, H., Chan, C. W. Y., et al. (2017). A micropatterned human pluripotent stem cell-based ventricular cardiac anisotropic sheet for visualizing drug-induced arrhythmogenicity. *Adv. Mater.* 29:1602448. doi: 10.1002/adma.201602448

Simon, D. T., Gabrielsson, E. O., Tybrandt, K., and Berggren, M. (2016). Organic bioelectronics: bridging the signaling gap between biology and technology. *Chem. Rev.* 116, 13009–13041. doi: 10.1021/acs.chemrev.6b00146

Srinivasan, A., Tahilramani, M., Bentley, J. T., Gore, R. K., Millard, D. C., Mukhatyar, V. J., et al. (2015). Microchannel-based regenerative scaffold for chronic peripheral nerve interfacing in amputees. *Biomaterials* 41, 151–165. doi: 10.1016/j.biomaterials.2014.11.035

Stieglitz, T., and Meyer, J. U. (1999). Implantable microsystems. Polyimide-based neuroprostheses for interfacing nerves. *Med. Device Technol.*10:28.

Stríteský, S., Marková, A., Víteček, J., Šafaříková, E., Hrabal, M., Kubáč, L., et al. (2018). Printing inks of electroactive polymer PEDOT: PSS: The study of biocompatibility, stability, and electrical properties. *J. Biomed. Mater. Res. A* 106, 1121–1128. doi: 10.1002/jbm.a.36314

Valero-Cabré, A., Tsironis, K., Skouras, E., Perego, G., Navarro, X., and Neiss, W. F. (2001). Superior muscle reinnervation after autologous nerve graft or poly-L-lactide-ϵ-caprolactone (PLC) tube implantation in comparison to silicone tube repair. *J. Neurosci. Res.* 63, 214–223. doi: 10.1002/1097-4547(20010115)63:2<214::AID-JNR1014>3.0.CO;2-D

Veraart, C., Grill, W. M., and Mortimer, J. T. (1993). Selective control of muscle activation with a multipolar nerve cuff electrode. *IEEE Trans. Biomed. Eng.* 40, 640–653. doi: 10.1109/10.237694

Wallman, L., Zhang, Y., Laurell, T., and Danielsen, N. (2001). The geometric design of micromachined silicon sieve electrodes influences functional nerve regeneration. *Biomaterials* 22, 1187–1193. doi: 10.1016/S0142-9612(00)00342-2

Wong, W. S., and Salleo, A. (2009). *Flexible Electronics: Materials and Applications*. Boston, MA: Springer Science and Business Media. doi: 10.1007/978-0-387-74363-9

Yannas, I. V., and Hill, B. J. (2004). Selection of biomaterials for peripheral nerve regeneration using data from the nerve chamber model. *Biomaterials* 25, 1593–1600. doi: 10.1016/S0142-9612(03)00505-2

Conflict of Interest: The authors declare that the research was conducted in the absence of any commercial or financial relationships that could be construed as a potential conflict of interest.

frontiers in Bioengineering and Biotechnology

ORIGINAL RESEARCH
published: 19 March 2021
doi: 10.3389/fbioe.2021.658176

Human Platelet Lysate Acts Synergistically With Laminin to Improve the Neurotrophic Effect of Human Adipose-Derived Stem Cells on Primary Neurons *in vitro*

*Martino Guiotto[1,2], Wassim Raffoul[1], Andrew M. Hart[2,3], Mathis O. Riehle[2] and Pietro G. di Summa[1]**

[1] Department of Plastic, Reconstructive and Hand Surgery, Centre Hospitalier Universitaire Vaudois (CHUV), University of Lausanne (UNIL), Lausanne, Switzerland, [2] Centre for the Cellular Microenvironment, University of Glasgow, Glasgow, United Kingdom, [3] Canniesburn Plastic Surgery Unit, Glasgow Royal Infirmary, Glasgow, United Kingdom

OPEN ACCESS

Edited by:
Xavier Navarro,
Universitat Autònoma de Barcelona, Spain

Reviewed by:
Kirsten Haastert-Talini,
Hannover Medical School, Germany
Adam Reid,
The University of Manchester, United Kingdom

***Correspondence:**
Pietro G. di Summa
pietro.di-summa@chuv.ch;
pietro.disumma@gmail.com

Specialty section:
This article was submitted to Tissue Engineering and Regenerative Medicine, a section of the journal Frontiers in Bioengineering and Biotechnology

Received: 25 January 2021
Accepted: 15 February 2021
Published: 19 March 2021

Citation:
Guiotto M, Raffoul W, Hart AM, Riehle MO and di Summa PG (2021) Human Platelet Lysate Acts Synergistically With Laminin to Improve the Neurotrophic Effect of Human Adipose-Derived Stem Cells on Primary Neurons in vitro. Front. Bioeng. Biotechnol. 9:658176. doi: 10.3389/fbioe.2021.658176

Background: Despite the advancements in microsurgical techniques and noteworthy research in the last decade, peripheral nerve lesions have still weak functional outcomes in current clinical practice. However, cell transplantation of human adipose-derived stem cells (hADSC) in a bioengineered conduit has shown promising results in animal studies. Human platelet lysate (hPL) has been adopted to avoid fetal bovine serum (FBS) in consideration of the biosafety concerns inherent with the use of animal-derived products in tissue processing and cell culture steps for translational purposes. In this work, we investigate how the interplay between hPL-expanded hADSC ($hADSC^{hPL}$) and extracellular matrix (ECM) proteins influences key elements of nerve regeneration.

Methods: hADSC were seeded on different ECM coatings (laminin, LN; fibronectin, FN) in hPL (or FBS)-supplemented medium and co-cultured with primary dorsal root ganglion (DRG) to establish the intrinsic effects of cell–ECM contact on neural outgrowth. Co-cultures were performed "direct," where neural cells were seeded in contact with hADSC expanded on ECM-coated substrates (*contact effect*), or "indirect," where DRG was treated with their conditioned medium (*secretome effect*). Brain-derived nerve factor (BDNF) levels were quantified. Tissue culture plastic (TCPS) was used as the control substrate in all the experiments.

Results: hPL as supplement alone did not promote higher neurite elongation than FBS when combined with DRG on ECM substrates. However, in the presence of hADSC, hPL could dramatically enhance the stem cell effect with increased DRG neurite outgrowth when compared with FBS conditions, regardless of the ECM coating (in both indirect and direct co-cultures). The role of ECM substrates in influencing neurite outgrowth was less evident in the FBS conditions, while it was significantly amplified in the presence of hPL, showing better neural elongation in LN conditions when compared with FN and TCPS. Concerning hADSC growth factor secretion, ELISA showed significantly higher concentrations of BDNF when cells were expanded in hPL compared with

FBS-added medium, without significant differences between cells cultured on the different ECM substrates.

Conclusion: The data suggest how hADSC grown on LN and supplemented with hPL could be active and prone to support neuron–matrix interactions. hPL enhanced hADSC effects by increasing both proliferation and neurotrophic properties, including BDNF release.

Keywords: human platelet lysate, extracellular matrix, laminin, adipose-derived adult stem cells, serum substitute supplement, peripheral nerve repair, cell therapy

INTRODUCTION

Peripheral nerve injuries (PNI), despite advancements of microsurgical techniques, lead to a profound reduction in patients' quality of life and pose a socioeconomic burden. Commonly, PNI result from trauma, tumor extirpation, or iatrogenic injuries to the upper and lower limb, mainly affecting young and adult working age classes.

Unlike the central nervous system, the peripheral nervous system (PNS) retains a spontaneous capacity to regenerate over short gaps, due to the plasticity of Schwann cells (SCs).

Currently, the gold-standard treatment is an end-to-end anastomosis in the case of short gap, while nerve grafts are generally chosen for long segment nerve defects (>2–3 cm) because of the otherwise excessive tension between the two stumps. These procedures lead to unsatisfactory outcomes and suboptimal functional recovery, followed by consequent donor site morbidity in the latter surgical option. Poor outcomes can be explained by the chronic denervation and fibrosis of the distal stump which rapidly affects the regenerative capability of the PNS (Jessen and Mirsky, 2016).

Tissue engineering pursues to find the ideal biodegradable conduit, in order to avoid the common nerve graft complications, preserving or even improving the functional outcomes in clinical care. In the last decade, the concept of an empty conduit was overcome by the application of intraluminal coatings or fillers containing extracellular matrix (ECM) molecules [laminin (LN), fibronectin (FN), or collagen], transplanted cells [SCs, SC-like cells, adipose-derived stem cell (ADSC)], and neurotrophic factors [mainly brain-derived nerve factor (BDNF), glial-derived nerve factor (GDNF), nerve growth factor (NGF)], which improve the recovery in the PNS (Resch et al., 2018).

The ideal cell type should be easily transplantable with no associated functional donor loss, proliferate rapidly in *in vitro* expansion, and successfully integrate into host tissue with minimal immunological reaction. Previous experimental studies in rodent have shown that ADSC transplantation represents effectively an alternative strategy to create a favorable environment for nerve regeneration without the drawbacks of SCs (need for nerve biopsy and sacrifice of a functional nerve, constant need for GF adjunction and more complex *in vitro* expansion) (Kingham et al., 2014; Mathot et al., 2019).

The growing interest in stem cell therapy in a wide range of medical fields opened new lines of investigation for nerve repair, with a particular focus on human ADSC (Lensch et al., 2018).

To achieve safe and reliable clinical translation, stem cell therapy has to be subjected to biosafety concerns (Paula et al., 2015; Condé-Green et al., 2016). The manipulation with xenogeneic components, including enzymatic adipose tissue dissociation and the use of fetal bovine serum (FBS) as culture medium supplement, showed the potential of immune reactions and exposure to viral, bacterial, or prion infection (Lalu et al., 2012; Sherman et al., 2019). Moreover, FBS is subject to batch-to-batch variability, which impacts on reproducibility. According to the good manufacturing practice (GMP) guidelines, the essential steps to ensure translationability for stem cell therapy are the avoidance of chemical- and/or animal-derived protein in tissue dissociation and culture supplementation (Kyllönen et al., 2013; Condé-Green et al., 2016).

According to these considerations, human platelet lysate (hPL) was suggested as a substitute to FBS for human cell expansion assuring the biosafety and consistent reliability in clinical translation, since it can be easily obtained, as pooled blood from apheresis products and buffy coats (Schallmoser et al., 2020).

Therefore, human adipose-derived stem cells (hADSC) expanded in hPL-supplemented medium ($hADSC^{hPL}$) can be seen as a viable cell population for therapy in nerve defects, with translational applicability and neurotrophic potential (Palombella et al., 2020).

Regarding a further potential actor involved in PNS regeneration, the ECM, an acellular component composed of proteoglycans and fibrous proteins such as collagen, elastin, fibronectin, and laminin, provides a well-defined environment for cell survival, differentiation, tissue morphogenesis, and homeostasis (Frantz et al., 2010; de Luca et al., 2014). LN is a main component of the ECM both in the central and the peripheral nervous systems, supporting a variety of functions including SC migration, axonal outgrowth, and axon myelination (Barros et al., 2011; di Summa et al., 2013). FN is secreted by glial cells promoting cell growth, survival, and motility. Both support the recovery after nerve injuries: the former (LN) stimulating

Abbreviations: BDNF, brain-derived growth factor; DRG, dorsal root ganglia; ECM, extracellular matrix; FBS, fetal bovine serum; FN, fibronectin; GDNF, glial cell line-derived neurotrophic factor; GMP, good manufacturing practice; GFs, growth factors; hADSC, human adipose-derived stem cells; hPL, human platelet lysate; $hADSC^{hPL}$, human adipose-derived stem cells pre-expanded with hPL-added medium; $hADSC^{FBS}$, human adipose-derived stem cells pre-expanded with FBS-added medium; IKVAV, Ile-Lys-Val-Ala-Val; LN, laminin; MSCs, mesenchymal stem cells; MBP, myelin basic protein; NGF, nerve-derived growth factor; PNI, peripheral nerve injuries; PNS, peripheral nervous system; dADSC, rat ADSC differentiated toward a glia-like phenotype; RGD, Arg-Gly-Asp; SCs, Schwann cells; TCPS, tissue culture plastic; YIGSR, Tyr-Ile-Gly-Ser-Arg.

axonal elongation and activating SCs in myelin production, the latter (FN) increasing neural cell adhesion and SC proliferation (Gao et al., 2013).

After a nerve lesion in PNS, SCs dedifferentiate into a "repair" SC phenotype, migrate, proliferate along the endothelial bridge across the nerve gap, secrete growth factors, support axonal elongation, and myelinate axons. The ECM provides the binding sites mediating interactions between cells, growth cone, and the surrounding microenvironment through specific integrin receptors, which regulate cell adhesion, proliferation, migration, and differentiation (Plow et al., 2000; Schmidt and Leach, 2003; Scheib and Höke, 2013). While being a critical component for cell-to-cell interactions, ECM also acts as a reservoir for soluble factors bound to its components through specific receptors (Harris et al., 2017).

By providing the cells with specific ECM cues, it is possible to influence and improve the regenerative process and gain further insights into its therapeutic potential.

Building on our previous works, and in order to define the most suitable and encouraging coating for a future bioconduit, we investigated the impact of $hADSC^{hPL}$ in combination with different ECM-molecule-coated surfaces, and we studied their individual and combined potentials to improve neurite outgrowth in a dorsal root ganglia (DRG) explant model.

MATERIALS AND METHODS

hADSC Extraction and Culture

hADSC were isolated from abdominal adipose tissue of three healthy women (age 49 ± 2) who underwent breast reconstruction using abdominal autologous flaps (deep inferior epigastric perforator flaps, DIEP) at Canniesburn Plastic Surgery Unit, Glasgow Royal Infirmary, Glasgow, Scotland. The discarded part of the flap and the adipose tissue were obtained after a signed informed consent. All protocols were reviewed and approved by the hospital ethics committees (local Biobank number 314 GGC) in accordance with the Declaration of Helsinki.

The adipose tissue was mechanically minced, microdissected, and mechanically dispersed in a 10-cm Petri dish, until the hADSC were selected according to their plastic adherence. They were resuspended in 7 ml of complete medium (see below for composition), plated in T75 flask, and cultured at 37°C and 5% CO_2. The medium was changed after 24 h to remove erythrocytes and, afterward, every 3–4 days until cell confluence.

Cells isolated were cultured in parallel in complete medium: alpha-MEM (Gibco, Paisley, United Kingdom) added with 5% hPL (Antibodies, Aachen, Germany) or 10% FBS (Sigma-Aldrich, United Kingdom) and 1% penicillin–streptomycin (GE Healthcare).

Extracellular Matrix Surface Preparation and Cell Seeding

Tissue culture plastic (TCPS) 24-well plates were use direct or coated according to the specific condition with either LN (LN-1, Engelbreth-Holm-Swarm murine sarcoma basement membrane, Sigma-Aldrich) for 2 h at 37°C at 10 μg/ml phosphate buffered saline (PBS) or FN (bovine plasma, Sigma-Aldrich) at 10 μg/ml PBS for 1 h at room temperature. For the control, TCPS well surface was used without any prior coating. Every coating step was followed by a double washing with PBS 1 × solution (Sigma-Aldrich). The concentration of the ECM proteins and the timing for coating procedures were based on our previous experience (di Summa et al., 2013; de Luca et al., 2018).

hADSC were trypsinized and homogeneously seeded at a density of 15,000 cells/cm^2 in 24-well plates, incubated for 48 h at 37°C, 5% CO_2, and then seeded with freshly dissected DRG.

DRG Organotypic Explants

All work was carried out in accordance with the Home Office Animals (Scientific Procedures) Act 1986. Neonatal Sprague–Dawley rats (1–3 days old) were euthanized by Euthatal® injection (Merial, 200 mg/ml, 500 mg/kg), carried out by an animal house technician in accordance with Home Office regulations, and DRG carefully dissected using the microsurgical technique under binocular magnification. Upon extraction, DRG were transferred to an ice-cooled Petri dish with Leibovitz's L-15 Medium (Thermo Fisher Scientific, Loughborough, United Kingdom) and processed to remove excess roots. DRG organotypic explants were, after delicate microsurgical root cleaning, immediately cultured (one single DRG/well) under the three conditions detailed below. After 48 h of co-culture, DRG were fixed and stained following the protocol below.

hADSC–DRG Co-Cultures

With the co-cultures, we wanted to reproduce *in vitro* the supposed *in vivo* effects of hADSC when used in a nerve conduit for peripheral nerve repair. We adapted the co-culture model to investigate the interactions between ECM proteins (condition 1), hADSC (condition 2), and hADSC secretome only (condition 3) with primary neurons. Considering the *in vivo* timescale of nerve repair, these three conditions could mimic the spatial–temporal contacts of the growth cone after the implantation of a cell-filled nerve conduit at the injury site (**Table 1**).

Condition 1 (DRG Alone)

Single DRG was grown on a 24-well plate coated with LN, FN, or TCPS only for 48 h at 37°C, 5% CO_2 in a mix of 100 μl of L-15 media (Thermo Fisher), 50 μg/ml *N*-acetylcysteine (NAC, Sigma-Aldrich) (West et al., 2007), 1% penicillin–streptomycin (Pen-Strep, GE Healthcare), 10 ng/ml NGF 2.5S (Invitrogen) (*DRG medium*), and 100 μl of Alpha-MEM (Gibco) with 5% hPL (Antibodies) or 10% FBS (Sigma-Aldrich) (*hADSC medium*). To make this condition comparable with the following ones, the co-culture medium was prepared by mixing in equal parts the DRG medium with complete hADSC medium.

Condition 2 (Direct Co-Cultures)

A single DRG was cultured on top of hADSC (15,000/cm^2 in a 24-well plate pre-expanded for 48 h on LN, FN-coated surface, or TCPS at 37°C, 5% CO_2) in a mixture of 100 μl of DRG medium and 100 μl of hADSC medium for 48 h at 37°C, 5% CO_2. The

TABLE 1 | DRG explant co-culture *in vitro* model to mimic the hPL–hADSC therapy on ECM-coated scaffold *in vivo*.

	Cells in culture	Culture medium	Substrate	*In vivo* interaction simulation
Condition 1—DRG alone	Primary DRG explant	50% DRG medium, 50% hADSC medium	24-well plate coated with LN, FN, or TCPS	Growth cone and ECM
Condition 2—direct co-culture	Primary DRG explant and hADSC	50% DRG medium, 50% hADSC medium Serum-free condition: 50% DRG medium, 50% hADSC medium (without 5% hPL or 10% FBS)	24-well plate coated with LN, FN, or TCPS	Growth cone, ECM, and hADSC (cells + secretome)
Condition 3—indirect co-culture	Primary DRG explant	50% DRG medium, 50% hADSC secretome	24-well plate coated with LN, FN, or TCPS	Growth cone, ECM, and hADSC (secretome)

hPL, human platelet lysate; hADSC, human adipose-derived stem cells; ECM, extracellular matrix; DRG, dorsal root ganglion; LN, laminin; FN, fibronectin; TCPS, tissue culture plastic.

same direct co-cultures were repeated in parallel without medium supplementation with FBS or hPL (*serum-free*) but keeping these additives only during hADSC expansion steps (to closely mimic the *in vivo* condition, **Table 1**).

Condition 3 (Indirect Co-Cultures)

A single DRG explant was cultured on a 24-well plate coated with either LN, FN, or TCPS for 48 h at 37°C, 5% CO_2 in a mixture of 100 μl of DRG medium and 100 μl of conditioned medium of the hADSC (*secretome*) previously grown (initial same cell density, 15,000/cm^2) on a substrate coated with either LN, FN, or TCPS for 48 h in the presence of hADSC complete medium (**Figure 1A**).

Immunofluorescence

After 48 h, DRG were fixed and stained with mouse anti-β3-tubulin (Sigma-Aldrich Tub III, 1:100) and FITC-coupled phalloidin (Thermo Fisher; 1:200) followed by Texas Red-labeled antimouse (1:100, Vector Laboratories, United States) and DAPI (VECTASHIELD, Vector Laboratories, Peterborough, United Kingdom).

Image Analysis

Samples were viewed on an Olympus BX51 fluorescent microscope using 10 × (Olympus, NA 0.3). Images were acquired using a high-resolution camera (QImaging, Retiga 2000i), an automated stage movement (Prior Scientific, United Kingdom) combined with the auto-stitching of mosaic images with Surveyor Viewer software (Objective Imaging, United States).

DRG scanning images (anti-β3-tubulin channel) were analyzed in Fiji ImageJ software (Schindelin et al., 2012).

Both image capturing and neurite outgrowth analysis were performed by the same examiner. Results were expressed as the longest neurite and "axonal area," which was defined as the area that was covered by β3-tubulin-positive neurites. This was used as the whole extension of the DRG and its outgrowth was imaged for each condition. The neurite length was manually evaluated using the Freehand line tool after setting the appropriate scale for calibration. For every picture, at least five different attempts were performed to identify the longest neurite. The area was identified with the Freehand area tool following the perimeter of each neurites. Experiments were repeated for three biological repeats and at least three technical repeats for each condition (**Figures 1B,C**).

Evaluation of BDNF-Secreted Factor

The conditioned medium was collected after expansion of hADSC for 48 h on coated (LN or FN) surfaces or on uncoated TCPS in the presence of either of the two supplements (FBS, hPL). After centrifugation step at 4,300 relative centrifugal force for 10 min to remove cellular debris, supernatants were transferred to a new tube and stored at −20°C until processing. Fresh non-conditioned medium was used as negative control. Subsequently, samples were analyzed with ELISA kits for BDNF (R&D Systems, Bio-Techne DuoSet ELISA Human BDNF, Abingdon, United Kingdom), according to the manufacturer's instruction. Each sample was assayed in duplicate and the absorbance determined at 450 and 570 nm with an infinite F50 spectrophotometer (Tecan Group, Männedorf, Switzerland). The quantity of the secreted factor, calculated from a standard curve produced using recombinant protein, was multiplied with the dilution factor. Experiments were conducted in technical and biological triplicates.

Statistical Analysis

All data were expressed as average ± standard error of the mean (SEM). To verify the data spread, D'Agostino and Pearson omnibus normality test was applied (D'Agostino, 1971).

One-way analysis of variance (ANOVA) with Tukey's multiple comparison test was used to assess statistical significance among groups.

Significance was expressed as $^{*}p < 0.05$, $^{**}p < 0.01$, $^{***}p < 0.001$, and $^{****}p < 0.0001$. All analysis was performed using GraphPad Prism 6 for Mac (GraphPad Software, La Jolla, CA, United States).

RESULTS

Serum Additives Significantly Influence DRG Neurite Outgrowth but Only in Combination With Laminin

To understand the impact of hPL on primary neurons, DRG explants were cultured on LN or FN-coated TCPS (with uncoated TCPS used as a negative control) for a time period of 48 h. The hypothesis that a higher concentration of trophic molecules present in hPL may enhance nerve regeneration on their own was not confirmed: DRG outgrowth, both in terms of the longest

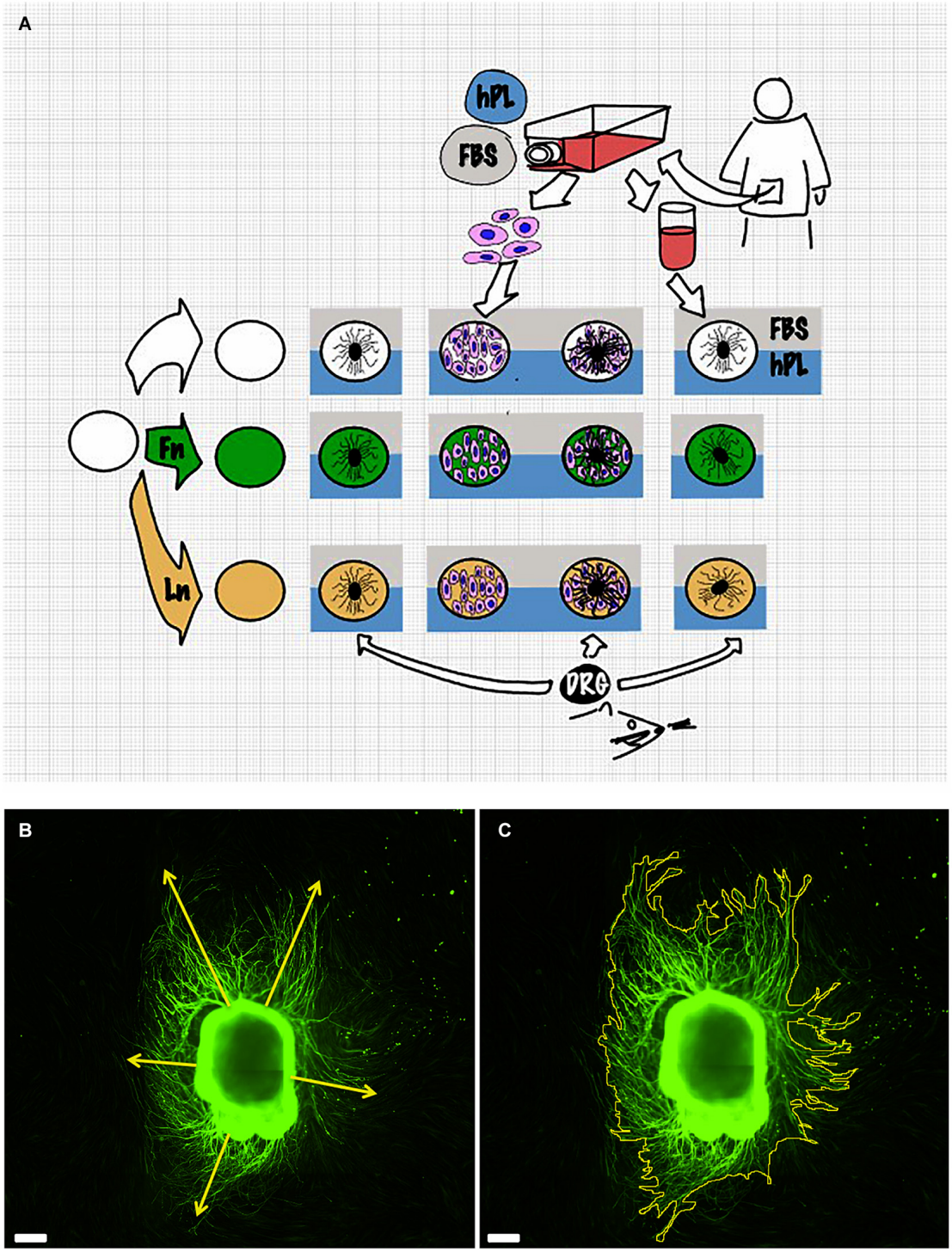

FIGURE 1 | Scheme of the experimental setup **(A)**. Details of the measurement method: dorsal root ganglion (DRG) longest neurite **(B)** and area **(C)**. Scale bar: 500 μm.

neurite as well as axonal area, was comparable regardless of the serum supplement (FBS or hPL) adopted for the medium.

However, when considering the ECM impact on DRG outgrowth, our results showed meaningful variation when DRG were cultured on LN-coated surfaces. This effect was visible in both DRG in media supplemented with either hPL or FBS in terms of neurite extension [LN vs TCPS (FBS), $^{****}p < 0.0001$; LN vs TCPS (hPL), $^{***}p < 0.001$; **Figure 2**], but only in

hPL conditions when considering axonal area [LN vs TCPS (hPL), $^{***}p < 0.001$]. Similarly, LN enhanced neurite elongation significantly more so than FN, but this effect was statistically significant only for hPL (LN vs FN: longest neurite, $^{*}p < 0.05$; axonal area, $^{**}p < 0.01$; **Figure 2**).

ECM, hADSC, and hPL Synergistically Enhance DRG Outgrowth

To assess the effect of hADSC on neural cells, comparing FBS to when hPL is applied as the medium additive in the pre-expansion steps ($hADSC^{FBS}$, $hADSC^{hPL}$), we performed a direct co-culture of $hADSC^{FBS}$ or $hADSC^{hPL}$ with single DRG on LN, FN-coated surface, or TCPS.

hPL and FBS differ considerably in their content (growth factors, adhesion factors, cytokines, and bulk protein), which may directly influence DRG explant outgrowth; therefore, the hADSC were only precultured with either media, then continued in serum-free conditions once the DRG were added. These experiments were performed in parallel to the same direct co-cultures (with serum additives) between hADSC and primary neurons.

The DRG explant outgrowth was the same, and no significant difference was found between serum-free and serum-added groups, independently of the ECM (**Appendix 1**), confirming that the medium additives themselves did not influence DRG outgrowth directly. Applying hPL only during the expansion steps of hADSC was sufficient to obtain a significant neurotrophic effect on neurons, which was consistent with our previous results (Palombella et al., 2020).

The DRG longest neurite was strongly increased by $hADSC^{hPL}$ in all conditions, compared with the same co-culture system with $hADSC^{FBS}$ ($^{****}p < 0.0001$ on LN, $^{***}p < 0.001$ on FN, $^{***}p < 0.001$ on TCPS, **Figure 3**). Similarly, the axonal area was higher in $hADSC^{hPL}$ conditions on LN ($^{****}p < 0.0001$), FN ($^{*}p < 0.05$), and TCPS ($^{**}p < 0.001$) when compared with the $ADSC^{FBS}$ (**Figure 3**).

Importantly, the $hADSC^{hPL}$ cultured on LN lead to a statistically stronger DRG outgrowth (both the longest neurite and axonal area) compared with any other condition, including versus $hADSC^{hPL}$ on FN (longest neurite and area: $^{****}p < 0.0001$) or TCPS (longest neurite $^{****}p < 0.0001$; area $^{**}p < 0.01$). The differences in DRG explant outgrowth between the different ECM coatings were less pronounced in any of the FBS conditions. Although DRG explants on $ADSC^{FBS}$ cultured on LN showed a significantly increased neurite outgrowth when compared with FN, this was not the case when compared with the outgrowth seen on $ADSC^{FBS}$ on TCPS (**Figure 3**).

$hADSC^{hPL}$ Secretome Supports DRG Outgrowth With High Affinity for ECM Molecules

To analyze the impact of the hADSC secretome alone on DRG outgrowth, without the effect of cell-to-cell interactions, we realized an indirect co-culture model with single DRG grown on LN, FN-coated surface, or TCPS and treated with hADSC-conditioned medium that was derived from hADSC cultures supplemented either with FBS or with hPL, cultured on TCPS alone, or TCPS coated with either LN or FN.

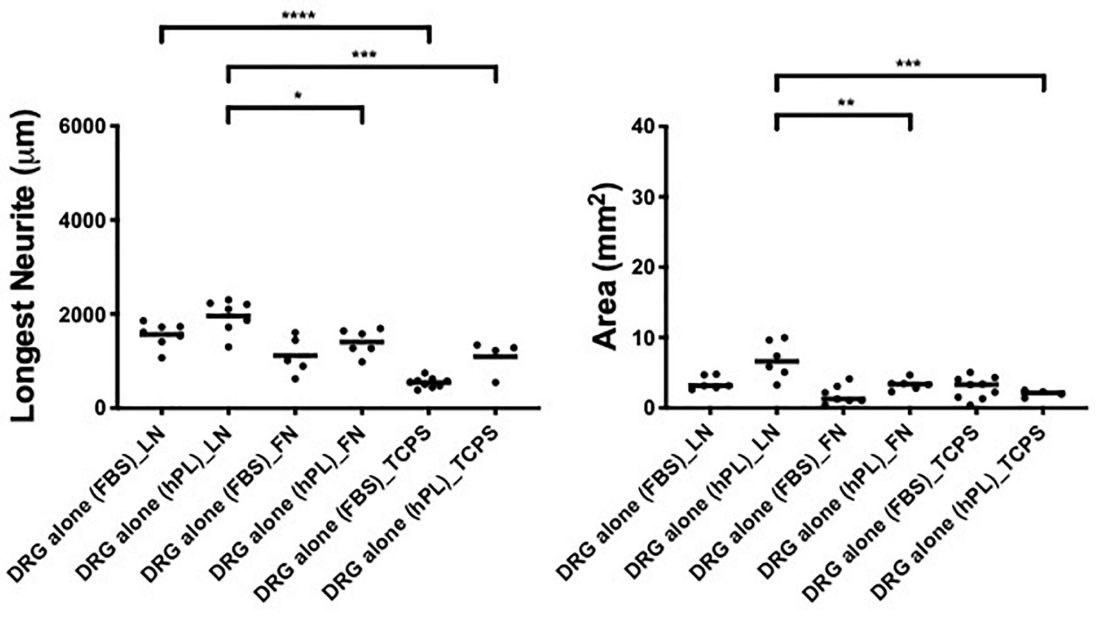

FIGURE 2 | Serum additives significantly influence DRG neurite outgrowth, but only in combination with laminin (condition 1—DRG alone). Longest neurite and axonal area of DRG alone on the extracellular matrix (ECM). Three biological repeats and at least three technical replicates (DRG) were assessed. One-way ANOVA with Tukey's multiple comparison tests was used for assessing statistical significance among the examined groups ($^{*}p < 0.05$, $^{**}p < 0.01$, $^{***}p < 0.001$, $^{****}p < 0.0001$). The number of DRG tested corresponds to the number of dots for each condition in the graph.

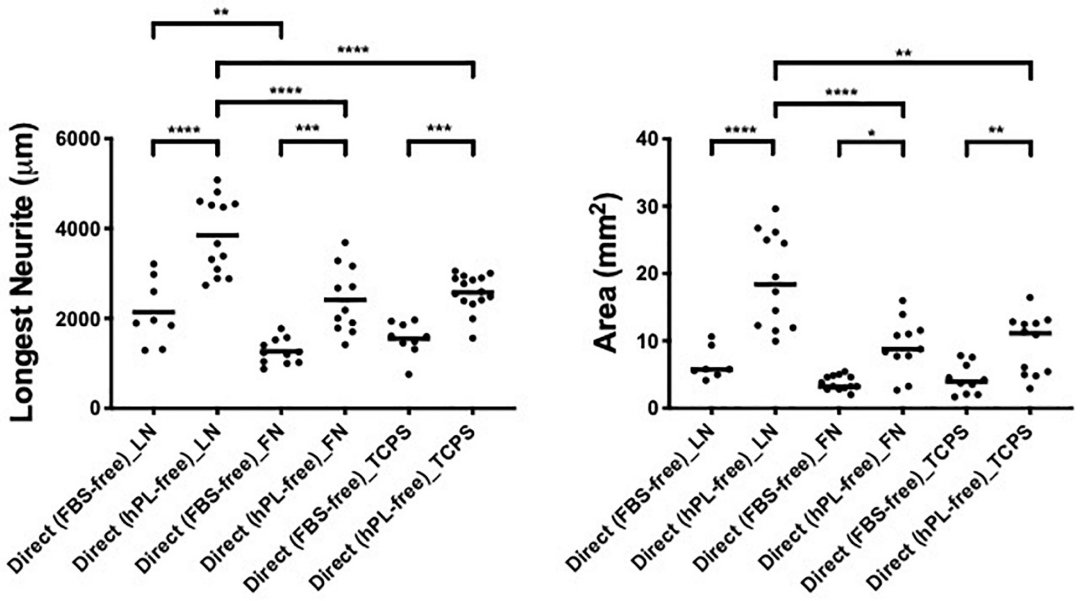

FIGURE 3 | ECM, human adipose-derived stem cells (hADSC), and human platelet lysate (hPL) synergistically interact enhancing DRG outgrowth (condition 2—direct co-culture). Longest neurite and axonal area of direct co-culture on ECM. Three biological repeats and at least three technical replicates (DRG) were assessed. One-way ANOVA with Tukey's multiple comparison tests was used for assessing statistical significance among the examined groups ($^{*}p < 0.05$, $^{**}p < 0.01$, $^{***}p < 0.001$, $^{****}p < 0.0001$). The number of DRG tested corresponds to the number of dots for each condition in the graph.

The DRG outgrowth (both the longest neurite and axonal area) was significantly increased by the hADSC^{hPL} secretome (vs ADSC^{FBS} secretome) on either of the two ECM substrates (longest neurite: LN $^{***}p < 0.001$, FN $^{*}p < 0.05$; axonal area: LN $^{**}p < 0.01$) but not on TCPS (**Figure 4**).

The strongest neurotrophic effect was seen on DRG explants placed on LN and stimulated by hADSC^{hPL} secretome. The hADSC^{hPL} secretome evoked the longest neurite to grow of DRG explants and lead to axonal areas that were significantly higher than on either FN or TCPS (longest neurite: vs FN $^{**}p < 0.01$, vs TCPS $^{***}p < 0.001$; area: vs FN $^{***}p < 0.001$, vs TCPS $^{****}p < 0.0001$).

The ADSC^{FBS} secretome showed no synergistic effects in combination with the different substrate types on axonal outgrowth of DRG (**Figure 4**).

Influence of ECM Molecules on DRG Outgrowth

The combination of a direct co-culture of the DRG explants on hADSC grown with hPL and on LN showed the most effective approach *in vitro* for nerve regeneration; this combination showed the longest DRG neurite outgrowth (almost 4,000 μm) and the largest axonal area (almost 20 mm^2). For the indirect co-culture, the secretome of hADSC^{hPL} on LN resulted in a significantly higher axonal elongation ($^{*}p < 0.05$) when compared with the DRG explant on its own on LN (**Figure 5**).

hADSC^{hPL} grown on FN-coated surfaces showed, once in contact with DRG explants, a beneficial effect on neurite outgrowth, when compared with the DRG alone on FN, even if with significantly lower values for the longest neurite or axonal area when compared with laminin-coated substrates (direct vs DRG alone, longest neurite: $^{**}p < 0.01$, axonal area: $^{***}p < 0.001$; direct vs indirect, area $^{*}p < 0.05$, **Figure 6**).

Interestingly, the positive effect of hADSC grown on FN was only visible in the direct co-culture system and only in the presence of hPL. When the secretome of hADSC grown on FN or TCPS was used as a culture medium (condition 2), DRG explant outgrowth was not significantly impacted when compared with the DRG explant grown directly on the respective ECM surface.

hADSC^{hPL} grown on TCPS evidenced a neurotrophic effect only when the primary DRG explants were in direct contact with the hADSC (longest neurite: vs indirect $^{****} < 0.0001$, vs DRG explant alone $^{****} < 0.0001$; area: vs indirect $^{**} < 0.01$, vs DRG explant alone $^{**} < 0.01$, **Figure 7**).

Here, the direct co-culture appeared significantly better than DRG explant alone even when FBS was used as additive medium (longest neurite: $^{****} < 0.0001$, **Figure 7**).

hADSC^{hPL} Show Enhanced BDNF Secretion

We evaluated the secretion of BDNF in hADSC-conditioned medium collected after 48 h of cell expansion on LN, FN, or TCPS with medium supplemented either with 5% hPL or 10% FBS.

The hPL alone had a significantly higher concentration of BDNF when compared with the hADSC-conditioned medium, regardless of the ECM-coating options. In all three ECM-coating conditions, the levels of BDNF detected in the 5% hPL-added

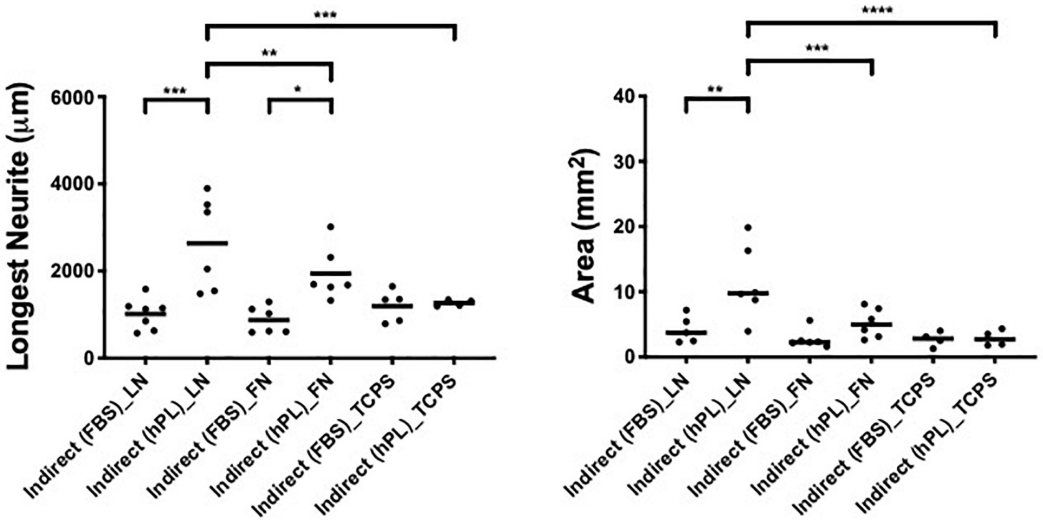

FIGURE 4 | hPL–hADSC secretome supports DRG outgrowth with high affinity for ECM molecules (condition 3—indirect co-cultures). Longest neurite and axonal area of indirect co-culture on ECM. Three biological repeats and at least three technical replicates (DRG) were assessed. One-way ANOVA with Tukey's multiple comparison tests was used for assessing statistical significance among the examined groups (*$p < 0.05$, **$p < 0.01$, ***$p < 0.001$, ****$p < 0.0001$). The number of DRG tested corresponds to the number of dots for each condition in the graph.

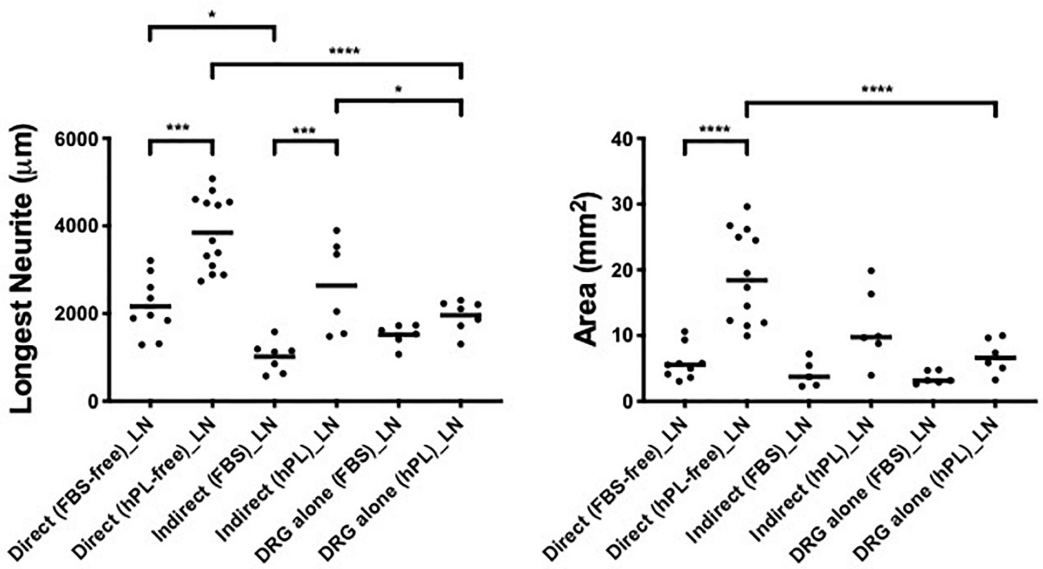

FIGURE 5 | Influence of laminin on DRG outgrowth. Longest neurite and axonal area of direct co-culture, indirect co-culture, and DRG alone on laminin (LN). Three biological repeats and at least three technical replicates (DRG) were assessed. One-way ANOVA with Tukey's multiple comparison tests was used for assessing statistical significance among the examined groups (*$p < 0.05$, **$p < 0.01$, ***$p < 0.001$, ****$p < 0.0001$). The number of DRG tested corresponds to the number of dots for each condition in the graph.

medium were significantly increased compared with the media supplemented with 10% FBS (****$p < 0.0001$, **Figure 8**).

The hADSC cultured under serum-free conditions did not show a significantly different change in BDNF release independently of the ECM substrate that they grew on. When focusing on a potential ECM effect con the GF release, hADSC^{hPL} on LN did not seem to result in any significant changes to the free BDNF levels in the supernatant (**Figure 8**).

DISCUSSION

PNI can cause motor, sensory, and autonomic disabilities. Despite the spontaneous regeneration of the peripheral nervous system and microsurgical advancements in nerve repair, the outcomes remain far from optimal, with unsatisfactory functional results and high morbidity (Xu et al., 2019). The necessity of ameliorating the restorative potential has guided research interest

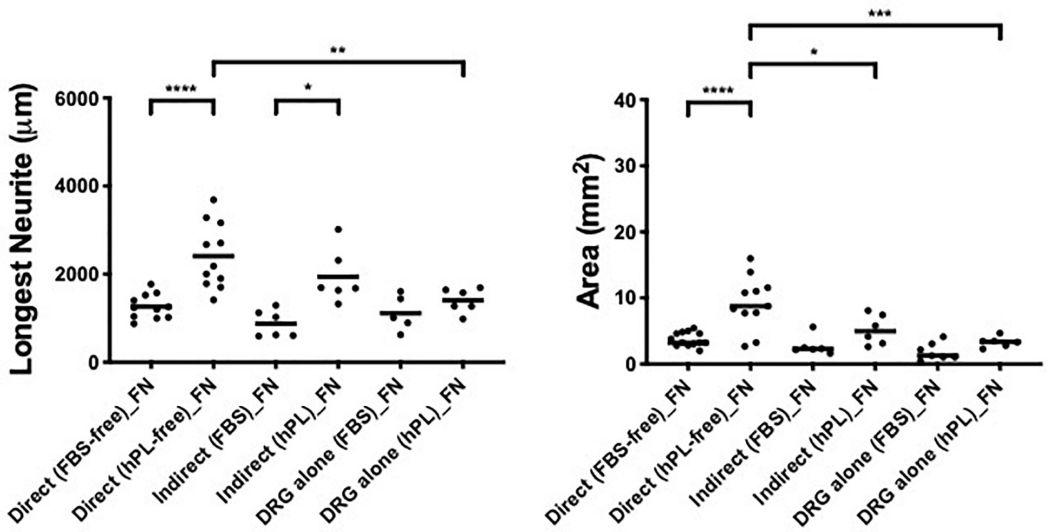

FIGURE 6 | Influence of fibronectin on DRG outgrowth. Longest neurite and axonal area of direct co-culture, indirect co-culture, and DRG alone on fibronectin (FN). Three biological repeats and at least three technical replicates (DRG) were assessed. One-way ANOVA with Tukey's multiple comparison tests was used for assessing statistical significance among the examined groups (*$p < 0.05$, **$p < 0.01$, ***$p < 0.001$, ****$p < 0.0001$). The number of DRG tested corresponds to the number of dots for each condition in the graph.

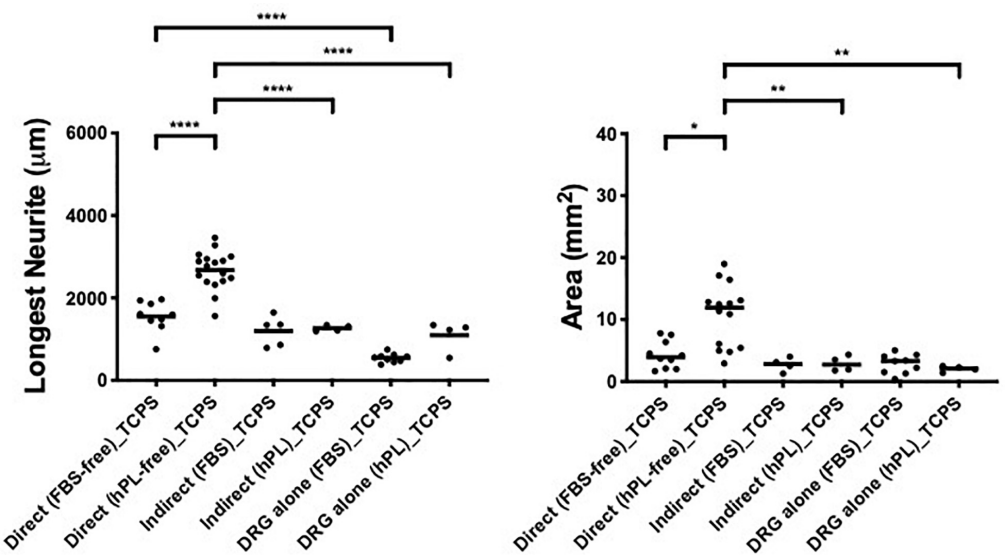

FIGURE 7 | Influence of tissue culture plastic (TCPS) on DRG outgrowth. Longest neurite and axonal area of direct co-culture, indirect co-culture, and DRG alone on TCPS. Three biological repeats and at least three technical replicates (DRG) were assessed. One-way ANOVA with Tukey's multiple comparison tests was used for assessing statistical significance among the examined groups (*$p < 0.05$, **$p < 0.01$, ***$p < 0.001$, ****$p < 0.0001$). The number of DRG tested corresponds to the number of dots for each condition in the graph.

toward cellular therapies, which aim to use autologous cells to support the host regeneration process (Guo et al., 2017).

hADSC have attracted interest for their cell-based therapy potential because of their abundance, ease of isolation, high proliferation rate, greater differentiation potential compared with other mesenchymal stem cells (MSCs), and their immunomodulatory and angiogenic properties (Kim et al., 2013; Palombella et al., 2017; Cowper et al., 2019). The regenerative capability is the synergy between the cell-to-cell interactions and what cells release in the surrounded milieu (Teixeira et al., 2015). Thus, recent cell therapy research has been focused on the potential applications of the MSC secretome due to its GF-enriched composition and extracellular vesicles. Nevertheless, the proteomic studies are still insufficient to explain the functional effects of the MSC secretome, and to specify the diverse protein spectra according to the type of

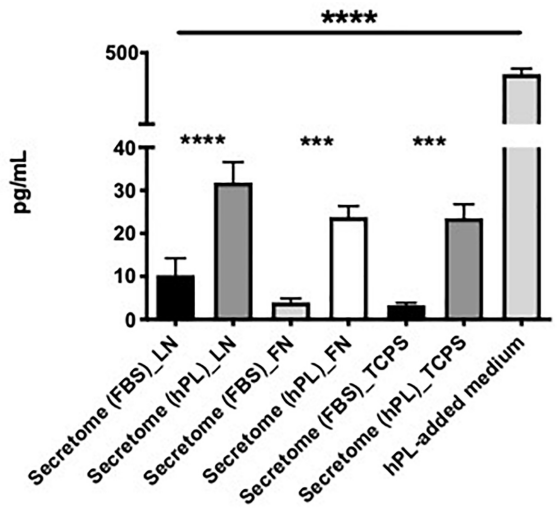

FIGURE 8 | hPL–hADSC show enhanced brain-derived nerve factor (BDNF) secretion. Evaluation of BDNF concentration (pg/ml) in hADSC-conditioned medium (secretome) on LN, FN, or TCPS. Both supplement media (FBS and hPL) were tested and compared according to the ECM-coating condition. BDNF concentration was evaluated in hPL-added medium alone (without cells), too. Three biological and technical (each one in duplicate) repeats were assessed. One-way ANOVA with Tukey's multiple comparison tests was used for assessing statistical significance among the examined groups (*$p < 0.05$, **$p < 0.01$, ***$p < 0.001$, ****$p < 0.0001$).

MSCs, some studies showed an increased neuronal and glial survival rate or a more pronounced neural/glial differentiation, when neural precursor cells were cultured with human umbilical cord perivascular cell (HUCPVC) secretome, possibly explained by the release of NGF, fibroblast growth factor-2 (FGF-2), or intracellular protein such as 14-3-3, Hsp70, and UCHL1 (Ribeiro et al., 2012; Teixeira et al., 2015).

Recently, we developed a completely animal protein-free method to extract, culture, and maintain *in vitro* hADSC, guaranteeing patient biosafety and potential for clinical translation (Palombella et al., 2020).

As a medium additive, hPL provides a safe, human-derived product, which has been shown to increase the proliferation of hADSC, preserve their stemness properties and differentiation potential, and even enhance their neural commitment (Guiotto et al., 2020; Lischer et al., 2020; Palombella et al., 2020). For all these reasons, hADSC pre-expanded in hPL (hADSC^{hPL}) are the ideal candidate for cell-based therapies and can play a role in nerve tissue engineering encouraging regeneration.

Functionalization of biomaterial surfaces to influence cellular behavior can be a fruitful approach to deliver and maintain transplanted cells for medical application. Such cells may be induced toward target cells by reproducing the original regeneration environment through physical and biochemical components (Zhang et al., 2019).

In this sense, when considering the interplay between the ECM and neural cells, the design of a hADSC^{hPL} cell delivery scaffold needs to simulate the physical and haptotactic cues of the ECM, guiding the axonal elongation across the nerve stumps, through both soluble signaling and contact integrin receptor pathways (Chen et al., 2000; Armstrong et al., 2007; Dodla and Bellamkonda, 2008; Guo et al., 2015, 2017; Poitelon et al., 2016).

According to the literature, ECM components (FN, LN, and collagen) have been successfully applied as inner coating of neural conduits in rodent *in vivo* models, successfully increasing SC and MSC proliferation, cell viability, and functional outcomes (Armstrong et al., 2007; Gámez Sazo et al., 2012; de Luca et al., 2013; Gonzalez-Perez et al., 2018). LN has been reported to be an important actor when considering ECM proteins that have been shown to promote nerve outgrowth, being essential for SC proliferation, morphological/phenotypical modifications, and myelination (Milner et al., 1997; Chernousov et al., 2008; Yu et al., 2009; Koh et al., 2010; di Summa et al., 2013; Hosseinkhani et al., 2013; de Luca et al., 2014).

Interestingly, LN impacts consistently not only on neural cell growth but also on ADSC attachment, survival, and SC-like differentiation. Our group previously showed that LN better supported rat ADSC differentiated toward a glia-like phenotype (dADSC) adhesion and survival and in co-culture with neurons supporting an increased neurite length. Consistently, we detected a boost to growth factor secretion (NGF and BDNF) when dADSC were grown on ECM (LN or FN) with DRG (di Summa et al., 2013).

Close to our outcomes, Zarinfard et al. (2016) found that human adipose cells transdifferentiated into SC-like, grown on LN surface exhibited higher cell viability and stronger gene expression of GFAP, S100-Beta, myelin basic protein (MBP), and even BDNF and GDNF.

Gonzalez-Perez et al. showed better *in vitro* proliferation and cell survival of SCs when cultured in LN than in FN. However, in their *in vivo* study, with a critical rat sciatic nerve gap, SCs seeded in FN-aligned matrices showed superior functional results than SCs loaded in LN-aligned matrices. Regarding the application of MSCs (derived from bone marrow) in the same aligned constructs, better outcomes were reported both *in vitro* and *in vivo*, when surfaces were coated with FN (Gonzalez-Perez et al., 2018).

With translation to the clinic in mind, and to avoid patient safety issues related to animal-derived protein extraction, whole ECM proteins are replaced with select functional motifs while preserving the same molecular functionality. In the context of nerve repair, a combination of synthetic peptides present on FN and LN, RGD (Arg-Gly-Asp), and LN-derived YIGSR (Tyr-Ile-Gly-Ser-Arg) and IKVAV (Ile-Lys-Val-Ala-Val) has been shown to be useful (Li et al., 2014). While YIGSR and RGD mediate SC adhesion and proliferation, IKVAV has been shown to support neural differentiation capability and axonal elongation both *in vitro* and *in vivo* (Motta et al., 2019).

Finally, Santiago et al. found that the hADSC adhere preferentially to substrates modified with the IKVAV peptide and less so to YIGSR or RGD (Santiago et al., 2006).

To further investigate the implications of hPL in cell therapy, in this work, we combined hADSC^{hPL} with ECM proteins (LN, FN) in co-culture models with primary DRG neurons in an organotypic tissue explant model. These investigations were conducted with the aim to clarify the effects resulting from a

combination of different sera, human ADSC, and two ECM molecules, on primary neurons *in vitro*.

When DRG explants were growing alone (condition 1, without hADSC influence), the two different medium supplements (FBS or hPL) did not influence neurite outgrowth, meaning that the hPL itself, despite its higher GF levels (Guiotto et al., 2020), did not provide significantly higher neurotrophic effects compared with standard FBS (**Figure 2**) (Palombella et al., 2020). Still, the presence of LN only (DRG alone—condition 1) manifested a meaningful promotion of neurite length and axonal area in comparison with FN or TCPS, independent of the medium supplement used (**Figure 2**).

When DRG explants were directly grown in contact with hADSC (condition 2), we show a significant difference between the regeneration (longest neurite and axonal extension area) observed for cultures supplemented with hPL and the ones with FBS, in all coating conditions (**Figure 3**). Remarkably, hPL enhanced the well-known positive effect of hADSC on nerve regeneration (Guo et al., 2017).

When DRG neurons were grown with hADSC-conditioned medium (condition 3), the data showed a significant difference between the hADSC^{FBS} and hADSC^{hPL} secretome where the latter increased neurite length and density, on either ECM-coated surfaces (LN, FN) but not on TCPS. This suggests a significant role of the secretome–matrix–neuron interaction system. Particularly, on LN, primary neurons evidenced the highest response to the hADSC^{hPL} secretome, confirming that LN coating forms part of an ideal environment for regenerating neurons, enabling their response to the neurotrophic effect of the secretome and sustaining axonal elongation (**Figure 4**) (Armstrong et al., 2007).

The critical role of the interplay between ECM, hADSC, and hPL was evident in the direct co-culture conditions, where we noticed a striking DRG explant outgrowth on LN–hADSC (**Figures 5**, **9**).

Overall, in direct and indirect co-cultures, the neurite outgrowth on LN was significantly increased when compared with the uncoated and even to the FN setting. Interestingly, this effect was only present when hPL was applied as the additive medium during the hADSC expansion steps. Importantly, keeping the hPL supplementation ongoing during the direct co-culture did not seem to further improve neurite outgrowth as we evaluated previously (Palombella et al., 2020).

Indeed, LN directly influences, on the one hand, hADSC adhesion, proliferation, and their neurotrophic properties [supporting GF release (Palombella et al., 2020)]. On the other hand, it creates an environment suitable for regenerating neural cells, prone to be stimulated by the hADSC and their secretome when in co-culture.

hPL stimulates hADSC proliferation and amplifies cell-to-cell interactions and the release of trophic factors synergistically: this effect could be related to the cell proliferation promoted by the hPL itself or to the neurotrophic properties that ADSC acquire when grown with hPL (Palombella et al., 2020).

From a functional point of view, our *in vitro* model can be interpreted as the temporo-spatial sequence of events, which occur after the implantation of a hADSC-loaded neural conduit between the two stumps of a severed nerve. Indeed, while the hADSC secretome (*indirect*) diffuses immediately after the surgery through the local microenvironment, influencing at an early stage (*Time 0*) the nerve growth cone, the hADSC themselves (*direct*) require more time (depending on cell proliferation) to come into contact (*Time 1*) with the axons at the proximal stump, stimulating further elongation.

Not surprisingly, a cumulative effect between the secretome and cell-to-cell interactions emerges from our results. Applying hPL in the pre-expansion steps of hADSC could improve cell performance, reduce the time that lapses (*Time 0-Time 1*), support the potential of hADSC to support nerve regeneration therapy at an earlier stage, and lead to an increase in repair when compared with the effect elicited by the same cells grown with FBS.

After peripheral nerve injury, the ECM and, particularly, LN are responsible for providing adequate adaptation signals, through specific integrin-binding receptors, for local cells in order to induce gene expression, metabolic activity, and cell behavior modifications. Similarly, ECM proteins modulate the soluble factor secretion, cellular homeostasis, and cell fate of the hADSC (Midwood et al., 2004; Rozario and DeSimone, 2010; Noro et al., 2013; Pope et al., 2016). Therefore, a LN-functionalized conduit combining ECM scaffold and hADSC^{hPL} could both allow a "neural-oriented" microenvironment for neural cells and a "neural-friendly"

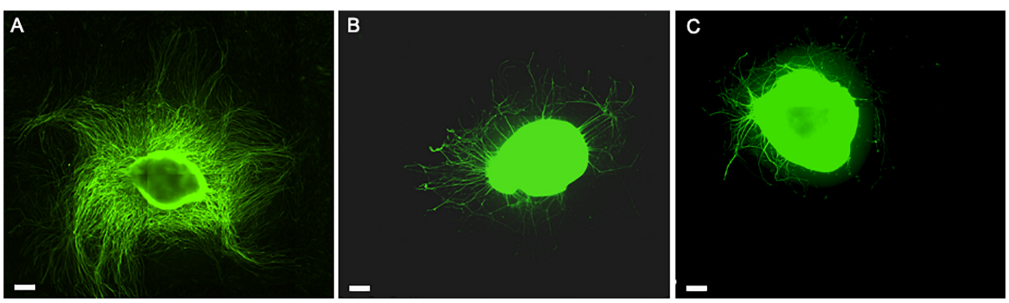

FIGURE 9 | The role of hADSC cell-to-cell interaction and secretome when expanded with the hPL in *in vitro* DRG co-culture model. Direct co-culture of DRG with hADSC^{hPL} on LN-coated surface **(A)**, indirect co-culture of DRG with hADSC^{hPL} secretome on LN-coated surface **(B)**, and DRG alone on LN **(C)**. Scale bar: 500 μm.

behavior of the hADSC themselves. Being expanded with hPL, the stronger proliferation of hADSC^{hPL} amplifies exponentially these benefits.

CONCLUSION

To date, this is the first study which investigated the relationship between hADSC, hPL, and ECM: considering our findings, due to the synergic functions, we can hypothesize that a LN-coated scaffold could support hADSC adhesion and proliferation and, in turn, cell activity through GF release and cell–matrix–neuron interactions, maximizing the potential of hADSC therapy.

In light of the remarkable increase of DRG neurite outgrowth obtained *in vitro* on laminin substrates, a combined cell therapy approach coupling hADSC^{hPL} with a LN-functionalized bioartificial conduit will be a matter of further *in vitro* and *in vivo* investigation by our group, to optimize a potential translatable route for peripheral nerve repair.

DATA AVAILABILITY STATEMENT

The raw data supporting the conclusions of this article will be made available by the authors, without undue reservation.

ETHICS STATEMENT

Ethical review and approval was not required for the animal study because dorsal root ganglia were explanted from euthanized neonatal rats and used as an *in vitro* model for cell culture.

AUTHOR CONTRIBUTIONS

MG did the experiments, analyzed the data, and wrote the manuscript. PS conceived the idea and with MR supervised the project and corrected the manuscript. All authors read, critically revised, and approved the final version of the manuscript.

FUNDING

Leenaards Fondation financially supported this research project.

ACKNOWLEDGMENTS

We are grateful to *Leenaards Fondation* for granting this project.

REFERENCES

Armstrong, S. J., Wiberg, M., Terenghi, G., and Kingham, P. J. (2007). ECM molecules mediate both Schwann cell proliferation and activation to enhance neurite outgrowth. *Tissue Eng.* 13, 2863–2870. doi: 10.1089/ten.2007.0055

Barros, C. S., Franco, S. J., and Müller, U. (2011). Extracellular matrix: functions in the nervous system. *Cold Spring Harb. Perspect. Biol.* 3:a005108. doi: 10.1101/cshperspect.a005108

Chen, Y. S., Hsieh, C. L., Tsai, C. C., Chen, T. H., Cheng, W. C., Hu, C. L., et al. (2000). Peripheral nerve regeneration using silicone rubber chambers filled with collagen, laminin and fibronectin. *Biomaterials* 21, 1541–1547. doi: 10.1016/s0142-9612(00)00028-4

Chernousov, M. A., Yu, W. M., Chen, Z. L., Carey, D. J., and Strickland, S. (2008). Regulation of Schwann cell function by the extracellular matrix. *Glia* 56, 1498–1507. doi: 10.1002/glia.20740

Condé-Green, A., Kotamarti, V. S., Sherman, L. S., Keith, J. D., Lee, E. S., Granick, M. S., et al. (2016). Shift toward mechanical isolation of adipose-derived stromal vascular fraction: review of upcoming techniques. *Plast. Reconstr. Surg. Glob Open.* 4, e1017. doi: 10.1097/gox.0000000000001017

Cowper, M., Frazier, T., Wu, X., Curley, L., Ma, M. H., Mohuiddin, O. A., et al. (2019). Human platelet lysate as a functional substitute for fetal bovine serum in the culture of human adipose derived stromal/stem cells. *Cells* 8:724. doi: 10.3390/cells8070724

D'Agostino, R. B. (1971). An omnibus test of normality for moderate and large sample size. *Biometrika* 58, 341–348. doi: 10.1093/biomet/58.2.341

de Luca, A. C., Fonta, C. M., Raffoul, W., di Summa, P. G., and Lacour, S. P. (2018). In vitro evaluation of gel-encapsulated adipose derived stem cells: biochemical cues for in vivo peripheral nerve repair. *J. Tissue Eng. Regen. Med.* 12, 676–686. doi: 10.1002/term.2486

de Luca, A. C., Lacour, S. P., Raffoul, W., and di Summa, P. G. (2014). Extracellular matrix components in peripheral nerve repair: how to affect neural cellular response and nerve regeneration? *Neural Regen. Res.* 9, 1943–1948.

de Luca, A. C., Stevens, J. S., Schroeder, S. L., Guilbaud, J. B., Saiani, A., Downes, S., et al. (2013). Immobilization of cell-binding peptides on poly-ε-caprolactone film surface to biomimic the peripheral nervous system. *J. Biomed. Mater. Res. A* 101, 491–501. doi: 10.1002/jbm.a.34345

di Summa, P. G., Kalbermatten, D. F., Raffoul, W., Terenghi, G., and Kingham, P. J. (2013). Extracellular matrix molecules enhance the neurotrophic effect of Schwann cell-like differentiated adipose-derived stem cells and increase cell survival under stress conditions. *Tissue Eng. Part A.* 19, 368–379. doi: 10.1089/ten.tea.2012.0124

Dodla, M. C., and Bellamkonda, R. V. (2008). Differences between the effect of anisotropic and isotropic laminin and nerve growth factor presenting scaffolds on nerve regeneration across long peripheral nerve gaps. *Biomaterials.* 29, 33–46. doi: 10.1016/j.biomaterials.2007.08.045

Frantz, C., Stewart, K. M., and Weaver, V. M. (2010). The extracellular matrix at a glance. *J. Cell Sci.* 123(Pt 24), 4195–4200.

Gámez Sazo, R. E., Maenaka, K., Gu, W., Wood, P. M., and Bunge, M. B. (2012). Fabrication of growth factor- and extracellular matrix-loaded, gelatin-based scaffolds and their biocompatibility with Schwann cells and dorsal root ganglia. *Biomaterials* 33, 8529–8539. doi: 10.1016/j.biomaterials.2012.07.028

Gao, X., Wang, Y., Chen, J., and Peng, J. (2013). The role of peripheral nerve ECM components in the tissue engineering nerve construction. *Rev. Neurosci.* 24, 443–453.

Gonzalez-Perez, F., Hernández, J., Heimann, C., Phillips, J. B., Udina, E., and Navarro, X. (2018). Schwann cells and mesenchymal stem cells in laminin- or fibronectin-aligned matrices and regeneration across a critical size defect of 15 mm in the rat sciatic nerve. *J. Neurosurg. Spine* 28, 109–118. doi: 10.3171/2017.5.spine161100

Guiotto, M., Raffoul, W., Hart, A. M., Riehle, M. O., and di Summa, P. G. (2020). Human platelet lysate to substitute fetal bovine serum in hMSC expansion for translational applications: a systematic review. *J. Transl. Med.* 18:351.

Guo, J., Guo, S., Wang, Y., and Yu, Y. (2017). Promoting potential of adipose derived stem cells on peripheral nerve regeneration. *Mol. Med. Rep.* 16, 7297–7304. doi: 10.3892/mmr.2017.7570

Guo, Z. Y., Sun, X., Xu, X. L., Zhao, Q., Peng, J., and Wang, Y. (2015). Human umbilical cord mesenchymal stem cells promote peripheral nerve repair via paracrine mechanisms. *Neural Regen. Res.* 10, 651–658. doi: 10.4103/1673-5374.155442

Harris, G. M., Madigan, N. N., Lancaster, K. Z., Enquist, L. W., Windebank, A. J., Schwartz, J., et al. (2017). Nerve guidance by a decellularized fibroblast extracellular matrix. *Matrix Biol.* 60–61, 176–189. doi: 10.1016/j.matbio.2016.08.011

Hosseinkhani, H., Hiraoka, Y., Li, C. H., Chen, Y. R., Yu, D. S., Hong, P. D., et al. (2013). Engineering three-dimensional collagen-IKVAV matrix to mimic neural microenvironment. *ACS Chem. Neurosci.* 4, 1229–1235. doi: 10.1021/cn400075h

Jessen, K. R., and Mirsky, R. (2016). The repair Schwann cell and its function in regenerating nerves. *J. Physiol.* 594, 3521–3531. doi: 10.1113/jp270874

Kim, N., Im, K. I., Lim, J. Y., Jeon, E. J., Nam, Y. S., Kim, E. J., et al. (2013). Mesenchymal stem cells for the treatment and prevention of graft-versus-host disease: experiments and practice. *Ann. Hematol.* 92, 1295–1308.

Kingham, P. J., Kolar, M. K., Novikova, L. N., Novikov, L. N., and Wiberg, M. (2014). Stimulating the neurotrophic and angiogenic properties of human adipose-derived stem cells enhances nerve repair. *Stem Cells Dev.* 23, 741–754. doi: 10.1089/scd.2013.0396

Koh, H. S., Yong, T., Teo, W. E., Chan, C. K., Puhaindran, M. E., Tan, T. C., et al. (2010). In vivo study of novel nanofibrous intra-luminal guidance channels to promote nerve regeneration. *J. Neural Eng.* 7:046003. doi: 10.1088/1741-2560/7/4/046003

Kyllönen, L., Haimi, S., Mannerström, B., Huhtala, H., Rajala, K. M., Skottman, H., et al. (2013). Effects of different serum conditions on osteogenic differentiation of human adipose stem cells in vitro. *Stem Cell Res. Ther.* 4:17. doi: 10.1186/scrt165

Lalu, M. M., McIntyre, L., Pugliese, C., Fergusson, D., Winston, B. W., Marshall, J. C., et al. (2012). Safety of cell therapy with mesenchymal stromal cells (SafeCell): a systematic review and meta-analysis of clinical trials. *PLoS One* 7:e47559. doi: 10.1371/journal.pone.0047559

Lensch, M., Muise, A., White, L., Badowski, M., and Harris, D. (2018). Comparison of synthetic media designed for expansion of adipose-derived mesenchymal stromal cells. *Biomedicines* 6:54. doi: 10.3390/biomedicines6020054

Li, X., Liu, X., Josey, B., Chou, C. J., Tan, Y., Zhang, N., et al. (2014). Short laminin peptide for improved neural stem cell growth. *Stem Cells Transl. Med.* 3, 662–670. doi: 10.5966/sctm.2013-0015

Lischer, M., di Summa, P. G., Oranges, C. M., Schaefer, D. J., Kalbermatten, D. F., Guzman, R., et al. (2020). Human platelet lysate stimulated adipose stem cells exhibit strong neurotrophic potency for nerve tissue engineering applications. *Regen. Med.* 15, 1399–1408. doi: 10.2217/rme-2020-0031

Mathot, F., Shin, A. Y., and Van Wijnen, A. J. (2019). Targeted stimulation of MSCs in peripheral nerve repair. *Gene* 710, 17–23. doi: 10.1016/j.gene.2019.02.078

Midwood, K. S., Williams, L. V., and Schwarzbauer, J. E. (2004). Tissue repair and the dynamics of the extracellular matrix. *Int. J. Biochem. Cell Biol.* 36, 1031–1037. doi: 10.1016/j.biocel.2003.12.003

Milner, R., Wilby, M., Nishimura, S., Boylen, K., Edwards, G., Fawcett, J., et al. (1997). Division of labor of Schwann cell integrins during migration on peripheral nerve extracellular matrix ligands. *Dev. Biol.* 185, 215–228. doi: 10.1006/dbio.1997.8547

Motta, C. M. M., Endres, K. J., Wesdemiotis, C., Willits, R. K., and Becker, M. L. (2019). Enhancing Schwann cell migration using concentration gradients of laminin-derived peptides. *Biomaterials* 218:119335. doi: 10.1016/j.biomaterials.2019.119335

Noro, A., Sillat, T., Virtanen, I., Ingerpuu, S., Bäck, N., Konttinen, Y. T., et al. (2013). Laminin production and basement membrane deposition by mesenchymal stem cells upon adipogenic differentiation. *J. Histochem. Cytochem.* 61, 719–730. doi: 10.1369/0022155413502055

Palombella, S., Guiotto, M., Higgins, G. C., Applegate, L. L., Raffoul, W., Cherubino, M., et al. (2020). Human platelet lysate as a potential clinical-translatable supplement to support the neurotrophic properties of human adipose-derived stem cells. *Stem Cell Res. Ther.* 11:432.

Palombella, S., Pirrone, C., Rossi, F., Armenia, I., Cherubino, M., Valdatta, L., et al. (2017). Effects of metal micro and nano-particles on hASCs: an in vitro model. *Nanomaterials* 7:212. doi: 10.3390/nano7080212

Paula, A. C., Martins, T. M., Zonari, A., Frade, S. P., Angelo, P. C., Gomes, D. A., et al. (2015). Human adipose tissue-derived stem cells cultured in xeno-free culture condition enhance c-MYC expression increasing proliferation but bypassing spontaneous cell transformation. *Stem Cell Res. Ther.* 6:76.

Plow, E. F., Haas, T. A., Zhang, L., Loftus, J., and Smith, J. W. (2000). Ligand binding to integrins. *J. Biol. Chem.* 275, 21785–21788.

Poitelon, Y., Lopez-Anido, C., Catignas, K., Berti, C., Palmisano, M., Williamson, C., et al. (2016). YAP and TAZ control peripheral myelination and the expression of laminin receptors in Schwann cells. *Nat. Neurosci.* 19, 879–887. doi: 10.1038/nn.4316

Pope, B. D., Warren, C. R., Parker, K. K., and Cowan, C. A. (2016). Microenvironmental control of adipocyte fate and function. *Trends Cell Biol.* 26, 745–755. doi: 10.1016/j.tcb.2016.05.005

Resch, A., Wolf, S., Mann, A., Weiss, T., Stetco, A. L., and Radtke, C. (2018). Co-culturing human adipose derived stem cells and schwann cells on spider silk-a new approach as prerequisite for enhanced nerve regeneration. *Int. J. Mol. Sci.* 20:71. doi: 10.3390/ijms20010071

Ribeiro, C. A., Fraga, J. S., Grãos, M., Neves, N. M., Reis, R. L., Gimble, J. M., et al. (2012). The secretome of stem cells isolated from the adipose tissue and Wharton jelly acts differently on central nervous system derived cell populations. *Stem Cell Res. Ther.* 3:18. doi: 10.1186/scrt109

Rozario, T., and DeSimone, D. W. (2010). The extracellular matrix in development and morphogenesis: a dynamic view. *Dev. Biol.* 341, 126–140. doi: 10.1016/j.ydbio.2009.10.026

Santiago, L. Y., Nowak, R. W., Peter Rubin, J., and Marra, K. G. (2006). Peptide-surface modification of poly(caprolactone) with laminin-derived sequences for adipose-derived stem cell applications. *Biomaterials* 27, 2962–2969. doi: 10.1016/j.biomaterials.2006.01.011

Schallmoser, K., Henschler, R., Gabriel, C., Koh, M. B. C., and Burnouf, T. (2020). Production and quality requirements of human platelet lysate: a position statement from the working party on cellular therapies of the international society of blood transfusion. *Trends Biotechnol.* 38, 13–23. doi: 10.1016/j.tibtech.2019.06.002

Scheib, J., and Höke, A. (2013). Advances in peripheral nerve regeneration. *Nat. Rev. Neurol.* 9, 668–676.

Schindelin, J., Arganda-Carreras, I., Frise, E., Kaynig, V., Longair, M., Pietzsch, T., et al. (2012). Fiji: an open-source platform for biological-image analysis. *Nat. Methods* 9, 676–682. doi: 10.1038/nmeth.2019

Schmidt, C. E., and Leach, J. B. (2003). Neural tissue engineering: strategies for repair and regeneration. *Annu. Rev. Biomed. Eng.* 5, 293–347. doi: 10.1146/annurev.bioeng.5.011303.120731

Sherman, L. S., Condé-Green, A., Naaldijk, Y., Lee, E. S., and Rameshwar, P. (2019). An enzyme-free method for isolation and expansion of human adipose-derived mesenchymal stem cells. *J. Vis. Exp.* doi: 10.3791/59419

Teixeira, F. G., Carvalho, M. M., Neves-Carvalho, A., Panchalingam, K. M., Behie, L. A., Pinto, L., et al. (2015). Secretome of mesenchymal progenitors from the umbilical cord acts as modulator of neural/glial proliferation and differentiation. *Stem Cell Rev. Rep.* 11, 288–297. doi: 10.1007/s12015-014-9576-2

West, C. A., Hart, A. M., Terenghi, G., and Wiberg, M. (2007). Analysis of the dose-response of N-acetylcysteine in the prevention of sensory neuronal loss after peripheral nerve injury. *Acta Neurochir. Suppl.* 100, 29–31. doi: 10.1007/978-3-211-72958-8_6

Xu, Z., Orkwis, J. A., DeVine, B. M., and Harris, G. M. (2019). Extracellular matrix cues modulate Schwann cell morphology, proliferation, and protein expression. *J. Tissue Eng. Regen. Med.* 14, 229–242. doi: 10.1002/term.2987

Yu, W. M., Chen, Z. L., North, A. J., and Strickland, S. (2009). Laminin is required for Schwann cell morphogenesis. *J. Cell Sci.* 122(Pt 7), 929–936. doi: 10.1242/jcs.033928

Zarinfard, G., Tadjalli, M., Razavi, S., and Kazemi, M. (2016). Effect of laminin on neurotrophic factors expression in Schwann-like cells induced from human adipose-derived stem cells in vitro. *J. Mol. Neurosci.* 60, 465–473. doi: 10.1007/s12031-016-0808-6

Zhang, Z., Qu, R., Fan, T., Ouyang, J., Lu, F., and Dai, J. (2019). Stepwise adipogenesis of decellularized cellular extracellular matrix regulates adipose tissue-derived stem cell migration and differentiation. *Stem Cells Int.* 2019:1845926.

Conflict of Interest: The authors declare that the research was conducted in the absence of any commercial or financial relationships that could be construed as a potential conflict of interest.

APPENDIX 1

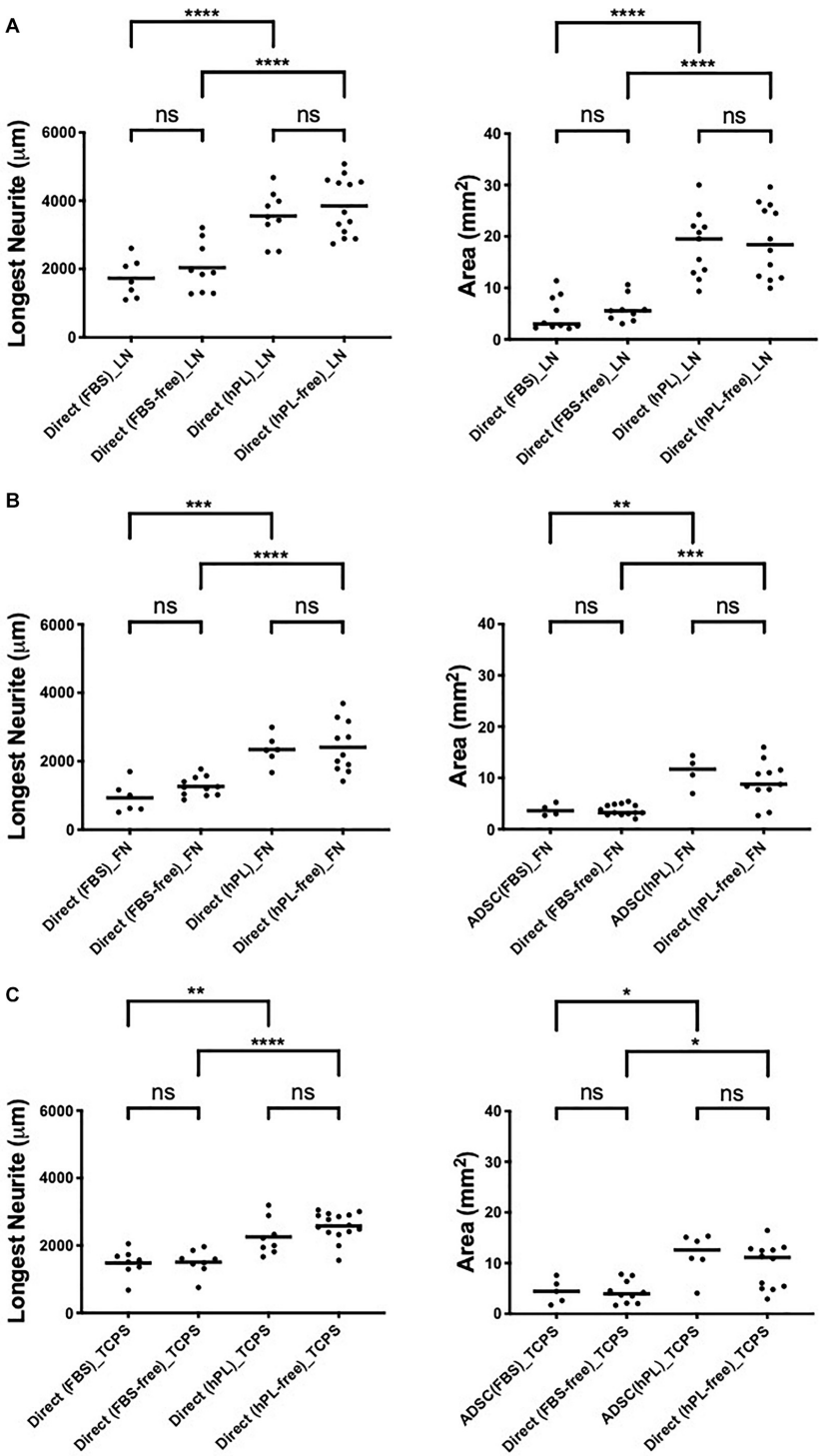

FIGURE A1 | hADSC maintain a neurotrophic effect despite serum deprivation in direct co-culture with primary neurons on LN **(A)**, FN **(B)**, and TCPS **(C)**. Longest neurite and axonal area of direct co-culture on LN **(A)**, FN **(B)**, and TCPS **(C)**. Three biological repeats and at least three technical replicates (DRG) were assessed. One-way ANOVA with Tukey's multiple comparison tests was used for assessing statistical significance among the examined groups (*$p < 0.05$, **$p < 0.01$, ***$p < 0.001$, ****$p < 0.0001$). The number of DRG tested corresponds to the number of dots for each condition in the graph.

frontiers in Bioengineering and Biotechnology

ORIGINAL RESEARCH
published: 22 March 2021
doi: 10.3389/fbioe.2021.627805

Chemotactic TEG3 Cells' Guiding Platforms Based on PLA Fibers Functionalized With the SDF-1α/CXCL12 Chemokine for Neural Regeneration Therapy

Oscar Castaño[1,2,3,4†], Ana López-Mengual[5,6,7,8†], Diego Reginensi[9,10†], Andreu Matamoros-Angles[5,6,7,8‡], Elisabeth Engel[2,3,11] and José Antonio del Rio[5,6,7,8*]*

[1] Electronics and Biomedical Engineering, Universitat de Barcelona, Barcelona, Spain, [2] Biomaterials for Regenerative Therapies, Institute of Bioengineering of Catalonia, Parc Cientific de Barcelona, Barcelona, Spain, [3] CIBER en Bioingeniería, Biomateriales y Nanomedicina, CIBER-BBN, Madrid, Spain, [4] Bioelectronics Unit and Nanobioeneering Laboratory, Institute for Nanoscience and Nanotechnology of the University of Barcelona, Barcelona, Spain, [5] Molecular and Cellular Neurobiotechnology, Institute of Bioengineering of Catalonia, Parc Cientific de Barcelona, Barcelona, Spain, [6] Department of Cell Biology, Physiology and Immunology, Faculty of Biology, Universitat de Barcelona, Barcelona, Spain, [7] Centro de Investigación Biomédica en Red sobre Enfermedades Neurodegenerativas, Barcelona, Spain, [8] Institute of Neurosciences, University of Barcelona, Barcelona, Spain, [9] School of Medicine, Universidad de Panamá, Panama City, Panama, [10] Biomedical Engineering Program, Universidad Latina de Panamá, Panama City, Panama, [11] IMEM-BRT Group, Department of Materials Science, EEBE, Technical University of Catalonia (UPC), Barcelona, Spain

(Following spinal cord injury, olfactory ensheathing cell (OEC) transplantation is a promising therapeutic approach in promoting functional improvement. Some studies report that the migratory properties of OECs are compromised by inhibitory molecules and potentiated by chemical concentration differences. Here we compare the attachment, morphology, and directionality of an OEC-derived cell line, TEG3 cells, seeded on functionalized nanoscale meshes of Poly(l/dl-lactic acid; PLA) nanofibers. The size of the nanofibers has a strong effect on TEG3 cell adhesion and migration, with the PLA nanofibers having a 950 nm diameter being the ones that show the best results. TEG3 cells are capable of adopting a bipolar morphology on 950 nm fiber surfaces, as well as a highly dynamic behavior in migratory terms. Finally, we observe that functionalized nanofibers, with a chemical concentration increment of SDF-1α/CXCL12, strongly enhance the migratory characteristics of TEG3 cells over inhibitory substrates.

Keywords: olfactory ensheathing cells, electrospinning, PLA nanofibers, cell migration, gradients, SDF-1alpha, CXCL12

OPEN ACCESS

Edited by:
Antonio Salgado, University of Minho, Portugal

Reviewed by:
Vasif Nejat Hasirci, Acıbadem University, Turkey
Eduardo D. Gomes, University of Minho, Portugal

****Correspondence:***
Elisabeth Engel
eengel@ibecbarcelona.eu
José Antonio del Rio
jadelrio@ibecbarcelona.eu; jadelrio@ub.edu

‡Present Address:
Andreu Matamoros-Angles Institute of Neuropathology, University Medical Center Hamburg-Eppendorf, Hamburg, Germany

† These authors have contributed equally to this work

Specialty section:
This article was submitted to Tissue Engineering and Regenerative Medicine, a section of the journal Frontiers in Bioengineering and Biotechnology

Received: *10 November 2020*
Accepted: *01 March 2021*
Published: *22 March 2021*

Citation:
Castaño O, López-Mengual A, Reginensi D, Matamoros-Angles A, Engel E and del Rio JA (2021) Chemotactic TEG3 Cells' Guiding Platforms Based on PLA Fibers Functionalized With the SDF-1α/CXCL12 Chemokine for Neural Regeneration Therapy. Front. Bioeng. Biotechnol. 9:627805. doi: 10.3389/fbioe.2021.627805

INTRODUCTION

Traumatic injuries to the central nervous system (CNS) are associated with the loss, in most cases, of crucial physiological functions. Spinal cord injury (SCI) is, unfortunately, a prime example, since it substantially affects the quality of life through loss of function (paralysis and anesthesia) and development of pain and secondary disabilities. Many biological limitations restrict the efficacy of current SCI repair strategies, and many of the regenerative mechanisms are impaired in patients

with neuropathies, further limiting their recovery (Silver et al., 2014; Pounders et al., 2019). As a consequence, although there have been advances [i.e., (Reichert, 2007)], repair of the damaged spinal cord continues to be a major paradigmatical challenge in regenerative medicine. Neural tissue engineering offers hope to patients and is a rapidly growing field aimed at creating engineered tissue able to replace dead tissue in affected regions and recover lost function (Akter, 2016).

Olfactory ensheathing cells (OECs) play a key role in the guidance of olfactory axons by trophic and physical support (Kafitz and Greer, 1999; Sonigra et al., 1999). These properties have led to their implementation in several cell therapeutical approaches in the damaged CNS. Several studies have demonstrated beneficial effects following OEC transplantation in animals after SCI. Evidence of anatomical regeneration (Ramón-Cueto and Nieto-Sampedro, 1994; Li et al., 1997; Imaizumi et al., 2000; Nash et al., 2002) and functional improvement (Li et al., 1997; Ramón-Cueto et al., 1998, 2000; Lu et al., 2001, 2002; López-Vales et al., 2007) has been observed in a variety of SCI models, including in hemisection and in complete transection of the spinal cord.

Olfactory ensheathing cell transplantation is a cellular alternative therapeutic approach for SCI. In general, five beneficial effects of OECs have been reported that can promote functional recovery: (i) stimulation of axonal growth; (ii) tissue and axon preservation; (iii) capability to mix intimately with healing glia; (iv) promotion of angiogenesis; and (v) capability to ensheath growing axons [i.e, see Roet and Verhaagen (2014) for review]. However, therapy based on the use of OECs has a series of problems that leads to variable and contradictory results, mostly caused by the inherent complexity of the regenerative process and the myriad variables involved [e.g., receptors, ligands (inhibitory substrates)] (Field et al., 2003; Thuret et al., 2006; Gómez et al., 2018). In addition, unfortunately, transplanted OECs show a high rate of cell death in the host as a result of the excitotoxicity associated with the lesion, in the primary as well as the penumbra regions (Torres-Espín et al., 2014), almost disappearing 2–3 weeks after transplantation. Therefore, the number of cells per transplant must be high ($\approx$ 200,000 cells; Guntinas-Lichius et al., 2001; Tabakow et al., 2013). Furthermore, transplanted OECs showed a low degree of migration in the lesioned spinal cord (Reginensi et al., 2015).

In the primary olfactory system, OECs migrate from the periphery (olfactory mucosa) into the CNS (olfactory bulb), and this organized migration is also able to enhance axonal extension after injury of the olfactory tract (Ekberg et al., 2012). However, as noted above, the migratory properties of OECs are extremely limited in the area of injury in the spinal cord due to the presence of inhibitory molecules in the extracellular environment (Gudiño-Cabrera and Nieto-Sampedro, 2000; Deng et al., 2006). Several factors have been described as modulators of the migration of OECs, including glial-derived neurotrophic factor (GDNF), fibulin-3, slit-2, myelin-associated inhibitors (MAIs; e.g., Nogo-A, MAG, or OMgp), and chondroitin sulfate proteoglycans (CSPG; Cao et al., 2006; Su et al., 2007; Vukovic et al., 2009; Huang et al., 2011; Nocentini et al., 2012; Reginensi et al., 2015). Most of these molecules inhibit the migration of OECs, and they are overexpressed in the meningo-glial scar after injury, acting as negative players in the migration of transplanted OECs.

For this reason, researchers seek to enhance the regenerative potential of OECs in combination with other treatments, for example, gene therapy, in order to obtain a local, continuous release of factors that improve axonal growth, neutralizing factors of the inhibitory signal present in the injured environment, and biomaterials to allow guided targeting and better structural support in the area of injury. In previous studies, we analyzed the migratory properties and biomechanical aspects of OECs growing on inhibitory substrates, such as MAIs (Nocentini et al., 2012; Reginensi et al., 2015), or CSPGs (Reginensi et al., 2015). We evidenced that in the presence of inhibitory molecules, the migratory capacity and traction force of OECs are drastically reduced, which correlates with profound changes in the F-actin cytoskeleton and the distribution of focal adhesion complexes (Nocentini et al., 2012; Reginensi et al., 2015). As noted above, several studies using ducts made with biomaterials have been reported with differing levels of success in regenerative strategies. These biomaterials, both natural and artificial, must meet a series of specific requirements. Natural biomaterials, in general, are difficult to handle due to their low mechanical resistance, while artificial materials stand out for their low bioactivity and signaling control to properly guide cells or lesioned axons in the repair process (Chen et al., 2018). Nanobiotechnology has been able to manufacture biodegradable materials at a controlled submicron scale using the technique of electrospinning to create nanofibers mimicking the extracellular matrix (ECM). The method is very versatile and allows for positioning of the fibers with relative precision. Electrospinning offers a topography that cells can easily recognize (Álvarez et al., 2013, 2014; Oliveira et al., 2016) and also provides a high-surface area-to-volume ratio that can be modified and functionalized with a bioactive group or signals to enhance cell adhesion, morphology, and fate control (Ghasemi-Mobarakeh et al., 2008; Beachley and Wen, 2009; Hackett et al., 2010). However, there have been few successful studies of the production of biocompatible matrices for the promotion of cell migration and axonal regrowth in models of CNS injury (Straley et al., 2010).

A significant field of investigation in SCI is the application of these biomaterials to perform as guiding supports at the place of damage and/or the application as a matrix for the release of signaling factors to encourage nerve regeneration (King et al., 2010). For example, fibers and scaffolds based on materials such as poly (lactic-co-glycolic acid; PLGA), Poly(l/dl-lactic acid; PLA), and NeuroGel (methacrylamide-based hydrogel) have shown an encouraing positive result in terms of functionality when used as support for axon growth. Additionally, gradients of biomolecules on synthetic biomaterials can efficiently mimic the natural, graded variation of properties with the ECM. Such gradients represent accessible study boards for improving understanding of cellular activities, and they also provide functional support for tissue engineering. The created morphological gradients regulate the settlement of cells, diffusion of nutrients, and removal of cellular waste products during cell proliferation and differentiation, while also providing a

progressive variation of mechanical properties within the overall support mechanism.

The combination of electrospinning techniques in the generation of nanofibers based on synthetic materials (e.g., PLA, PLGA), functionalized with bioactive molecules that act with a chemical gradient (e.g., SDF-1α, TNF-α) for certain biological systems, may be relevant for the development of new approaches to tissue engineering. TEG3 cells are an immortalized cell line of OECs that preserve the pro-regenerative features of primary cells (Moreno-Flores et al., 2003), and they also express the C-X-C chemokine type 4 receptor (CXCR-4) with a high affinity to the chemokine stromal cell-derived factor 1 (SDF1alpha also known C-X-C motif chemokine 12, SDF-1α/CXCL12) triggering intracellular signaling processes mediated by several kinases [i.e., Akt and extracellular signal-regulated kinase (pERK)1/2] (Levoye et al., 2009).

We hypothesize that less rigid and more amorphous topographies, such as PLA (PLDLA 80/20) nanostructured fibers, functionalized on their surface with different concentrations of a chemotactic agent, would guide the migration of TEG3 cells toward more chemokine-concentrated surfaces. We then modeled a damaged gap by creating an inhibiting microenvironment using a growth inhibitory molecule as the CSPG, in contrast to the adhesive permissive laminin coatings. The bridging system was designed and optimized using PLA electrospun fibers, which were functionalized with a chemotactic agent such as the SDF-1α/CXCL12 chemokine to get an *in situ* increment of migration signaling on the surface to drive cells through the fibers.

MATERIALS AND METHODS

Antibodies and Biochemicals Reagents

The reagents used for coating treatments were Poly-*L*-Lysine (P4707; Sigma-Aldrich, Merck Life Science), Laminin (L2020; Sigma-Aldrich, Merck Life Science), CSPG (CC117; Millipore, Merck Life Science), Phalloidin-TRITC (P5282; Sigma-Aldrich, Merck Life Science), diamidino-2-phenylindole (DAPI; B2261; Sigma-Aldrich, Merck Life Science), Rhodamine B (R6626, Sigma-Aldrich, Merck Life Science), SYLGARD™ 184 Silicone Elastomer Kit (1673921; Dow Corning, Belgium), and recombinant murine SDF-1α (CXCL12; 250–20A; Peprotech).

The primary antibodies used in immunocytochemistry were SDF-1α antibody (Abcam; AB25117), b3 integrin (MAB2514; Millipore, Merck Life Science), Vinculin (Abcam, ab155120), and green fluorescence protein (GFP; A11122; Invitrogen™, Thermo Fisher Scientific, Waltham, MA, United States). The secondary antibodies used were Alexa Fluor 488 donkey anti-rabbit (A21206; Invitrogen™, Thermo Fisher Scientific, Waltham, MA, United States) and Alexa Fluor 488 goat anti-rat (A11006; Invitrogen™, Thermo Fisher Scientific, Waltham, MA, United States).

TEG3 Cultures

The immortalized clonal cell line TEG3 was used in this study. These are rat OEC primary cultures transfected with the simian vacuolating virus 40 (SV40) large *T* antigen (Moreno-Flores et al., 2003). In the study we used the original TEG3 cell line and a modified TEG3 cell line that expressed the enhanced green fluorescent protein (eGFP; Reginensi et al., 2015). Cells were maintained in Dulbecco's Modified Eagle Medium/Nutrient Mixture F-12 (DMEM–F12, 11320033; Invitrogen™, Thermo Fisher Scientific, Waltham, MA, United States) supplemented with 10% bovine calf serum (12133C; Sigma-Aldrich, Merck Life Science), 20 μg/ml pituitary extract (13028014; Invitrogen™, Thermo Fisher Scientific, Waltham, MA, United States), 2 μM forskolin (F6886; Sigma-Aldrich, Merck Life Science), 1% penicillin-streptomycin (15140122; Invitrogen™, Thermo Fisher Scientific, Waltham, MA, United States), and 1% fungizone (15290026; Invitrogen™, Thermo Fisher Scientific, Waltham, MA, United States). TEG3 cells between passages 4–8 were used for the experiments.

Culture Surface Coating and Immunocytochemical Methods

Glass coverslips (12 mm Ø) were coated essentially as described (Nocentini et al., 2012; Reginensi et al., 2015). Briefly, coverslips were pre-coated with Poly-*L*-Lysine 10 μg/ml dissolved in 0.1 M phosphate-buffered saline solution (PBS, pH 7.3) and then washed. After rinsing, they were coated with laminin (2 mg/ml, dissolved in 0.1 M PBS) and washed twice with 0.1 M PBS. In inhibition experiments, CSPG (20 μg/ml) was added instead of Laminin. TEG3 cells were cultured for 20 h and then the coverslips were fixed in 4% buffered paraformaldehyde for 30 min, permeabilized with 0.1% Triton X-100, and blocked with 10% fetal bovine serum (FBS), both diluted in 0.1 M PBS. Cells were sequentially incubated overnight with primary antibodies at 4°C and with the corresponding Alexa Fluor-tagged secondary antibodies for 1 h at room temperature. After rinsing in 0.1 M PBS, cells were stained with 0.1 M 4′,6- DAPI diluted in 0.1 M PBS for 10 min, rinsed, and mounted on Fluoromount™ (Vector Labs, Burlingame, CA, United States); they were then analyzed using an Olympus BX61 fluorescence microscope equipped with a DP12L cooled camera or a Zeiss LSCM 500 confocal microscopy. Digital image processing was performed with ImageJ™ software.

Fabrication of PLA Nanofibers Using Electrospinning

Poly(l/dl-lactic acid; PLA, PURASORB® PLDL 8038 Corbion, Amsterdam, Netherlands, inherent viscosity midpoint 3.8 dl/g) fibers were produced by electrospinning onto square windows of Parafilm™ (Bemis Company, Inc, Neenah, WI, United States) hollow frames (12 mm × 12 mm inner window; 15 mm × 15 mm outer frame) and cover slides (15 mm diameter × 0.1 mm thick) attached to a rotary collector using adhesive tape. Cover slides were previously washed with soap and water and then cleaned in water, acetone, and methanol for 10 min in an ultrasound bath. Several concentrations (3, 4, 6, 8, and 9% w/w in 2,2,2-trifluoroethanol; 99.8%; Panreac, Barcelona, Spain) were tested to optimize the fiber thickness. Rhodamine B 0.01% related to PLA was added to the solutions to stain the fibers. The electrospinning

process took just 30 s at 14 kV, 20 cm tip-collector distance, 1,200 rpm rotary speed, and the ambient humidity was kept at RH = 30% at 16°C. In the spinning process of the PLA-aligned nanofibers (Álvarez et al., 2014), the fibers were oriented perpendicular to the permissive (laminin) and inhibitory (CSPG) coatings and attached to coverslips in sterile conditions.

Manufacture of PLA Biofunctionalized SDF-1α/CXCL12 Nanofibers for *in situ* Surface Concentration Increments

Both fibrous frames and fibrous coated cover slides with PLA nanofibers (diameter, 950 nm) were functionalized with SDF-1α/CXCL12 (Peprotech) chemokine using a dip-coating method to obtain a surface concentration difference. Briefly, fiber surfaces were first hydrolyzed for 10 min with a 0.01 M sodium hydroxide (NaOH) solution. After rinsing in pure water, they were immersed in an MES pH = 5.5 buffered solution of 1-ethyl-3-(3-dimethylaminopropyl)carbodiimide/N-hydroxysuccinimide (EDC/NHS) 1/1.2 for 10 min. Afterward, fibers were again rinsed and dip-coated in a solution of SDF-1α/CXCL12 of 50 ng/ml at a speed of 10 mm/min. Fibers were then rinsed again and store for further assays.

Mechanical Characterization of PLA Fibers

The mechanical assessment was performed by uniaxial tensile-strain Zwiki Z0.5TN (Zwick-Roell, Ulm, Germany) analysis parallel with the direction of the fibers. Fibers were electrospun following the same conditions as section "Fabrication of PLA nanofibers using electrospinning" but for 3 h, yielding a mat of about 20–30 μm thickness in the center of the aluminum foil used to collect fibers. Then samples were cut following an ISO 527-1 standard with a bone shape. Then the bone-shaped mat was wrapped to form a cylinder that was coupled to the tensile-strain grips. The cell-load used had a maximum of 5N. The section was assessed by measuring the half-width of the cylinders using a high precision digital Mitutoyo micrometer 293–344 (Mitutoyo, Kanagawa, Japan). Measurement was performed at a speed of 10 mm/min until rupture. Elastic or Young's modulus was approached by linear regression of the linear area of the elastic area.

Crystallinity Content (χc) and Glass Transition Temperature (T_g) of the PLA Fibers

Thermal features were assessed using differential calorimetric analysis (DSC, Q20, TA Instruments, Waters, DE, United States). 5 mg of fibers were encapsulated in aluminum pans and held to a thermal treatment between room temperature and 200°C at a 10°C/min rate for 2 cycles under N_2 atmosphere. Degree of crystallinity was obtained following the relation $\%\chi c = (\Delta H_m - \Delta H_c)/\Delta H^0{}_m$, where $\%\chi c$ is crystallinity content expressed as a percentage, ΔHm is the latent melting point, and ΔHc is the heat of the crystallization, both obtained integrating the corresponding DSC peaks, and $\Delta H^0{}_m$ is the melting point of PLA with an assumed degree of crystallinity of 100%. This has a value of 93.1 J/g (Álvarez et al., 2013).

Morphological Characterization of PLA Fibers and Fixed Cells

Micro-and nano-morphology of PLA was assessed using field emission scanning electron microscope (FESEM, Nova^{TM}-Nano SEM-230; FEI Co., Hillsboro, OR, United States) operating at 5.00 kV. Before imaging, samples were coated with an ultra-thin carbon layer to improve conductivity. Mean fiber diameter was measured considering at least 25 randomly selected fibers and using the ImageJ^{TM} analysis software (Schneider et al., 2012), and quantification of the fibers directionality was assessed using Fiji open-source platform (Schindelin et al., 2012) and its directionality plugin. Images of fibers and cells were produced by fixing cells with a solution in paraformaldehyde at 4% (PFA, Electron Microscopy Sciences, United States) for 15 min after rinsing cells twice with sterile 1 × PBS. Then they were washed again with 1 × phosphate-buffered saline (PBS).

As PLA fibers cannot be immersed in ethanol solutions due to the damage caused by alkoholisis, we decided to freeze them gradually, first at 4°C, then a −20°C, and finally at −80°C, followed by a process of lyophilization for 12 h. Afterward, they were coated with an ultra-thin layer of gold.

Circularity Index and Morphological Cell Analysis

Coverslips were coated with Laminin (control) or CSPG (inhibitory substrate). 3×10^4 TEG cells were seeded in coverslips with nanofibers for *in vitro* experiments. For cell imaging, thresholded images are previously pretreated with a bandpass filter and are subjected to circularity analysis. The index circularity with a value of 1.0 indicates a cell with rounded morphology, while as it approaches 0 it indicates that the cell has a bipolar structure based on the formula: $4\pi \times (\text{Area}/\text{Perimeter}^2)$. The digital analysis process was performed using ImageJ^{TM} software.

Time-Lapse Analysis of TEG3 Migration Over PLA Nanofibers

For time-lapse analysis, Fluorodish cell culture dishes (World Precision Instruments, Sarasota, FL, United States) were coated with Poly-L-lysine and then with Laminin or CSPG as indicated above. Next, PLA nanofibers (functionalized or not) were placed over the coverslip in a parallel orientation. In order to analyze cell/fiber interaction and migration, we placed a polydimethylsiloxane (PDMS) membrane with a 500-μm-wide rectangular opening on top of the coated plate and PLA fibers. Next, 2×10^4 TEG3 cells were seeded in the PDMS hole for 12 h to improve cell attachment, and the PDMS mask was gently removed, preserving the PLA fibers and allowing TEG cells to interact with fibers or the substrate while avoiding detached cells. TEG cells were cultured, and the time-lapse analysis was performed. In some cases, cultures were fixed after different time points (4 and 6 days) and immunochemically processed as above. For live imaging, culture dishes were transferred to a Live

Cell Instruments system (LCI Instruments, Seoul, South Korea) for 25 h. Tracking was performed with an inverted Olympus microscope IX71 (20X objective), and images (5 megapixels each) were captured with either an ORCA Flash 4 or CX50 Olympus camera (17 fields, 190 frames each field, one frame every 8 min. 25 h in total; Nocentini et al., 2012; Reginensi et al., 2015). Images were then compiled as single image stacks and exported as uncompressed Audio Video Interleave (AVI) video files. The migration of TEG3 cells was analyzed using the MTrack plug-in from the ImageJ^{TM} software.

Statistical Analysis

Quantitative data are expressed as mean ± S.E.M. (standard error of the mean) of at least three independent experiments. Means were compared with a one-way ANOVA test. *A* value of $p < 0.05$ was considered statistically significant.

RESULTS

TEG3 Cytoskeletal Dynamics and Cell Morphology

TEG3 is a clonal OEC line that shows similar growth-promoting potential to non-modified OECs (Moreno-Flores et al., 2003). In the first experiments, we seeded TEG3 cells in a permissive substrate (Laminin) to study their cytoskeletal characteristics and phenotype morphology. Lifeact, a small peptide with an affinity for actin microfilaments, has become one of the gold standards in cell imaging of actin, especially in cell morphology (Flores et al., 2019). Lentiviral transfected LifeAct-eGFP TEG3 cells showed high expression of membrane protrusions through the presence of motile lamellipodia, both in their trailing process and in the cell body (white and red asterisk, respectively, in **Figure 1A**). Also, we determined the presence of focal adhesions (FAs; vinculin-positive) on the laminin-coated substrate. TEG3 cells adopted two different morphologies as represented by the F-actin (Phalloidin-TRITC) distribution (**Figure 1B**) as well as the presence of integrin αvβ3 (**Figure 1C**). This indicates that TEG3 presents an active and dynamic mechanotransduction system able to sense physical properties (i.e., substrate stiffness) of the surrounding environment and thus modulate adhesion and traction forces with the ECM. Also, as described in other studies (Aguzzi et al., 2013; Reginensi et al., 2015), we observed the presence of two phenotype subpopulations of cultured OEC-TEG3 cells: bipolar morphology [Schwann cell-like OEC (sOEC-TEG3)] (red arrows), and flattened morphology [astrocyte-like OEC (aOEC-TEG3)] with planar stellate morphology (white arrows; **Figures 1D,E**). F-actin distribution showed the morphological plasticity of TEG3 cells. The bipolar TEG3 cells tend to have a single leading process and extensive trailing process (red arrows), while the flattened TEG3 cells tend to have a large membrane protrusion from one or both sides (**Figure 1D**). Also, using high-resolution microscopy (FESEM) we observed what it seems a mix of bipolar (Schwann-like OEC-TEG3 cells) and flattened (astrocyte-like OEC-TEG3 cells) under *in vitro* conditions (**Figure 1E**).

Cytomorphometric Analysis and Cell Tracking of TEG3 Over PLA Nanofibers

Electrospinning was applied to create aligned fiber meshes with differing average fiber diameters. Fibers were satisfactorily

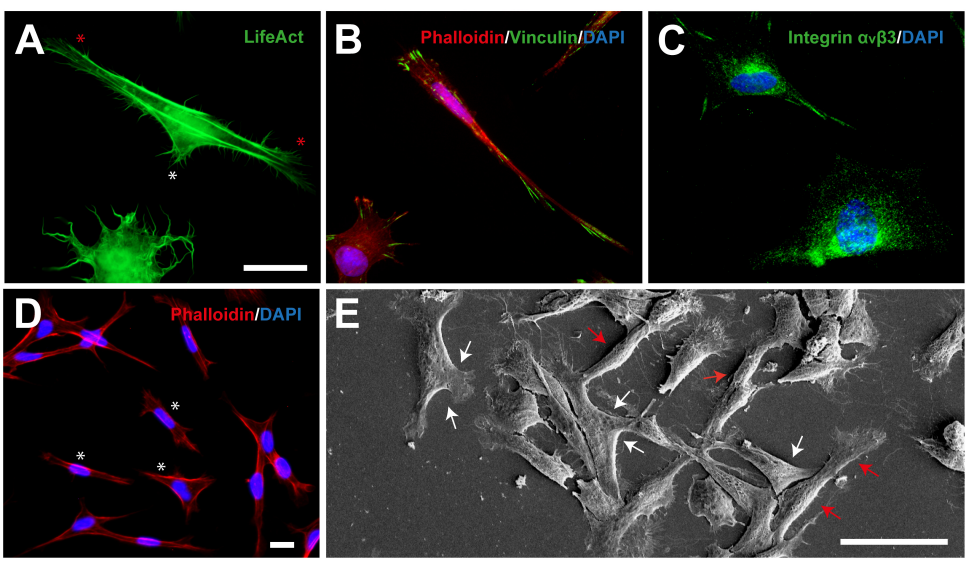

FIGURE 1 | TEG3 cytoskeletal dynamics and phenotype morphology. **(A)** Lentiviral transfected LifeAct-eGFP TEG3 showing a high expression of membrane protrusions through the presence of motile lamellipodia; trailing process (white asterisk) and in the cell body (red asterisk); **(B)** intracellular distribution of *F*-actin and focal adhesions (FAs) on laminin substrate; **(C)** stain of integrin αvβ3; **(D)** flattened TEG3 cells showing membrane protrusion on one or both sides; and **(E)** FESEM image of a mix of bipolar (Schwann-type OECs, red arrows) and flattened (astrocyte-type OECs, white arrows) cells under *in vitro* conditions. Scale bars **(A–C)** – 10 μm; **(D)** – 10 μm; and **(E)** – 50 μm.

produced using PLA 80LL/20DL isomeric copolymer ratios, and the control of the thickness was reproducible by modifying the electrospinning solution concentration and viscosity. Fibers were slightly crystalline according to DSC measurements ($\%\chi_c$ = 10.2%) with a Tg of 59.1°C, and mechanical tensile-strain assessment showed maximum stress of 97.4 ± 34.3 MPa and an approached elastic modulus of 2.2 ± 1.0 GPa. Fiber diameters were measured from FESEM micrographs using ImageJ^{TM} software. A minimum of 30 fibers was measured to obtain the average fiber diameter of each sample. TEG3 cells were seeded at low-density ratio on coverslips coated with laminin together with PLA nanofibers of various diameters. Several thicknesses were prepared in the range between 300 and 1,400 nm (**Figures 2A–C**). A higher cell attachment was found for 950 nm fibers (**Figure 2E**). In cell imaging, different shape descriptors can measure the perimeter, area, length, and roundness of individual cells, once an ellipse is fitted over a given cell. Circularity index is a normalized ratio of area to the perimeter (1 for a circular shape and 0 for a linear shape) and, biologically, lower circularity values describe elongated cell over the fibers. According to our cell morphology analysis, TEG3 cells have the lowest circularity index of 0.13 ± 0.04 when cultured on 950 nm

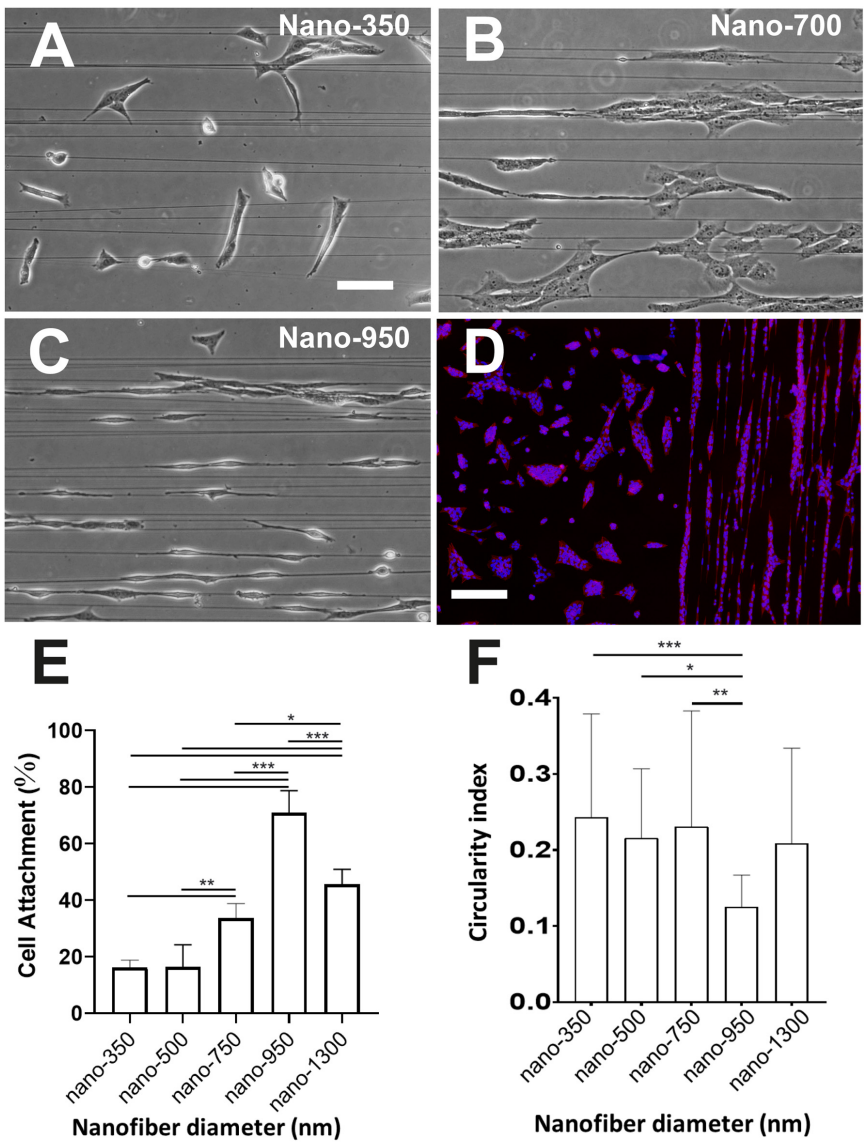

FIGURE 2 | Cytomorphometric analysis of TEG3 over different diameter PLA nanofibers. Cells adhered onto fibers on coverslips with associated laminin of an averaged fiber diameter of **(A)** 350 nm, **(B)** 700 nm, and **(C)** 950 nm; **(D)** DAPI/phalloidin fluorescent image of cells adhered to a surface with (right) and without (left) 950 nm-fibers over an inhibiting coating of CSPG; **(E)** histogram showing the percentage of attachment of the cells with the different diameters of PLA nanofibers (biomaterial; ***p-value < 0.0001; **p-values 0,0017 and 0.0020; *p-value 0.0411; and N = 5); and **(F)** their shape circularity index of cells attached to the different fibers assessed in this work (***p-value < 0.0002; **p-value 0.0019; *p-value 0.0170; and N > 25). Scale bars **(A)** (same for **B,C**) – 50 μm; and **(D)** – 300 μm.

fibers (**Figure 2F**). In PLA nanofibers, with a diameter of 950 nm., the cells have an elongated, bipolar-type structure associated with deformation of the cytoskeleton, in alignment with the direction of nanofibers. Furthermore, the rest of the PLA fiber diameters (350, 500, 750, and 1,300 nm) present a higher index of circularity over 0.2 (350 nm = 0.24 ± 0,14; 500 nm = 0.22 ± 0.09; 700 nm = 0.23 ± 0.15; and 1,300 nm = 0.21 ± 0,13) which indicates that the TEG3 cells are more irregular and anysotropic, and they have less presence of membrane protrusions, as well as a trailing process of cell-biomaterial interaction (**Figure 2D**).

Aligned fibers were achieved by targeting the charged polymer jet toward the edge of a rapid rotating collector. FESEM showed that 950 nm nanofibers aligned on Laminin-coated coverslips (**Figure 3A**) induced cell bodies to elongate along the axis of the fiber and to extend trailing processes guided by fiber directionality (**Figures 3B,C**). Directionality quantification can be assessed by processing the image (**Supplementary Figure 1D**) mathematically by a Fast Fourier Transform (FFT) algorithm (Sachot et al., 2016) represented in a distribution curve (**Supplementary Figure 1E**) and the full width at half maximum (FWHM). The lower the FMHM, the more oriented the fibers. Interestingly, at the cellular level, TEG3 showed, in some cases, the activity of peripheral lamellipodial waves which bear numerous fine filopodia. This resulted in an increased cell-cell contact and the migration of groups of TEG3 cells over the nanofibers (**Figure 3B**), as well as single migrations where TEG3 cells extended their long cytoskeleton to align completely following the surface of the PLA nanofiber (950 nm; **Figure 3C**; **Supplementary Videos 1–3**). In **Supplementary Video 1**, the process of adhesion of a single TEG3 cell on a 950 nm PLA nanofiber can be seen. In addition, we can observe, through a high magnification zoom, the interaction of the cell membrane on the migratory front with the nanotopography of PLA nanofiber (**Figures 3D,E**). **Figure 3E** details the protrusion of the TEG3 cells when adhering to the fiber. Using immunofluorescence techniques, we were able to show how eGFP-TEG3 cells are capable of associating with fluorescent nanofibers (red; **Figure 3F**).

Migratory Properties of TEG3 Cell Over PLA Biofunctionalized SDF-1α Nanofibers on CSPG Substrate

TEG3 cells growing over CSPG presented a loss of a leading and trailing process and, as well, the presence of membrane protrusions (**Supplementary Figures 2C,D**) compared to laminin permissive control cells (**Supplementary Figures 2A,B**). We decided then to create a doubled area with a different concentration of SDF-1α/CXCL12 linked to the surface of the PLA fibers through an EDC/NHS covalent bonding process. First, carboxylate groups had to be generated in a very controlled manner to avoid water meniscus destroying the fibers

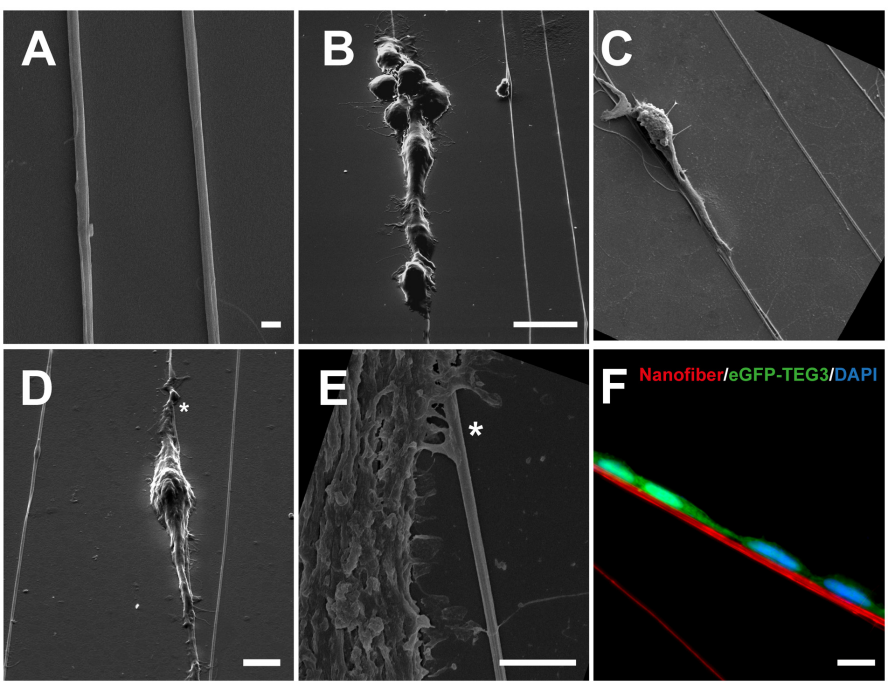

FIGURE 3 | FESEM analysis of TEG3 over PLA nanofibers of differing diameters. FESEM images of **(A)** pure nanofibers of an average size of 950 nm aligned on coverslips with a laminin coating; **(B, C)** analysis of the cell morphology on the fibrous substrates showing that cell bodies are elongated along the axis of the fiber and extended trailing processes that are guided by fiber directionality; **(D)** peripheral lamellipodial waves bearing fine filopodia showing cell-cell contact and cell group migration over the nanofibers; **(E)** cell membrane on the migratory front interacting with the nanotopography of PLA nanofiber (asterisk); **(F)** detail of the elongation of eGFP-TEG3 over a stained fiber (red) with immunofluorescence techniques. Scale bars: **(A)** – 1 μm., **(B)** (same for **(C)**) – 50 μm; **(D)** – 5 μm; **(E)** – 7.5 μm; and **(F)** – 10 μm.

on the hollow part of the frame. NaOH was selected as the base to break surface PLA chains and induce the creation of carboxylate functional groups (Mateos-Timoneda et al., 2014). The level of concentration of SDF-1α/CXCL12 on the surface was defined by the time of immersion in the solution (**Figure 4A**). After subsequent controlled immersions in the EDC/NHS and the SDF-1α/CXCL12 solutions, fibers maintained their aligned structure (**Figure 4B**) and the chemokine was observed

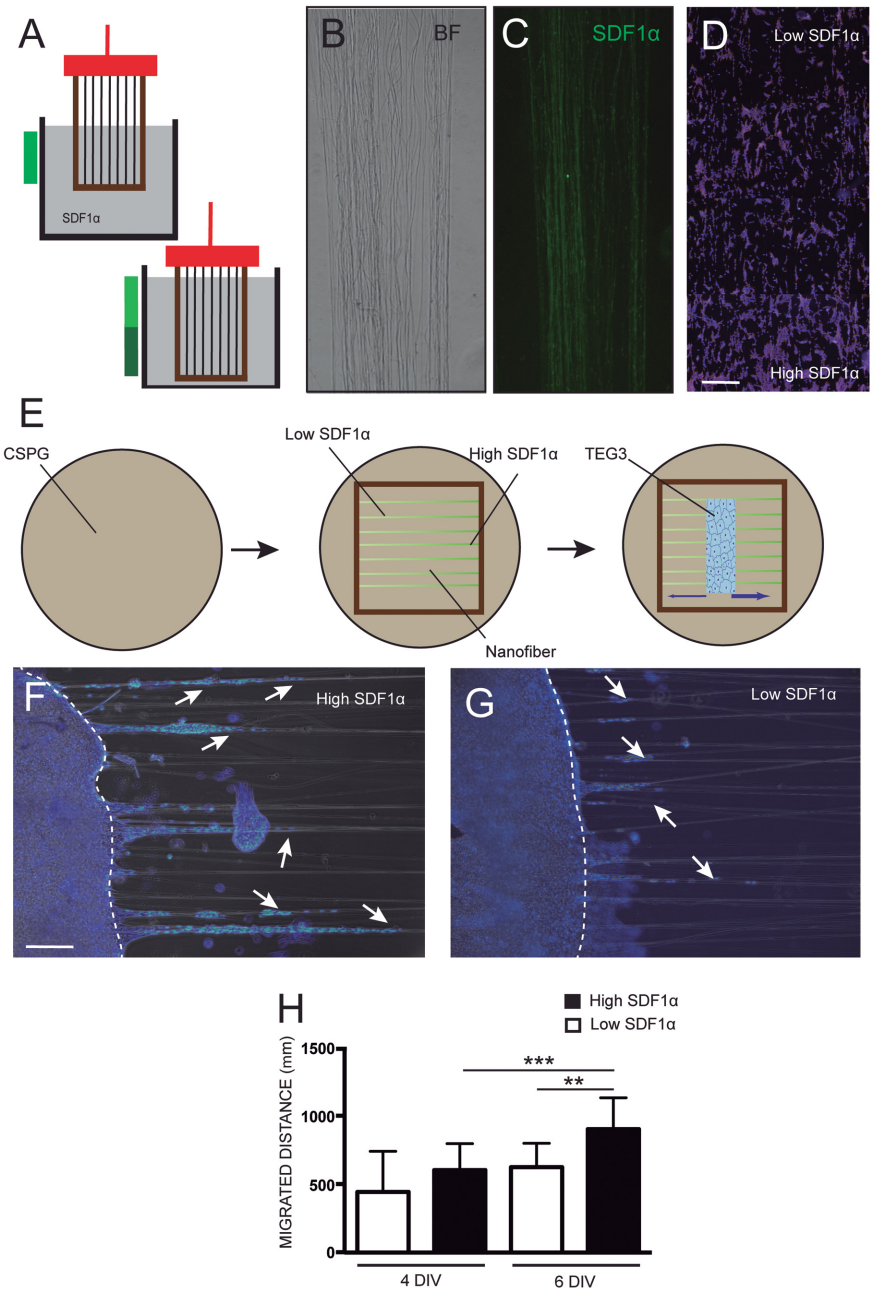

FIGURE 4 | Enhanced adhesion and migration of TEG on SDF-1α functionalized nanofibers. Scheme showing how the paraffin frames with the fibers on the top were dipped into the different aqueous solutions for activation and functionalization **(A)**; optical microscope images showing the maintained structure of the coated fibers in bright-field **(B)**, the homogeneous functionalization of the nanofibers with the chemotactic agent SDF-1α/CXCL12 by linking fluorescent SDF-1α antibodies **(C)**, and **(D)** the concentration of TEG3 cells in two areas with different concentrations of the chemotactic SDF-1α/CXCL12; **(E)** detailed instrumental scheme of the fibers within the paraffin frame laid onto a glass cover-slide coated with inhibitory CSPG where the cells are seeded using a PDMS template container and removed after confluence to let the cells migrate; **(F,G)** immunofluorescence images of the culture on both sides of the initial cell deposit at a time-point of 6 days showing the differences in number and distance migrated (white arrows); and **(H)** quantification of the covered distance by the cells at 4 and 6 days. Kruskal–Wallis test. ***p-value 0,0006; **p-value 0,0026. Scale bars **(C,D)** – 150 μm and **(F,G)** 300 μm.

with immunofluorescence through the nanofiber (**Figure 4C**), although with limitations due to the small diameter of the fibers.

Previous to the final test, fibers were electrospun onto conventional glass slides and functionalized with SDF-1α/CXCL12. After sterilization, 2×10^5 TEG3 cells were seeded and cultured for 48 h. **Figure 4D** shows the preference of TEG3 cells to migrate to high concentrated SDF-1α/CXCL12 functionalized areas rather than areas of lower concentration. In the second set of experiments, the same treatment (with low and high functionalized SDF-1α/CXCL12 areas) was performed for fibers within paraffin frames. However, no functionalization was carried out in the middle of the mats in order to leave a free area for cell deposition. A PDMS mask was placed over the precise location of the non-functionalized area of the fibers (see section "Materials and Methods" for details). 2×10^5 TEG3 cells were seeded in the PDMS hole. After cell adhesion, PDMS was removed and cells were allowed to migrate for between 4 and 6 days (**Figure 4E**). Cells were observed to advance from the non-functionalized area to the functionalized, especially the highly concentrated areas, as may be observed in **Figures 4F–H** shows the quantification of the distance migrated by the cells for 4 and 6 days in the effort to find a relevant statistical difference at day 6. The nanofibers then act as a guiding platform for cell migration. On day 6, TEG3 cells migrated an average distance of 625.6 mm ± 175.5 mm (N of 28) for low concentrate SDF-1α/CXCL12 while for high concentrate the average distance migrated was relevantly higher: 903.4 mm ± 230.1 mm (N of 28).

DISCUSSION

Various studies have indicated that the regenerative properties of OECs seem to be largely associated with their migratory capacities (Wang and Huang, 2012; Roloff et al., 2013), which has led to great interest in improving cell dynamics and survival of OECs after transplantation. Deng et al. (2006) showed that both rat and human OECs migrated relatively short distances, both rostrally and caudally, in animals with spinal cord lesions with a concomitant contralateral hemisection. Smale et al. (1996) reported non-significant cell migration when fetal rat olfactory bulb OECs were transplanted into the brain of damaged adult rats. Also, it has been shown that transplanted OECs migrate shorter distances in injured spinal cord compared to controls (uninjured spinal cord; Gudiño-Cabrera and Nieto-Sampedro, 2000; Collazos-Castro et al., 2005). These results have been confirmed in xenograft experiments using GFP expressing mouse OECs (Ramer et al., 2004).

Determining the molecular and cellular mechanisms by which OECs regulate migratory properties will lead to a better understanding of the role of OECs in regeneration within the olfactory system and will identify how the use of OECs can be optimized for regenerative therapies.

In this study, a parallel polylactic acid PLA electrospun nanofiber with low crystallinity – which improves their flexibility and biodegradability – is proposed. The effect of the diameter was studied and optimized to create a chemotactic concentration increment with a signaling biomolecule such as SDF-1α/CXCL12, which was covalently attached to the fiber surface. Both the topography and the increase in concentration effects were observed to improve the migration and proliferation of the OEC-derived TEG3 cell line over surface coatings with permissive Laminin and, more relevantly, with the inhibitory substrate CSPG. A biodegradable and metabolizable artificial material such as PLA can be processed and modified to introduce specific signaling. This method makes this synthetic polymer comparable to natural materials with the advantage of greater control over processing, and therefore, over the fate of the cell.

Fibers had a high amorphous grade which ensures that the PLA 80/20 is as flexible as possible, although still far from the lack of stiffness of nerve tissue (**Supplementary Figure 1A**; Sachot et al., 2014). This seems not to be a drawback; as in our previous studies, similar glial cells were able to adhere, proliferate, and even dedifferentiate (Álvarez et al., 2014). FESEM images showed a great affinity of TEG3 cells for pristine PLA fibers without the need for functionalization, evidencing good attachment, adhesion, and alignment on the PLA surface.

We tried to suggest a new strategy for the implantation of those cells in SCI in conjunction with a topographical biomaterial with a signaling chemotactic concentration difference. Biomaterial supports have been proposed in the literature, although to date no one has tried to improve glial migration through a chemotactic integrated signal that bypasses the inhibitory region of the scar. Considering that TEG3 cells express CXCR4, SDF-1α/CXCL12 was an excellent option to enhance not only migration, but also cell adhesion.

Electrospun PLA fibers can be a potent tool to guide TEG3 cells and avoid the inhibition mechanism of the spinal cord environment, as may be observed in the present study. We showed in a previous study that glia can be sensitive to lactate coming from PLA 70/30 fibers and metabolized as an energy source in a glucose-poor environment (Álvarez et al., 2014). However, for this purpose, we needed a less degradable PLA source and a stiffer one that could support aggressive treatment like the process of functionalization shown here. PLA 80/20 meets the requirements to work as a stable bridging platform for neuron migration. As well, the aligned distribution together with the proper thickness work as a perfect tandem for cell alignment and migration. The only thing we needed was to show cells which direction to follow. The possibility of creating a gradient or concentration difference with a chemotactic agent such as SDF-1α/CXCL12 covalently attached by a conventional EDC/NHS chemistry (Sachot et al., 2015) makes the platform ideal for use as a model to bypass the inhibiting CSPG and push the cells toward the concentrated side of the fibers.

The first stages of the research implied the deposition of the fibers and their functionalization onto coverslides. However, that is not practical for a real damaged spinal cord. The idea of using paraffin frames is an attractive option for easy 3D integration of ECM-like fibers. The process here applied has been reproducible and efficient in producing fibers with no background so they can be easily coupled to any 3D tissue, model, device, or material for bridging. They have the option of being stacked, creating different layers of a controlled number of fibers and porosity.

Although the results obtained by several researchers are positive, more research is needed to achieve functional recovery from an SCI. The key phase for axon regeneration is the evolution

of the damaged proximal wound into a new growth tip that sums up a regeneration process, which must then cross the lesion through the glial scar and the inflammation to reconnect with its original target (Silver and Miller, 2004). Factors that control the formation of the growth tip and the recovery of axonal growth include the inherent regenerative capacity of neuronal cells, as well as the previously developed multifaceted inhibitory biochemical microenvironment that prevents the growth of the damaged axon. Indeed, they form physical and molecular walls for anatomical and functional recovery. CSPG is a good example of an inhibitory molecule.

Understanding the fundamental mechanism of the type of migration of TEG3 cells from the configuration of a cylindrical topography of diameter around the micrometer, and being able to analyze the spatio-temporal behavior of the cells without subjecting them to a disruption in their structural integrity, were our main concerns. The platform shown here allows us to analyze and characterize the migratory properties of TEG3 cells by microscopy in real-time to obtain a certain migratory pattern. Preliminary, but not conclusive, results indicate that TEG3 cells are capable of migrating collectively, but with free disposition. A lack of stable cell-cell junctions was observed (see **Supplementary Video 2** in the **Supplementary Data**) during the migratory process; however, transitory physical interactions were observed, and perhaps they could also be molecular, which would allow free movement within a coordinated migration.

The approach presented here needs to be tested in a real inhibitory environment. However, the process can be further optimized, for example with the combination of SDF-1α/CXCL12 surface concentration increments and TEG3 cell lines expressing the ectodomain of the Nogo receptor 1 (NgR1), an antagonist of MAIs. Finally, the application of neurons and determination of whether the growth tip and the recovery of axonal growth can be controlled within the inherent regenerative capacity of neuronal cells need to be examined. We are convinced that TEG3 cells in our platform can form physical and molecular walls for anatomical and functional recovery.

The next steps involve the addition of other interesting experiments such as inhibiting the CXCR4 co-receptor in the TEG3 cell line as a proof of concept to evidence that molecular interactions through this receptor-ligand complex are fundamental for the growth of OECs over CSPGs; as well, co-cultures with neurons are envisaged, to show that OECs higher levels of directionality and migration can positively influence the neurons growth and their axonal extension; and finally, explore the adhesion molecules/proteins, or other overexpressed markers that might explain the increased cell adhesion and migration. However, identification of the main targets and the increase of the dimension and the number of cells adhered to the fibers is needed and a challenge.

CONCLUSION

Poly(l/dl-lactic acid electrospun fibers with a covalently linked signaling SDF-1α/CXCL12 surface increment act as an efficient bridge for TEG3 cell migration. Although fiber stiffness is far from the natural stiffness of the nerve tissue, topographical morphology, and the possibility to effectively link an amino-containing biomolecule with time-dependent dip-coating using a well-known chemistry method, opens the way to developing more suitable platforms involving biomaterials. TEG3 cells migrate onto the fiber despite being surrounded by an inhibitory environment of CSPG. Real-time migration analysis and characterization over a nanostructure pattern are easily achieved without the need for micronanufacture with sophisticated instrumentation techniques. Indeed, we increase the migration of the cells over inhibitory substrates (as happens after SCI) on compatible fibers most probably their immunomodulatory effects can be preserved for longer times to enhance axon regrowth of lesioned neurons. However, these are the next step not only *in vitro* but also *in vivo*. Further experiments are needed to explore the mechanisms behind OECs migration and adhesion, which would be of paramount importance to enhance surfaces in terms of healing efficiency.

DATA AVAILABILITY STATEMENT

The raw data supporting the conclusions of this article will be made available by the authors, without undue reservation.

AUTHOR CONTRIBUTIONS

OC, EE, and JR conceived the project. OC, AL-M, DR, and AM-A implemented and carried out the experiments, characterized the outcomes, and analyzed the data. OC, AL-M, DR, and JR wrote the manuscript. OC, EE, and JR provided the funding and the needed infrastructure. All authors contributed to the article and approved the submitted version.

FUNDING

The authors thank the European Commission-ERANET (nAngioderm JTC2018-103) and the Spanish Ministry MICINN for the funding support (BES-2015-071997, MAT2015-62725-ERC, RTI2018-096320-B-C21, RTI2018-097038-B-C22, and *PRPSEM* Project: RTI2018-099773-B-I00), the Severo Ochoa Program for Centers of Excellence and R&D 2016-2019 and Obra Social la Caixa (CaixaImpulse CI0015). Authors also thanks the CERCA Program, and by the Commission for Universities and Research of the Department of Innovation, Universities, and Enterprise of the Generalitat de Catalunya (SGR2017-648 and SGR2017-359), CIBERNED (CMED2018-2) CIBER-BBN and the Spanish network of cell therapy (TERCEL). The project leading to these results received funding from "la Caixa" Foundation (ID 100010434) under the agreement LCF/PR/HR19/52160007 to JR; and the María de Maeztu Unit of Excellence (Institute of Neurosciences, University of Barcelona) MDM-2017-0729 to JR. AM-A was supported by a fellowship from La Fundación Tatiana Pérez de Guzmán el Bueno and AL-M was supported by FPI Program. DR was supported by a fellowship from CONICYT, Chile

and actually from SENACYT, Panamá (Grants FID17-078 and FID18-042).

SUPPLEMENTARY MATERIAL

The Supplementary Material for this article can be found online at: https://www.frontiersin.org/articles/10.3389/fbioe.2021.627805/full#supplementary-material

Resulted plots form mechanical and thermal characterization; Electronic and optical fluorescence microscope images of TEG3 cells both on adhesive and inhibitory coatings.

Supplementary Video 1 | TEG3 cells running over 950 nm fibers.

Supplementary Video 2 | TEG3 cells migration front over 950 nm fiber.

Supplementary Video 3 | TEG3 cells advance over a 950 nm fiber in a CSPG inhibtory coating.

REFERENCES

Aguzzi, A., Barres, B. A., and Bennett, M. L. (2013). Microglia: scapegoat, saboteur, or something else? *Science* 339, 156–161. doi: 10.1126/science.1227901

Akter, F. (2016). *Tissue Engineering Made Easy*. Amsterdam: Elsevier Science.

Álvarez, Z., Castaño, O., Castells, A. A., Mateos-Timoneda, M. A., Planell, J. A., Engel, E., et al. (2014). Neurogenesis and vascularization of the damaged brain using a lactate-releasing biomimetic scaffold. *Biomaterials* 35, 4769–4781. doi: 10.1016/j.biomaterials.2014.02.051

Álvarez, Z., Mateos-Timoneda, M. A., Hyroššová, P., Castaño, O., Planell, J. A., Perales, J. C., et al. (2013). The effect of the composition of PLA films and lactate release on glial and neuronal maturation and the maintenance of the neuronal progenitor niche. *Biomaterials* 34, 2221–2233. doi: 10.1016/j.biomaterials.2012.12.001

Beachley, V., and Wen, X. (2009). Fabrication of nanofiber reinforced protein structures for tissue engineering. *Mater. Sci. Eng. C. Mater. Biol. Appl.* 29, 2448–2453. doi: 10.1016/j.msec.2009.07.008

Cao, L., Su, Z., Zhou, Q., Lv, B., Liu, X., Jiao, L., et al. (2006). Glial cell line-derived neurotrophic factor promotes olfactory ensheathing cells migration. *Glia* 54, 536–544. doi: 10.1002/glia.20403

Chen, Y.-S., Harn, H.-J., and Chiou, T.-W. (2018). The role of biomaterials in implantation for central nervous system injury. *Cell Transplant.* 27, 407–422. doi: 10.1177/0963689717732991

Collazos-Castro, J. E., Muñetón-Gómez, V. C., and Nieto-Sampedro, M. (2005). Olfactory glia transplantation into cervical spinal cord contusion injuries. *J. Neurosurg. Spine* 3, 308–317. doi: 10.3171/spi.2005.3.4.0308

Deng, C., Gorrie, C., Hayward, I., Elston, B., Venn, M., Mackay-Sim, A., et al. (2006). Survival and migration of human and rat olfactory ensheathing cells in intact and injured spinal cord. *J. Neurosci. Res.* 83, 1201–1212. doi: 10.1002/jnr.20817

Ekberg, J. A. K., Amaya, D., Mackay-Sim, A., and St John, J. A. (2012). The migration of olfactory ensheathing cells during development and regeneration. *Neurosignals* 20, 147–158. doi: 10.1159/000330895

Field, P., Li, Y., and Raisman, G. (2003). Ensheathment of the olfactory nerves in the adult rat. *J. Neurocytol.* 32, 317–324. doi: 10.1023/B:NEUR.0000010089.37032.48

Flores, L. R., Keeling, M. C., Zhang, X., Sliogeryte, K., and Gavara, N. (2019). Lifeact-TagGFP2 alters F-actin organization, cellular morphology and biophysical behaviour. *Sci. Rep.* 9:3241. doi: 10.1038/s41598-019-40092-w

Ghasemi-Mobarakeh, L., Prabhakaran, M. P., Morshed, M., Nasr-Esfahani, M.-H., and Ramakrishna, S. (2008). Electrospun poly(epsilon-caprolactone)/gelatin nanofibrous scaffolds for nerve tissue engineering. *Biomaterials* 29, 4532–4539. doi: 10.1016/j.biomaterials.2008.08.007

Gómez, R. M., Sánchez, M. Y., Portela-Lomba, M., Ghotme, K., Barreto, G. E., Sierra, J., et al. (2018). Cell therapy for spinal cord injury with olfactory ensheathing glia cells (OECs). *Glia* 66, 1267–1301. doi: 10.1002/glia.23282

Gudiño-Cabrera, G., and Nieto-Sampedro, M. (2000). Schwann-like macroglia in adult rat brain. *Glia* 30, 49–63. doi: 10.1002/(SICI)1098-1136(200003)30:1<49::AID-GLIA6>3.0.CO;2-M

Guntinas-Lichius, O., Angelov, D. N., Tomov, T. L., Dramiga, J., Neiss, W. F., and Wewetzer, K. (2001). Transplantation of olfactory ensheathing cells stimulates the collateral sprouting from axotomized adult rat facial motoneurons. *Exp. Neurol.* 172, 70–80. doi: 10.1006/exnr.2001.7774

Hackett, J. M., Dang, T. T., Tsai, E. C., and Cao, X. (2010). Electrospun biocomposite polycaprolactone/collagen tubes as scaffolds for neural stem cell differentiation. *Materials (Basel)* 3, 3714–3728. doi: 10.3390/ma3063714

Huang, Z., Wang, Y., Su, Z., Geng, J., Chen, Y., Yuan, X., et al. (2011). Slit-2 repels the migration of olfactory ensheathing cells by triggering Ca2+-dependent cofilin activation and RhoA inhibition. *J. Cell Sci.* 124, 186–197. doi: 10.1242/jcs.071357

Imaizumi, T., Lankford, K. L., Burton, W. V., Fodor, W. L., and Kocsis, J. D. (2000). Xenotransplantation of transgenic pig olfactory ensheathing cells promotes axonal regeneration in rat spinal cord. *Nat. Biotechnol.* 18, 949–953. doi: 10.1038/79432

Kafitz, K. W., and Greer, C. A. (1999). Olfactory ensheathing cells promote neurite extension from embryonic olfactory receptor cells in vitro. *Glia* 25, 99–110. doi: 10.1002/(SICI)1098-1136(19990115)25:2<99::AID-GLIA1<3.0.CO;2-V

King, V. R., Alovskaya, A., Wei, D. Y. T., Brown, R. A., and Priestley, J. V. (2010). The use of injectable forms of fibrin and fibronectin to support axonal ingrowth after spinal cord injury. *Biomaterials* 31, 4447–4456. doi: 10.1016/j.biomaterials.2010.02.018

Levoye, A., Balabanian, K., Baleux, F., Bachelerie, F., and Lagane, B. (2009). CXCR7 heterodimerizes with CXCR4 and regulates CXCL12-mediated G protein signaling. *Blood* 113, 6085–6093. doi: 10.1182/blood-2008-12-196618

Li, Y., Field, P. M., and Raisman, G. (1997). Repair of adult rat corticospinal tract by transplants of olfactory ensheathing cells. *Science* 277, 2000–2002. doi: 10.1126/science.277.5334.2000

López-Vales, R., Forés, J., Navarro, X., and Verdú, E. (2007). Chronic transplantation of olfactory ensheathing cells promotes partial recovery after complete spinal cord transection in the rat. *Glia* 55, 303–311. doi: 10.1002/glia.20457

Lu, J., Féron, F., Ho, S. M., Mackay-Sim, A., and Waite, P. M. (2001). Transplantation of nasal olfactory tissue promotes partial recovery in paraplegic adult rats. *Brain Res.* 889, 344–357. doi: 10.1016/s0006-8993(00)03235-2

Lu, J., Féron, F., Mackay-Sim, A., and Waite, P. M. E. (2002). Olfactory ensheathing cells promote locomotor recovery after delayed transplantation into transected spinal cord. *Brain* 125, 14–21. doi: 10.1093/brain/awf014

Mateos-Timoneda, M. A., Castano, O., Planell, J. A., and Engel, E. (2014). Effect of structure, topography and chemistry on fibroblast adhesion and morphology. *J. Mater. Sci. Mater. Med.* 25:1781–1787. doi: 10.1007/s10856-014-5199-z

Moreno-Flores, M. T., Lim, F., Martín-Bermejo, M. J., Díaz-Nido, J., Ávila, J., and Wandosell, F. (2003). Immortalized olfactory ensheathing glia promote axonal regeneration of rat retinal ganglion neurons. *J. Neurochem.* 85, 861–871. doi: 10.1046/j.1471-4159.2003.01729.x

Nash, H. H., Borke, R. C., and Anders, J. J. (2002). Ensheathing cells and methylprednisolone promote axonal regeneration and functional recovery in the lesioned adult rat spinal cord. *J. Neurosci.* 22, 7111–7120. doi: 10.1523/JNEUROSCI.22-16-07111.2002

Nocentini, S., Reginensi, D., Garcia, S., Carulla, P., Moreno-Flores, M. T., Wandosell, F., et al. (2012). Myelin-associated proteins block the migration of olfactory ensheathing cells: an in vitro study using single-cell tracking and traction force microscopy. *Cell. Mol. Life Sci.* 69, 1689–1703. doi: 10.1007/s00018-011-0893-1

Oliveira, H., Catros, S., Boiziau, C., Siadous, R., Marti-Munoz, J., Bareille, R., et al. (2016). The proangiogenic potential of a novel calcium releasing biomaterial: impact on cell recruitment. *Acta Biomater.* 29, 435–445. doi: 10.1016/j.actbio.2015.10.003

Pounders, V., McArthur, L., Rinehart, J., McQueen, R., Raynes, E., and Roca-Menchavez, M. (2019). Physical therapy and regenerative medicine: current knowledge and future prospects. *FASEB J.* 33:802.57. doi: 10.1096/fasebj.2019.33.1_supplement.802.57

Ramer, L. M., Au, E., Richter, M. W., Liu, J., Tetzlaff, W., and Roskams, A. J. (2004). Peripheral olfactory ensheathing cells reduce scar and cavity formation and promote regeneration after spinal cord injury. *J. Comp. Neurol.* 473, 1–15. doi: 10.1002/cne.20049

Ramón-Cueto, A., Cordero, M. I., Santos-Benito, F. F., and Avila, J. (2000). Functional recovery of paraplegic rats and motor axon regeneration in their spinal cords by olfactory ensheathing glia. *Neuron* 25, 425–435. doi: 10.1016/s0896-6273(00)80905-8

Ramón-Cueto, A., and Nieto-Sampedro, M. (1994). Regeneration into the spinal cord of transected dorsal root axons is promoted by ensheathing glia transplants. *Exp. Neurol.* 127, 232–244. doi: 10.1006/exnr.1994.1099

Ramón-Cueto, A., Plant, G. W., Avila, J., and Bunge, M. B. (1998). Long-distance axonal regeneration in the transected adult rat spinal cord is promoted by olfactory ensheathing glia transplants. *J. Neurosci.* 18, 3803–3815. doi: 10.1523/JNEUROSCI.18-10-03803.1998

Reginensi, D., Carulla, P., Nocentini, S., Seira, O., Serra-Picamal, X., Torres-Espín, A., et al. (2015). Increased migration of olfactory ensheathing cells secreting the Nogo receptor ectodomain over inhibitory substrates and lesioned spinal cord. *Cell. Mol. Life Sci.* 72, 2719–2737. doi: 10.1007/s00018-015-1869-3

Reichert, W. M. (2007). *Indwelling Neural Implants: Strategies for Contending with the In Vivo Environment*. Boca Raton, FL: CRC Press.

Roet, K. C. D., and Verhaagen, J. (2014). Understanding the neural repair-promoting properties of olfactory ensheathing cells. *Exp. Neurol.* 261, 594–609. doi: 10.1016/j.expneurol.2014.05.007

Roloff, F., Ziege, S., Baumgärtner, W., Wewetzer, K., and Bicker, G. (2013). Schwann cell-free adult canine olfactory ensheathing cell preparations from olfactory bulb and mucosa display differential migratory and neurite growth-promoting properties in vitro. *BMC Neurosci.* 14:141. doi: 10.1186/1471-2202-14-141

Sachot, N., Castaño, O., Oliveira, H., Martí-Muñoz, J., Roguska, A., Amedee, J., et al. (2016). A novel hybrid nanofibrous strategy to target progenitor cells for cost-effective: in situ angiogenesis. *J. Mater. Chem. B* 4:6967. doi: 10.1039/c6tb02162j

Sachot, N., Engel, E., and Castaño, O. (2014). Hybrid organic-inorganic scaffolding biomaterials for regenerative therapies. *Curr. Org. Chem* 18, 2299–2314. doi: 10.2174/1385272819666140806200355

Sachot, N., Mateos-Timoneda, M. A., Planell, J. A., Velders, A. H., Lewandowska, M., Engel, E., et al. (2015). Towards 4th generation biomaterials: a covalent hybrid polymer-ormoglass architecture. *Nanoscale* 7, 15349–15361. doi: 10.1039/C5NR04275E

Schindelin, J., Arganda-Carreras, I., Frise, E., Kaynig, V., Longair, M., Pietzsch, T., et al. (2012). Fiji: an open-source platform for biological-image analysis. *Nat. Methods* 9, 676–682. doi: 10.1038/nmeth.2019

Schneider, C. A., Rasband, W. S., and Eliceiri, K. W. (2012). NIH image to ImageJ: 25 years of image analysis. *Nat. Methods* 9, 671–675. doi: 10.1038/nmeth.2089

Silver, J., and Miller, J. H. (2004). Regeneration beyond the glial scar. *Nat. Rev. Neurosci.* 5, 146–156. doi: 10.1038/nrn1326

Silver, J., Schwab, M. E., and Popovich, P. G. (2014). Central nervous system regenerative failure: role of oligodendrocytes, astrocytes, and microglia. *Cold Spring Harb. Perspect. Biol.* 7:a020602. doi: 10.1101/cshperspect.a020602

Smale, K. A., Doucette, R., and Kawaja, M. D. (1996). Implantation of olfactory ensheathing cells in the adult rat brain following fimbria-fornix transection. *Exp. Neurol.* 137, 225–233. doi: 10.1006/exnr.1996.0021

Sonigra, R. J., Brighton, P. C., Jacoby, J., Hall, S., and Wigley, C. B. (1999). Adult rat olfactory nerve ensheathing cells are effective promoters of adult central nervous system neurite outgrowth in coculture. *Glia* 25, 256–269. doi: 10.1002/(SICI)1098-1136(19990201)25:3<256::AID-GLIA6<3.0.CO;2-Y

Straley, K. S., Foo, C. W. P., and Heilshorn, S. C. (2010). Biomaterial design strategies for the treatment of spinal cord injuries. *J. Neurotrauma* 27, 1–19. doi: 10.1089/neu.2009.0948

Su, Z., Cao, L., Zhu, Y., Liu, X., Huang, Z., Huang, A., et al. (2007). Nogo enhances the adhesion of olfactory ensheathing cells and inhibits their migration. *J. Cell Sci.* 120, 1877–1887. doi: 10.1242/jcs.03448

Tabakow, P., Jarmundowicz, W., Czapiga, B., Fortuna, W., Miedzybrodzki, R., Czyz, M., et al. (2013). Transplantation of autologous olfactory ensheathing cells in complete human spinal cord injury. *Cell Transplant.* 22, 1591–1612. doi: 10.3727/096368912X663532

Thuret, S., Moon, L. D. F., and Gage, F. H. (2006). Therapeutic interventions after spinal cord injury. *Nat. Rev. Neurosci.* 7, 628–643. doi: 10.1038/nrn1955

Torres-Espín, A., Redondo-Castro, E., Hernández, J., and Navarro, X. (2014). Bone marrow mesenchymal stromal cells and olfactory ensheathing cells transplantation after spinal cord injury – a morphological and functional comparison in rats. *Eur. J. Neurosci.* 39, 1704–1717. doi: 10.1111/ejn.12542

Vukovic, J., Ruitenberg, M. J., Roet, K., Franssen, E., Arulpragasam, A., Sasaki, T., et al. (2009). The glycoprotein fibulin-3 regulates morphology and motility of olfactory ensheathing cells in vitro. *Glia* 57, 424–443. doi: 10.1002/glia.20771

Wang, Y., and Huang, Z. (2012). Morphological phenotypes of olfactory ensheathing cells display different migratory responses upon Slit-2. *Exp. Cell Res.* 318, 1889–1900. doi: 10.1016/j.yexcr.2012.05.024

Conflict of Interest: The authors declare that the research was conducted in the absence of any commercial or financial relationships that could be construed as a potential conflict of interest.

frontiers in Bioengineering and Biotechnology

REVIEW
published: 25 May 2021
doi: 10.3389/fbioe.2021.674473

Natural Biomaterials as Instructive Engineered Microenvironments That Direct Cellular Function in Peripheral Nerve Tissue Engineering

Rebecca Powell[1,2], Despoina Eleftheriadou[1,2,3], Simon Kellaway[1,2] and James B. Phillips[1,2]*

[1] UCL Centre for Nerve Engineering, University College London, London, United Kingdom, [2] Department of Pharmacology, UCL School of Pharmacy, University College London, London, United Kingdom, [3] Department of Mechanical Engineering, University College London, London, United Kingdom

Nerve tissue function and regeneration depend on precise and well-synchronised spatial and temporal control of biological, physical, and chemotactic cues, which are provided by cellular components and the surrounding extracellular matrix. Therefore, natural biomaterials currently used in peripheral nerve tissue engineering are selected on the basis that they can act as instructive extracellular microenvironments. Despite emerging knowledge regarding cell-matrix interactions, the exact mechanisms through which these biomaterials alter the behaviour of the host and implanted cells, including neurons, Schwann cells and immune cells, remain largely unclear. Here, we review some of the physical processes by which natural biomaterials mimic the function of the extracellular matrix and regulate cellular behaviour. We also highlight some representative cases of controllable cell microenvironments developed by combining cell biology and tissue engineering principles.

Keywords: peripheral nerve, tissue engineering, biomaterials, microenvironment, regeneration

OPEN ACCESS

Edited by:
Antonio Salgado, University of Minho, Portugal

Reviewed by:
Kirsten Haastert-Talini, Hannover Medical School, Germany
Pavel Makarevich, Lomonosov Moscow State University, Russia

****Correspondence:***
Rebecca Powel
rebecca.powell.17@ucl.ac.uk

Specialty section:
This article was submitted to Tissue Engineering and Regenerative Medicine, a section of the journal Frontiers in Bioengineering and Biotechnology

Received: *01 March 2021*
Accepted: *16 April 2021*
Published: *25 May 2021*

Citation:
Powell R, Eleftheriadou D, Kellaway S and Phillips JB (2021) Natural Biomaterials as Instructive Engineered Microenvironments That Direct Cellular Function in Peripheral Nerve Tissue Engineering. Front. Bioeng. Biotechnol. 9:674473. doi: 10.3389/fbioe.2021.674473

INTRODUCTION

Despite significant research and progress in microsurgical techniques over recent decades, peripheral nerve repair remains challenging for clinicians. Recovery from larger gap injuries is especially problematic, with patients commonly living with unsatisfactory restoration of sensory and motor function (Muheremu and Ao, 2015) which can have a substantial impact on quality of life (Wojtkiewicz et al., 2015). Depending on the severity of the injury, a number of interventions may be employed by clinicians to aid the innate regeneration potential of the peripheral nervous system. Where possible, end-to-end suturing of the nerve stumps will be performed following a transection injury. However, when the damage involves a gap which cannot be sutured directly this is not possible, and the gold standard for repair is autologous transplantation of nerve tissue, or autograft. Autografts do come with drawbacks, with patients potentially presenting with morbidity at the donor site, subsequent sensory deficits, neuroma development and having a greater risk of infection. Furthermore, there is a limited amount of available graft material (Lee and Wolfe, 2000). Therefore, a critical need remains for developing effective nerve repair strategies that overcome limitations of autografting.

The design and production of nerve guidance conduits is multidisciplinary and may draw from engineering, biology, and chemistry to provide optimal conditions for the support of axonal regeneration. Nerve repair technology has progressed from the development of simple hollow tubes to more sophisticated engineered tissues, designed to mimic additional features of the nerve autograft. To be successful, engineered tissues must integrate with the host nerve tissue and provide an appropriate environment to support and guide the regeneration of neurons from the proximal to the distal side of the injury site.

There is little consensus in peripheral nerve engineering, despite the wide range of biomaterials available, on which are most suited to supporting cells involved in the repair process such as neurons, Schwann cells, macrophages, and blood vessels. As is the case for many tissue engineering solutions, both natural and synthetic material avenues have been extensively explored with tangible advantages and disadvantages attributed to both options (Zhang et al., 2014; Di Summa et al., 2015; Muheremu and Ao, 2015; Gregory and Phillips, 2021). Synthetic polymers are popular as they can be adapted, through various modifications, to improve cell adhesion and finely tune mechanical properties (Li et al., 2015; Mobasseri et al., 2015; Shahriari et al., 2017). However, natural materials (typically derived from extracellular matrix components) possess innate cell binding motifs, produce harmless degradation products, and effectively invoke natural tissue remodelling and repair pathways (Bonnans et al., 2014; Nicolas et al., 2020). Using extracellular matrix proteins in the form of hydrogels gives the benefit of structural integrity for supporting regenerating axons, whilst maintaining the hydrogel viscoelastic properties and their capability to act as carriers for drugs, growth factors and cells to further improve function (Bhatnagar et al., 2016).

Cell behaviour and nerve extracellular matrix have been characterised extensively. Of particular importance in engineered nerve tissue are interactions between neurons, Schwann cells, macrophages, and endothelial cells with collagen, laminin, and fibronectin due to their presence in native nerve extracellular matrix and the ability of these to be used in hydrogel form. Cells interact with these proteins in an integrin-dependent manner, binding to peptides in fibronectin and laminin such as RGD which is recognised by α5β1 integrins and attaching to collagen via interactions involving α_1-integrins in particular (Brown and Phillips, 2007; O'Rourke et al., 2015). Fibrin is another protein used in peripheral nerve repair that, although not present in the native extracellular matrix, is deposited after injury. Fibrin forms a nerve bridge joining the two ends of an injured peripheral nerve which acts as early guidance for fibroblasts, endoneurial cells, and repair Schwann cells (Hodde et al., 2016) and therefore has an important role in the peripheral nerve injury response. There have been various studies that have used extracellular matrix protein hydrogels inside outer tubes to influence cell behaviour in animal models, shown in **Table 1**. Included in the table are those studies which investigated the impact of the biomaterial on the phenotype of cells involved in the repair process–namely Schwann cells, neurons, and macrophages. Both cellular and acellular implanted constructs have been included, in addition to more complex hydrogels such as those releasing growth factors. *In vitro* and *in vivo* experimental outcomes that have shown to have a positive effect on peripheral nerve regeneration are the increased viability, adhesion, proliferation, and elongation of Schwann cells in addition to increased neurite extension from neural cells and the polarisation of macrophages towards an M2, pro-regenerative phenotype (Badylak et al., 2008; Georgiou et al., 2015; Jessen and Mirsky, 2019).

In this review, we have identified common extracellular matrix proteins used in hydrogels for peripheral nerve repair applications and the way in which these can mimic the function of native extracellular matrix and regulate cellular behaviour (**Figures 1**, **2**). We highlight some representative examples of controllable cell microenvironments developed by combining cell biology and tissue engineering principles which will be useful for future development of cellular nerve guidance conduits. Understanding how these different cell types interact with extracellular matrix protein hydrogels will allow us to choose the most appropriate materials for nerve guidance conduits and hopefully improve outcomes for translational therapies.

CELLULAR BEHAVIOUR SUPPORTING PERIPHERAL NERVE REGENERATION

Schwann cells provide neurotropic support and are involved in the inherent regeneration response. They transform after denervation into repair Schwann cells which proliferate and elongate to form Bands of Büngner which support and guide the regenerating axons (Deumens et al., 2010; Jessen et al., 2015; Jessen and Mirsky, 2016). Without this Schwann cell guidance, undirected growth of axons can occur resulting in unsuccessful repair alongside muscle atrophy at the distal target and neuroma formation at the proximal stump (Deumens et al., 2010; Gomez-Sanchez et al., 2015; Jessen et al., 2015; Jessen and Arthur-Farraj, 2019). Accelerating organised Schwann cell migration may be critical in improving axonal regeneration throughout the conduit (Chen et al., 2019). Ensuring viability and the spatial organisation of supporting cells is important to the success of the nerve guidance conduit in peripheral nerve regeneration (Smith and Stevenson, 1988). Repair Schwann cells are also an integral part of many other intercellular interactions (Pan et al., 2020), for example the recruitment of macrophages, which aid in the formation of a pro-regenerative environment in addition to releasing VEGF to encourage the growth of blood vessels (Lindborg et al., 2017; Roberts et al., 2017; Zigmond and Echevarria, 2019). Blood vessels in turn help guide the Schwann cells across the nerve bridge and supply oxygen to the injury area (Cattin et al., 2015). If oxygen deprivation is prolonged, the repair Schwann cells, neurons and other cell types in the regenerative region will die and impair axon regeneration (Krock et al., 2011). Schwann cells also remyelinate the regenerated axons, allowing complete reinnervation (Stratton et al., 2018). Supporting Schwann cell survival and proliferation alongside blood vessel formation is therefore likely to be essential to the overall success of nerve guidance constructs.

Another aspect to consider is the role of immune cells such as macrophages in the peripheral nerve regeneration process.

TABLE 1 | Summary of extracellular matrix hydrogels as nerve guidance conduit luminal fillers in *in vivo* models.

Conduit	Hydrogel material	Additional components	Implanted cell	Species	Gap length	Cell type of interest	Cell behaviour	References
COLLAGEN	Collagen I	None	Differentiated adipose-derived stem cells	Rat	10 mm sciatic	Schwann cells	Collagen-cell combination conduits promoted Schwann cell infiltration, preferentially along the walls of the conduit	Di Summa et al., 2014
COLLAGEN	Collagen	None	Acellular	Dog	35 mm sciatic	Neurons	More nerve fibres and larger myelinated area with NGF versus without, although thinner compared to autograft	Yao et al., 2018
ACRYLONITRILE VINYLCHLORIDE COPOLYMER	Matrigel	None	Primary rat Schwann cells	Rat	8 mm sciatic	Neurons, Schwann cells	Greater number of myelinated axons with Schwann cells, which increased with Schwann cell density, although Matrigel alone was inhibitory. Heterologous induced immune response impeding regeneration	Guenard et al., 1992
CHITOSAN	Collagen	Laminin or fibronectin	Acellular	Rat	15 mm sciatic	Schwann cells	Greatest infiltration of Schwann cells observed in stabilised fibronectin and laminin conduits	Gonzalez-Perez et al., 2017
SMALL INTESTINE SUBMUCOSA	Collagen I	Hyaluronic acid	Acellular	Rat	10 mm sciatic	Schwann cells	Aligned hydrogels resulted in elevated Schwann cell migration and proliferation at 4 weeks	Lacko et al., 2020
CHITOSAN	Collagen I	Laminin or fibronectin	MSCs/ Schwann cells	Rat	15 mm sciatic	Neurons, Schwann cells, MSCs	Better functional results in those with implanted Schwann cells in fibronectin-aligned constructs, despite *in vitro* greater proliferation on laminin	Gonzalez-Perez et al., 2018
COLLAGEN	Collagen	Collagen-gag	Acellular	Rat	10 mm sciatic	Neurons	Comparable axon and nerve fibre density between collagen/GAG and autograft, although number of myelinated nerves reduced	Lee et al., 2012
COLLAGEN I	Collagen I	Hyaluronic acid	Neural stem cells	Rabbit	5 mm facial	Neurons, macrophages	No infiltration of macrophages. HA supported developmentally immature neurons and promotes neurite outgrowth	Zhang et al., 2008
POLY-L-LACTIDE-CO-CAPROLACTONE	Collagen I	Hyaluronic acid, NGF	Acellular	Rat	10 mm sciatic	Neurons	Additions of hydrogel to conduits did not improve motor neuron recovery, but sensory neurite outgrowth increased in presence of NGF	Jin et al., 2013
POLY-D,L-LACTATES	Laminin	Collagen IV, heparan sulfate, proteoglycan	Acellular	Mouse	4–5 mm sciatic	Neurons	Laminin had stimulatory effect on axon growth	Madison et al., 1985
COLLAGEN I	Hyaluronic acid	Laminin-simulating peptide, sodium dismutase	Acellular	Rat	15 mm sciatic	Neurons	Myelinated axons, axonal sprouting comparable to autograft	Rochkind and Nevo, 2014
SILICONE	Collagen I	Fibrin gel	Schwann cells	Rat	10 mm sciatic	Neurons, endothelial cells	Blood vessel numbers in GAE-EngNT comparable to autograft, 8-fold more axons in GAE than the empty tube with neural extensions following aligned Schwann cells	Muangsanit et al., 2020
SILICONE	Peripheral-nerve specific extracellular matrix	None	Acellular	Rat	15 mm sciatic	Macrophages, Schwann cells	M1 and M2 macrophages and Schwann cell numbers were increased with PNSECM in addition to the M2:M1 ratio compared to silicone conduit alone	Prest et al., 2017
POLY (L-LACTIC ACID)-CO-POLY (TRIMETHYLENE CARBONATE)	Porcine decellularised nerve matrix	NGF (3.3 μg/ml)	Acellular	Rat	15 mm sciatic		Schwann cell migration increased with porcine decellularised nerve matrix with NGF compared to conduits without NGF	Rao et al., 2021

GAG, glycosaminoglycans; MSCs, mesenchymal stem cells; NGF, nerve growth factor.

The majority of nerve guidance conduits are formed of a stiffer/stronger conduit filled with a soft hydrogel material to give greater structural integrity to the implant, and the hydrogel can be used as an acellular construct or seeded with cells prior to implantation (column 4). In vivo models of nerve repair involved the transection of a peripheral nerve, commonly sciatic (column 6), with critical gap lengths (over which no repair is possible without a graft or bridging) of around 15 mm in rats, 30 mm in rabbits and dogs and 40 mm in pigs and humans. The studies included were those that implanted conduits in vivo with an extracellular matrix luminal filler surrounded by an outer tube, and measured outcomes related to the behaviour of key cells involved in the repair process–Schwann cells, macrophages and neurons (columns 7 and 8).

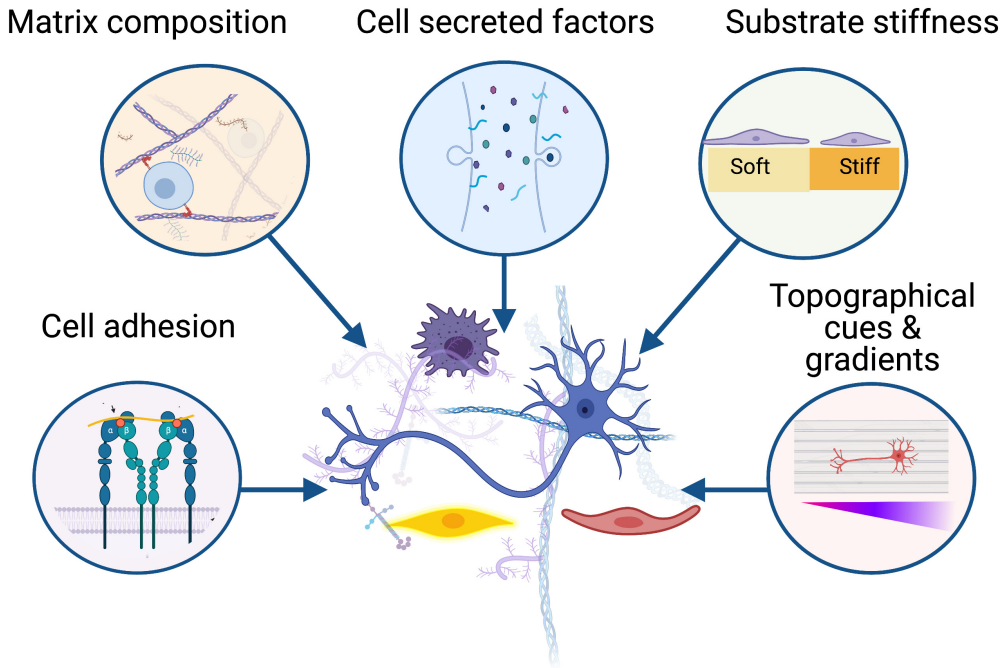

FIGURE 1 | Biomaterials influence the behaviour of key cellular players in peripheral nerve regeneration including neurons, Schwann cells, immune cells, and vasculature. Successful regeneration is dependent on the interactions between these cells and the surrounding microenvironment, from cell adhesion to substrate stiffness, growth factors, and topographical gradients. Created with BioRender.com.

Inflammatory events following peripheral nerve injury are complex (Dubový et al., 2013). Initially it is crucial macrophages phagocytose cellular and extracellular debris, however, like many other tissues, regeneration of the peripheral nerve is impaired until inflammation is resolved with the activation of the anti-inflammatory immune response (Ydens et al., 2012). Over-activation of the inflammatory response will result in the formation of fibrotic tissue at the injury site which impairs regeneration as regenerating axons and supporting Schwann cells cannot penetrate fibrotic scars (Wang et al., 2019). The differing macrophages can be characterised broadly as M1 (inflammatory) or M2 (anti-inflammatory). The employment of materials that promote the polarisation of macrophages towards the M2 phenotype is often desired but must be carefully timed to allow initial clearance of debris.

THE ADDITION OF LAMININ OR FIBRONECTIN AND CERTAIN PEPTIDES CAN IMPROVE FUNCTIONAL OUTCOMES

Laminin, fibronectin and other components have been added to collagen hydrogels to try and improve cell proliferation and the regenerative potential of the biomaterials. Schwann cells both deposit and interact with laminin (Chernousov and Carey, 2000). Schwann cell migration across the nerve bridge is also aided by the presence of laminin (Mccarthy et al., 1983; Motta et al., 2019), as well as it being a key factor affecting the ability of Schwann cells to sense and respond to mechanical properties of matrices (Urbanski et al., 2016). Mice with Schwann cells expressing disrupted laminin γ1 display impaired peripheral nerve myelination and regeneration (Chen and Strickland, 2003), suggesting the presence of laminin in the nerve bridge is important for successful regeneration. Suri and Schmidt (2010) added 100 μg/ml laminin to collagen and hyaluronic acid hydrogels and found the release of neurotrophic factors, proliferation rate and metabolic activity was increased from the encapsulated primary rat Schwann cells. This was compared with both cell-laden collagen and hyaluronic acid hydrogels containing lower concentrations of laminin, and Schwann cells encapsulated in collagen-only hydrogels (Suri and Schmidt, 2010). Although this study shows the presence of laminin has a positive effect on Schwann cell behaviour, this nerve guidance construct was not implanted and it is therefore unclear if and how this effect will translate *in vivo*.

The use of extracellular matrix peptides may be relevant for translational therapies as synthesising peptides is more reproducible than isolating natural extracellular matrix molecules. In addition, specific cell functions may be targeted by carefully choosing the peptides (Boontheekul and Mooney, 2003). In fact, the active peptides of laminin–those important for Schwann cell adhesion–have also been isolated and combined with hydrogels to try to improve the behaviour of neurons and other cell types (Hiraoka et al., 2009; Hosseinkhani et al., 2013;

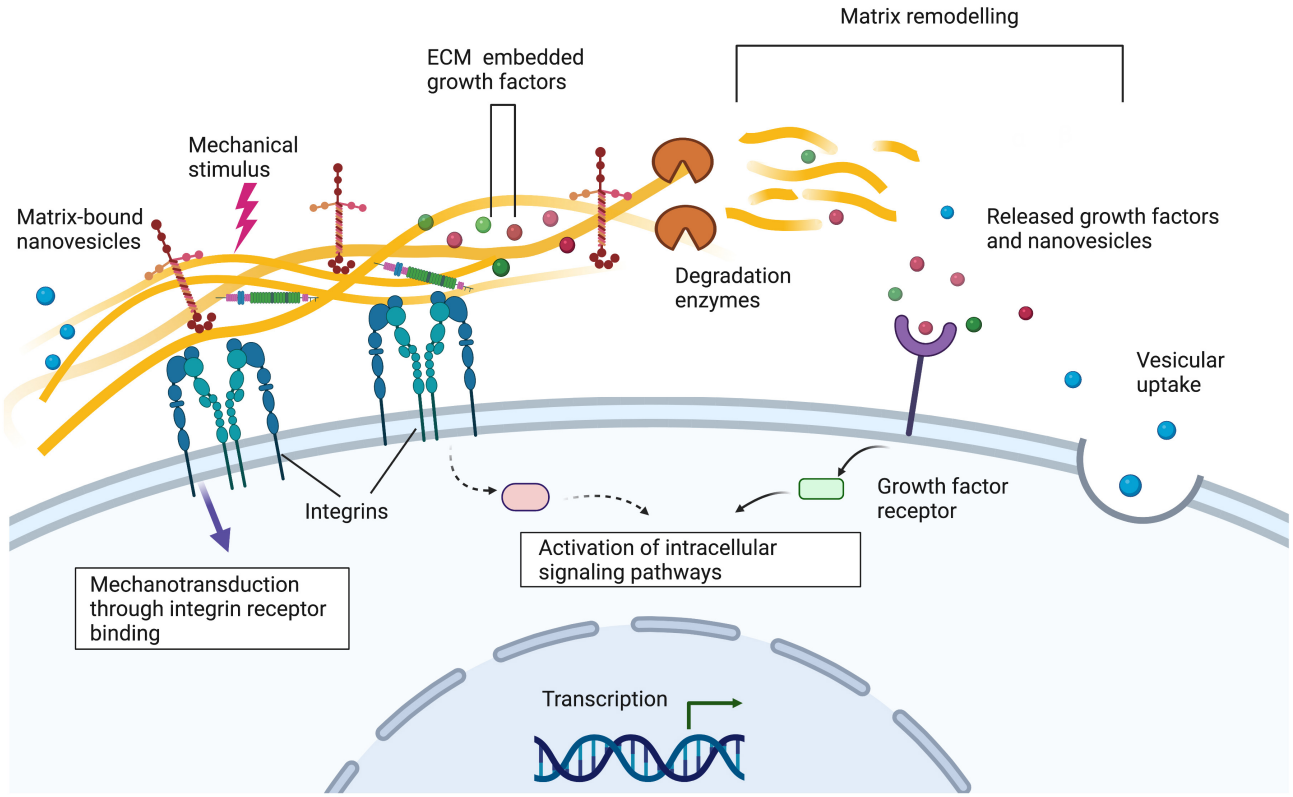

FIGURE 2 | Integrins on the cell surface bind to extracellular matrix proteins such as laminin and collagen. Alterations to the extracellular matrix via matrix remodelling, the addition of matrix-bound nanovesicles and growth factors and mechanical stimuli can alter cellular behaviour. Understanding these interactions is important when designing nerve guidance constructs for peripheral nerve tissue engineering applications. Created with Biorender.com.

Rochkind and Nevo, 2014; Motta et al., 2019). Motta et al. (2019) compared a number of these and assessed the proliferation and adhesion behaviour of Schwann cells alongside that of fibroblasts. Hosseinkhani et al. (2013) also looked at the laminin peptides IKVAV and RGD on dorsal root ganglia (DRG) proliferation and differentiation. They found collagen matrices modified with the peptides RGD, IKVAV, and RGD-IKVAV increased attachment, proliferation and increased potential to differentiate in media with acidic fibroblast growth factor (aFGF). Including IKVAV had the most significant results in all outcomes compared to RGD alone, as well as collagen modified with VVIAK and those on 2D culture. Taken together, these studies indicate the laminin peptide IKVAV has positive effects *in vitro* on both Schwann cells and neurons. Immune cells are also able to bind to and be affected by cryptic peptides in collagen such as discoidin domain receptors (DDR) 1 and 2, leukocyte-associated immunoglobulin-like receptor 1 (LAIR-1) as well as RGD, suppressing immune cell activity. Fibrin also contains P1, P2, and RGD peptides which immune cells can interact with via αMβ2 integrins (Rowley et al., 2019), with fibrin inducing both inflammatory and anti-inflammatory responses.

Using materials which encourage longer processes to form in implanted cells can also aid the growth of axons over a longer distance. Gonzalez-Perez et al. (2017) developed aligned constructs formed of laminin or fibronectin blended with collagen 1 hydrogel and contained these in a chitosan conduit. Later, this construct was seeded with Schwann cells or mesenchymal stem cells and implanted into a 15 mm sciatic nerve gap in rats (Gonzalez-Perez et al., 2018). Improved functional outcomes, such as electrophysiology, were seen with fibronectin and laminin as well as an increased number of axons and myelinated fibres when compared to collagen alone (Gonzalez-Perez et al., 2017). Schwann cells also migrated to a slightly greater degree in these blends although this was not significant compared to collagen alone (Gonzalez-Perez et al., 2017). Fibronectin and laminin seem to induce generally similar outcomes in cell behaviour, although the *in vivo* cellular constructs with fibronectin and rat Schwann cells showed a greater increase in motor neuron reinnervation compared to laminin or those containing mesenchymal stem cells. In addition, at the distal nerve end, the fibronectin and Schwann cell constructs had a significant increase in myelinated fibres (Gonzalez-Perez et al., 2018). This aligns with *in vitro* data that showed Schwann cells elongated to a greater extent on fibronectin compared to laminin (Gonzalez-Perez et al., 2017, 2018), indicating that Schwann cell elongation is associated with

positive effects on neuron growth. Stem cells have been widely used either directly in peripheral nerve guidance constructs or differentiated into Schwann cell-like cells with promising results (Ziegler et al., 2011; Martens et al., 2014; Georgiou et al., 2015; Sakaue and Sieber-Blum, 2015; Jung et al., 2016; Cai et al., 2017; Huang et al., 2017, 2020; Kim et al., 2017; Sanen et al., 2017; Jones et al., 2018; Kubiak et al., 2020). However, it is not known in these cases if these differentiated cells will behave comparably in response to different biomaterials to the Schwann cells found in a native injury environment.

Another more complex hydrogel addition to nerve guidance conduits is Matrigel, a basement membrane hydrogel containing laminin, collagen IV, heparan sulphate proteoglycans and growth factors, which is commonly used as a cell carrier and coating for neural stem cells (Rodriguez et al., 2000; Kim et al., 2007; Koutsopoulos and Zhang, 2013; Li et al., 2018; Liu et al., 2020). Including Matrigel in collagen conduits has been shown to improve regeneration compared with collagen alone, which was not improved with the addition of Schwann cells (Udina et al., 2004), as well as encouraging Schwann cell infiltration into the proximal and distal device of a hollow conduit, resulting in improved axonal regeneration in short gap repair models (Madison et al., 1985; Labrador et al., 1998). Although Matrigel supports neural cells and Schwann cell migration *in vitro* it is unclear if this translates well to *in vivo* peripheral nerve regeneration as in other studies the inclusion of Matrigel decreased axon number compared to the empty tube control or autograft (Guenard et al., 1992). The source and variability of this material mean it would also not be appropriate for clinical therapy.

As previously discussed, the M2 macrophage response is important to successful regeneration. Macrophages also express integrins which allow them to bind to the RGD peptides found in laminin and fibronectin. Binding of integrins activates macrophages and induces the release of pro-inflammatory cytokines such as Tumour Necrosis Factor-alpha (TNF-α) and Interleukin 6 (IL-6). In addition, they can respond to biomaterials too large to phagocytose by binding together to form foreign body giant cells (Anderson et al., 2008; Sheikh et al., 2015). Blocking the RGD-binding integrins on macrophages resulted in a thinner foreign body capsule, as well as reduced release of inflammatory cytokines in response to lipopolysaccharides (Zaveri et al., 2014). This study suggests the binding of macrophages to biomaterials expressing RGD peptides via integrins may result in the release of inflammatory cytokines, which could be detrimental to regeneration. This is in contrast to those studies suggesting the presence of RGD peptides are beneficial due to the interaction between neurons and Schwann cells.

In addition to protein hydrogels increasing neurotrophic factor release, metabolic activity and adherence of Schwann cells, the addition of guiding fibres from fibrillar collagen or synthetic compounds can aid cell elongation reminiscent of the repair Schwann cell phenotype. Repair Schwann cells interact with fibrin deposited in the nerve bridge after injury, and when Schwann cell proliferation was assessed in response to a two-dimensional fibrin substrate versus a fibrin hydrogel, there was found to be increased Schwann cell proliferation in two-dimensional cultures. However, the Schwann cells in fibrin hydrogels formed more complex branching which may indicate a greater potential to form Bands of Büngner-like structures despite the lower proliferation rates (Hodde et al., 2016). With polycaprolactone aligned fibres included in the hydrogel, the Schwann cells also extended long processes. Schuh et al. found a collagen-fibrin blend containing 10% fibrin and 90% collagen type I promoted Schwann cell viability compared with collagen alone. *In vitro*, there was also shown to be increased neurite viability, alignment and outgrowth of NG108 cells (a neuroblastoma cell line) on the collagen-fibrin gels. Both of these studies translated to *in vivo* experiments showing increased axonal regeneration (Hodde et al., 2016; Schuh et al., 2018), suggesting that fibrin increases the viability of Schwann cells, but additional guiding fibres such as the polycaprolactone and fibrillar collagen are required to allow longer processes to form and contribute to regenerating axonal guidance.

Alternatively, biologically complex materials may be produced via the decellularisation of animal tissues and their subsequent processing to form extracellular matrix hydrogels. When implanted *in vivo*, these materials provide site appropriate extracellular matrix components and modulate cellular behaviour, such as macrophage phenotype, to promote positive tissue remodelling (Crapo et al., 2011; Medberry et al., 2013; Saldin et al., 2017; Spang and Christman, 2018). Tissue specific effects of hydrogels derived from decellularised extracellular matrix have been observed in neural tissue repair; peripheral nerve extracellular matrix derived hydrogels were biochemically distinct from spinal cord extracellular matrix derived hydrogels and thus had specific effects on the transcriptome of neural stem cells (Xu et al., 2021). Prest et al. (2017) employed a canine peripheral nerve derived extracellular matrix hydrogel within a silicone conduit that improved Schwann cell infiltration and increased the M2:M1 macrophage population ratio when compared to an empty conduit in a critical sized defect. Moreover, decellularised extracellular matrix hydrogels may act as a growth factor reservoir, improving their efficacy *in vivo* as controlled delivery systems (Briquez et al., 2015; Martino et al., 2015a,b). For example, Rao et al. (2021) reported elevated Schwann cell migration at the proximal and distal stumps in conduits filled with porcine derived peripheral nerve extracellular matrix hydrogels when they were bound with NGF. Furthermore, synergistic effects were observed in the proliferation and migration of Schwann cells using peripheral nerve derived extracellular matrix hydrogels as a system for the codelivery of VEGF and NGF resulting in improved functional recovery (Li et al., 2020) after sciatic nerve crush.

EFFECT OF STIFFNESS ON MACROPHAGES AND SCHWANN CELLS

Recent studies examined how the local microenvironment influences human macrophage M1/M2 polarisation, with polarisation toward the M2 phenotype being induced by increasing the stiffness of the substrate (Friedemann et al., 2017). Friedemann et al. embedded human macrophages in 3D porous type I collagen hydrogels and found that the higher the rigidity of the matrix (27–100 Pa), the higher the secretion of

Interleukin-10 (IL−10) and the lower the secretion of TNF-α and Interleukin-12 (IL−12). These changes in the cytokine expression profiles are indicative of a more pro-regenerative macrophage phenotype. However, a subsequent study using 3D collagen gels with elastic moduli equivalent to 0.5–1.5 kPa did not observe any consistent differences in the macrophage response to the stiffness of the scaffolds. Instead, the authors demonstrated a clear correlation between macrophage polarisation and the cross-linking method employed to alter the mechanical properties of the scaffold (Sridharan et al., 2019). 3D matrix architecture, rather than stiffness, was also found to be the major factor directing macrophage migration through collagen hydrogels (Van Goethem et al., 2010). For instance, the fibril density of collagen hydrogels has been shown to control macrophage activation and infiltration (Sapudom et al., 2020), creating a complex picture of macrophage behaviour and hydrogel mechanical properties.

Several studies have shown that Schwann cells can develop normally on both stiff and soft hydrogels but activate different intracellular pathways in response to different substrate stiffness. Urbanski et al. (2016) found no significant differences in Schwann cell attachment or viability between soft (1.5 kPa) and rigid matrices (30 kPa), while a slight increase in proliferation was observed on the rigid substrates. This limited response may be expected as under physiological conditions, Schwann cells have to adapt to the wide range of elastic moduli that may occur in the native microenvironment. Variations in extracellular matrix elasticity were also found to induce some changes in Schwann cell morphology, albeit less significantly compared to other glial cell types. When cultured on soft substrates enriched with collagen and laminin, Schwann cells acquired a more elongated phenotype and exhibited more actin-rich processes along the membrane. On rigid matrices, Schwann cells adopted a more flat and polygonal shape. Adjusting the elasticity of hydrogels to promote elongated phenotypes that could potentially form structures mimicking Bands of Büngner may improve the support of axon regeneration by these implanted cellular hydrogels.

Mechanical stimuli have also been found to affect the expression of downstream Hippo pathway co-activators Yap and Taz in Schwann cells, which in turn induce the expression of basal lamina receptor genes. These co-activators are vital for radial sorting of axons and subsequent myelination (Poitelon et al., 2016)–important at the later stages of injury when remyelination of the regenerated axon occurs (Taveggia et al., 2010; Stratton et al., 2018). Interestingly, similar to the limited responsiveness of Schwann cells to substrate stiffness, there seems to be a threshold after which Schwann cells appear to be unaffected–they showed insignificant morphological changes and no variations in the expression of YAP/TAZ mechanotransducers from 40 kPa to 4 MPa (Poitelon et al., 2016). The presence of laminin again can greatly change Schwann cell response to mechanical stimuli as it acts as a co-factor in activating YAP/TAZ mechanotransducers (Poitelon et al., 2016).

Neurite extension is affected by both interfibre spacing and mechanical stiffness within collagen hydrogels (Willits and Skornia, 2004). DRG neurite outgrowth on three-dimensional (3D) collagen hydrogels was shown to be biphasic and increased on softer to intermediate substrates (<10 Pa). The slower neurite extension rates observed on more stiff collagen gels could be linked to the denser fibre network (Willits and Skornia, 2004). DRG co-cultures are commonly used to model the growth of neurons on top of cellular and acellular constructs, as an indicator of the regenerative potential (Bozkurt et al., 2007; Kingham et al., 2011; Stettner et al., 2013). DRG explants are also useful as a model of myelination as they contain a mixed population of neurons and glial cells (Hanani, 2005; Emery and Ernfors, 2018), with the neurons in DRGs known to regenerate their axons actively after injury (Khoshakhlagh et al., 2018). Matrix elasticity also regulated neurite outgrowth in fibrin gels (Man et al., 2011). More recently, Nichol et al. demonstrated that human motor neurons differentiated from induced pluripotent stem cells generate longer neurites and extend faster within more rigid three-dimensional collagen I hydrogels (∼5 kPa). The authors suggested that the strong adhesion of leading-edge protrusions was responsible for accelerated neurite extension, and correlated with increased activation of ras homolog gene family member A (RHOA) expression (Nichol et al., 2019). RHOA signalling could thus play an important role in controlling mechanosensitive neuronal responses in elastic environments. The results of the previous studies indicate that the regulation of human neuritogenesis by 3D environmental elasticity may differ depending on neuronal subtype. It is nevertheless important to highlight that the methods of characterising the mechanical properties of hydrogels in these studies are very diverse, which makes direct comparisons of the results more challenging.

STIFFNESS GRADIENTS AND TOPOGRAPHICAL FEATURES DIRECT NEURITE OUTGROWTH AND SCHWANN CELL ELONGATION

The presence of stiffness gradients can also affect neurite extension, cell migration, and axonal branching. Guided cell migration is a key element in neural tissue engineering, where recent efforts have focused on strategies that guide neurons and support cells across gaps resulting from peripheral nerve injury (Wrobel and Sundararaghavan, 2013). Using a microfluidic system, Sundararaghavan et al. studied the durotactic response of neurites from chick DRG explants to 3D collagen gels with tailored mechanical gradients of varied stiffness. Results indicate that the presence of gradients can enhance and orientate growth, with the length of neurites growing down the steeper gradient of $377 \pm 25 - 57 \pm 2.8$ Pa being increased, without altering cell adhesion (Sundararaghavan et al., 2009). In collagen hydrogels containing substrate gradients, Kayal et al. (2020) found the extension of neurites from NG108-15 neural cells was dependent on both the gradient and absolute stiffness of the hydrogel. This study highlights again the importance of considering both cues–gradient and stiffness–in controlling orientation of neurites.

Experimental observations have also demonstrated that topographical features such as matrix alignment could potentially

encourage nerve regeneration by manipulating and directing neurite outgrowth (Ceballos et al., 1999). For instance, the uniaxial orientation of collagen fibres in magnetically aligned collagen gel rods has been shown to increase the invasion of neurites and their preferential elongation *in vitro*, a response likely caused by contact guidance of growth cones at the neurite tips (Dubey et al., 1999). Similarly, chick DRG explants cultured on aligned freeze -dried collagen scaffolds exhibited preferential outgrowth along the length of the aligned fibres (Lowe et al., 2016). It should be noted when comparing studies using DRGs, that overall embryonic DRGs have a higher regenerative potential compared to adult ones, with embryonic chick DRGs undergoing earlier pseudo-unipolarisation compared to their rat counterparts (Matsuda et al., 1996).

Finally, Schwann cell migration can be guided by different durotactic or topological cues, a response that can be vital for nerve regeneration (Bruder et al., 2007; Evans et al., 2018). Long-term culture (after 21 days) of DRG explants on highly oriented 3D collagen scaffolds showed that migrating Schwann cells aligned within the guidance channels and self-assembled in columns that resembled Bands of Büngner (Bozkurt et al., 2009).

ADDING NEUROTROPHIC FACTORS HAS SHOWN TO BE BENEFICIAL WITHIN CERTAIN CONCENTRATION RANGES

Neurotrophic factors are released by repair Schwann cells and contribute to the creation of a pro-regenerative environment in the nerve bridge. The inclusion of these and other growth factors in hydrogels may boost neurotrophic support. Overexpression of growth factors such as glial cell line-derived neurotrophic factor (GDNF) can, however, result in axonal entrapment (Eggers et al., 2019), so any inclusion or release of neurotrophic factors must be carefully controlled in peripheral nerve repair. Allodi et al. (2011) found motor and sensory neurons increase their outgrowth if brain-derived neurotrophic factor (BDNF) or nerve growth factor (NGF) was added to collagen type I hydrogels, respectively. Although Schwann cells were included in experiments, this was only to assess if they could associate with neurons rather than directly measuring the effect of the neurotrophic factors on them (Allodi et al., 2011). NGF has also been incorporated in a fibrin and heparin hydrogel and implanted into rat sciatic nerve gaps (Lee et al., 2003). The NGF was released in a controlled manner and the number of nerve fibres increased corresponding to the NGF concentration up to 2 ng/ml, with no significant differences found between 20 and 50 ng/ml. The addition of NGF to hydrogels may especially target sensory rather than motor neuron regeneration to improve functional outcomes. *In vitro*, DRG outgrowth was impacted in a dose-dependent manner by NGF carried in collagen and hyaluronan hydrogels on a poly-L-caprolactone (PLCL) scaffold developed by Jin et al. (2013) Although this did not translate to significant effects on motor recovery *in vivo*, this study did find NGF improved sensory recovery *in vivo*. The addition of NGF has also been shown to improve regeneration over longer gaps. Yao et al. (2018) contained NGF in a longitudinally orientated collagen conduit (LOCC) which was used *in vivo* to repair a 35 mm nerve gap in dogs. Here, gastrocnemius muscle mass was significantly higher in the LOCC/NGF group than the LOCC alone group.

The effect of including growth factors such as basic fibroblast growth factor (FGF-2) in hydrogels has a positive effect on neuron growth (Sakiyama-Elbert and Hubbell, 2000; Al-Zer et al., 2015; Fujimaki et al., 2017). Indeed, although Dietzmeyer et al. (2020) saw an impairment of regeneration when Schwann cells modified to overexpress FGF-2 were present in their hyaluronic acid and laminin conduit versus the acellular conduits, it was found the inclusion of the Schwann cells had instead induced a downregulation of neurotrophic factor expression compared to that of the *in vitro* 2D culture. Sakiyama-Elbert and Hubbell (2000) additionally modelled the release of FGF-2 from fibrin hydrogels and found its inclusion would improve neurite extension as long as the immobilised heparin it was bound to was in 500-molar excess relative to the FGF-2. FGF-2 may positively impact peripheral nerve regeneration but, similar to neurotrophic factors, only if release is controlled.

CONCLUSION

Complex structural support in nerve guidance conduits has been extensively studied with the development of porous materials, and those with internal supporting and guiding structures (Konofaos and Ver Halen, 2013; Bozkurt et al., 2016; Meyer et al., 2016; Belanger et al., 2018). This review is, to our knowledge, the first to focus on how common nerve guidance constructs made with extracellular protein hydrogels alter the phenotype of cells involved in the nerve injury process (**Figure 2**). Unfortunately, there is very little in common in terms of outcome measures between studies, so it is difficult to compare results directly and any conclusions should be treated with a suitable degree of caution. Still, there is some consensus that the addition of laminin or fibronectin improves functional outcomes by increasing Schwann cell survival and release of neurotrophic factors, as well as making the cells more able to sense and respond to the surrounding mechanical properties (Suri and Schmidt, 2010; Hosseinkhani et al., 2013; Urbanski et al., 2016). There is also an indication that relatively soft gels promote a desirable macrophage response (Van Goethem et al., 2010; Sridharan et al., 2015, 2019), with Schwann cells being less sensitive to mechanical changes (Urbanski et al., 2016). In terms of neurons, it may be beneficial to create gels with a gradient of stiffness or aligned fibres to improve guidance and increase neurite extension (Ceballos et al., 1999; Dubey et al., 1999; Sundararaghavan et al., 2009). Adding neurotrophic factors has also shown to be beneficial although concentration plays a critical role in this and, like with mechanical cues, the response is dependent on neuronal subtype (Allodi et al., 2011; Jin et al., 2013; Yao et al., 2018; Nichol et al., 2019).

Understanding the behaviour of cells in response to altered biomaterials is an essential consideration when combining cells

and materials in tissue engineering efforts, and more research should be undertaken in this area. We acknowledge the focus of this review on extracellular matrix protein hydrogels–chosen due to the role of these in the innate peripheral regeneration response and common use of these materials in peripheral nerve guidance constructs–does therefore not include a host of information on cellular behaviour in response to other hydrogels such as alginate, as well as synthetic constructs. Naturally derived extracellular matrix, such as those from bone, small intestine and bladder, of course contain all the proteins mentioned here and therefore the information in this review may be found to be applicable.

AUTHOR CONTRIBUTIONS

All authors contributed equally to preparing, advising, and approving the manuscript.

FUNDING

This work is supported by Medical Research Council (MRC) MR/N013867/1 (RP), UCL Mechanical Engineering (DE), Advanced Therapeutics and Nano-medicines CDT EP/L01646X (SK) and EP/R004463/1 (JP).

REFERENCES

Allodi, I., Guzman-Lenis, M. S., Hernandez, J., Navarro, X., and Udina, E. (2011). In vitro comparison of motor and sensory neuron outgrowth in a 3D collagen matrix. *J. Neurosci. Methods* 198, 53–61. doi: 10.1016/j.jneumeth.2011.03.006

Al-Zer, H., Apel, C., Heiland, M., Friedrich, R. E., Jung, O., Kroeger, N., et al. (2015). Enrichment and schwann cell differentiation of neural crest-derived dental pulp stem cells. *In Vivo* 29, 319–326.

Anderson, J. M., Rodriguez, A., and Chang, D. T. (2008). Foreign body reaction to biomaterials. *Semin. Immunol.* 20, 86–100. doi: 10.1016/j.smim.2007.11.004

Badylak, S. F., Valentin, J. E., Ravindra, A. K., Mccabe, G. P., and Stewart-Akers, A. M. (2008). Macrophage phenotype as a determinant of biologic scaffold remodeling. *Tissue Eng. Part A* 14, 1835–1842. doi: 10.1089/ten.tea.2007.0264

Belanger, K., Schlatter, G., Hebraud, A., Marin, F., Testelin, S., Dakpe, S., et al. (2018). A multi-layered nerve guidance conduit design adapted to facilitate surgical implantation. *Health Sci. Rep.* 1:e86. doi: 10.1002/hsr2.86

Bhatnagar, D., Simon, M., and Rafailovich, M. H. (2016). *Hydrogels for Regenerative Medicine*. London: InTech.

Bonnans, C., Chou, J., and Werb, Z. (2014). Remodelling the extracellular matrix in development and disease. *Nat. Rev. Mol. Cell Biol.* 15, 786–801. doi: 10.1038/nrm3904

Boontheekul, T., and Mooney, D. J. (2003). Protein-based signaling systems in tissue engineering. *Curr. Opin. Biotechnol.* 14, 559–565. doi: 10.1016/j.copbio.2003.08.004

Bozkurt, A., Boecker, A., Tank, J., Altinova, H., Deumens, R., Dabhi, C., et al. (2016). Efficient bridging of 20 mm rat sciatic nerve lesions with a longitudinally micro-structured collagen scaffold. *Biomaterials* 75, 112–122. doi: 10.1016/j.biomaterials.2015.10.009

Bozkurt, A., Deumens, R., Beckmann, C., Olde Damink, L., Schügner, F., Heschel, I., et al. (2009). In vitro cell alignment obtained with a Schwann cell enriched microstructured nerve guide with longitudinal guidance channels. *Biomaterials* 30, 169–179. doi: 10.1016/j.biomaterials.2008.09.017

Bozkurt, A., Lassner, F., Tank, J., Beckmann, C., Wöltje, M., Smeets, R., et al. (2007). A bioartifical nerve guide using a resorbable collagen matrix. *J. Plastic Reconst. Aesthetic Surg.* 60, S4–S4.

Briquez, P. S., Hubbell, J. A., and Martino, M. M. (2015). Extracellular matrix-inspired growth factor delivery systems for skin wound healing. *Adv. Wound Care (New Rochelle)* 4, 479–489. doi: 10.1089/wound.2014.0603

Brown, R. A., and Phillips, J. B. (2007). Cell responses to biomimetic protein scaffolds used in tissue repair and engineering. *Int. Rev. Cytol.* 262, 75–150. doi: 10.1016/s0074-7696(07)62002-6

Bruder, J. M., Lee, A. P., and Hoffman-Kim, D. (2007). Biomimetic materials replicating Schwann cell topography enhance neuronal adhesion and neurite alignment in vitro. *J. Biomat. Sci. Polymer Ed.* 18, 967–982. doi: 10.1163/156856207781494412

Cai, S., Tsui, Y. P., Tam, K. W., Shea, G. K., Chang, R. S., Ao, Q., et al. (2017). Directed differentiation of human bone marrow stromal cells to fate-committed schwann cells. *Stem Cell Rep.* 9, 1097–1108. doi: 10.1016/j.stemcr.2017.08.004

Cattin, A. L., Burden, J. J., Van Emmenis, L., Mackenzie, F. E., Hoving, J. J., Garcia Calavia, N., et al. (2015). Macrophage-induced blood vessels guide schwann cell-mediated regeneration of peripheral nerves. *Cell* 162, 1127–1139. doi: 10.1016/j.cell.2015.07.021

Ceballos, D., Navarro, X., Dubey, N., Wendelschafer-Crabb, G., Kennedy, W. R., and Tranquillo, R. T. (1999). Magnetically aligned collagen gel filling a collagen nerve guide improves peripheral nerve regeneration. *Exp. Neurol.* 158, 290–300. doi: 10.1006/exnr.1999.7111

Chen, B., Chen, Q., Parkinson, D. B., and Dun, X. P. (2019). Analysis of schwann cell migration and axon regeneration following nerve injury in the sciatic nerve bridge. *Front. Mol. Neurosci.* 12:308. doi: 10.3389/fnmol.2019.00308

Chen, Z. L., and Strickland, S. (2003). Laminin gamma1 is critical for Schwann cell differentiation, axon myelination, and regeneration in the peripheral nerve. *J. Cell Biol.* 163, 889–899. doi: 10.1083/jcb.200307068

Chernousov, M. A., and Carey, D. J. (2000). Schwann cell extracellular matrix molecules and their receptors. *Histol. Histopathol.* 15, 593–601.

Crapo, P. M., Gilbert, T. W., and Badylak, D. V. M. (2011). An overview of tissue and whole organ decellularization processes. *Biomaterials* 32, 3233–3243. doi: 10.1016/j.biomaterials.2011.01.057

Deumens, R., Bozkurt, A., Meek, M. F., Marcus, M. A., Joosten, E. A., Weis, J., et al. (2010). Repairing injured peripheral nerves: Bridging the gap. *Prog. Neurobiol.* 92, 245–276. doi: 10.1016/j.pneurobio.2010.10.002

Di Summa, P., De Luca, A., Raffoul, W., Giacalone, F., and Bertolini, M. (2015). Tissue-engineered constructs for peripheral nerve repair: current research concepts and future perspectives. *Plastic Aesthetic Res.* 2, 213–213. doi: 10.4103/2347-9264.160889

Di Summa, P. G., Kingham, P. J., Campisi, C. C., Raffoul, W., and Kalbermatten, D. F. (2014). Collagen (NeuraGen®) nerve conduits and stem cells for peripheral nerve gap repair. *Neurosci. Lett.* 572, 26–31. doi: 10.1016/j.neulet.2014.04.029

Dietzmeyer, N., Huang, Z., Schüning, T., Rochkind, S., Almog, M., Nevo, Z., et al. (2020). *In Vivo and In Vitro evaluation of a novel hyaluronic acid–laminin hydrogel as luminal filler and carrier system for genetically engineered schwann cells in critical gap length tubular peripheral nerve graft in rats. Cell Trans.* 29, 096368972091009-096368972091009

Dubey, N., Letourneau, P. C., and Tranquillo, R. T. (1999). Guided neurite elongation and schwann cell invasion into magnetically aligned collagen in simulated peripheral nerve regeneration. *Exp. Neurol.* 158, 338–350. doi: 10.1006/exnr.1999.7095

Dubový, P., Jančálek, R., and Kubek, T. (2013). *Role of Inflammation and Cytokines in Peripheral Nerve Regeneration*. Cambridge, MA: Academic Press Inc, 173–206.

Eggers, R., De Winter, F., Hoyng, S. A., Hoeben, R. C., Malessy, M. J. A., Tannemaat, M. R., et al. (2019). Timed GDNF gene therapy using an immune-evasive gene switch promotes long distance axon regeneration. *Brain* 142, 295–311. doi: 10.1093/brain/awy340

Emery, E. C., and Ernfors, P. (2018). "Dorsal root ganglion neuron types and their functional specialization," in *The Oxford Handbook of the Neurobiology of Pain*, ed. J. N. Wood (Oxford: Oxford University Press).

Evans, E. B., Brady, S. W., Tripathi, A., and Hoffman-Kim, D. (2018). Schwann cell durotaxis can be guided by physiologically relevant stiffness gradients. *Biomaterials Research* 22, 14–14.

Friedemann, M., Kalbitzer, L., Franz, S., Moeller, S., Schnabelrauch, M., Simon, J. C., et al. (2017). Instructing human macrophage polarization by stiffness and glycosaminoglycan functionalization in 3D collagen networks. *Adv. Healthc. Mater.* 6:1600967. doi: 10.1002/adhm.201600967

Fujimaki, H., Uchida, K., Inoue, G., Miyagi, M., Nemoto, N., Saku, T., et al. (2017). Oriented collagen tubes combined with basic fibroblast growth factor promote peripheral nerve regeneration in a 15 mm sciatic nerve defect rat model. *J. Biomed. Mater. Res. Part A* 105, 8–14. doi: 10.1002/jbm.a.35866

Georgiou, M., Golding, J. P., Loughlin, A. J., Kingham, P. J., and Phillips, J. B. (2015). Engineered neural tissue with aligned, differentiated adipose-derived stem cells promotes peripheral nerve regeneration across a critical sized defect in rat sciatic nerve. *Biomaterials* 37, 242–251. doi: 10.1016/j.biomaterials.2014.10.009

Gomez-Sanchez, J. A., Carty, L., Iruarrizaga-Lejarreta, M., Palomo-Irigoyen, M., Varela-Rey, M., Griffith, M., et al. (2015). Schwann cell autophagy, myelinophagy, initiates myelin clearance from injured nerves. *J. Cell Biol.* 210, 153–168. doi: 10.1083/jcb.201503019

Gonzalez-Perez, F., Cobianchi, S., Heimann, C., Phillips, J. B., Udina, E., and Navarro, X. (2017). Stabilization, rolling, and addition of other extracellular matrix proteins to collagen hydrogels improve regeneration in chitosan guides for long peripheral nerve gaps in rats. *Neurosurgery* 80, 465–474. doi: 10.1093/neuros/nyw068

Gonzalez-Perez, F., Hernández, J., Heimann, C., Phillips, J. B., Udina, E., and Navarro, X. (2018). Schwann cells and mesenchymal stem cells in laminin- or fibronectin-aligned matrices and regeneration across a critical size defect of 15 mm in the rat sciatic nerve. *J. Neurosurg. Spine* 28, 109–118. doi: 10.3171/2017.5.spine161100

Gregory, H., and Phillips, J. B. (2021). Materials for peripheral nerve repair constructs: natural proteins or synthetic polymers? *Neurochem. Int.* 143:104953. doi: 10.1016/j.neuint.2020.104953

Guenard, V., Kleitman, N., Morrissey, T. K., Bunge, R. P., and Aebischer, P. (1992). Syngeneic Schwann cells derived from adult nerves seeded in semipermeable guidance channels enhance peripheral nerve regeneration. *J. Neurosci.* 12, 3310–3320. doi: 10.1523/jneurosci.12-09-03310.1992

Hanani, M. (2005). Satellite glial cells in sensory ganglia: from form to function. *Brain Res. Brain Res. Rev.* 48, 457–476. doi: 10.1016/j.brainresrev.2004.09.001

Hiraoka, M., Kato, K., Nakaji-Hirabayashi, T., and Iwata, H. (2009). Enhanced survival of neural cells embedded in hydrogels composed of collagen and laminin-derived cell adhesive peptide. *Bioconjug. Chem.* 20, 976–983. doi: 10.1021/bc9000068

Hodde, D., Gerardo-Nava, J., Wohlk, V., Weinandy, S., Jockenhovel, S., Kriebel, A., et al. (2016). Characterisation of cell-substrate interactions between Schwann cells and three-dimensional fibrin hydrogels containing orientated nanofibre topographical cues. *Eur. J. Neurosci.* 43, 376–387. doi: 10.1111/ejn.13026

Hosseinkhani, H., Hiraoka, Y., Li, C. H., Chen, Y. R., Yu, D. S., Hong, P. D., et al. (2013). Engineering three-dimensional collagen-IKVAV matrix to mimic neural microenvironment. *ACS Chem. Neurosci.* 4, 1229–1235. doi: 10.1021/cn400075h

Huang, C. W., Huang, W. C., Qiu, X., Fernandes Ferreira Da Silva, F., Wang, A., Patel, S., et al. (2017). The differentiation stage of transplanted stem cells modulates nerve regeneration. *Sci. Rep.* 7:17401.

Huang, Z., Powell, R., Phillips, J. B., and Haastert-Talini, K. (2020). Perspective on schwann cells derived from induced pluripotent stem cells in peripheral nerve tissue engineering. *Cells* 9:2497. doi: 10.3390/cells9112497

Jessen, K. R., and Arthur-Farraj, P. (2019). Repair Schwann cell update: adaptive reprogramming, EMT, and stemness in regenerating nerves. *Glia* 67, 421–437. doi: 10.1002/glia.23532

Jessen, K. R., and Mirsky, R. (2016). The repair Schwann cell and its function in regenerating nerves. *J. Physiol.* 594, 3521–3531. doi: 10.1113/jp270874

Jessen, K. R., and Mirsky, R. (2019). Schwann cell precursors; multipotent glial cells in embryonic nerves. *Front. Mol. Neurosci.* 12:69. doi: 10.3389/fnmol.2019.00069

Jessen, K. R., Mirsky, R., and Lloyd, A. C. (2015). Schwann cells: development and role in nerve repair. *Cold Spring Harb. Perspect. Biol.* 7:a020487. doi: 10.1101/cshperspect.a020487

Jin, J., Limburg, S., Joshi, S. K., Landman, R., Park, M., Zhang, Q., et al. (2013). Peripheral nerve repair in rats using composite hydrogel-filled aligned nanofiber conduits with incorporated nerve growth factor. *Tissue Eng. Part A* 19, 2138–2146. doi: 10.1089/ten.tea.2012.0575

Jones, I., Novikova, L. N., Novikov, L. N., Renardy, M., Ullrich, A., Wiberg, M., et al. (2018). Regenerative effects of human embryonic stem cell-derived neural crest cells for treatment of peripheral nerve injury. *J. Tissue Eng. Regen. Med.* 12, e2099–e2109.

Jung, N., Park, S., Choi, Y., Park, J.-W., Hong, Y., Park, H., et al. (2016). Tonsil-derived mesenchymal stem cells differentiate into a schwann cell phenotype and promote peripheral nerve regeneration. *Int. J. Mol. Sci.* 17, 1867–1867. doi: 10.3390/ijms17111867

Kayal, C., Moeendarbary, E., Shipley, R. J., and Phillips, J. B. (2020). Mechanical response of neural cells to physiologically relevant stiffness gradients. *Adv. Healthcare Mater.* 9:1901036. doi: 10.1002/adhm.201901036

Khoshakhlagh, P., Sivakumar, A., Pace, L. A., Sazer, D. W., and Moore, M. J. (2018). Methods for fabrication and evaluation of a 3D microengineered model of myelinated peripheral nerve. *J. Neural Eng.* 15:064001. doi: 10.1088/1741-2552/aae129

Kim, H. S., Lee, J., Lee, D. Y., Kim, Y. D., Kim, J. Y., Lim, H. J., et al. (2017). Schwann cell precursors from human pluripotent stem cells as a potential therapeutic target for myelin repair. *Stem Cell Rep.* 8, 1714–1726. doi: 10.1016/j.stemcr.2017.04.011

Kim, S. M., Lee, S. K., and Lee, J. H. (2007). Peripheral nerve regeneration using a three dimensionally cultured schwann cell conduit. *J. Craniofac. Surg.* 18, 475–488. doi: 10.1097/01.scs.0000249362.41170.f3

Kingham, P. J., Mantovani, C., and Terenghi, G. (2011). "Stem cell and neuron co-cultures for the study of nerve regeneration," in *3D Cell Culture: Methods and Protocols*, ed. J. W. Haycock (Totowa, NJ: Humana Press), 115–127. doi: 10.1007/978-1-60761-984-0_8

Konofaos, P., and Ver Halen, J. P. (2013). Nerve repair by means of tubulization: past, present, future. *J. Reconstr. Microsurg.* 29, 149–164. doi: 10.1055/s-0032-1333316

Koutsopoulos, S., and Zhang, S. G. (2013). Long-term three-dimensional neural tissue cultures in functionalized self-assembling peptide hydrogels, Matrigel and Collagen I. *Acta Biomaterialia* 9, 5162–5169. doi: 10.1016/j.actbio.2012.09.010

Krock, B. L., Skuli, N., and Simon, M. C. (2011). Hypoxia-induced angiogenesis: good and evil. *Genes Cancer* 2, 1117–1133. doi: 10.1177/1947601911423654

Kubiak, C. A., Grochmal, J., Kung, T. A., Cederna, P. S., Midha, R., and Kemp, S. W. P. (2020). Stem-cell-based therapies to enhance peripheral nerve regeneration. *Muscle Nerve* 61, 449–459. doi: 10.1002/mus.26760

Labrador, R. O., Buti, M., and Navarro, X. (1998). Influence of collagen and laminin gels concentration on nerve regeneration after resection and tube repair. *Exp Neurol* 149, 243–252. doi: 10.1006/exnr.1997.6650

Lacko, C. S., Singh, I., Wall, M. A., Garcia, A. R., Porvasnik, S. L., Rinaldi, C., et al. (2020). Magnetic particle templating of hydrogels: engineering naturally derived hydrogel scaffolds with 3D aligned microarchitecture for nerve repair. *J. Neural Eng.* 17:016057. doi: 10.1088/1741-2552/ab4a22

Lee, A. C., Yu, V. M., Lowe, J. B., Brenner, M. J., Hunter, D. A., Mackinnon, S. E., et al. (2003). Controlled release of nerve growth factor enhances sciatic nerve regeneration. *Exp. Neurol.* 184, 295–303. doi: 10.1016/s0014-4886(03)00258-9

Lee, J. Y., Giusti, G., Friedrich, P. F., Archibald, S. J., Kemnitzer, J. E., Patel, J., et al. (2012). The effect of collagen nerve conduits filled with collagen-glycosaminoglycan matrix on peripheral motor nerve regeneration in a rat model. *J. Bone Joint Surg. Am.* 94, 2084–2091. doi: 10.2106/jbjs.k.00658

Lee, S. K., and Wolfe, S. W. (2000). Peripheral nerve injury and repair. *JAAOS J. Am. Acad. Orthopaedic Surg.* 8, 243–252.

Li, B., Qiu, T., Iyer, K. S., Yan, Q., Yin, Y., Xie, L., et al. (2015). PRGD/PDLLA conduit potentiates rat sciatic nerve regeneration and the underlying molecular mechanism. *Biomaterials* 55, 44–53. doi: 10.1016/j.biomaterials.2015.03.028

Li, H., Ye, A. Q., and Su, M. (2018). Application of stem cells and advanced materials in nerve tissue regeneration. *Stem Cells Int.* 2018:4243102.

Li, R., Xu, J., Rao, Z., Deng, R., Xu, Y., Qiu, S., et al. (2020). Facilitate angiogenesis and neurogenesis by growth factors integrated decellularized matrix hydrogel. *Tissue Eng. Part A* doi: 10.1089/ten.TEA.2020.0227 [Epup ahead of print],

Lindborg, J. A., Mack, M., and Zigmond, R. E. (2017). Neutrophils are critical for myelin removal in a peripheral nerve injury model of wallerian degeneration. *J. Neurosci.* 37, 10258–10277. doi: 10.1523/jneurosci.2085-17.2017

Liu, D., Pavathuparambil Abdul Manaph, N., Al-Hawwas, M., Bobrovskaya, L., Xiong, L. L., and Zhou, X. F. (2020). Coating materials for neural stem/progenitor cell culture and differentiation. *Stem Cells Dev.* 29, 463–474. doi: 10.1089/scd.2019.0288

Lowe, C. J., Reucroft, I. M., Grota, M. C., and Shreiber, D. I. (2016). Production of highly aligned collagen scaffolds by freeze-drying of self-assembled, fibrillar collagen gels. *ACS Biomater. Sci. Eng.* 2, 643–651. doi: 10.1021/acsbiomaterials.6b00036

Madison, R., Da Silva, C. F., Dikkes, P., Chiu, T. H., and Sidman, R. L. (1985). Increased rate of peripheral nerve regeneration using bioresorbable nerve guides and a laminin-containing gel. *Exp. Neurol.* 88, 767–772. doi: 10.1016/0014-4886(85)90087-1

Man, A. J., Davis, H. E., Itoh, A., Leach, J. K., and Bannerman, P. (2011). Neurite outgrowth in fibrin gels is regulated by substrate stiffness. *Tissue Eng. Part A* 17, 2931–2942. doi: 10.1089/ten.tea.2011.0030

Martens, W., Sanen, K., Georgiou, M., Struys, T., Bronckaers, A., Ameloot, M., et al. (2014). Human dental pulp stem cells can differentiate into Schwann cells and promote and guide neurite outgrowth in an aligned tissue-engineered collagen construct *in vitro*. *Faseb J.* 28, 1634–1643. doi: 10.1096/fj.13-243980

Martino, M. M., Briquez, P. S., Maruyama, K., and Hubbell, J. A. (2015a). Extracellular matrix-inspired growth factor delivery systems for bone regeneration. *Adv. Drug Deliv. Rev.* 94, 41–52. doi: 10.1016/j.addr.2015.04.007

Martino, M. M., Brkic, S., Bovo, E., Burger, M., Schaefer, D. J., Wolff, T., et al. (2015b). Extracellular matrix and growth factor engineering for controlled angiogenesis in regenerative medicine. *Front. Bioeng. Biotechnol.* 3:45. doi: 10.3389/fbioe.2015.00045

Matsuda, S., Baluk, P., Shimizu, D., and Fujiwara, T. (1996). Dorsal root ganglion neuron development in chick and rat. *Anat Embryol. (Berl).* 193, 475–480.

Mccarthy, J. B., Palm, S. L., and Furcht, L. T. (1983). Migration by haptotaxis of a schwann-cell tumor line to the basement-membrane glycoprotein laminin. *J. Cell Biol.* 97, 772–777. doi: 10.1083/jcb.97.3.772

Medberry, C. J., Crapo, P. M., Siu, B. F., Carruthers, C. A., Wolf, M. T., Nagarkar, S. P., et al. (2013). Hydrogels derived from central nervous system extracellular matrix. *Biomaterials* 34, 1033–1040. doi: 10.1016/j.biomaterials.2012.10.062

Meyer, C., Stenberg, L., Gonzalez-Perez, F., Wrobel, S., Ronchi, G., Udina, E., et al. (2016). Chitosan-film enhanced chitosan nerve guides for long-distance regeneration of peripheral nerves. *Biomaterials* 76, 33–51. doi: 10.1016/j.biomaterials.2015.10.040

Mobasseri, A., Faroni, A., Minogue, B. M., Downes, S., Terenghi, G., and Reid, A. J. (2015). Polymer scaffolds with preferential parallel grooves enhance nerve regeneration. *Tissue Eng. Part A* 21, 1152–1162. doi: 10.1089/ten.tea.2014.0266

Motta, C. M. M., Endres, K. J., Wesdemiotis, C., Willits, R. K., and Becker, M. L. (2019). Enhancing Schwann cell migration using concentration gradients of laminin-derived peptides. *Biomaterials* 218:119335. doi: 10.1016/j.biomaterials.2019.119335

Muangsanit, P., Day, A., Dimiou, S., Atac, A. F., Kayal, C., Park, H., et al. (2020). Rapidly formed stable and aligned dense collagen gels seeded with Schwann cells support peripheral nerve regeneration. *J. Neural Eng.* 17, 46036–46036.

Muheremu, A., and Ao, Q. (2015). Past, present, and future of nerve conduits in the treatment of peripheral nerve injury. *Biomed. Res. Int.* 2015:237507.

Nichol, R. H., Catlett, T. S., Onesto, M. M., Hollender, D., and Gomez, T. M. (2019). Environmental elasticity regulates cell-type specific RHOA signaling and neuritogenesis of human neurons. *Stem Cell Rep.* 13, 1006–1021. doi: 10.1016/j.stemcr.2019.10.008

Nicolas, J., Magli, S., Rabbachin, L., Sampaolesi, S., Nicotra, F., and Russo, L. (2020). 3D extracellular matrix mimics: fundamental concepts and role of materials chemistry to influence stem cell fate. *Biomacromolecules* 21, 1968–1994. doi: 10.1021/acs.biomac.0c00045

O'Rourke, C., Drake, R.a.L, Cameron, G. W. W., Loughlin, A. J., and Phillips, J. B. (2015). Optimising contraction and alignment of cellular collagen hydrogels to achieve reliable and consistent engineered anisotropic tissue. *J. Biomater. Appl.* 30, 599–607. doi: 10.1177/0885328215597818

Pan, D., Mackinnon, S. E., and Wood, M. D. (2020). Advances in the repair of segmental nerve injuries and trends in reconstruction. *Muscle Nerve* 61, 726–739. doi: 10.1002/mus.26797

Poitelon, Y., Lopez-Anido, C., Catignas, K., Berti, C., Palmisano, M., Williamson, C., et al. (2016). YAP and TAZ control peripheral myelination and the expression of laminin receptors in Schwann cells. *Nat. Neurosci.* 19, 879–887. doi: 10.1038/nn.4316

Prest, T. A., Yeager, E., Lopresti, S. T., Zygelyte, E., Martin, M. J., Dong, L., et al. (2017). Nerve-specific, xenogeneic extracellular matrix hydrogel promotes recovery following peripheral nerve injury. *J. Biomed. Mater. Res. Part A* 106, 450–459. doi: 10.1002/jbm.a.36235

Rao, Z., Lin, T., Qiu, S., Zhou, J., Liu, S., Chen, S., et al. (2021). Decellularized nerve matrix hydrogel scaffolds with longitudinally oriented and size-tunable microchannels for peripheral nerve regeneration. *Mater. Sci. Eng. C Mater. Biol. Appl.* 120:111791. doi: 10.1016/j.msec.2020.111791

Roberts, S. L., Dun, X. P., Doddrell, R. D. S., Mindos, T., Drake, L. K., Onaitis, M. W., et al. (2017). Sox2 expression in Schwann cells inhibits myelination in vivo and induces influx of macrophages to the nerve. *Development* 144, 3114–3125. doi: 10.1242/dev.150656

Rochkind, S., and Nevo, Z. (2014). Recovery of peripheral nerve with massive loss defect by tissue engineered guiding regenerative gel. *Biomed. Res. Int.* 2014:327578.

Rodriguez, F. J., Verdu, E., Ceballos, D., and Navarro, X. (2000). Nerve guides seeded with autologous schwann cells improve nerve regeneration. *Exp. Neurol.* 161, 571–584. doi: 10.1006/exnr.1999.7315

Rowley, A. T., Nagalla, R. R., Wang, S. W., and Liu, W. F. (2019). Extracellular matrix-based strategies for immunomodulatory biomaterials engineering. *Adv. Healthcare Mater.* 8:1801578. doi: 10.1002/adhm.201801578

Sakaue, M., and Sieber-Blum, M. (2015). Human epidermal neural crest stem cells as a source of Schwann cells. *Development* 142, 3188–3197. doi: 10.1242/dev.123034

Sakiyama-Elbert, S. E., and Hubbell, J. A. (2000). Development of fibrin derivatives for controlled release of heparin-binding growth factors. *J. Control Release* 65, 389–402. doi: 10.1016/s0168-3659(99)00221-7

Saldin, L. T., Cramer, M. C., Velankar, S. S., White, L. J., and Badylak, S. F. (2017). Extracellular matrix hydrogels from decellularized tissues: Structure and function. *Acta Biomaterialia* 49, 1–15. doi: 10.1016/j.actbio.2016.11.068

Sanen, K., Martens, W., Georgiou, M., Ameloot, M., Lambrichts, I., and Phillips, J. (2017). Engineered neural tissue with Schwann cell differentiated human dental pulp stem cells: potential for peripheral nerve repair? *J. Tissue Eng. Regen. Med.* 11, 3362–3372. doi: 10.1002/term.2249

Sapudom, J., Mohamed, W. K. E., Garcia-Sabate, A., Alatoom, A., Karaman, S., Mahtani, N., et al. (2020). Collagen fibril density modulates macrophage activation and cellular functions during tissue repair. *Bioengineering (Basel)* 7:33. doi: 10.3390/bioengineering7020033

Schuh, C., Day, A. G. E., Redl, H., and Phillips, J. (2018). An optimized collagen-fibrin blend engineered neural tissue promotes peripheral nerve repair. *Tissue Eng. Part A* 24, 1332–1340. doi: 10.1089/ten.tea.2017.0457

Shahriari, D., Shibayama, M., Lynam, D. A., Wolf, K. J., Kubota, G., Koffler, J. Y., et al. (2017). Peripheral nerve growth within a hydrogel microchannel scaffold supported by a kink-resistant conduit. *J. Biomed. Mater. Res. A* 105, 3392–3399. doi: 10.1002/jbm.a.36186

Sheikh, Z., Brooks, P., Barzilay, O., Fine, N., and Glogauer, M. (2015). Macrophages, foreign body giant cells and their response to implantable biomaterials. *Materials* 8, 5671–5701. doi: 10.3390/ma8095269

Smith, G. V., and Stevenson, J. A. (1988). Peripheral nerve grafts lacking viable Schwann cells fail to support central nervous system axonal regeneration. *Exp. Brain Res.* 69, 299–306.

Spang, M. T., and Christman, K. L. (2018). Extracellular matrix hydrogel therapies: *In vivo* applications and development. *Acta Biomaterialia* 68, 1–14. doi: 10.1016/j.actbio.2017.12.019

Sridharan, R., Cameron, A. R., Kelly, D. J., Kearney, C. J., and O'brien, F. J. (2015). *Biomaterial Based Modulation of Macrophage Polarization: A Review and Suggested Design Principles*. Amsterdam: Elsevier.

Sridharan, R., Ryan, E. J., Kearney, C. J., Kelly, D. J., and O'brien, F. J. (2019). Macrophage polarization in response to collagen scaffold stiffness is dependent on cross-linking agent used to modulate the stiffness. *Acs Biomater. Sci. Eng.* 5, 544–552. doi: 10.1021/acsbiomaterials.8b00910

Stettner, M., Wolffram, K., Mausberg, A. K., Wolf, C., Heikaus, S., Derksen, A., et al. (2013). A reliable *in vitro* model for studying peripheral nerve myelination in mouse. *J. Neurosci. Methods* 214, 69–79. doi: 10.1016/j.jneumeth.2013.01.009

Stratton, J. A., Holmes, A., Rosin, N. L., Sinha, S., Vohra, M., Burma, N. E., et al. (2018). Macrophages regulate schwann cell maturation after nerve injury. *Cell Rep.* 24, 2561–2572 e6.

Sundararaghavan, H. G., Monteiro, G. A., Firestein, B. L., and Shreiber, D. I. (2009). Neurite growth in 3D collagen gels with gradients of mechanical properties. *Biotechnol. Bioeng.* 102, 632–643. doi: 10.1002/bit.22074

Suri, S., and Schmidt, C. E. (2010). Cell-laden hydrogel constructs of hyaluronic acid, collagen, and laminin for neural tissue engineering. *Tissue Eng. Part A* 16, 1703–1716. doi: 10.1089/ten.tea.2009.0381

Taveggia, C., Feltri, M. L., and Wrabetz, L. (2010). Signals to promote myelin formation and repair. *Nat. Rev. Neurol.* 6, 276–287.

Udina, E., Rodriguez, F. J., Verdu, E., Espejo, M., Gold, B. G., and Navarro, X. (2004). FK506 enhances regeneration of axons across long peripheral nerve gaps repaired with collagen guides seeded with allogeneic Schwann cells. *Glia* 47, 120–129. doi: 10.1002/glia.20025

Urbanski, M. M., Kingsbury, L., Moussouros, D., Kassim, I., Mehjabeen, S., Paknejad, N., et al. (2016). Myelinating glia differentiation is regulated by extracellular matrix elasticity. *Sci. Rep.* 6:33751.

Van Goethem, E., Poincloux, R., Gauffre, F., Maridonneau-Parini, I., and Le Cabec, V. (2010). Matrix architecture dictates three-dimensional migration modes of human macrophages: differential involvement of proteases and podosome-like structures. *J. Immunol.* 184, 1049–1061. doi: 10.4049/jimmunol.0902223

Wang, M. L., Rivlin, M., Graham, J. G., and Beredjiklian, P. K. (2019). Peripheral nerve injury, scarring, and recovery. *Connect Tissue Res.* 60, 3–9. doi: 10.1080/03008207.2018.1489381

Willits, R. K., and Skornia, S. L. (2004). Effect of collagen gel stiffness on neurite extension. *J. Biomater. Sci. Polym. Ed.* 15, 1521–1531. doi: 10.1163/1568562042459698

Wojtkiewicz, D. M., Saunders, J., Domeshek, L., Novak, C. B., Kaskutas, V., and Mackinnon, S. E. (2015). Social impact of peripheral nerve injuries. *Hand (N Y)* 10, 161–167.

Wrobel, M. R., and Sundararaghavan, H. G. (2013). Directed migration in neural tissue engineering. *Tissue Eng. Part B Rev.* 20, 93–105. doi: 10.1089/ten.teb.2013.0233

Xu, Y., Zhou, J., Liu, C., Zhang, S., Gao, F., Guo, W., et al. (2021). Understanding the role of tissue-specific decellularized spinal cord matrix hydrogel for neural stem/progenitor cell microenvironment reconstruction and spinal cord injury. *Biomaterials* 268:120596. doi: 10.1016/j.biomaterials.2020.120596

Yao, Y., Cui, Y., Zhao, Y., Xiao, Z., Li, X., Han, S., et al. (2018). Effect of longitudinally oriented collagen conduit combined with nerve growth factor on nerve regeneration after dog sciatic nerve injury. *J. Biomed. Mater. Res. B Appl. Biomater.* 106, 2131–2139. doi: 10.1002/jbm.b.34020

Ydens, E., Cauwels, A., Asselbergh, B., Goethals, S., Peeraer, L., Lornet, G., et al. (2012). Acute injury in the peripheral nervous system triggers an alternative macrophage response. *J. Neuroinflammation* 9:176.

Zaveri, T. D., Lewis, J. S., Dolgova, N. V., Clare-Salzler, M. J., and Keselowsky, B. G. (2014). Integrin-directed modulation of macrophage responses to biomaterials. *Biomaterials* 35, 3504–3515. doi: 10.1016/j.biomaterials.2014.01.007

Zhang, B. G. X., Quigley, A. F., Myers, D. E., Wallace, G. G., Kapsa, R. M. I., and Choong, P. F. M. (2014). Recent advances in nerve tissue engineering. *Int. J. Artif. Organs.* 37, 277–291.

Zhang, H., Wei, Y., Tsang, K., Sun, C., Li, J., Huang, H., et al. (2008). Implantation of neural stem cells embedded in hyaluronic acid and collagen composite conduit promotes regeneration in a rabbit facial nerve injury model. *J. Transl. Med.* 6:67. doi: 10.1186/1479-5876-6-67

Ziegler, L., Grigoryan, S., Yang, I. H., Thakor, N. V., and Goldstein, R. S. (2011). Efficient generation of schwann cells from human embryonic stem cell-derived neurospheres. *Stem Cell Rev. Rep.* 7, 394–403. doi: 10.1007/s12015-010-9198-2

Zigmond, R. E., and Echevarria, F. D. (2019). Macrophage biology in the peripheral nervous system after injury. *Prog. Neurobiol.* 173, 102–121. doi: 10.1016/j.pneurobio.2018.12.001

Conflict of Interest: The reviewer KH-T declared a past collaboration with several of the authors (RP and JP) to the handling editor.

The remaining authors declare that the research was conducted in the absence of any commercial or financial relationships that could be construed as a potential conflict of interest.

frontiers in Bioengineering and Biotechnology

REVIEW
published: 24 June 2021
doi: 10.3389/fbioe.2021.695850

Insulin-Like Growth Factor-1: A Promising Therapeutic Target for Peripheral Nerve Injury

*Benjamin R. Slavin[1,2], Karim A. Sarhane[1], Nicholas von Guionneau[1], Phillip J. Hanwright[1], Chenhu Qiu[3,4], Hai-Quan Mao[3,4,5,6], Ahmet Höke[7,8] and Sami H. Tuffaha[1]**

[1] Department of Plastic and Reconstructive Surgery, School of Medicine, Johns Hopkins University, Baltimore, MD, United States, [2] Division of Plastic and Reconstructive Surgery, University of Miami Miller School of Medicine, Miami, FL, United States, [3] Department of Materials Science and Engineering, Whiting School of Engineering, Johns Hopkins University, Baltimore, MD, United States, [4] Institute for Nanobiotechnology, Johns Hopkins University, Baltimore, MD, United States, [5] Department of Biomedical Engineering, School of Medicine, Johns Hopkins University, Baltimore, MD, United States, [6] Translational Tissue Engineering Center, School of Medicine, Johns Hopkins University, Baltimore, MD, United States, [7] Department of Neurology, School of Medicine, Johns Hopkins University, Baltimore, MD, United States, [8] Department of Neuroscience, School of Medicine, Johns Hopkins University, Baltimore, MD, United States

OPEN ACCESS

Edited by:
Xavier Navarro, Universitat Autònoma de Barcelona, Spain

Reviewed by:
Haim Werner, Tel Aviv University, Israel
Kirsten Haastert-Talini, Hannover Medical School, Germany
Matthew Wood, Washington University in St. Louis, United States

***Correspondence:**
Sami H. Tuffaha
stuffah1@jhmi.edu

Specialty section:
This article was submitted to Tissue Engineering and Regenerative Medicine, a section of the journal Frontiers in Bioengineering and Biotechnology

Received: *15 April 2021*
Accepted: *02 June 2021*
Published: *24 June 2021*

Citation:
Slavin BR, Sarhane KA, von Guionneau N, Hanwright PJ, Qiu C, Mao H-Q, Höke A and Tuffaha SH (2021) Insulin-Like Growth Factor-1: A Promising Therapeutic Target for Peripheral Nerve Injury. Front. Bioeng. Biotechnol. 9:695850. doi: 10.3389/fbioe.2021.695850

Patients who sustain peripheral nerve injuries (PNIs) are often left with debilitating sensory and motor loss. Presently, there is a lack of clinically available therapeutics that can be given as an adjunct to surgical repair to enhance the regenerative process. Insulin-like growth factor-1 (IGF-1) represents a promising therapeutic target to meet this need, given its well-described trophic and anti-apoptotic effects on neurons, Schwann cells (SCs), and myocytes. Here, we review the literature regarding the therapeutic potential of IGF-1 in PNI. We appraised the literature for the various approaches of IGF-1 administration with the aim of identifying which are the most promising in offering a pathway toward clinical application. We also sought to determine the optimal reported dosage ranges for the various delivery approaches that have been investigated.

Keywords: IGF-1, PNI, peripheral nerve injury, nerve regeneration, somatomedin C, nanoparticle carrier

INTRODUCTION

Peripheral nerve injuries (PNIs) affect approximately 67 800 people annually in the United States alone (Wujek and Lasek, 1983; Noble et al., 1998; Taylor et al., 2008). Despite optimal management, many patients experience lasting motor and sensory deficits, the majority of whom are unable to return to work within 1 year of the injury (Wujek and Lasek, 1983). The lack of clinically available therapeutic options to enhance nerve regeneration and functional recovery remains a major challenge.

The amount of time that elapses between initial nerve injury and end-organ reinnervation has consistently been shown to be the most important predictor of functional recovery following PNI (Scheib and Hoke, 2013), with proximal injuries and delayed repairs resulting in worse outcomes (Carlson et al., 1996; Tuffaha et al., 2016b). This is primarily due to denervation-induced atrophy of muscle and Schwann cells (SCs) (Fu and Gordon, 1995). Following surgical repair, axons often must regenerate over long distances at a relatively slow rate of 1–3 mm/day to reach and reinnervate distal motor endplates. Throughout this process, denervated muscle undergoes irreversible loss of myofibrils and loss of neuromuscular junctions (NMJs), thereby resulting in progressive and permanent muscle atrophy. It is well known that the degree of muscle atrophy

increases with the duration of denervation (Ishii et al., 1994). Chronically denervated SCs within the distal nerve are also subject to time-dependent senescence. Following injury, proliferating SCs initially maintain the basal lamina tubes through which regenerating axons travel. SCs also secrete numerous neurotrophic factors that stimulate and guide axonal regeneration. However, as time elapses without axonal interaction, SCs gradually lose the capacity to perform these important functions, and the distal regenerative pathway becomes inhospitable to recovering axons (Ishii et al., 1993; Glazner and Ishii, 1995; Grinsell and Keating, 2014).

Research efforts to improve PNI outcomes have primarily focused on isolated processes, including the acceleration of intrinsic axonal outgrowth and maintenance of the distal regenerative environment. In order to maximize functional recovery, a multifaceted therapeutic approach that both limits the damaging effects of denervation atrophy on muscle and SCs and accelerates axonal regeneration is needed.

A number of promising potential therapies have been under investigation for PNI. Many such experimental therapies are growth factors including glial cell line-derived neurotrophic factor (GDNF), fibroblast growth factor (FGF), and brain-derived neurotrophic growth factor (Fex Svenningsen and Kanje, 1996; Lee et al., 2007; Gordon, 2009). Tacrolimus (FK506), delivered either systemically or locally, has also shown promise in a number of studies (Konofaos and Terzis, 2013; Davis et al., 2019; Tajdaran et al., 2019).

Insulin-like growth factor-1 (IGF-1) is a particularly promising candidate for clinical translation because it has the potential to address the need for improved nerve regeneration while simultaneously acting on denervated muscle to limit denervation-induced atrophy. However, like other growth factors, IGF-1 has a short half-life of 5 min, relatively low molecular weight (7.6 kDa), and high water-solubility: all of which present significant obstacles to therapeutic delivery in a clinically practical fashion (Gold et al., 1995; Lee et al., 2003; Wood et al., 2009). Here, we present a comprehensive review of the literature describing the trophic effects of IGF-1 on neurons, myocytes, and SCs. We then critically evaluate the various therapeutic modalities used to upregulate endogenous IGF-1 or deliver exogenous IGF-1 in translational models of PNI, with a special emphasis on emerging bioengineered drug delivery systems. Lastly, we analyze the optimal dosage ranges identified for each mechanism of IGF-1 with the goal of further elucidating a model for future clinical translation.

METHODS

We comprehensively reviewed the literature for original studies examining the efficacy of IGF-1 in treating PNI. We queried the PubMed and Embase databases for terms including "Insulin-Like Growth Factor I," "IGF1," "IGF-1," "somatomedin C," "PNIs," "peripheral nerves," "nerve injury," "nerve damage," "nerve trauma," "nerve crush," "nerve regeneration," and "nerve repair." Following title review, our search yielded 218 results. Inclusion criteria included original basic science studies utilizing IGF-1 as a means of addressing PNI. Following abstract review, 56 studies were sorted by study type and mechanism of delivery into the following categories: (1) *in vitro*, (2) *in vivo* endogenous upregulation of IGF-1, or (3) *in vivo* delivery of exogenous IGF-1. Studies included in the *in vivo* exogenous IGF-1 group were further sub-stratified into systemic or local delivery, and the local IGF-1 delivery methods were further sub-divided into free IGF-1 injection, hydrogel, or mini-pump studies. Following categorization by mechanism of IGF-1 delivery, the optimal dosage range for each group was calculated by converting all reported IGF-1 dosages to nM for ease of comparison using the standard molecular weight of IGF-1 of 7649 Daltons. After standardization of dosages to nM, the IGF-1 concentration reported as optimal from each study was used to calculate the overall mean, median, and range of optimal IGF-1 dosage for each group.

IN VITRO EFFECTS OF IGF-1 ON NEURONS, SCHWANN CELLS, AND MYOCYTES

The positive trophic and anti-apoptotic effects of IGF-1 are primarily mediated via the PI3K-Akt and MAP-kinase pathways (Ho and 2007 GH Deficiency Consensus Workshop Participants, 2007; Chang et al., 2017). Autophosphorylation of the intracellular domain of IGF-1 receptors results in the activation of insulin receptor substrates 1–4, followed by activation of Ras GTPase, and then the successive triggering of Raf, MEK, and lastly ERK. Through activation of Bcl-2, ERK has been shown to prevent apoptosis and foster neurite growth. Ras activation also triggers aPKC and Akt (Homs et al., 2014), with the active form of the latter inhibiting GSK-3β and thus inhibiting a number of pro-apoptotic pathways (Kanje et al., 1988; Schumacher et al., 1993; Chang et al., 2017). Additionally, the JAK-STAT pathway is an important contributor toward the stimulation of neuronal outgrowth and survival by facilitating Growth Hormone (GH) receptor binding on target tissue to induce IGF-1 release (Meghani et al., 1993; Cheng et al., 1996; Seki et al., 2010; Chang et al., 2017). These biochemical mechanisms enable GH and IGF-1 to exert anabolic and anti-apoptotic effects on neurons, SCs, and myocytes (Tuffaha et al., 2016b).

A number of *in vitro* studies have highlighted the neurotrophic effects of IGF-1 (**Table 1**). Using cultured nerve, SCs, and dorsal root ganglion (DRG) cells, these studies demonstrate that IGF-1 promotes neurite outgrowth and limits neuronal apoptosis (Caroni and Grandes, 1990; Sumantran and Feldman, 1993; Akahori and Horie, 1997; Delaney et al., 2001; Ogata et al., 2004; Liang et al., 2007; Scheib and Hoke, 2013, 2016a,b). Additionally, several *in vitro* studies have shown that IGF-1 supports SC myelination and inhibits SC apoptosis whilst also stimulating nerve sprouting into denervated muscle and reducing muscle atrophy (Caroni and Grandes, 1990; Sumantran and Feldman, 1993; Ogata et al., 2004; Liang et al., 2007; Scheib and Hoke, 2016a,b).

TABLE 1 | *In vitro* studies of IGF-1 on neurons, SCs, and DRG cells (IGF-1, insulin-like growth factor 1; SC, schwann cells; DRG, dorsal root ganglion, bFGF, basic fibroblast growth factor; Bcl-xL, B-cell lymphoma-extra large; C-myc, cellular-myc; GAP-43, growth-associated protein 43; GGF, glial growth factor).

Cell Target	IGF-1 Concentrations Tested (in originally concentrations)	Optimal IGF-1 Concentration Reported (standardized to nM)	Key Finding (Citation)
Neurons	10 and 100 ng/mL	1.31	Insulin, IGF-1 and 2 are mitogenic to cultured rat sciatic nerve segments, stimulate [3H]thymidine incorporation through their receptors Ho and 2007 GH Deficiency Consensus Workshop Participants, 2007.
Neurons/Myocytes	0.1, 0.3, 0.5, 2, and 10 nM	2	Nerve sprouting in innervated adult skeletal muscle is induced by exposure to elevated levels of insulin-like growth factors Gorio et al., 2001.
SCs	20 ng/mL	2.61	IGF-1 serves as a mitogen for rat SCs Wood et al., 2009.
SCs	0.1, 0.3, 1.0, and 3.0 nM	3	IGF-1 induces mitogenesis in cultured SCs Gold et al., 1995.
DRGs	(50 or 100 ng/mL IGF-1) + (5, 10, 20, or 50 ng/mL bFGF)	6.54	FGF and insulin-like growth factor rescue growth cones of sensory neurites from collapse after tetracaine-induced injury Chang et al., 2017.
DRGs	1–10 nM IGF-1	10	IGF-I enhances neurite regeneration but is not required for its survival in adult DRG explant Schumacher et al., 1993.
SCs	0.3 and 10 nM	10	Insulin-like growth factor-I and over-expression of Bcl-xL prevent glucose-mediated apoptosis in Schwann cells Kanje et al., 1988.
Neurons	0, 3, and 10 nM	10	Insulin-like growth factor I regulates c-myc and GAP-43 messenger ribonucleic acid expression in SH-SY5Y human neuroblastoma cells Delaney et al., 2001.
Neurons	0.1, 1.0, 3.0, and 10 nM	10	Insulin-like growth factor has a positive trophic effect on human neuroblastoma cell growth Homs et al., 2014.
SCs	10, (100 ng/mL IGF-1 + 20 ng/mL GGF)	13.07	Extracellular control of cell size can be achieved through combination of IGF + GGF to augment cell cycle progression Scheib and Hoke, 2013.
SCs	150 ng/mL	19.61	IGF1 has a positive trophic effect on SC myelination Cheng et al., 1996.
SCs	20 nM	20	IGF1 stimulates *de novo* fatty acid synthesis for SC myelination Seki et al., 2010.

The neurotrophic effects of IGF-1 have been found to be dose-dependent and independent of cell-cycle stage (Sumantran and Feldman, 1993; Tuffaha et al., 2016b). Specific trophic benefits to neurons include the promotion of neurite outgrowth, prevention of neuronal apoptosis, and the promotion of growth cone motility. As the proximal end of an injured nerve begins to recover, regenerating axons are guided to reinnervate their distal targets by numerous chemotrophic factors, resulting in the formation of a growth cone. IGF-1 plays a key role in the motility of the growth cone by inducing reorganization of actin and activation of focal adhesion molecules via the PI3K/Akt pathway (Tuffaha et al., 2016b). IGF-1 further augments growth cone motility via downregulation of c-myc, a cell proliferation transcription factor indicative of neuronal differentiation, and upregulation of growth cone-associated protein 43 (GAP-43), a vital component of neurite formation.

Schwann cells are instrumental to recovery following PNI given their ability to support and guide axonal regeneration via the secretion of neurotrophic factors and maintenance of basal lamina tubes (Scheib and Hoke, 2013, 2016a,b; Tuffaha et al., 2016b). Initially after injury, myelinating SCs distal to the site of injury undergo conversion to a more immature, proliferating repair phenotype (Nocera and Jacob, 2020). Throughout this process, SCs express a variety of genes that dynamically control the regenerative process by promoting survival of neurons, breakdown of damaged axons, clearance of myelin, axonal regrowth, and guidance to the axons' former targets, finally leading to remyelination of the regenerated axon (Chen et al., 2015; Gordon, 2020; Nocera and Jacob, 2020). Unfortunately, upregulation of pro-regenerative gene expression is temporary and the SCs gradually lose the continued ability to support axonal regrowth as time elapses without axonal interaction (Gordon, 2020). A more detailed description of the biological processes underpinning the role of SCs in peripheral nerve regeneration can be found in a recent review article by Nocera and Jacob (2020). IGF-1 supports SCs by promoting their proliferation, maturation, and differentiation to myelinating phenotypes, while concurrently inhibiting SC apoptosis via the PI3K pathway (Scheib and Hoke, 2013; Tuffaha et al., 2016b). IGF-1's ability to initiate myelination centers around regulating the balance between ERK, a pathway suppressing SC differentiation, and PI3K-Akt, a pathway promoting SC differentiation via increased expression of myelin basic protein and myelin-associated glycoprotein (Schumacher et al., 1993; Stewart et al., 1996; Conlon et al., 2001; Scheib and Hoke, 2016a).

Peripheral nerve injury subjects muscle to prolonged denervation that results in myofiber atrophy with increased proteolysis, decreased contractility, and interstitial fibrosis. As the period of denervation extends, these proteolytic and fibrotic processes continue, thereby decreasing the viability of muscle to accept regenerating axons (Shavlakadze et al., 2005; Tuffaha et al., 2016b). In addition to the deleterious effects of prolonged

denervation and fibrosis on muscle, functional recovery is hindered by the failure of regenerating motor nerve fibers to come into contact with the specific motor pathways that guide them back to their original motor endplates (Gordon, 2020). A more thorough description of the biological processes and pathways implicated in denervation-induced muscle atrophy can be found in this recent review article by Ehmsen and Hoke (2020). Following nerve injury, local levels of IGF-1 increase and stimulate axonal sprouting into denervated muscle (Homs et al., 2014). IGF-1 also activates the Akt/mTOR pathway, thereby decreasing atrophy markers including MAFbx and MuRF1 (Bodine et al., 2001; Stitt et al., 2004). Also of note, IGF-1's propensity for decreasing inflammation via promotion of a pro-regenerative M2 macrophage shift over pro-inflammatory M1 reduces the degree of scarring and fibrosis that could otherwise interfere with the targeting of regenerating motor axons (Labandeira-Garcia et al., 2017; Zhao et al., 2021).

Studies included in **Table 1** tested an array of dosages of *in vitro* IGF-1. After considering the individual results of each study, we found that many reported a maximally efficacious IGF-1 dosage. Using each of the reported dosage ranges with the highest efficacy from the *in vitro* studies, we estimated the optimal concentration range for *in vitro* IGF-1 to be 2.61–20.0 nM (mean = 9.81 nM, median = 10.0 nM) (Rinderknecht and Humbel, 1978).

IN VIVO UPREGULATION OF ENDOGENOUS IGF-1

Many of the *in vitro* benefits of IGF-1 to neurons, SCs, and myocytes have also been observed *in vivo*. IGF-1 is produced endogenously by the liver. There has also been documentation of autocrine and paracrine IGF-1 production by multiple cell and tissue types including SCs and myocytes (Laron, 2001; McMullen et al., 2004; Apel et al., 2010). Multiple studies have found that following PNI, IGF-1 increases axon number and maintains SC proliferation at near-normal levels while also enhancing NMJ recovery to promote end-organ reinnervation (Caroni and Grandes, 1990; Kanje et al., 1991; Apel et al., 2010; Emel et al., 2011; Bayrak et al., 2017). Studies administering anti-IGF-1 antibodies to a sciatic nerve crush model further validated the role of IGF-1 in PNI, finding a diminished capacity for regeneration (Kanje et al., 1989; Sjoberg and Kanje, 1989).

One strategy that has been used to take advantage of the therapeutic benefits of IGF-1 involves systemic upregulation of endogenous IGF-1 production at the protein level in injured nerves via upstream augmentation of the GH axis (**Table 2**; Kanje et al., 1988; Gorio et al., 1998, 2001; Losa et al., 1999; Madaschi et al., 2003; Flint et al., 2004; Rabinovsky and Draghia-Akli, 2004; Saceda et al., 2011; Bagriyanik et al., 2014; Homs et al., 2014; Nagata et al., 2014; Wang et al., 2015; Tsai et al., 2016; Tuffaha et al., 2016a; Chang et al., 2017; Lopez et al., 2019). The most straightforward approach to accomplish this aim involves systemic administration of GH (Saceda et al., 2011; Tuffaha et al., 2016a; Lopez et al., 2019). This has been shown to be efficacious in both acute PNI repair models and also in a model in which chronic denervation is induced prior to nerve repair (Lopez et al., 2019). One of the strengths of this approach is that it offers a clear pathway to clinical translation, as GH is already available as an FDA-approved drug for other indications. However, it is limited by the need for systemic treatment, which requires daily parenteral dosing and carries a number of side effects, in addition to a lack of fine control over local IGF-1 levels.

Heparin is another upregulator of endogenous IGF-1 that was shown to be effective in promoting nerve and muscle recovery following PNI, as demonstrated by Madaschi et al. (2003) with intraperitoneal injection of a dosage of 1 mg/kg (Madaschi et al., 2003). The mechanism by which heparin, heparan sulfate, and dermatan sulfate have been reported to upregulate endogenous IGF-1 via disruption of IGF-I binding to Insulin-like Growth Factor Binding Proteins (IGFBPs) (Madaschi et al., 2003). Heparin is also thought to inhibit the binding of IGFBP-3 to extracellular matrix heparan sulfate proteoglycans, thereby reducing the affinity of IGFBPs for IGF-I administration and resulting in the release of IGFBP-3 from the cell surface (Gorio et al., 2001). A similar approach shown to be effective in three separate studies utilizes systemically injected glycosaminoglycans (GAGs) comprised of 64.4% heparin, 28.8% dermatan sulfate, and 6.7% chondroitin sulfate. The effectiveness of GAGs in enhancing the recovery process following PNI was evidenced by a marked increase in IGF-1 levels in denervated muscle, leading to enhanced recovery as measured by nerve-evoked muscle force testing and the extent of muscle reinnervation (Gorio et al., 1998, 2001; Losa et al., 1999).

Gene delivery targeted to skeletal myocytes has also demonstrated promise as a method of upregulating IGF-1 production in PNI models (Flint et al., 2004; Rabinovsky and Draghia-Akli, 2004; Nagata et al., 2014; Tsai et al., 2016). This approach has been applied both systemically as well as directly to the local site of PNI. Amongst the gene delivery protocols included in **Table 2**, the work of Nagata et al. (2014) is notable given its use of a biocompatible polyplex nanomicelle as a means of delivering IGF-1 plasmid DNA (pDNA) to the local site of PNI (Nagata et al., 2014). The diverse strategies employed by these systemic GH axis modifiers demonstrate the flexibility with which IGF-1 can potentially be incorporated into future translational approaches. However, these systemic therapeutic approaches are all limited by the resulting systemic upregulation of IGF-1 with the associated risks and side effects as well as the lack of fine control of IGF-1 levels within the target tissues, specifically the injured nerve and denervated muscle.

DELIVERY OF EXOGENOUS IGF-1

Both systemic and local techniques have been tested for exogenous IGF-1 administration. Local delivery was further categorized into three different approaches: targeted injection of free IGF-1, implantable mini-pumps, and IGF-1-eluting hydrogels. As with the *in vitro* studies, reported optimal dosages varied. When possible, we calculated an optimal concentration

TABLE 2 | *In vivo* studies using upregulators of endogenous IGF-1 (AAVrh, adeno-associated virus rhesus isolate; EPO, erythropoietin; GAGs, glycosaminoglycans; pDNA, plasmid DNA; hIGF-1, human IGF-1; GH, growth hormone; HGH, human growth hormone).

Cell Target	Local Delivery?	Endogenous IGF-1 Upregulator Dosage and Delivery	Specific GH Axis Modifier (Citation)
Nerve	Y/N	400 nL/min AAVrh10 via "micropump" directly into sciatic nerve and also intrathecally	AAVrh10 Virus delivery of IGF-1 Tajdaran et al., 2019
Nerve	Y	30, 60, 100, 150, and 200 mg/mL/kg Alpinia oxyphylla fruit locally applied to nerve gap	Alpinia oxyphylla Bodine et al., 2001
Nerve	Y	5000 U/kg EPO	EPO Apel et al., 2010
Nerve/Muscle	N	1 mg/kg GAGs (64.4% heparin, 28.8% dermatan sulfate, and 6.7% chondroitin sulfate) injected intraperitoneally daily	GAGs Kanje et al., 1991
Nerve/Muscle	N	5 mg/kg GAGs via daily intraperitoneal injections (64.4% heparin, 28.8% dermatan sulfate, and 6.7% chondroitin sulfate)	GAGs Bayrak et al., 2017
Nerve/Muscle	N	1 mg/kg GAGs (64.4% heparin, 28.8% dermatan sulfate, and 6.7% chondroitin sulfate)	GAGs Sjoberg and Kanje, 1989
Nerve/Muscle	Y	134 ug/mL IGF-1-expressing pDNA, delivered via biocompatible polyplex nanomicelle	Gene Delivery Labandeira-Garcia et al., 2017
Nerve/Muscle	N	0.35 mg/kg myostatin propeptide plasmid injected at five different locations on shaved rat abdomen	Gene Delivery Zhao et al., 2021
Nerve/Muscle	Y	30 uL hIGF-1 vector solution (90 ug DNA)	Gene Transfer Laron, 2001
Nerve	N	0.4 mg/day subcutaneous GH injection	GH Chang et al., 2017
Nerve	N	0.1 mg/kg/day subcutaneous GH injection	GH Kanje et al., 1989
Nerve	N	0.6 mg/day subcutaneous GH injection	GH Homs et al., 2014
Nerve	N	400 mIU/day HGH via mini pump	GH Lee et al., 2003
Nerve/Muscle	N	1 mg/kg intraperitoneal heparin injections daily	Heparin Emel et al., 2011
Muscle	Y	Plasmid-IGF-1 delivery via intramuscular injection increased blood flow and angiogenesis in diabetic/diseased limb	Plasmid Therapy Rinderknecht and Humbel, 1978
Nerve	N	10 mg/kg injections of resveratrol for 14 days	Resveratrol McMullen et al., 2004

mean, median, and range for each method of *in vivo* IGF-1 administration.

Systemic *in vivo* Delivery of IGF-1

Systemic delivery of IGF-1 is achieved via either daily subcutaneous or intraperitoneal injections of free IGF-1. Reported optimal dosages for regeneration of nerve, SC, and muscle range from 0.001 to 1.00 mg/kg/day with a mean of 0.59 mg/kg/day and a median of 0.75 mg/kg/day of IGF-1 (Contreras et al., 1993, 1995; Vaught et al., 1996; Vergani et al., 1998; Lutz et al., 1999; Mohammadi and Saadati, 2014; **Table 3**). The calculated mean and median IGF-1 concentrations for systemic delivery were the highest of any of the delivery mechanisms included in our analysis. This finding emphasizes that the use of a systemic approach necessitates greater dosages of IGF-1 to account for off-target distribution and degradation/clearance prior to reaching the injury site. Notably, almost none of the systemic studies included in this analysis quantified the concentration of IGF-1 at the target injury site, which raises significant concerns about the validity of the findings. With regards to clinical applicability, systemic IGF-1 delivery is severely limited by the risk of side effects, including hypoglycemia, lymphoid hyperplasia, body fat accumulation, electrolyte imbalances, and mental status changes (Elijah et al., 2011; Tuffaha et al., 2016b; Vilar et al., 2017). In contrast to upregulation of systemic IGF-1 via GH Releasing Hormone (GHRH), treatment with systemic IGF-1 does not have the benefit of upstream negative feedback control and therefore poses a greater risk of resulting in spiking IGF-1 levels.

Local Injection of Free IGF-1

Local administration of IGF-1 was achieved by several targeted approaches including direct application of free IGF-1 to the injured nerve at the time of surgical transection as well as single, periodic, and daily local injections of free IGF-1 to the injury site (Caroni and Grandes, 1990; Welch et al., 1997; Day et al., 2001, 2002; Stitt et al., 2004; Emel et al., 2011; García Medrano et al., 2013; Mohammadi et al., 2013; Gu et al., 2015; Kostereva et al., 2016; **Table 4**). Local injection of free IGF-1 is not practical for clinical application as the half-life of IGF-1 is 10 min while the time required for regeneration to occur is often many months (Mayocliniclabs.com, 2020). Multiple injections per day would thus be required to maintain local tissue concentrations. We therefore did not attempt to ascertain the optimal dosages for this approach.

Local Mini-Pump Delivery of IGF-1

Mini-osmotic pumps provide a sustained, local delivery of exogenous IGF-1 (**Table 5**; Kanje et al., 1989; Sjoberg and Kanje, 1989; Ishii and Lupien, 1995; Tiangco et al., 2001; Fansa et al., 2002; Apel et al., 2010; Luo et al., 2016). This technique involves subcutaneous implantation of an osmotic pump in the abdomen with extension of a catheter from the pump to the transected nerve site. The positioning of the catheter is maintained by suturing it to local connective tissue. A fixed concentration and

TABLE 3 | *In vivo* studies using systemic administration of IGF-1 (rhIGF-1, recombinant human IGF-1; subq, subcutaneously).

Cell Target	IGF-1 Dosage	Optimal Reported Dosage of IGF-1 Injected Daily (in mg/kg/day) (Citation)
Nerve/Muscle	100 ng/kg/day intraperitoneal injections	0.0001 Nagata et al., 2014
Nerve/Muscle	0.02 mg/kg/day, 1 mg/kg/day	0.02 Tsai et al., 2016
Nerve	0.5 mg/kg rhIGF-1	0.50 Rabinovsky and Draghia-Akli, 2004
Nerve	0.1, 0.3, 1, 3, 10, and 30 mg/kg/day rhIGF-1 for 14 days	1.00 Flint et al., 2004
Nerve	1 mg/kg subq for delay of grip strength deterioration, 0.3–1.0 mg/kg subq for motor/sensory neuroprotection	1.00 Wang et al., 2015
Nerve	1 mg/kg subq	1.00 Bagriyanik et al., 2014

TABLE 4 | *In vivo* studies using targeted local application/injection of IGF-1 (BSA, bovine serum albumin; PBS, phosphate-buffered saline; PRP, platelet-rich plasma; pcDNA, plasmid-cloning DNA; hIGF1, human IGF-1; PNI, peripheral nerve injury; PDGF, platelet-derived growth factor).

Cell Target	IGF-1 Protocol	Optimal Quantity IGF-1 Used and Application Regimen	Study Results (Citation)
Nerve	Three sub-epineural 10 uL injections along distal nerve prior to transection, 200 ng/30 mL daily injections to transplanted limb	0.0067 ug/mL daily injection	IGF-1 increased nerve regeneration Losa et al., 1999
Nerve	0.2 nM IGF-1 achieved half-maximal response, 100 ng IGF-1 in 100–200 uL BSA in PBS injected daily for 4, 7, or 14 days	0.1 ug daily injection	IGF-1 induced nerve sprouting Gorio et al., 1998
Nerve	15 ug IGF-1 (0.125 mL) injections/day for 8 days, delivered via injection port at crush-injured nerve site, IGF-1 better than PRP	15 ug daily injection	IGF-1 decreased muscle atrophy Saceda et al., 2011
Nerve/Muscle	Intramuscular injection of 200 ug into the gastrocnemius muscle on the 3rd, 5th, 7th, and 9th day	200 ug periodic injection	IGF-1 partially rescues denervation-induced muscle loss Tuffaha et al., 2016a
Muscle	100 ng at 0, 3, and 7 days post-denervation	0.1 ug periodic injection	IGF-1 resulted in relative preservation of muscle diameter, weight, contractile properties Lopez et al., 2019
Nerve/Muscle	100 ug on day 1, 3, and 7	100 ug periodic injection	IGF-1 decreased muscle atrophy following chronic denervation Mohammadi and Saadati, 2014
Nerve	4 ug/10 uL pcDNA-IGF-1 injected into clamped epineurium immediately	0.4 ug/uL single injection	Exogenous hIGF-1 is capable of protecting spinal cord motoneurons following PNI Lutz et al., 1999
Nerve	Graft filled with 10 uL (30 ng/kg) IGF-1 at time of procedure	0.03 ug/kg single application	IGF-1 accelerated and improved functional recovery and morphometric indices of sciatic nerve Vergani et al., 1998
Nerve	Combination of 1.5 ug IGF-1 and 0.75 ug PDGF	1.5 ug single application paired with 0.75 ug PDGF	Combined PDGF/IGF-1 did not significantly enhance PNI regeneration after 6 weeks Contreras et al., 1995
Nerve	2 mL rhIGF-1 with concentration 10 mg/mL injected into graft site	2.0×10^4 ug single application	47–62% increase in % of nerve endings in distal sciatic region Vaught et al., 1996

TABLE 5 | *In vivo* studies using mini pumps for local administration of IGF-1.

Cell Target	IGF-1 Concentrations	Pump Rate (in uL/h)	Optimal Concentration of IGF-1 Loaded into Mini-Pump (in ug/mL) (Citation)
Nerve	100 mg/mL total in the mini pump, continuous pump rate of 0.25 uL/h over 28 days	0.25	1.00×10^5 Elijah et al., 2011
Nerve	100 ug/mL @ 0.25 uL/h (0.025 ug/h) over 12 weeks w/pump replacement at 6 weeks	0.25	100.00 Gordon, 2020
Nerve	50 or 100 ug/mL @ 0.25 uL/h over 28 days (no significant difference between the 50 and 100 ug/mL concentrations initially loaded into mini pump)	0.25	50.00 Vilar et al., 2017
Nerve	0.10 ug/uL @ 0.25 uL/h over 1–4 weeks	0.25	0.10 Kostereva et al., 2016
Nerve	50, 100, 200 ug/mL, 100 or 200 ug/mL "optimal, 25% increase in regeneration" over 6 days	1.05	100.00 Shavlakadze et al., 2005
Nerve	Local mini pump: 10 ug/mL released at a rate of 0.5 uL/h over 7 days Systemic mini pump: 200 ug/mL IGF-1 released at a rate of 1 uL/h over 7 days	0.50	10.00 Caroni and Grandes, 1990
Nerve	100 ug/mL IGF-1 concentration released over 3–4 days	Unspecified	100.00 Ehmsen and Hoke, 2020

quantity of IGF-1 is then loaded into the pump and released at a constant rate (Kanje et al., 1989).

Studies using mini-pump delivery of IGF-1 tested a variety of initial concentrations (mean = 143 μg/mL, median = 100 μg/mL, and range: 50 μg/mL – 100 mg/mL), pump rates (mean = 0.425 μL/h, median = 0.25 μL/h, and range: 0.25 – 1.05 μL/h), and release durations (mean = 26 days, median = 7 days, and range: 3 days–12 weeks). The highest dose was reported by Fansa et al. (2002) using a starting concentration of IGF-1 of 100 mg/mL dosed at a continuous pump rate of 0.25 uL/h over 28 days, a value several orders of magnitude higher than any of the other mini pump studies included in **Table 5**. This concentration discrepancy relative to other mini-pump studies is possibly attributable to the design of this particular study, which set out to investigate the benefits of IGF-1 on a tissue-engineered nerve graft model containing cultured, viable SCs. When the study by Fansa et al. (2002) is excluded, the reported initial optimal concentration for mini pump studies centers on a much more focused range of 0.1–100 μg/mL with a mean of 60 μg/mL and median of 75 μg/mL. Overall, all mini-pump studies included in **Table 5** found a positive impact of IGF-1 on nerve regeneration.

Local Delivery of Exogenous IGF-1 Using Hydrogels

The use of hydrogels encapsulated with varying concentrations of IGF-1 allows for a prolonged and potentially tunable release *in vivo* (Yuan et al., 2000; Mathonnet et al., 2001; Kikkawa et al., 2014; Bayrak et al., 2017). The specific hydrogel formulations that have been evaluated vary with regards to IGF-1 release kinetics, degradation rate, and biocompatibility. Despite differences in study design, the majority of hydrogel studies included in **Table 6** used a water-soluble polymer oligo(poly(ethylene glycol) fumarate) (OPF) hydrogel with encapsulated gelatin microparticles (Yuan et al., 2000; Holland et al., 2005; Kikkawa et al., 2014; Bayrak et al., 2017). The extent of crosslinking within the OPF hydrogel as well as the use of encapsulated gelatin particles with variable isoelectric points allows for tunability of IGF-1 release. The cumulative release of IGF-1 by this hydrogel formulation was reported to be 95.2% ± 2.9% by Day 28, with some studies achieving a similar cumulative release within 48 h (Yuan et al., 2000; Kikkawa et al., 2014).

The hydrogels were soaked in IGF-1 solutions, with concentrations ranging from 0.05 to 1 mg/ml. The duration of soaking time and biomaterials used for fabrication differed between studies, thereby complicating further direct comparisons beyond individual consideration. Regardless of concentration of IGF-1 soaking solution, duration of soaking time, or hydrogel composition, the fundamental property in predicting utility for nerve regeneration is the sustained concentration of released IGF-1 that is reaching the site of PNI. Unfortunately, only two of the studies included in **Table 6** quantified IGF-1 release *in vivo* using either fluid sampling with ELISA or radiolabeled IGF-1 (Yuan et al., 2000; Kikkawa et al., 2014). Using ELISA, one study reported significantly greater *in vivo* IGF-1 concentration, peaking at 1.25 μg/mL at Post-operative Day 1 (POD 1) and returning to the physiologic levels of the control group by POD 7 (Kikkawa et al., 2014). Using radiolabeling, the other *in vivo* quantification study reported a biphasic IGF-1 release profile with an initial burst of approximately 80% of the starting concentration of IGF-1 at 1 h followed by sustained release of the remaining 15% ± 2.9% over the subsequent 48-h period (Yuan et al., 2000). Conversely, a different study reported failure of IGF-1 to prevent motoneuron death, a finding which was noted to be contrary to previous results and required additional investigation. This study described the use of a soaked gel foam plug but did not specify the IGF-1 release profile of this material (Bayrak et al., 2017). As such, further analysis and testing is needed to determine the optimal fabrication parameters, loading strategy, and concentration of released IGF-1 required for successful local delivery via hydrogel.

DISCUSSION

Although numerous studies have demonstrated the benefit of IGF-1 to SCs, myocytes, and neurons *in vitro* and following PNI in animal models, several factors must be examined prior to proposing a treatment modality that is suitable for clinical translation. Besides efficacy, additional considerations include ease of regulatory clearance and safety. With regard to regulatory clearance, GH, Growth Hormone Releasing Hormone, and IGF-1 are already clinically available, FDA-approved drugs approved for other indications. With regards to safety, hypoglycemia is the most commonly seen short-term effect of IGF-1 use, although accumulation of body fat, coarsening of facial features, and lymphoid hyperplasia necessitating surgical correction have also been observed with long-term use (Contreras et al., 1995; Tuffaha et al., 2016b). Clinical trials investigating a link between malignancy and exogenous GH therapy have been equivocal, with multiple studies in children undergoing GH therapy demonstrating a low risk of associated malignancy. Additionally, GH therapy in adults has not been found to increase the risk of cancer (Yang et al., 2004; Xu et al., 2005; Chung et al., 2008; Renehan and Brennan, 2008; Svensson and Bengtsson, 2009; Tuffaha et al., 2016b). Given the potential systemic effects of IGF-1, a practical delivery system that can provide sustained release of bioactive IGF-1 to nerve and muscle tissue affected by PNI is of great importance. It will also be important to determine the minimum dose and duration required to achieve therapeutic efficacy.

Optimal dosage of IGF-1 is dependent upon its administration method. As demonstrated by **Tables 1–6**, there is great variation in IGF-1 dosing and frequency of administration between the various methods of delivery, with narrower ranges for ideal dosage that emerge within groups. These reported dosage ranges may serve as a useful reference point when developing and testing IGF-1 delivery strategies in pre-clinical models. Achieving the required pharmacokinetic profile for IGF-1 delivery is challenging due to the small size and short half-life of IGF-1. Therefore, designing drug delivery systems that provide targeted or local treatment of affected muscle and nerve tissue will

TABLE 6 | *In vivo* studies using IGF-1-eluting hydrogels for local administration (BDNF, brain-derived neurotrophic factor; CNTF, ciliary neurotrophic factor; GDNF, glial cell line-derived neurotrophic factor).

Cell Target	Quantity IGF-1 Used and Application Regimen	IGF-1 Protocol	Study Results (Citation)
Nerve	0.05 ug/uL hydrogel	Hydrogels soaked in 0.05 mg/mL IGF-1 for 12 h, released over 48 h	Hydrogel-coated electrodes absorbed significantly more IGF-1 and released it over 48 h Emel et al., 2011
Nerve	40 ug/uL hydrogel	0.025–0.25 ug/uL IGF-1 (1278 ng/mL @ peak release)	Hydrogels are tunable Stitt et al., 2004
Nerve/Spinal Cord	1 ug/uL soaked gel	1 ug/uL soaked gel foam, soaked with either IGF-1, BDNF, CNTF, or GDNF	CNTF and IGF-1 soaked gels failed to prevent motoneuron death Day et al., 2001
Nerve/SC	100 ug soaked gel	100 ug IGF-1 soaked hydrogel added at time of surgical transection	Axonal order/myelination preserved in IGF-1 group, SC proliferation close to normal Day et al., 2002
Nerve	200 ug soaked plug	Two plugs soaked in 200 ug IGF-1 placed at axotomy site, spaced 12 h apart	IGF-1 induced survival in axotomized chick olfactory neurons Mohammadi et al., 2013

facilitate clinical translatability of IGF-1 therapy. Local delivery of IGF-1 would reduce the side effects and potential toxicities of systemic exposure while permitting titration of loading levels to improve efficacy. However, the use of daily or frequent injections to an injury site, as described in previous studies, increases the risk of iatrogenic damage to the recovering nerve and surrounding vasculature (Caroni and Grandes, 1990; Day et al., 2001, 2002; Stitt et al., 2004; Emel et al., 2011; Mohammadi et al., 2013; Kostereva et al., 2016). In addition, the potential scarring induced by repeated local injections could preclude regenerating axons from reaching their distal targets, leading to decreased NMJ reinnervation as well as potential neuroma formation. Furthermore, the local injection of free IGF-1 without a biocompatible carrier misses an opportunity to improve its bioavailability. While the mini-pump technique provides a level of automated control over IGF-1 administration unmatched by the other previously described methods, the subcutaneous implantation of a mini-pump in a human patient introduces the risks of infection and device migration. More importantly, given the duration of time needed for regeneration to occur, the implanted pump would also likely induce a high degree of foreign body reaction resulting in fibrotic encapsulation and potential deleterious effects on the injured nerve being treated.

Despite the well-documented positive effects of IGF-1 in the setting of PNI, the major obstacle for clinical translation remains the lack of a practical delivery system that offers tunable and sustained release of bioactive IGF-1 targeted to nerve and muscle tissue downstream of the nerve injury. Such a delivery system would avoid the potential risks and side effects associated with systemic IGF-1 administration and provide a practical means of applying this treatment for both patients and clinicians (Contreras et al., 1995). The ideal IGF-1 delivery system should also demonstrate biocompatibility without inducing inflammation or encapsulation over time. In addition to the pre-soaked IGF-1 eluting hydrogels detailed in **Table 6**, several bioengineering approaches to local IGF-1 delivery have recently been reported in animal models. Notable amongst these studies are a delivery system which makes use of biodegradable poly(lactic-co-glycolic acid) (PLGA)/graphene oxide (GO) nanofibers embedded with immobilized IGF-1 for spinal cord repair, as well as a system of IGF-1 loaded polymeric PLGA microspheres for use in bilateral cavernous nerve injury (Santos et al., 2016; Haney et al., 2019; Pan et al., 2019).

Several bioengineered carriers have been developed in recent years for local delivery of IGF-1. Comprised of amine-terminated polyamidoamine dendrimers functionalized with polyethylene glycol (PEG), alginate, poly(γ-glutamic acid)/β-tricalcium phosphate, chitosan, gelatin, and PLGA/hyaluronic acid, these carriers have been shown to provide sustained, *in vivo* IGF-1 release profiles up to 30 days for applications including bone and cartilage regeneration (Geiger et al., 2018; Zhang et al., 2020).

The combination of nanoparticle carriers with hydrogels as a hybrid delivery system has recently come into favor for purposes including passively controlled drug release, stimuli-responsive drug delivery, site-specific drug delivery, and detoxification. The addition of a hydrogel to a nanoparticle delivery system allows for an added level of tunability as well as increased assurance that the nanoparticles remain at the local site of delivery *in vivo* (Gao et al., 2016; Norouzi et al., 2016). A promising approach being pursued by our group for repair of PNI involves encapsulation of IGF-1 into nanoparticles that provide sustained release of IGF-1 for over 6 weeks. The nanoparticles are then suspended within a biomimetic nanofiber hydrogel composite carrier to facilitate *in vivo* application and preliminary results have been encouraging (Santos et al., 2016). The approach involves injection of the composite hydrogel into the denervated target muscle and around the nerve distal to the site of injury, such that the released bioactive IGF-1 diffuses through the target tissues. Our unpublished data suggests that IGF-1 does not act on regenerating axons in gradient-dependent fashion, as uniform delivery along the distal nerve results in a robust treatment effect. However, the question of gradient dependence has not been specifically addressed to our knowledge and warrants further investigation. To achieve maximal treatment effect, IGF-1 will likely need to be delivered for the duration of the regenerative period, which can last many months or even years. It is unlikely that an engineered drug delivery system will be developed that can achieve this duration of release with a single dose. We therefore anticipate that interval ultrasound-guided reinjections will be needed, with the dosing schedule being dependent on the duration of drug release.

CONCLUSION

There is strong evidence behind the supportive role of IGF-1 in recovery after PNI in animal models. IGF-1 can prevent SC apoptosis, foster axonal growth, and decrease the rate of denervation-induced muscle atrophy. Beyond the mechanistic studies that have demonstrated these positive effects *in vitro*, a number of *in vivo* studies have demonstrated efficacy by direct delivery or upregulation of IGF-1, either systemically or locally. An optimized delivery system is critically needed that can offer sustained delivery of bioactive IGF-1 to target tissues in a safe and clinically practical fashion. The optimal dosing ranges of IGF-1 vary substantially depending upon mechanism of delivery, and further work will be needed to define the dose-response relationship for any delivery method prior to clinical application.

AUTHOR CONTRIBUTIONS

BS, KS, NG, PH, and ST contributed to conception and design of the study. BS and ST performed the literature review, organized the database in collaboration with KS, NG, and PH, and wrote the first draft of the manuscript. BS performed preliminary stoichiometric calculations. KS, NG, and PH contributed the revisions to the manuscript draft. CQ verified all stoichiometric values and calculations and provided revisions. H-QM and AH contributed invaluable perspectives, insights, and revisions to the manuscript. ST supervised all aspects and stages of the project as corresponding author. All authors contributed to the article and approved the submitted version.

REFERENCES

Akahori, Y., and Horie, H. (1997). IGF-I enhances neurite regeneration but is not required for its survival in adult DRG explant. *Neuroreport* 8, 2265–2269. doi: 10.1097/00001756-199707070-00034

Apel, P. J., Ma, J., Callahan, M., Northam, C. N., Alton, T. B., Sonntag, W., et al. (2010). Effect of locally delivered IGF-1 on nerve regeneration during aging: an experimental study in rats. *Muscle Nerve* 41, 335–341. doi: 10.1002/mus.21485

Bagriyanik, H. A., Ersoy, N., Cetinkaya, C., Ikizoglu, E., Kutri, D., Ozcana, T., et al. (2014). The effects of resveratrol on chronic constriction injury of sciatic nerve in rats. *Neurosci. Lett.* 561, 123–127. doi: 10.1016/j.neulet.2013.12.056

Bayrak, A. F., Olgun, Y., Ozbakan, A., Aktas, S., Kulan, C. A., Kamaci, G., et al. (2017). The effect of insulin like growth factor-1 on recovery of facial nerve crush injury. *Clin. Exp. Otorhinolaryngol.* 10, 296–302. doi: 10.21053/ceo.2016.00997

Bodine, S. C., Stitt, T. N., Gonzalez, M., Kline, W. O., Stover, G. L., Bauerlein, R., et al. (2001). Akt/mTOR pathway is a crucial regulator of skeletal muscle hypertrophy and can prevent muscle atrophy in vivo. *Nat. Cell Biol.* 3, 1014–1019. doi: 10.1038/ncb1101-1014

Carlson, B. M., Billington, L., and Faulkner, J. (1996). Studies on the regenerative recovery of long-term denervated muscle in rats. *Restor. Neurol. Neurosci.* 10, 77–84. doi: 10.3233/RNN-1996-10203

Caroni, P., and Grandes, P. (1990). Nerve sprouting in innervated adult skeletal muscle induced by exposure to elevated levels of insulin-like growth factors. *J. Cell Biol.* 110, 1307–1317. doi: 10.1083/jcb.110.4.1307

Chang, Y. M., Chang, H. H., Tsai, C. C., Lin, H. J., Ho, T. J., Ye, C. X., et al. (2017). Alpinia oxyphylla Miq. fruit extract activates IGFR-PI3K/Akt signaling to induce Schwann cell proliferation and sciatic nerve regeneration. *BMC Complement. Altern. Med.* 17:184. doi: 10.1186/s12906-017-1695-2

Chen, P., Piao, X., and Bonaldo, P. (2015). Role of macrophages in wallerian degeneration and axonal regeneration after peripheral nerve injury. *Acta Neuropathol.* 130, 605–618. doi: 10.1007/s00401-015-1482-4

Cheng, H. L., Randolph, A., Yee, D., Delafontaine, P., Tennekoon, G., and Feldman, E. L. (1996). Characterization of insulin-like growth factor-I and its receptor and binding proteins in transected nerves and cultured Schwann cells. *J. Neurochem.* 66, 525–536. doi: 10.1046/j.1471-4159.1996.66020525.x

Chung, T. T., Evanson, J., Walker, D., Akker, S. A., Besser, G. M., Monson, J. P., et al. (2008). Safety of GH replacement in hypopituitary patients with nonirradiated pituitary and peripituitary tumours. *Clin. Endocrinol. (Oxf.)* 68, 965–969. doi: 10.1111/j.1365-2265.2007.03135.x

Conlon, I. J., Dunn, G. A., Mudge, A. W., and Raff, M. C. (2001). Extracellular control of cell size. *Nat. Cell Biol.* 3, 918–921. doi: 10.1038/ncb1001-918

Contreras, P. C., Steffler, C., and Vaught, J. L. (1993). rhIGF-I enhances functional recovery from sciatic crush. Time-course and dose-response study. *Ann. N. Y. Acad. Sci.* 692, 314–316. doi: 10.1111/j.1749-6632.1993.tb26245.x

Contreras, P. C., Steffler, C., Yu, E., Callison, K., Stong, D., and Vaught, J. L. (1995). Systemic administration of rhIGF-I enhanced regeneration after sciatic nerve crush in mice. *J. Pharmacol. Exp. Ther.* 274, 1443–1449.

Davis, B., Hilgart, D., Erickson, S., Labroo, P., Burton, J., Sant, H., et al. (2019). Local FK506 delivery at the direct nerve repair site improves nerve regeneration. *Muscle Nerve* 60, 613–620. doi: 10.1002/mus.26656

Day, C. S., Buranapanitkit, B., Riano, F. A., Tomaino, M. M., Somogyi, G., Sotereanos, D. G., et al. (2002). Insulin growth factor-1 decreases muscle atrophy following denervation. *Microsurgery* 22, 144–151. doi: 10.1002/micr.21742

Day, C. S., Riano, F., Tomaino, M. M., Buranatanitkit, B., Somogyi, G., Sotereanos, D., et al. (2001). Growth factor may decrease muscle atrophy secondary to denervation. *J. Reconstr. Microsurg.* 17, 51–57.

Delaney, C. L., Russell, J. W., Cheng, H. L., and Feldman, E. L. (2001). Insulin-like growth factor-I and over-expression of Bcl-xL prevent glucose-mediated apoptosis in Schwann cells. *J. Neuropathol. Exp. Neurol.* 60, 147–160. doi: 10.1093/jnen/60.2.147

Ehmsen, J. T., and Hoke, A. (2020). Cellular and molecular features of neurogenic skeletal muscle atrophy. *Exp. Neurol.* 331:113379. doi: 10.1016/j.expneurol.2020.113379

Elijah, I. E., Branski, L. K., Finnerty, C. C., and Herndon, D. N. (2011). The GH/IGF-1 system in critical illness. *Best Pract. Res. Clin. Endocrinol. Metab.* 25, 759–767. doi: 10.1016/j.beem.2011.06.002

Emel, E., Ergün, S. S., Kotan, D., Gürsoy, E. B., Parman, Y., Zengin, A., et al. (2011). Effects of insulin-like growth factor-I and platelet-rich plasma on sciatic nerve crush injury in a rat model. *J. Neurosurg.* 114, 522–528. doi: 10.3171/2010.9.JNS091928

Fansa, H., Schneider, W., Wolf, G., and Keilhoff, G. (2002). Influence of insulin-like growth factor-I (IGF-I) on nerve autografts and tissue-engineered nerve grafts. *Muscle Nerve* 26, 87–93. doi: 10.1002/mus.10165

Fex Svenningsen, A., and Kanje, M. (1996). Insulin and the insulin-like growth factors I and II are mitogenic to cultured rat sciatic nerve segments and stimulate [3H]thymidine incorporation through their respective receptors. *Glia* 18, 68–72. doi: 10.1002/(sici)1098-1136(199609)18:1<68::aid-glia7>3.0.co;2-#

Flint, P. W., Nakagawa, H., Shiotani, A., Coleman, M. E., and O'Malley, B. W. Jr. (2004). Effects of insulin-like growth factor-1 gene transfer on myosin heavy chains in denervated rat laryngeal muscle. *Laryngoscope* 114, 368–371. doi: 10.1097/00005537-200402000-00035

Fu, S. Y., and Gordon, T. (1995). Contributing factors to poor functional recovery after delayed nerve repair: prolonged denervation. *J. Neurosci.* 15(5 Pt 2), 3886–3895. doi: 10.1523/jneurosci.15-05-03886.1995

Gao, W., Zhang, Y., Zhang, Q., and Zhang, L. (2016). Nanoparticle-hydrogel: a hybrid biomaterial system for localized drug delivery. *Ann. Biomed. Eng.* 44, 2049–2061. doi: 10.1007/s10439-016-1583-9

García Medrano, B., Barrio Sanz, P., Simón Pérez, C., León Andrino, A., Garrosa García, M., Martín Ferrero, M. A., et al. (2013). [Regeneration of critical injuries of the peripheral nerve with growth factors]. *Rev. Esp Cir. Ortop. Traumatol.* 57, 162–169. doi: 10.1016/j.recot.2013.03.007

Geiger, B. C., Wang, S., Padera, R. F., Grodzinsky, A. J., and Hammond, P. T. (2018). Cartilage-penetrating nanocarriers improve delivery and efficacy of growth factor treatment of osteoarthritis. *Sci. Transl. Med.* 10:eaat8800. doi: 10.1126/scitranslmed.aat8800

Glazner, G. W., and Ishii, D. N. (1995). Insulinlike growth factor gene expression in rat muscle during reinnervation. *Muscle Nerve* 18, 1433–1442. doi: 10.1002/mus.880181214

Gold, B. G., Katoh, K., and Storm-Dickerson, T. (1995). The immunosuppressant FK506 increases the rate of axonal regeneration in rat sciatic nerve. *J. Neurosci.* 15, 7509–7516. doi: 10.1523/jneurosci.15-11-07509.1995

Gordon, T. (2009). The role of neurotrophic factors in nerve regeneration. *Neurosurg. Focus* 26:E3.

Gordon, T. (2020). Peripheral nerve regeneration and muscle reinnervation. *Int. J. Mol. Sci.* 21:8652. doi: 10.3390/ijms21228652

Gorio, A., Citterio, C., Muller, E. E., and Di Giulio, A. M. (2001). Glycosaminoglycan-promoted muscle reinnervation and insulin-like growth factor-I levels are affected by anti-growth hormone-releasing hormone exposure. *J. Neurosci. Res.* 66, 1112–1117. doi: 10.1002/jnr.10025

Gorio, A., Vergani, L., De Tollis, A., Di Giulio, A. M., Torsello, A., Cattaneo, L., et al. (1998). Muscle reinnervation following neonatal nerve crush. Interactive effects of glycosaminoglycans and insulin-like growth factor-I. *Neuroscience* 82, 1029–1037. doi: 10.1016/s0306-4522(97)00257-1

Grinsell, D., and Keating, C. P. (2014). Peripheral nerve reconstruction after injury: a review of clinical and experimental therapies. *Biomed. Res. Int.* 2014:698256. doi: 10.1155/2014/698256

Gu, J., Liu, H., Zhang, N., Tian, H., Pan, J., Zhang, W., et al. (2015). Effect of transgenic human insulin-like growth factor-1 on spinal motor neurons following peripheral nerve injury. *Exp. Ther. Med.* 10, 19–24. doi: 10.3892/etm.2015.2472

Haney, N. M., Talwar, S., Akula, P. K., Reddy, A. G., Pema, G. S., Ninh, T. V., et al. (2019). Insulin-like growth factor-1-loaded polymeric poly(lactic-co-glycolic) acid microspheres improved erectile function in a rat model of bilateral cavernous nerve injury. *J. Sex. Med.* 16, 383–393. doi: 10.1016/j.jsxm.2018.12.018

Ho, K. K., and 2007 GH Deficiency Consensus Workshop Participants (2007). Consensus guidelines for the diagnosis and treatment of adults with GH deficiency II: a statement of the GH Research Society in association with the European Society for Pediatric Endocrinology, Lawson Wilkins Society, European Society of Endocrinology, Japan Endocrine Society, and Endocrine Society of Australia. *Eur. J. Endocrinol.* 157, 695–700. doi: 10.1530/eje-07-0631

Holland, T. A., Tabata, Y., and Mikos, A. G. (2005). Dual growth factor delivery from degradable oligo(poly(ethylene glycol) fumarate) hydrogel scaffolds for cartilage tissue engineering. *J. Control. Release* 101, 111–125. doi: 10.1016/j.jconrel.2004.07.004

Homs, J., Pagès, G., Ariza, L., Casas, C., Chillón, M., Navarro, X., et al. (2014). Intrathecal administration of IGF-I by AAVrh10 improves sensory and motor deficits in a mouse model of diabetic neuropathy. *Mol. Ther. Methods Clin. Dev.* 1:7. doi: 10.1038/mtm.2013.7

Ishii, D. N., and Lupien, S. B. (1995). Insulin-like growth factors protect against diabetic neuropathy: effects on sensory nerve regeneration in rats. *J. Neurosci. Res.* 40, 138–144. doi: 10.1002/jnr.490400116

Ishii, D. N., Glazner, G. W., and Pu, S. F. (1994). Role of insulin-like growth factors in peripheral nerve regeneration. *Pharmacol. Ther.* 62, 125–144. doi: 10.1016/0163-7258(94)90007-8

Ishii, D. N., Glazner, G. W., and Whalen, L. R. (1993). Regulation of peripheral nerve regeneration by insulin-like growth factors. *Ann. N. Y. Acad. Sci.* 27, 172–182. doi: 10.1111/j.1749-6632.1993.tb26215.x

Kanje, M., Skottner, A., and Lundborg, G. (1988). Effects of growth hormone treatment on the regeneration of rat sciatic nerve. *Brain Res.* 475, 254–258. doi: 10.1016/0006-8993(88)90613-0

Kanje, M., Skottner, A., Lundborg, G., and Sjoberg, J. (1991). Does insulin-like growth factor I (IGF-1) trigger the cell body reaction in the rat sciatic nerve? *Brain Res.* 563, 285–287. doi: 10.1016/0006-8993(91)91547-e

Kanje, M., Skottner, A., Sjoberg, J., and Lundborg, G. (1989). Insulin-like growth factor I (IGF-I) stimulates regeneration of the rat sciatic nerve. *Brain Res.* 486, 396–398. doi: 10.1016/0006-8993(89)90531-3

Kikkawa, Y. S., Nakagawa, T., Ying, L., Tabata, Y., Tsubouchi, H., Ido, A., et al. (2014). Growth factor-eluting cochlear implant electrode: impact on residual auditory function, insertional trauma, and fibrosis. *J. Transl. Med.* 12:280. doi: 10.1186/s12967-014-0280-4

Konofaos, P., and Terzis, J. K. (2013). FK506 and nerve regeneration: past, present, and future. *J. Reconstr. Microsurg.* 29, 141–148. doi: 10.1055/s-0032-1333314

Kostereva, N. V., Wang, Y., Fletcher, D. R., Unadkat, J. V., Schnider, J. T., Komatsu, C., et al. (2016). IGF-1 and chondroitinase ABC augment nerve regeneration after vascularized composite limb allotransplantation. *PLoS One* 11:e0156149. doi: 10.1371/journal.pone.0156149

Labandeira-Garcia, J. L., Costa-Besada, M. A., Labandeira, C. M., Villar-Cheda, B., and Rodriguez-Perez, A. I. (2017). Insulin-like growth factor-1 and neuroinflammation. *Front. Aging Neurosci.* 9:365. doi: 10.3389/fnagi.2017.00365

Laron, Z. (2001). Insulin-like growth factor 1 (IGF-1): a growth hormone. *Mol. Pathol.* 54, 311–316.

Lee, A. C., Yu, V. M., Lowe, J. B. III, Brenner, M. J., Hunter, D. A., Mackinnon, S. E., et al. (2003). Controlled release of nerve growth factor enhances sciatic nerve regeneration. *Exp. Neurol.* 184, 295–303. doi: 10.1016/s0014-4886(03)00258-9

Lee, K. Y., Nakagawa, T., Okano, T., Hori, R., Ono, K., Tabata, Y., et al. (2007). Novel therapy for hearing loss: delivery of insulin-like growth factor 1 to the cochlea using gelatin hydrogel. *Otol. Neurotol.* 28, 976–981. doi: 10.1097/mao.0b013e31811f40db

Liang, G., Cline, G. W., and Macica, C. M. (2007). IGF-1 stimulates de novo fatty acid biosynthesis by Schwann cells during myelination. *Glia* 55, 632–641. doi: 10.1002/glia.20496

Lopez, J., Quan, A., Budihardjo, J., Xiang, S., Wang, H., Koshy, K., et al. (2019). Growth hormone improves nerve regeneration, muscle re-innervation, and functional outcomes after chronic denervation injury. *Sci. Rep.* 9:3117.

Losa, M., Vergani, L., Lesma, E., Rossoni, G., Di Giulio, A. M., Vercelli, A., et al. (1999). Glycosaminoglycans treatment increases IGF-I muscle levels and counteracts motor neuron death: a novel nonanticoagulant action. *J. Neurosci. Res.* 55, 496–505. doi: 10.1002/(sici)1097-4547(19990215)55:4<496::aid-jnr9>3.0.co;2-6

Luo, T. D., Alton, T. B., Apel, P. J., Cai, J., Barnwell, J. C., Sonntag, W. E., et al. (2016). Effects of age and insulin-like growth factor-1 on rat neurotrophin receptor expression after nerve injury. *Muscle Nerve* 54, 769–775. doi: 10.1002/mus.25106

Lutz, B. S., Ma, S. F., Chuang, D. C., and Wei, F. C. (1999). Effects of systemically applied IGF-1 on motor nerve recovery after peripheral nerve transection and repair in the rat – a functional study. *Hand Surg.* 4, 131–136. doi: 10.1142/s0218810499000319

Madaschi, L., Di Giulio, A. M., and Gorio, A. (2003). Muscle reinnervation and IGF-I synthesis are affected by exposure to heparin: an effect partially antagonized by anti-growth hormone-releasing hormone. *Neurochem. Res.* 28, 163–168.

Mathonnet, M., Comte, I., Lalloué, F., and Ayer-Le Lièvre, C. (2001). Insulin-like growth factor I induced survival of axotomized olfactory neurons in the chick. *Neurosci. Lett.* 308, 67–70. doi: 10.1016/s0304-3940(01)01715-3

Mayocliniclabs.com (2020). *IGFGP - Clinical: Insulin-Like Growth Factor 1 (IGF1), LC-MS And Insulin-Like Growth Factor-Binding Protein 3 (IGFBP3) Growth Panel, Serum*. Available online at: https://www.mayocliniclabs.com/test-catalog/Clinical+and+Interpretive/36365 (accessed August 7, 2020).

McMullen, J. R., Shioi, T., Huang, W. Y., Zhang, L., Tarnavski, O., Bisping, E., et al. (2004). The insulin-like growth factor 1 receptor induces physiological heart growth via the phosphoinositide 3-kinase(p110alpha) pathway. *J. Biol. Chem.* 279, 4782–4793. doi: 10.1074/jbc.m310405200

Meghani, M. A., Martin, D. M., Singleton, J. R., and Feldman, E. L. (1993). Effects of serum and insulin-like growth factors on human neuroblastoma cell growth. *Regul. Pept.* 48, 217–224. doi: 10.1016/0167-0115(93)90350-h

Mohammadi, R., and Saadati, A. (2014). Influence of insulin-like growth factor I on nerve regeneration using allografts: a sciatic nerve model. *J. Craniofac. Surg.* 25, 1510–1514. doi: 10.1097/SCS.0000000000000783

Mohammadi, R., Esmaeil-Sani, Z., and Amini, K. (2013). Effect of local administration of insulin-like growth factor I combined with inside-out artery graft on peripheral nerve regeneration. *Injury* 44, 1295–1301. doi: 10.1016/j.injury.2013.04.014

Nagata, K., Itaka, K., Baba, M., Uchida, S., Ishii, T., and Kataoka, K. (2014). Muscle-targeted hydrodynamic gene introduction of insulin-like growth factor-1 using polyplex nanomicelle to treat peripheral nerve injury. *J. Control. Release* 183, 27–34. doi: 10.1016/j.jconrel.2014.03.021

Noble, J., Munro, C. A., Prasad, V. S., and Midha, R. (1998). Analysis of upper and lower extremity peripheral nerve injuries in a population of patients with multiple injuries. *J. Trauma* 45, 116–122. doi: 10.1097/00005373-199807000-00025

Nocera, G., and Jacob, C. (2020). Mechanisms of schwann cell plasticity involved in peripheral nerve repair after injury. *Cell. Mol. Life Sci.* 77, 3977–3989. doi: 10.1007/s00018-020-03516-9

Norouzi, M., Nazari, B., and Miller, D. W. (2016). Injectable hydrogel-based drug delivery systems for local cancer therapy. *Drug Discov. Today* 21, 1835–1849. doi: 10.1016/j.drudis.2016.07.006

Ogata, T., Iijima, S., Hoshikawa, S., Miura, T., Yamamoto, S., Oda, H., et al. (2004). Opposing extracellular signal-regulated kinase and Akt pathways control Schwann cell myelination. *J. Neurosci.* 24, 6724–6732. doi: 10.1523/jneurosci.5520-03.2004

Pan, S., Qi, Z., Li, Q., Ma, Y., Fu, C., Zheng, S., et al. (2019). Graphene oxide-PLGA hybrid nanofibres for the local delivery of IGF-1 and BDNF in spinal cord repair. *Artif. Cells Nanomed. Biotechnol.* 47, 651–664.

Rabinovsky, E. D., and Draghia-Akli, R. (2004). Insulin-like growth factor I plasmid therapy promotes in vivo angiogenesis. *Mol. Ther.* 9, 46–55. doi: 10.1016/j.ymthe.2003.10.003

Renehan, A. G., and Brennan, B. M. (2008). Acromegaly, growth hormone and cancer risk. *Best Pract. Res. Clin. Endocrinol. Metab.* 22, 639–657. doi: 10.1016/j.beem.2008.08.011

Rinderknecht, E., and Humbel, R. E. (1978). The amino acid sequence of human insulin-like growth factor I and its structural homology with proinsulin. *J. Biol. Chem.* 253, 2769–2776. doi: 10.1016/s0021-9258(17)40889-1

Saceda, J., Isla, A., Santiago, S., Morales, C., Odene, C., Hernández, B., et al. (2011). Effect of recombinant human growth hormone on peripheral nerve regeneration: experimental work on the ulnar nerve of the rat. *Neurosci. Lett.* 504, 146–150. doi: 10.1016/j.neulet.2011.09.020

Santos, J. L., Ren, Y., Vandermark, J., Archang, M. M., Williford, J., Liu, H., et al. (2016). Continuous production of discrete plasmid DNA-polycation nanoparticles using flash nanocomplexation. *Small* 12, 6214–6222. doi: 10.1002/smll.201601425

Scheib, J. L., and Hoke, A. (2016a). An attenuated immune response by schwann cells and macrophages inhibits nerve regeneration in aged rats. *Neurobiol. Aging* 45, 1–9. doi: 10.1016/j.neurobiolaging.2016.05.004

Scheib, J. L., and Hoke, A. (2016b). Impaired regeneration in aged nerves: clearing out the old to make way for the new. *Exp. Neurol.* 284(Pt A), 79–83. doi: 10.1016/j.expneurol.2016.07.010

Scheib, J., and Hoke, A. (2013). Advances in peripheral nerve regeneration. *Nat. Rev. Neurol.* 9, 668–676.

Schumacher, M., Jung-Testas, I., Robel, P., and Baulieu, E. E. (1993). Insulin-like growth factor I: a mitogen for rat schwann cells in the presence of elevated levels of cyclic AMP. *Glia* 8, 232–240. doi: 10.1002/glia.440080403

Seki, T., Abdel Nazeer, A., Sekimoto, K., Guao, Y., Al-jahdari, W., and Saito, S. (2010). Fibroblast growth factor and insulin-like growth factor rescue growth cones of sensory neurites from collapse after tetracaine-induced injury. *Anesth. Analg.* 110, 1468–1472. doi: 10.1213/ANE.0b013e3181d31ea6

Shavlakadze, T., White, J. D., Davies, M., Hoh, J. F., and Grounds, M. D. (2005). Insulin-like growth factor I slows the rate of denervation induced skeletal muscle atrophy. *Neuromuscul. Disord.* 15, 139–146. doi: 10.1016/j.nmd.2004.10.013

Sjoberg, J., and Kanje, M. (1989). Insulin-like growth factor (IGF-1) as a stimulator of regeneration in the freeze-injured rat sciatic nerve. *Brain Res.* 485, 102–108. doi: 10.1016/0006-8993(89)90671-9

Stewart, H. J., Bradke, F., Tabernero, A., Morrell, D., Jessen, K. R., and Mirsky, R. (1996). Regulation of rat schwann cell po expression and DNA synthesis by insulin-like growth factors in vitro. *Eur. J. Neurosci.* 8, 553–564. doi: 10.1111/j.1460-9568.1996.tb01240.x

Stitt, T. N., Drujan, D., Clarke, B. A., Panaro, F., Timofeyva, Y., Kline, W. O., et al. (2004). The IGF-1/PI3K/akt pathway prevents expression of muscle atrophy-induced ubiquitin ligases by inhibiting FOXO transcription factors. *Mol. Cell* 14, 395–403. doi: 10.1016/s1097-2765(04)00211-4

Sumantran, V. N., and Feldman, E. L. (1993). Insulin-like growth factor I regulates c-myc and GAP-43 messenger ribonucleic acid expression in SH-SY5Y human neuroblastoma cells. *Endocrinology* 132, 2017–2023. doi: 10.1210/endo.132.5.8477653

Svensson, J., and Bengtsson, B. A. (2009). Safety aspects of GH replacement. *Eur. J. Endocrinol.* 161(Suppl. 1), S65–S74. doi: 10.1530/EJE-09-0287

Tajdaran, K., Chan, K., Shoichet, M. S., Gordon, T., and Borschel, G. H. (2019). Local delivery of FK506 to injured peripheral nerve enhances axon regeneration after surgical nerve repair in rats. *Acta Biomater.* 96, 211–221. doi: 10.1016/j.actbio.2019.05.058

Taylor, C. A., Braza, D., Rice, J. B., and Dillingham, T. (2008). The incidence of peripheral nerve injury in extremity trauma. *Am. J. Phys. Med. Rehabil.* 87, 381–385. doi: 10.1097/PHM.0b013e31815e6370

Tiangco, D. A., Papakonstantinou, K. C., Mullinax, K. A., and Terzis, J. K. (2001). IGF-I and end-to-side nerve repair: a dose-response study. *J. Reconstr. Microsurg.* 17, 247–256. doi: 10.1055/s-2001-14516

Tsai, S. W., Tung, Y. T., Chen, H. L., Yang, S. H., Liu, C. Y., Lu, M., et al. (2016). Myostatin propeptide gene delivery by gene gun ameliorates muscle atrophy in a rat model of botulinum toxin-induced nerve denervation. *Life Sci.* 146, 15–23. doi: 10.1016/j.lfs.2015.12.056

Tuffaha, S. H., Budihardjo, J. D., Sarhane, K. A., Khusheim, M., Song, D., Broyles, J. M., et al. (2016a). Growth hormone therapy accelerates axonal regeneration, promotes motor reinnervation, and reduces muscle atrophy following peripheral nerve injury. *Plast. Reconstr. Surg.* 137, 1771–1780. doi: 10.1097/prs.0000000000002188

Tuffaha, S. H., Singh, P., Budihardjo, J. D., Means, K. R., Higgins, J. P., Shores, J. T., et al. (2016b). Therapeutic augmentation of the growth hormone axis to improve outcomes following peripheral nerve injury. *Expert Opin. Ther. Targets* 20, 1259–1265. doi: 10.1080/14728222.2016.1188079

Vaught, J. L., Contreras, P. C., Glicksman, M. A., and Neff, N. T. (1996). Potential utility of rhIGF-1 in neuromuscular and/or degenerative disease. *Ciba Found. Symp.* 196, 18–27; discussion 27-38.

Vergani, L., Di Giulio, A. M., Losa, M., Rossoni, G., Muller, E. E., and Gorio, A. (1998). Systemic administration of insulin-like growth factor decreases motor neuron cell death and promotes muscle reinnervation. *J. Neurosci. Res.* 54, 840–847. doi: 10.1002/(sici)1097-4547(19981215)54:6<840::aid-jnr12>3.0.co;2-1

Vilar, L., Vilar, C. F., Lyra, R., Lyra, R., and Naves, L. A. (2017). Acromegaly: clinical features at diagnosis. *Pituitary* 20, 22–32.

Wang, W., Li, D., Li, Q., Wang, L., Bai, G., Yang, T., et al. (2015). Erythropoietin promotes peripheral nerve regeneration in rats by upregulating expression of insulin-like growth factor-1. *Arch. Med. Sci.* 11, 433–437. doi: 10.5114/aoms.2015.50976

Welch, J. A., Kraus, K. H., Wells, M. R., Blunt, D. G., and Weremowitz, J. (1997). Effect of combined administration of insulin-like growth factor and platelet-derived growth factor on the regeneration of transected and anastomosed sciatic nerve in rats. *Am. J. Vet. Res.* 58, 1033–1037.

Wood, M. D., Moore, A. M., Hunter, D. A., Tuffaha, S., Borschel, G. H., Mackinnon, S. E., et al. (2009). Affinity-based release of glial-derived neurotrophic factor from fibrin matrices enhances sciatic nerve regeneration. *Acta Biomater.* 5, 959–968. doi: 10.1016/j.actbio.2008.11.008

Wujek, J. R., and Lasek, R. J. (1983). Correlation of axonal regeneration and slow component B in two branches of a single axon. *J. Neurosci.* 3, 243–251. doi: 10.1523/jneurosci.03-02-00243.1983

Xu, X. Q., Emerald, B. S., Goh, E. L., Kannan, N., Miller, L. D., Gluckman, P. D., et al. (2005). Gene expression profiling to identify oncogenic determinants of autocrine human growth hormone in human mammary carcinoma. *J. Biol. Chem.* 280, 23987–24003. doi: 10.1074/jbc.m503869200

Yang, X., Liu, F., Xu, Z., Chen, C., Li, G., Wu, X., et al. (2004). Growth hormone receptor expression in human colorectal cancer. *Dig. Dis. Sci.* 49, 1493–1498. doi: 10.1023/b:ddas.0000042254.35986.57

Yuan, Q., Wu, W., So, K. F., Cheung, A. L., Prevette, D. M., and Oppenheim, R. W. (2000). Effects of neurotrophic factors on motoneuron survival following axonal injury in newborn rats. *Neuroreport* 11, 2237–2241. doi: 10.1097/00001756-200007140-00035

Zhang, X., Xing, H., Qi, F., Liu, H., Gao, L., and Wang, X. (2020). Local delivery of insulin/IGF-1 for bone regeneration: carriers, strategies, and effects. *Nanotheranostics* 4, 242–255. doi: 10.7150/ntno.46408

Zhao, L., Zhang, B., Huang, S., Zhou, Z., Jia, X., Qiao, C., et al. (2021). Insulin-like growth factor-1 enhances motoneuron survival and inhibits neuroinflammation after spinal cord transection in zebrafish. *Cell. Mol. Neurobiol.* [Epub ahead of print].

Conflict of Interest: The authors declare that the research was conducted in the absence of any commercial or financial relationships that could be construed as a potential conflict of interest.

frontiers in Bioengineering and Biotechnology

ORIGINAL RESEARCH
published: 09 December 2021
doi: 10.3389/fbioe.2021.744230

Micropatterned Poly(D,L-Lactide-Co-Caprolactone) Conduits With KHI-Peptide and NGF Promote Peripheral Nerve Repair After Severe Traction Injury

Xing Yu[1†], Deteng Zhang[2†], Chang Liu[3], Zhaodi Liu[3], Yujun Li[3], Qunzi Zhao[1], Changyou Gao[2] and Yong Wang[1*]*

[1]Department of Thyroid Surgery, The Second Affiliated Hospital, Zhejiang University School of Medicine, Hangzhou, China, [2]MOE Key Laboratory of Macromolecular Synthesis and Functionalization, Department of Polymer Science and Engineering, Zhejiang University, Hangzhou, China, [3]College of Medicine, Zhejiang University, Hangzhou, China

OPEN ACCESS

Edited by:
Srinivas Madduri,
University Hospital of Basel, Switzerland

Reviewed by:
Huaqiong Li,
University of Chinese Academy of Sciences, China
Pavel Makarevich,
Lomonosov Moscow State University, Russia

***Correspondence:**
Changyou Gao
cygao@zju.edu.cn
Yong Wang
surgwy@zju.edu.cn

[†]These authors have contributed equally to this work

Specialty section:
This article was submitted to Tissue Engineering and Regenerative Medicine, a section of the journal Frontiers in Bioengineering and Biotechnology

Received: 20 July 2021
Accepted: 15 November 2021
Published: 09 December 2021

Citation:
Yu X, Zhang D, Liu C, Liu Z, Li Y, Zhao Q, Gao C and Wang Y (2021) Micropatterned Poly(D,L-Lactide-Co-Caprolactone) Conduits With KHI-Peptide and NGF Promote Peripheral Nerve Repair After Severe Traction Injury. Front. Bioeng. Biotechnol. 9:744230. doi: 10.3389/fbioe.2021.744230

Severe traction injuries after stretch to peripheral nerves are common and challenging to repair. The nerve guidance conduits (NGCs) are promising in the regeneration and functional recovery after nerve injuries. To enhance the repair of severe nerve traction injuries, in this study KHIFSDDSSE (KHI) peptides were grafted on a porous and micropatterned poly(D,L-lactide-co-caprolactone) (PLCL) film (MPLCL), which was further loaded with a nerve growth factor (NGF). The adhesion number of Schwann cells (SCs), ratio of length/width (L/W), and percentage of elongated SCs were significantly higher in the MPLCL-peptide group and MPLCL-peptide-NGF group compared with those in the PLCL group *in vitro*. The electromyography (EMG) and morphological changes of the nerve after severe traction injury were improved significantly in the MPLCL-peptide group and MPLCL-peptide-NGF group compared with those in the PLCL group *in vivo*. Hence, the NGCs featured with both bioactive factors (KHI peptides and NGF) and physical topography (parallelly linear micropatterns) have synergistic effect on nerve reinnervation after severe traction injuries.

Keywords: severe traction injury, biodegradable polyester, nerve guidance conduit, KHIFSDDSSE peptide, nerve growth factor

INTRODUCTION

The peripheral nerve traction injury is one of the most common iatrogenic injuries in clinic (Schwartzman and Grothusen, 2008). The traction-related injury of the peripheral nerve, including brachial plexus, recurrent laryngeal nerve, and sciatic nerve, results in neuropathic pain, dysfunction of sensory, and motor systems (Liu H. et al., 2020). The tractive damage on the nerve takes place mainly at the outer epineurium and perineurium, whereas the structure inside the endoneurium remains relatively intact (Chiang et al., 2008). These morphologic findings suggest that the nerve palsies from traction injuries are temporary, and the electromyography (EMG) would gradually gain partial recovery (Brauckhoff et al., 2018). However, if the traction is prolonged or repeated, the resulted nerve root avulsion or widespread longitudinal damage would restrict the EMG recovery due to the limited possibilities for nerve reconstructions (Malessy et al., 2004). The current standard of

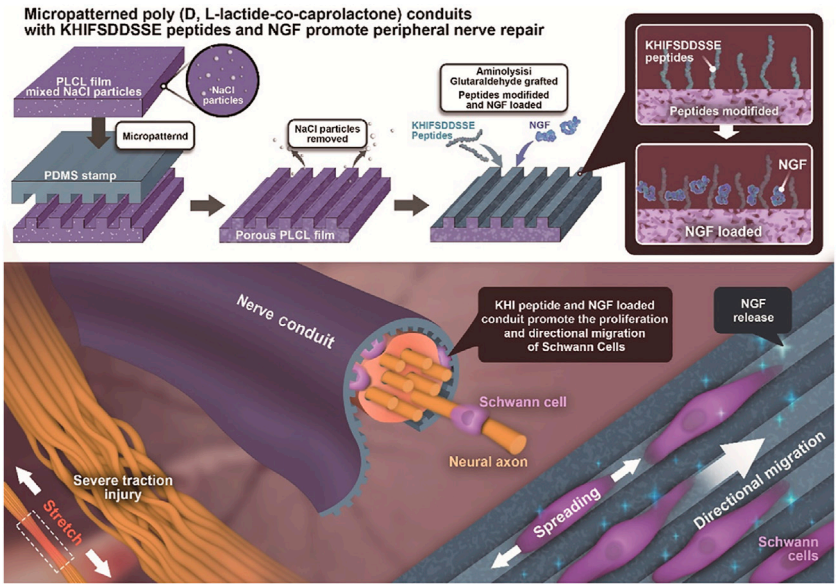

FIGURE 1 | Illustration of PLCL NGC fabrication, KHI peptide modification, and NGF loading and its application in nerve reinnervation after traction injury. The PLCL film mixed with NaCl porogen particles is endowed with a micropattern structure by pressing a micropatterned PDMS stamp under heating. After rinsing out the NaCl particles, the porous micropatterned PLCL film is aminolyzed to introduce free amine groups and is then successively grafted with KHI peptides and NGF *via* glutaraldehyde coupling and/or physical adsorption. The Schwann cells are guided along the micro-stripes *in vitro*. The recovery of the sciatic nerve is enhanced by the functionalized PLCL NGCs *in vivo*.

nerve repair for severe traction injury is autografting (Zheng et al., 2018). This procedure involves the harvest of a section of donor nerve, and the transplantation into the defect (Ray and Mackinnon, 2010). However, the autografting will cause an additional surgery to excise the peripheral nerve, which increases the chance of surgical complications. Additionally, the donor nerve may be insufficient, and the autografts are also restricted to the diameter mismatch between the donor and acceptor nerves (Cheah et al., 2017). Hence, there is a strong demand to find a new way for nerve repair after severe traction injury.

The nerve guidance conduits (NGCs) have shown great promise in the regeneration and functional recovery of peripheral nerves (Zhang et al., 2020a). However, NGCs are rarely used for the nerve traction injury repair, and the underlying impact needs to be elucidated. The morphologic characteristics of nerve traction injury are different from the transection or thermal injury, which are described as neural fiber nonlinearity, myelin degeneration, and internal structural collapse (Gluck et al., 2018). Although at a later stage the nerves experience partial structural and myelin regeneration, the continuity, linearity, and density of myelin cannot fully be recovered (Lopez-Silva et al., 2021). To create an appropriate microenvironment for nerve regeneration, a graphene oxide/poly(D,L-lactide-co-caprolactone) (PLCL) nerve conduit has been developed (Zhang et al., 2020b). Besides the surface chemical property, the surface morphology of NGCs is sculptured by longitudinally oriented structures, which has been found helpful in the orientation and motility of nervous system cells (Zhang et al., 2018a). Moreover, neural recovery can be also improved by using bioactive molecules such as cell growth factors and peptides (Xia et al., 2017; Sarker et al., 2018). For instance, KHIFSDDSSE (KHI) peptides, derived from neural cell adhesion molecules (NCAM), are immobilized onto a substrate, showing efficiency in selective guidance of migration of Schwann cells (SCs) (Ren et al., 2015).

In this study, a porous PLCL film with longitudinally oriented structure and KHI peptides/nerve growth factor (NGF) loading is designed to explore its applicability for the nerve repair after traction injury. The PLCL film mixed with NaCl particles is micropatterned by using a polydimethylsiloxane (PDMS) stamp under heating. After removal of the NaCl particles *via* water rinsing, the obtained porous micropatterned PLCL film is aminolyzed and grafted with the KHI peptides *via* glutaraldehyde coupling. The NGF is grafted/loaded on the film by reaction with the unreacted aldehyde groups and physical adsorption. The SCs are cultured on the modified PLCL film to investigate their adhesion, ratio of length/width (L/W), and elongation behavior (**Figure 1**). Moreover, the NGCs manufactured from the modified PLCL film are used in the sciatic nerve repair *in vivo*, whose overall performance is evaluated by EMG analysis, morphological observation, and neuromuscular junction (NMJ) during the process of reinnervation after traction injury.

MATERIALS AND METHODS

Materials

PLCL with two different molar ratios of L-lactide and ε-caprolactone copolymers (50: 50, Mw = 50 kDa and 75: 25, Mw = 25 kDa) were purchased from Daigang Biotech (Jinan,

China). Trichloromethane, methanol, acetone, NaCl, tertiary butanol, isopropyl alcohol, 1,6-hexanediamine, formaldehyde, ethanol, glutaraldehyde, and paraformaldehyde were supplied by Sinopharm Chemical Reagent (Shanghai, China). Ninhydrin hydrate (98%) and 5,5′-dithiobis-(2-nitrobenzoic acid) (DTNB) were purchased from Macklin Biochemical Co., Ltd. (Shanghai, China). KHIFSDDSSEK-Pra (KHI, Pra: L-C-propargylglycine) peptides were synthesized by Sangon Biotech (Shanghai, China). The water used in all the experiments was purified by a Milli-Q cycle purification system (Millipore, Bedford, MA, USA).

Fabrication of Porous Micropatterned PLCL Films With Peptide Modification and NGF Loading

As described in our previous study (Zhang et al., 2018b), PLCL 50: 50, 0.07 g, and PLCL 75: 25, 0.03 g, were both dissolved in 2.8 ml trichloromethane under stirring for 12 h at room temperature. Then, the NaCl porogen particles, which were ground in a mortar and sieved through a 200-mesh sieve, were added into the PLCL solution, followed by a 1-h stirring. The mixed solution was cast onto a polytetrafluoroethylene (PTFE) mould to obtain the original PLCL/NaCl film after volatilization of the solvent. The micropatterns were created on the surface of PLCL film according to the following procedures. 1) A PDMS template was cross-linked with microstructures of grooves and ridges (4–5 μm in depth, and 5/5 μm in width) by copying from a micropatterned silicon wafer. 2) The PDMS stamp was pressed on the PLCL/NaCl films at 170°C to obtain the micropatterned surface of 5/5 μm in groove width/ridge width. 3) The micropatterned film was immersed in water for 3 days to remove NaCl particles to obtain the macropores. 4) The porous and micropatterned film was aminolyzed in 10% (v/v) 1,6-hexanediamine/isopropanol solution at 37°C for 3 min and then reacted with glutaraldehyde, followed by grafting of KHI peptides. Glutaraldehyde was washed in PBS (pH 7.2) for 3 times, each for 15 min (Abay et al., 2019). 5) The obtained film was immersed in 10 μg/ml NGF water solution to chemically graft/physically adsorb NGF *via* the remained aldehyde groups and porous structure under negative pressure, respectively. The cumulative release amount of NGF was detected by ELISA at 1, 3, and 7 days after NGF loading.

The surface morphology of the films was observed and verified by a scanning electron microscope (SEM, Hitachi S-4800, Tokyo, Japan). The amount of the -NH_2 group on the aminolyzed PLCL films was detected by a ninhydrin assay method (Zhu et al., 2013). In order to measure the density of the peptides on the PLCL film, a calibration curve was firstly obtained by detecting the absorbance of various concentrations of peptides reacted with the DTNB, according to which the peptide density was calculated.

SC Culture *in vitro*

SCs (from Sprague Dawley rat) were supplied by the Cell Bank of Typical Culture Collection of Chinese Academy of Sciences (Shanghai, China) and cultured in high-glucose Dulbecco's modified Eagle's medium (DMEM, Gibco, Grand Island, NY, USA) supplemented with 10% (v/v) fetal bovine serum (FBS, Sijiqing Inc., Hangzhou, China), 100 U/ml penicillin, and 100 μg/ml streptomycin at 37°C in a 5% CO_2-humidified cell incubator. The PLCL films were soaked in 75% ethanol for 15 min and washed 3 times with phosphate-buffered saline (PBS).

SC Morphology

SCs were seeded onto the PLCL films at a density of 2×10^4 cells/cm^2 for 12 h and then freeze-dried after being fixed and dehydrated in gradient absolute ethanol/tertiary butanol for morphology detection using SEM. The L/W ratio and number of elongate SCs were measured by the Image-Pro Plus software.

Animal Experiments

Thirty-two male Sprague-Dawley rats weighing 200–220 g were randomly divided into 4 groups (8 animals in each group). The corresponding films were reeled onto a steel bar (diameter 1.5 mm) in advance and then surrounded onto the surface of injured nerves. The NGCs were obtained *in situ* by sewing with 8–0 nylon monofilament suture stitches, where the injured nerve was ensured to locate at the middle of NGCs. The length of the NGCs was 12 mm, and the inner diameter and wall thickness were 1.5 and 0.2 mm, respectively (Zhang et al., 2020a). The groups were repaired with PLCL film (PLCL group), parallelly linear micropatterned PLCL film (MPLCL group), micropatterned PLCL film with KHI peptides modification (MPLCL-peptide group), and micropatterned PLCL film grafted with KHI peptides and loaded with NGF (MPLCL-peptide-NGF group), respectively. All the animal experiments were carried out in accordance to the institutional animal care guidelines. The procedures were reviewed and approved by the Institutional Review Board (Ethics Committee, the Second Affiliated Hospital of Zhejiang University, School of Medicine).

The rats were anesthetized by intraperitoneal injection of 3% pentobarbital saline (0.1 ml/100 g). The left sciatic nerve was dissected and exposed by dorsal gluteal muscle splitting. The nerve was continuously stretched by a tension meter (Ai Debao, Wenzhou, China) at 3.5 N for 30 s. The electrophysiological (EMG) evaluation and gross and microscopic observation (optical and electron microscope) were performed to confirm the establishment of the traction injury model.

EMG Analysis

As the protocol described before (Yu et al., 2021), the simulating cathode composed of a stainless-steel monopolar needle was placed at the sciatic nerve trunk, with a parallel distance of 10 mm between the two cathodes. The motor response was recorded distally with a unipolar steel needle electrode inserted into the gastrocnemius muscle. The compound motor action potential (CMAP) and nerve conduction velocity (NCV) were recorded using a digital neurophysiological system (Neuro-MEP-Micro, Neurosoft Ltd., 5, Voronin str., Ivanovo, 153032, Russia).

Transmission Electron Microscopy

Transmission electron microscopy (TEM) was used to record the changes in the nerve's structure. The resected part of the nerve

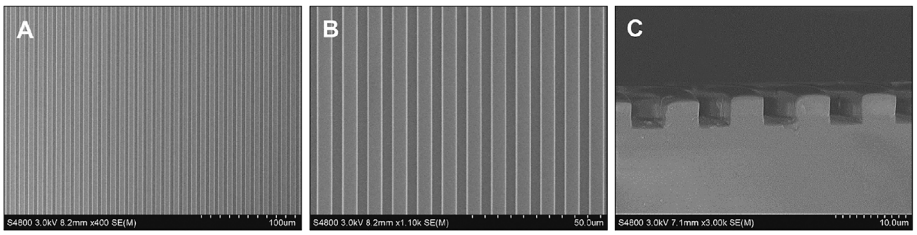

FIGURE 2 | SEM images showing the micropatterns of ridges/grooves of 5/5 μm **(A,B)** and depth of 4–5 μm **(C)**.

was fixed in 2.5% glutaraldehyde overnight in a refrigerator and washed in PBS (pH 7.2) for 3 times, each for 15 min. It was then placed in 1% osmium tetroxide for 1 h. After being stained in 4% uranyl acetate for 30 min, the sample was dehydrated by a series of concentrations of ethanol (70%, 80%, 90%, 95% ethanol, 10 min each) and embedded in a resin mixture. After sectioned, the sample was observed under a Tecnai 10 transmission electron microscope (Philips, Amsterdam, Netherlands) (Zhang et al., 2020b).

Statistical Analysis

The results are presented as number (%) and average ±SD appropriate. Data were analyzed by one-way ANOVA, Welch ANOVA, Student *t*-test, the $\chi 2$ test, Fisher's exact test, and non-parametric Wilcoxon–Mann–Whitney test appropriately using SPSS 20.0 software (SPSS Inc., Chicago, IL, USA). A p value less than 0.05 was considered to be statistically significant.

RESULTS

Fabrication and Characterization of Micropatterns on the Surface of PLCL Films

The guidance of directional migration of SCs is helpful to the functional recovery from severe damage in the peripheral nerve system, yet the application in practice still remains challenging despite of some pioneering studies (Zhang et al., 2018a). Inspired by the highly aligned microstructure of native nerve fibers, organized topographical guidance and bioactive molecules have been introduced to the inner wall of various types of NGCs to enhance their nerve regeneration (Huang et al., 2020). Linear micropatterns can induce the elongation of SC and nerite orientation of dorsal root ganglion (Zhang et al., 2020a). Therefore, in this study the linear micropatterns were created firstly on the PLCL film by using a stamp made from PDMS, which has very low surface energy for anti-adhesion. **Figure 2** shows that the micropatterns were regular and anisotropic, and the parameters of grooves and ridges were replica of the stamp with features of 4–5 μm in depth and 5/5 μm in width.

Next, the same technology was applied to the PLCL film having NaCl particles with a diameter of 75.6 ± 19.1 μm (**Supplementary Figure S1**) to obtain a porous micropatterned PLCL film after porogen leaching. The topographical morphology of the PLCL film was observed by SEM. The film shows a plenty of pores on both the surface and interior (**Figure 3A**) with a diameter of ~63.6 ± 29.9 μm (**Figure 3B**), regardless of the further grafting/loading of KHI peptides and NGF. Although the micropatterns were destroyed at the porous regions on the surface, the overall linear pattern structure was well maintained, which is important in guiding the spreading and elongation of cells contacted. After a series of surface treatment, the linear stripes on the film in each group were still maintained. Quantitative analysis found that the amount of $-NH_2$ was 7.3 μg/cm^2, and the density of KHI was 4.3 μg/cm^2. NGF can accelerate the process of nerve repair and regeneration, and its release plays a vital role for axon stretching. As shown in **Supplementary Figure S2**, the release of NGF from the film increased along with time prolongation at least for 1 week, with a total released amount of 35 ng.

Adhesion and Elongation of SCs *in Vitro*

SCs, the main glial cells in the peripheral nervous system, take a critical role during nerve reconstruction. After the nerve injury, SCs proliferate and migrate to form the Bunger bands and to guide the newborn axon to bridge the two injured stumps. The affinity and elongation of SCs on the surface of NGCs directly decide the outcomes of the functional recovery. As shown in **Figure 4A**, SCs spread slightly with a round shape and random direction in the PLCL group. However, the cells tended to elongate along the microgrooves in the MPLCL group. By contrast, the cells showed a lathy shape in the MPLCL-peptide group and MPLCL-peptide-NGF group.

The adhesion numbers of SCs (~250) in the MPLCL-peptide group and MPLCL-peptide-NGF group were significantly larger than that in the PLCL group ($p < 0.05$) (**Figure 4B**). As the irregular misconnection leads to functional disorder during the repair process, the regularly elongated and orientated cells can better guide the direction of newborn axons. The elongation factor, a parameter displaying the cell morphology index, is defined as the L/W ratio of SCs. The ratio of L/W was significantly increased in the MPLCL-peptide group and MPLCL-peptide-NGF group compared with that in the PLCL group ($p < 0.05$) (**Figure 4C**). The percentages of the elongated SCs in the MPLCL-peptide group and MPLCL-peptide-NGF group were significantly larger than that in the PLCL group as well ($p < 0.05$) (**Figure 4D**).

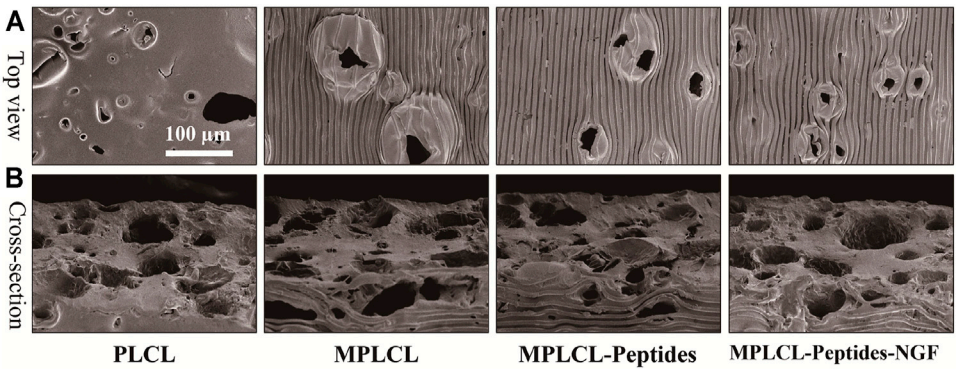

FIGURE 3 | Top-view **(A)** and cross-sectional **(B)** SEM images of different PLCL films, including the groups of PLCL, micropatterned PLCL (MPLCL), micropatterned PLCL grafted with KHI peptides (MPLCL-peptides), and micropatterned PLCL grafted with KHI peptides and loaded with NGF (MPLCL-peptides-NGF).

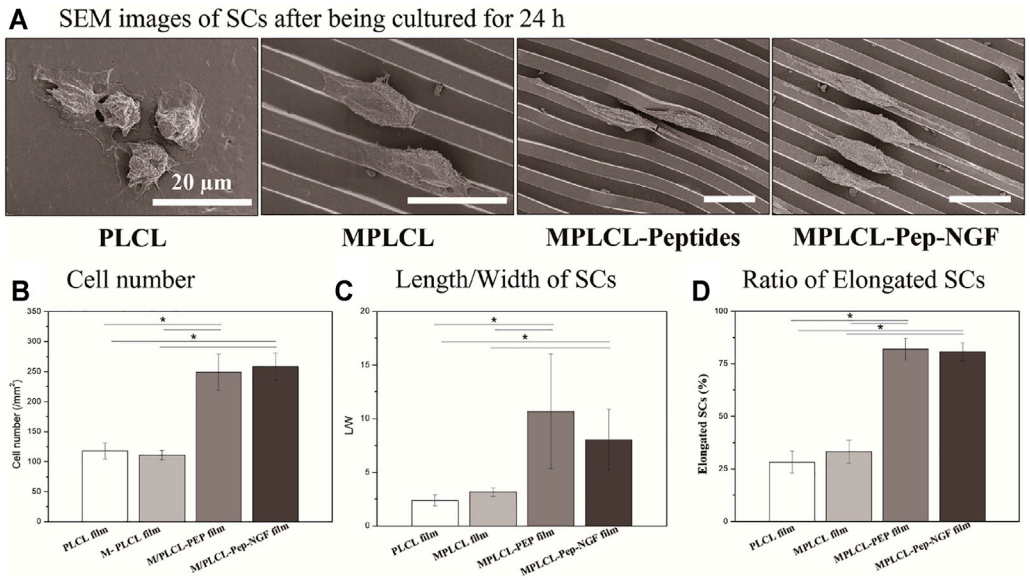

FIGURE 4 | The growth status of SCs on the different PLCL films, including the groups of PLCL, MPLCL, MPLCL-peptides, and MPLCL-peptides-NGF. **(A)** SEM images of SCs after being cultured for 24 h. **(B)** The statistical data of cell number. **(C)** The length/width (L/W) of SCs. **(D)** The ratio of elongated SCs. Asterisk (*) indicates statistically significant difference at the $p < 0.05$ level, $n = 3$.

Animal Evaluation

To evaluate the effects of KHI peptide grafting, NGF loading, and micropatterns *in vivo*, the PLCL film (PLCL group), micropatterned PLCL film (MPLCL group), micropatterned PLCL grafted with KHI peptides (MPLCL-peptide group), and micropatterned PLCL film grafted with KHI peptides and loaded with NGF (MPLCL-peptide-NGF group) were implanted to wrap the tractive injury points, respectively. All the animals were raised in the same environment for 4 weeks. The nerve conduction ability was detected by EMG analysis, and the morphology changes of nerves and gastrocnemius muscles (representing the recovery of reinnervation) were evaluated by optical and electron microscopy.

The Animal Model of Nerve Severe Traction Injury

To establish the animal model of the nerve severe traction injury, the sciatic nerve in one side was continuously stretched at 3.5 N for 30 s. The successful establishment of animal models was confirmed by nerve congestive gross observation, decreased NCV, and the representative CMAP results (amplitude decrease > 50%, or latency prolongation >10%). Hematein and eosin (H&E) staining showed that the injured nerve exhibited nonlinear internal fibers and increased the fiber spacing apart from a distinct region of wavy. The structural damages were also observed as fiber shredding and myelin sheathe degradation (**Figure 5**).

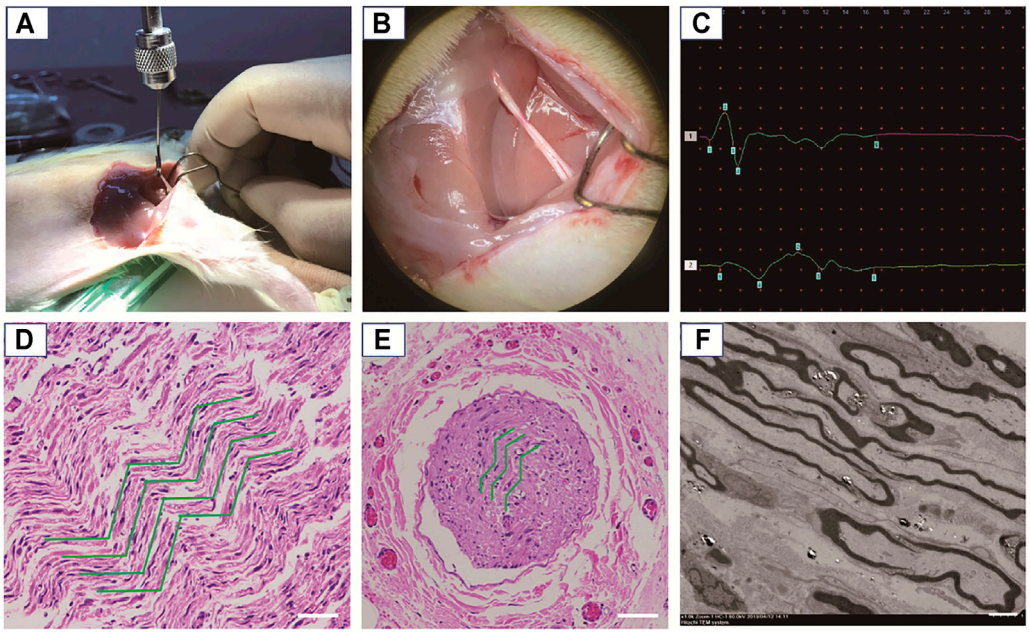

FIGURE 5 | Establishment and confirmation of an animal model for nerve severe traction injury. **(A)** The nerve was continuously stretched at 3.5 N for 30 s. **(B)** Gross observation of the damaged nerve, exhibiting edema and congestion. **(C)** The representative CMAP results after traction injury (amplitude decrease > 50%, or latency prolongation > 10%). **(D)** The damaged nerve point was observed by an optical microscope after H&E staining, where the green curves show circuitous axons in the longitudinal section. Scale bars: 50 μm. **(E)** The damaged nerve point was observed by an optical microscope after H&E staining, where the green curves show the circuitous axons in the cross section. Scale bars: 200 μm. **(F)** TEM observation of the circular axons and myelin sheathes in cross section being stretched as elliptical appearance. Scale bars: 5 μm.

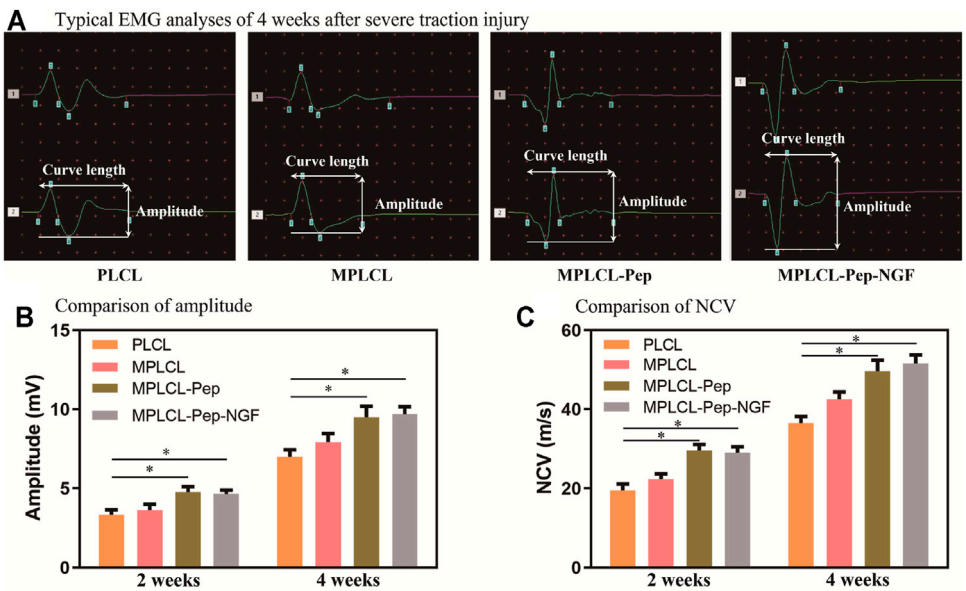

FIGURE 6 | Neural conductive abilities were shown in the groups of PLCL, MPLCL, MPLCL-peptides, and MPLCL-peptide-NGF groups, respectively. **(A)** Typical EMG analyses of 4 weeks after severe traction injury. **(B)** The comparison of amplitude. **(C)** The comparison of NCV. Asterisk (*) indicates statistically significant difference at the $p < 0.05$ level, $n = 8$.

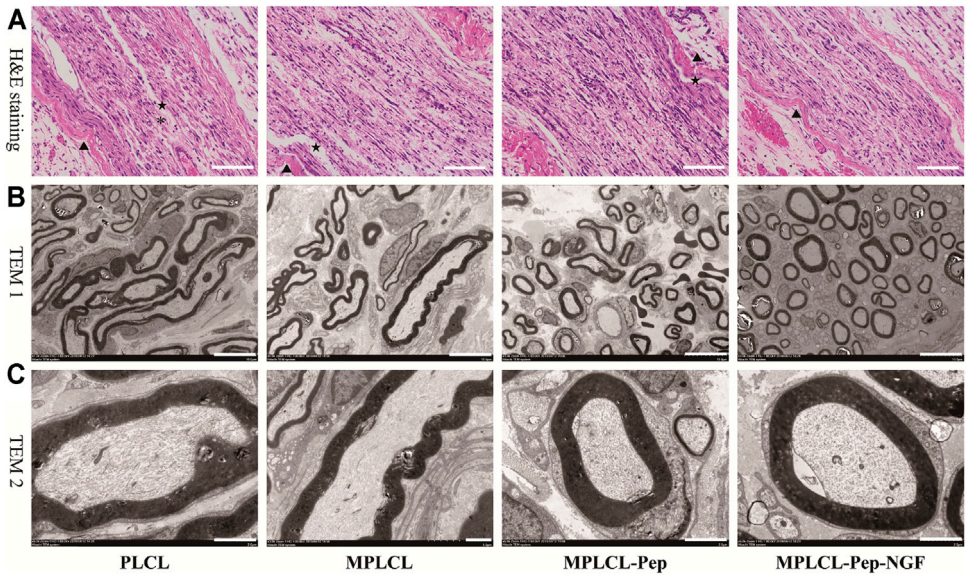

FIGURE 7 | The typical nerve morphological changes in each treatment group of PLCL, MPLCL, MPLCL-peptides, and MPLCL-peptides-NGF. **(A)** H&E staining of the neural in the longitudinal section, where ▲, *, and ★ refer to the circuitous structure of epineurium, the circuitous structure of axons, and the fracture of axons. Scale bars: 100 μm. **(B)** Cross-sectional TEM images showing the circular or elliptical appearance of axons. Scale bars: 10 μm. **(C)** Cross-sectional TEM images showing axons and myelin sheathes. Scale bars: 2 μm.

EMG Analyses

To evaluate the recovery of nerve conduction ability, EMG analyses (including CMAP and NCV) were performed in each treatment group at 2 and 4 weeks postoperatively. The representative waveforms for typical biphasic CMAP responses at 4 weeks postoperative for each treatment group are shown in **Figure 6A**. The CMAP amplitude was significantly increased in the MPLCL-peptide group and MPLCL-peptide-NGF group compared with that in the PLCL group at 2 and 4 weeks postoperative, respectively ($p < 0.05$) (**Figure 6B**). The NCV was also increased significantly in the MPLCL-peptide group and MPLCL-peptide-NGF group compared with that in the PLCL group at 2 and 4 weeks postoperative, respectively ($p < 0.05$) (**Figure 6C**).

Nerve Morphological Changes

The nerve morphological changes were observed by optical and electron microscopy at 4 weeks after NGC implantation (**Figure 7**). In the view of optical microscopy, the nonlinear structures at the injured point of axon fibers were alleviated in each treatment group. In the PLCL group, irregular structures (long, narrow, and wavy) of myelin sheath with lessoned anchoring particles were observed, accompanied with some fractures on the myelin sheath. By contrast, in the MPLCL-peptide group and MPLCL-peptide-NGF group, the remained fiber spacing was reduced, and the ratio of fiber fragment was significantly decreased. TEM images show circular myelinated axons and a thick myelin sheath, where the anchoring particles were observed for maintaining the integrity of the myelin sheath in the MPLCL-peptide group and MPLCL-peptide-NGF group.

Morphological Changes of Gastrocnemius Muscle

The macro- and micro-morphological changes of gastrocnemius muscles are recognized as a vital index to evaluate nerve functional recovery. At 4 weeks after surgery, the gross and microscopic changes of gastrocnemius muscles were observed (**Figure 8**). H&E staining indicates that the skeletal muscle cells have lost their cytoplasm, and the myofibers were sparse and separated by large distances with fibrosis increased and fatty infiltration in the PLCL group and MPLCL group. By contrast, the atrophic manifestation was significantly decreased in the MPLCL-peptide and MPLCL-peptide-NGF groups. The weight of gastrocnemius muscle in the MPLCL-peptide and MPLCL-peptide-NGF groups was significantly higher than that in the PLCL group, whereas there was no significant difference between the PLCL group and MPLCL group.

DISCUSSION

Complete recovery of neural functions after severe traction injury is a great challenge in clinic (Mahan et al., 2019). The treatment by using artificially engineered NGCs can provide an appropriate peripheral nerve growth environment *via* the improvement of physicochemical properties, surface longitudinally oriented microstructures, and bioactive molecule modification (Carvalho et al., 2019; Vijayavenkataraman, 2020). It was found that the NGCs having aligned topology and bioactive molecules on their inner surface can effectively control cell behaviors and nerve regeneration (Oh et al., 2018; Shah et al., 2019; Samadian et al., 2020). However, the effects of combination

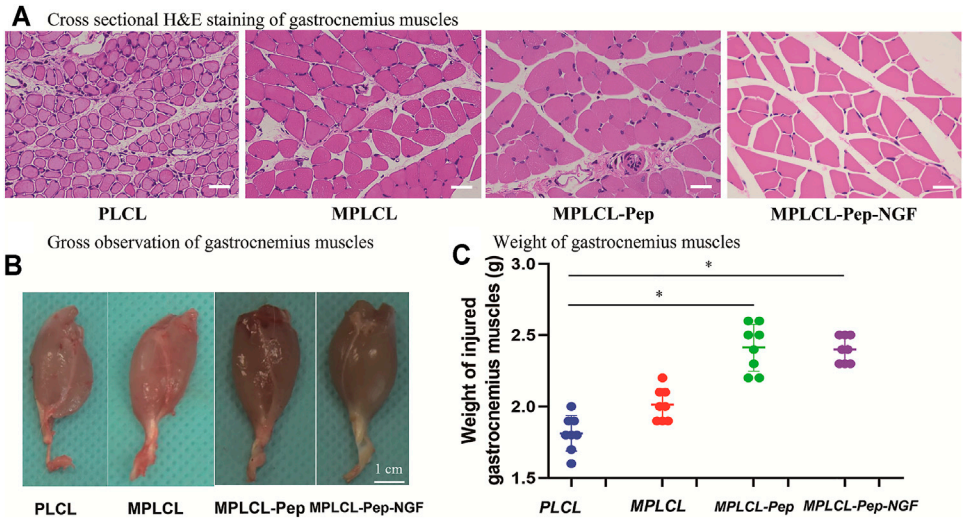

FIGURE 8 | Morphological changes of gastrocnemius muscles in each treatment group of PLCL, MPLCL, MPLCL-peptides, and MPLCL-peptides-NGF. **(A)** Cross-sectional H&E staining of gastrocnemius muscles. Scale bars: 50 μm. **(B)** Gross observation of gastrocnemius muscles. Scale bars: 1 cm. **(C)** Weight of the gastrocnemius muscles. Asterisk (*) indicates statistically significant difference at $p < 0.05$ level, $n = 8$.

in the repair of nerve traction injury are still unknown. The aim of this work is to explore the beneficial combinations of KHI peptide modification, NGF loading, and surface linear micropatterns in the reinnervation after severe traction.

The biodegradation of PLCL is very slow and would not take place apparently within 21 days (Zhang et al., 2015; Zhang et al., 2020b). The macroprous structures on the surface of PLCL films were obtained after leaching of the NaCl porogen particles (**Supplementary Figure S1**). The porous structures with a suitable pore size were beneficial for cell loading and adhesion, which is consistent with previous report (Sun et al., 2021). The 3D and porous structures offer a larger surface area, enabling the efficient grafting/loading of KHI peptides and NGF. Besides, the porous structure allows better supply of nutrients and oxygen *via* the pores on the NGCs, which are extremely important for cell proliferation and nerve regeneration inside the NGCs. Nonetheless, the overall linear (grooves and ridges) pattern structure was maintained although the patterns on the porous regions were distorted or absent.

The groove and ridge morphologic surface belongs to one of the longitudinally oriented microstructures, which can affect the nerve cellular behaviors and guide the directional migration of SCs (Wang et al., 2015). It has been found that the surface anisotropic stripes of grooves and ridges can bring meaningful improvement to nerve repair by adapting the morphology, orientation, and motility of nervous system cells (Tonazzini et al., 2015). Besides, Zhang et al. (2018b) found that SCs cultured on 20/40 μm polyester migrate along the stripes, with a higher ratio of L/W compared to those on the flat film. Furthermore, the migration rate of SCs was also increased significantly when being cultured on the 3/3-μm parallel stripe PLCL, which may promote the M2 polarization of macrophage (Zhang et al., 2020a). In this study, the microstructures of parallel grooves and ridges were created on the surface of the PLCL film, which could similarly guide the direction of SCs and enhance the ability of migration even though the macroprous structure was further implemented. Moreover, these microstructures were also sculptured on the surface of NGCs and implemented in the recovery of severe nerve traction injury *in vivo*. The results reveal that the microstructures of parallel grooves and ridges on the NGCs were helpful in alleviating the nonlinear structures at the injured point after severe traction injury.

The KHI peptide (sequence Lys-His-Ile-Phe-Ser-Asp-Asp-Ser-Ser-Glu-Lys-Pra) is derived from an NCAM, which is a transmembrane protein specifically expressed on neural cells, including neuron, SCs, and other neuroglial cells (Kam et al., 2002; Turner et al., 2019). In our previous study, we developed a complementary density gradient of KHI peptides and demonstrated that the SCs spread better and directionally migrate to the direction of a higher concentration of KHI peptides (Ren et al., 2015). After KHI peptides are immobilized on substrates, the activated NCAM sites can trigger the formation of focal adhesion, improving SC migration (Maness and Schachner, 2007; Lehembre et al., 2008). Furthermore, it was also reported that the KHI peptides can promote the adhesion of neuroglial cells but not affect the adhesion of fibroblasts (Kam et al., 2002). These results prevent the consequence of aberrant reinnervation, which leads to synkinesis rather than physiologic motion (Crumley, 2000). In the present study, the KHI peptides were modified on the surface of a PLCL film, showing a beneficial effect in promoting SC adhesion *in vitro*. Moreover, the NGCs modified with KHI peptides were also firstly implemented to repair peripheral nerve traction injury *in vivo*, showing much effective in elevating the level of recovery and accelerating the process of nerve reinnervation.

The NGF is a well-known neurotrophic factor and widely used in the clinical treatment for peripheral nerve regeneration (Liu

M.-Y. et al., 2020). However, a platform for controlled delivery is required because of its short half-life *in vivo* and its potential to impede axonal regeneration when used in supraphysiological doses (Lackington et al., 2019). Hence, we introduced a PLCL porous film loaded with NGF to investigate its effect on the promotion of nerve regeneration. It has been found that KHI-peptide modification did not influence on NGF release. Besides, the porous property of the films would prolong the release time of NGF till reaching 1 week. As shown in **Supplementary Figure S2**, the loaded NGF could be released in a sustained manner, and the cumulative dose of NGF reached up to 35 ng. The loading of NGF was found beneficial in nerve regeneration on the PLCL film having KHI peptides and micropatterns. As shown in **Figure 4**, the proliferation and elongation of SCs were increased significantly in the MPLCL-peptide-NGF group compared with those in the PLCL group. Furthermore, the MPLCL-peptide-NGF conduits were also found more beneficial in nerve regeneration after severe traction injury compared with the PLCL group *in vivo*. The results reveal that NGF loading is helpful to nerve reinnervation after severe traction injury, and the molecular mechanism would be investigated in our following work.

The macroprous structures, groove and ridge morphologic surface, KHI peptide, and NGF modifications were found helpful in nerve regeneration after severe traction injury *in vivo*. As shown in **Figure 5**, the animal model of peripheral nerve severe traction injury was validated. The injured peripheral nerves were treated by the NGCs of PLCL, MPLCL, MPLCL-peptides, and MPLCL-peptide-NGF respectively for 4 weeks. It was found that the neural EMG functions were recovered best in the group of MPLCL-peptide-NGF, including the amplitude increase and NCV acceleration (**Figure 6**). The gait analysis has been performed widely for evaluating the recovery of motor function as a result of functional recovery after peripheral nerve injury in the rat (Varejao et al., 2001). However, it had been reported that paw contraction and autotomy confounded the measurement of toe spread, a factor that is given particular weighting in the formula for sciatic function index determination (Ao et al., 2011). The conduction velocity is an objective and reliable index for evaluation of the conduction of action potential in peripheral nerves (Jiao et al., 2009). Therefore, we chose neural monitoring and nerve conductive velocity as the indexes to evaluate nerve functional recovery. It can be also found that the fiber spacing was reduced, and the ratio of fiber fragment was significantly decreased in the MPLCL-peptide group and MPLCL-peptide-NGF group (**Figure 7**). Besides, the atrophic manifestation of gastrocnemius muscle was significantly decreased in the MPLCL-peptide and MPLCL-peptide-NGF groups, showing the weight of gastrocnemius muscle gaining and the diameter of muscle bundle increasing (**Figure 8**). As a result, the combination of KHI peptide modification, NGF loading, and parallel linear micropattern surface could promote the reinnervation of the sciatic nerve after severe traction injury *in vivo*.

CONCLUSION

The PLCL films/NGCs were successfully modified with KHI peptides, NGF loading, and parallelly linear micropatterns. The KHI peptide modification and NGF loading were beneficial in SC proliferation, migration, and adhesion. The groove and ridge morphologic surface on the NGCs were helpful in alleviating the nerve nonlinear structures at the injured point after severe traction injury. The KHI peptide modification, NGF loading, and parallel linear micropattern surface could promote the adhesion and elongation of SCs *in vitro* and the reinnervation of the sciatic nerve after severe traction injury *in vivo*. Nonetheless, the underlying molecular mechanisms need to be elucidated further in the future.

DATA AVAILABILITY STATEMENT

The original contributions presented in the study are included in the article/**Supplementary Material**; further inquiries can be directed to the corresponding authors.

ETHICS STATEMENT

The animal study was reviewed and approved by The Second Affiliated Hospital, Zhejiang University School of Medicine.

AUTHOR CONTRIBUTIONS

XY, DZ, CG, and YW substantially contributed to the conception and design; CL, ZL, and YL contributed to the acquisition of data; CL and QZ analyzed and interpreted the data; YW, CG, XY, and DZ contributed to draft the article; YW and CG approved the final version to be published. This manuscript has been read and approved by all co-authors before submission.

FUNDING

This study is financially supported by the Health Innovation Talents Project of Zhejiang Province (2021RC004) and Natural Science Foundation of Zhejiang Province (LQ21H090011).

SUPPLEMENTARY MATERIAL

The Supplementary Material for this article can be found online at: https://www.frontiersin.org/articles/10.3389/fbioe.2021.744230/full#supplementary-material

Supplementary Figure S1 | SEM image of NaCl particles. The average diameter was measured as 75.6 ± 19.1 μm from the SEM images.

Supplementary Figure S2 | The cumulative release of NGF after 1, 3 and 7 days.

REFERENCES

Abay, A., Simionato, G., Chachanidze, R., Bogdanova, A., Hertz, L., Bianchi, P., et al. (2019). Glutaraldehyde - A Subtle Tool in the Investigation of Healthy and Pathologic Red Blood Cells. *Front. Physiol.* 10, 514. doi:10.3389/fphys.2019.00514

Ao, Q., Fung, C.-K., Yat-Ping Tsui, A., Cai, S., Zuo, H.-C., Chan, Y.-S., et al. (2011). The Regeneration of Transected Sciatic Nerves of Adult Rats Using Chitosan Nerve Conduits Seeded with Bone Marrow Stromal Cell-Derived Schwann Cells. *Biomaterials* 32, 787–796. doi:10.1016/j.biomaterials.2010.09.046

Brauckhoff, K., Svendsen, Ø. S., Stangeland, L., Biermann, M., Aas, T., and Husby, P. J. A. (2018). Injury Mechanisms and Electromyographic Changes after Injury of the Recurrent Laryngeal Nerve: Experiments in a Porcine Model. *Head and Neck* 40, 274–282. doi:10.1002/hed.24940

Carvalho, C. R., Oliveira, J. M., and Reis, R. L. (2019). Modern Trends for Peripheral Nerve Repair and Regeneration: Beyond the Hollow Nerve Guidance Conduit. *Front. Bioeng. Biotechnol.* 7, 337. doi:10.3389/fbioe.2019.00337

Cheah, M., Fawcett, J. W., and Haenzi, B. (2017). Differential Regenerative Ability of Sensory and Motor Neurons. *Neurosci. lett.* 652, 35–40. doi:10.1016/j.neulet.2016.11.004

Chiang, F.-Y., Lu, I.-C., Kuo, W.-R., Lee, K.-W., Chang, N.-C., and Wu, C.-W. (2008). The Mechanism of Recurrent Laryngeal Nerve Injury during Thyroid Surgery-The Application of Intraoperative Neuromonitoring. *Surgery* 143, 743–749. doi:10.1016/j.surg.2008.02.006

Crumley, R. L. (2000). Laryngeal Synkinesis Revisited. *Ann. Otol Rhinol Laryngol.* 109, 365–371. doi:10.1177/000348940010900405

Gluck, M. J., Vijayaraghavan, S., Sinclair, E. B., Ashraf, A., Hausman, M. R., and Cagle, P. J. (2018). Detecting Structural and Inflammatory Response after *In Vivo* Stretch Injury in the Rat Median Nerve via Second Harmonic Generation. *J. Neurosci. Methods* 303, 68–80. doi:10.1016/j.jneumeth.2018.02.006

Huang, L., Gao, J., Wang, H., Xia, B., Yang, Y., Xu, F., et al. (2020). Fabrication of 3D Scaffolds Displaying Biochemical Gradients along Longitudinally Oriented Microchannels for Neural Tissue Engineering. *ACS Appl. Mater. Inter.* 12, 48380–48394. doi:10.1021/acsami.0c15185

Jiao, H., Yao, J., Yang, Y., Chen, X., Lin, W., Li, Y., et al. (2009). Chitosan/polyglycolic Acid Nerve Grafts for Axon Regeneration from Prolonged Axotomized Neurons to Chronically Denervated Segments. *Biomaterials* 30, 5004–5018. doi:10.1016/j.biomaterials.2009.05.059

Kam, L., Shain, W., Turner, J. N., and Bizios, R. (2002). Selective Adhesion of Astrocytes to Surfaces Modified with Immobilized Peptides. *Biomaterials* 23, 511–515. doi:10.1016/s0142-9612(01)00133-8

Lackington, W. A., Kočí, Z., Alekseeva, T., Hibbitts, A. J., Kneafsey, S. L., Chen, G., et al. (2019). Controlling the Dose-dependent, Synergistic and Temporal Effects of NGF and GDNF by Encapsulation in PLGA Microparticles for Use in Nerve Guidance Conduits for the Repair of Large Peripheral Nerve Defects. *J. Controlled Release* 304, 51–64. doi:10.1016/j.jconrel.2019.05.001

Lehembre, F., Yilmaz, M., Wicki, A., Schomber, T., Strittmatter, K., Ziegler, D., et al. (2008). NCAM-induced Focal Adhesion Assembly: a Functional Switch upon Loss of E-Cadherin. *Embo J.* 27, 2603–2615. doi:10.1038/emboj.2008.178

Liu, H., Tan, N., Xu, D., Li, C.-Y., and Xian, G.-J. (2020a). NGF and CNTF Expression and Regulation Mechanism by miRNA in Acute Paralytic Strabismus. *Int. Ophthalmol.* 40, 975–984. doi:10.1007/s10792-019-01270-x

Liu, M.-Y., Chang, C.-P., Hung, C.-L., Hung, C.-J., and Huang, S.-M. (2020b). Traction Injury of Recurrent Laryngeal Nerve during Thyroidectomy. *World J. Surg.* 44, 402–407. doi:10.1007/s00268-019-05178-6

Lopez-Silva, T. L., Cristobal, C. D., Edwin Lai, C. S., Leyva-Aranda, V., Lee, H. K., and Hartgerink, J. D. (2021). Self-assembling Multidomain Peptide Hydrogels Accelerate Peripheral Nerve Regeneration after Crush Injury. *Biomaterials* 265, 120401. doi:10.1016/j.biomaterials.2020.120401

Mahan, M. A., Warner, W. S., Yeoh, S., and Light, A. (2020). Rapid-stretch Injury to Peripheral Nerves: Implications from an Animal Model. *J. Neurosurg.* 133, 1537–1547. doi:10.3171/2019.6.JNS19511

Malessy, M. J. A., de Ruiter, G. C. W., de Boer, K. S., and Thomeer, R. T. W. M. (2004). Evaluation of Suprascapular Nerve Neurotization after Nerve Graft or Transfer in the Treatment of Brachial Plexus Traction Lesions. *J. Neurosurg.* 101, 377–389. doi:10.3171/jns.2004.101.3.0377

Maness, P. F., and Schachner, M. (2007). Neural Recognition Molecules of the Immunoglobulin Superfamily: Signaling Transducers of Axon Guidance and Neuronal Migration. *Nat. Neurosci.* 10, 19–26. doi:10.1038/nn1827

Oh, S. H., Kang, J. G., Kim, T. H., Namgung, U., Song, K. S., Jeon, B. H., et al. (2018). Enhanced Peripheral Nerve Regeneration through Asymmetrically Porous Nerve Guide Conduit with Nerve Growth Factor Gradient. *J. Biomed. Mater. Res.* 106, 52–64. doi:10.1002/jbm.a.36216

Ray, W. Z., and Mackinnon, S. E. (2010). Management of Nerve Gaps: Autografts, Allografts, Nerve Transfers, and End-To-Side Neurorrhaphy. *Exp. Neurol.* 223, 77–85. doi:10.1016/j.expneurol.2009.03.031

Ren, T., Yu, S., Mao, Z., and Gao, C. (2015). A Complementary Density Gradient of Zwitterionic Polymer Brushes and NCAM Peptides for Selectively Controlling Directional Migration of Schwann Cells. *Biomaterials* 56, 58–67. doi:10.1016/j.biomaterials.2015.03.052

Samadian, H., Ehterami, A., Sarrafzadeh, A., Khastar, H., Nikbakht, M., Rezaei, A., et al. (2020). Sophisticated Polycaprolactone/gelatin Nanofibrous Nerve Guided Conduit Containing Platelet-Rich Plasma and Citicoline for Peripheral Nerve Regeneration: *In Vitro* and *In Vivo* Study. *Int. J. Biol. Macromolecules* 150, 380–388. doi:10.1016/j.ijbiomac.2020.02.102

Sarker, M. D., Naghieh, S., McInnes, A. D., Schreyer, D. J., and Chen, X. (2018). Regeneration of Peripheral Nerves by Nerve Guidance Conduits: Influence of Design, Biopolymers, Cells, Growth Factors, and Physical Stimuli. *Prog. Neurobiol.* 171, 125–150. doi:10.1016/j.pneurobio.2018.07.002

Schwartzman, R. J., and Grothusen, J. R. (2008). Brachial Plexus Traction Injury: Quantification of Sensory Abnormalities. *Pain Med.* 9, 950–957. doi:10.1111/j.1526-4637.2007.00394.x

Shah, M. B., Chang, W., Zhou, G., Glavy, J. S., Cattabiani, T. M., and Yu, X. (2019). Novel Spiral Structured Nerve Guidance Conduits with Multichannels and Inner Longitudinally Aligned Nanofibers for Peripheral Nerve Regeneration. *J. Biomed. Mater. Res.* 107, 1410–1419. doi:10.1002/jbm.b.34233

Sun, Y., Chi, X., Meng, H., Ma, M., Wang, J., Feng, Z., et al. (2021). Polylysine-decorated Macroporous Microcarriers Laden with Adipose-Derived Stem Cells Promote Nerve Regeneration *In Vivo*. *Bioactive Mater.* 6, 3987–3998. doi:10.1016/j.bioactmat.2021.03.029

Tonazzini, I., Jacchetti, E., Meucci, S., Beltram, F., and Cecchini, M. (2015). Schwann Cell Contact Guidance versus Boundary -Interaction in Functional Wound Healing along Nano and Microstructured Membranes. *Adv. Healthc. Mater.* 4, 1849–1860. doi:10.1002/adhm.201500268

Turner, C. A., Lyons, D. M., Buckmaster, C. L., Aurbach, E. L., Watson, S. J., Schatzberg, A. F., et al. (2019). Neural Cell Adhesion Molecule Peptide Mimetics Modulate Emotionality: Pharmacokinetic and Behavioral Studies in Rats and Non-human Primates. *Neuropsychopharmacol* 44, 356–363. doi:10.1038/s41386-018-0052-6

Varejão, A. S. P., Meek, M. F., Ferreira, A. J. A., Patrício, J. A. B., and Cabrita, A. M. S. (2001). Functional Evaluation of Peripheral Nerve Regeneration in the Rat: Walking Track Analysis. *J. Neurosci. Methods* 108, 1–9. doi:10.1016/s0165-0270(01)00378-8

Vijayavenkataraman, S. (2020). Nerve Guide Conduits for Peripheral Nerve Injury Repair: A Review on Design, Materials and Fabrication Methods. *Acta Biomater.* 106, 54–69. doi:10.1016/j.actbio.2020.02.003

Wang, Y., Wang, W., Wo, Y., Gui, T., Zhu, H., Mo, X., et al. (2015). Orientated Guidance of Peripheral Nerve Regeneration Using Conduits with a Microtube Array Sheet (MTAS). *ACS Appl. Mater. Inter.* 7, 8437–8450. doi:10.1021/acsami.5b00215

Xia, J., Zhang, L., Qian, M., Bao, Y., Wang, J., and Li, Y. (2017). Specific Light-Up Pullulan-Based Nanoparticles with Reduction-Triggered Emission and Activatable Photoactivity for the Imaging and Photodynamic Killing of Cancer Cells. *J. Colloid Interf. Sci.* 498, 170–181. doi:10.1016/j.jcis.2017.03.059

Yu, X., Liu, C., Yan, M., Gong, W., and Wang, Y. (2021). Hyperthermal Liquid, spray, and Smog May Be Potential Risk Factors for Recurrent Laryngeal Nerve thermal Injury during Thyroid Surgeries. *Endocrine* 72, 198–207. doi:10.1007/s12020-020-02451-w

Zhang, D., Ni, N., Chen, J., Yao, Q., Shen, B., Zhang, Y., et al. (2015). Electrospun SF/PLCL Nanofibrous Membrane: a Potential Scaffold for Retinal Progenitor Cell Proliferation and Differentiation. *Sci. Rep.* 5, 14326. doi:10.1038/srep14326

Zhang, D., Wu, S., Feng, J., Duan, Y., Xing, D., and Gao, C. (2018a). Micropatterned Biodegradable Polyesters Clicked with CQAASIKVAV

Promote Cell Alignment, Directional Migration, and Neurite Outgrowth. *Acta Biomater.* 74, 143–155. doi:10.1016/j.actbio.2018.05.018

Zhang, D., Xu, S., Wu, S., and Gao, C. (2018b). Micropatterned Poly(d,l-Lactide-Co-Caprolactone) Films Entrapped with Gelatin for Promoting the Alignment and Directional Migration of Schwann Cells. *J. Mater. Chem. B* 6, 1226–1237. doi:10.1039/c7tb03073h

Zhang, D., Yang, W., Wang, C., Zheng, H., Liu, Z., Chen, Z., et al. (2020a). Methylcobalamin-Loaded PLCL Conduits Facilitate the Peripheral Nerve Regeneration. *Macromol. Biosci.* 20, 1900382. doi:10.1002/mabi.201900382

Zhang, D., Yao, Y., Duan, Y., Yu, X., Shi, H., Nakkala, J. R., et al. (2020b). Surface-Anchored Graphene Oxide Nanosheets on Cell-Scale Micropatterned Poly(d,l-Lactide-Co-Caprolactone) Conduits Promote Peripheral Nerve Regeneration. *ACS Appl. Mater. Inter.* 12, 7915–7930. doi:10.1021/acsami.9b20321

Zheng, M.-X., Hua, X.-Y., Feng, J.-T., Li, T., Lu, Y.-C., Shen, Y.-D., et al. (2018). Trial of Contralateral Seventh Cervical Nerve Transfer for Spastic Arm Paralysis. *N. Engl. J. Med.* 378, 22–34. doi:10.1056/NEJMoa1615208

Zhu, Y., Mao, Z., and Gao, C. (2013). Control over the Gradient Differentiation of Rat BMSCs on a PCL Membrane with Surface-Immobilized Alendronate Gradient. *Bio. Macro. Mol.* 14, 342–349. doi:10.1021/bm301523p

Conflict of Interest: The authors declare that the research was conducted in the absence of any commercial or financial relationships that could be construed as a potential conflict of interest.

Publisher's Note: All claims expressed in this article are solely those of the authors and do not necessarily represent those of their affiliated organizations, or those of the publisher, the editors, and the reviewers. Any product that may be evaluated in this article, or claim that may be made by its manufacturer, is not guaranteed or endorsed by the publisher.

Advantages of publishing in Frontiers

OPEN ACCESS
Articles are free to read for greatest visibility and readership

FAST PUBLICATION
Around 90 days from submission to decision

HIGH QUALITY PEER-REVIEW
Rigorous, collaborative, and constructive peer-review

TRANSPARENT PEER-REVIEW
Editors and reviewers acknowledged by name on published articles

Frontiers
Avenue du Tribunal-Fédéral 34
1005 Lausanne | Switzerland

Visit us: www.frontiersin.org
Contact us: frontiersin.org/about/contact

REPRODUCIBILITY OF RESEARCH
Support open data and methods to enhance research reproducibility

DIGITAL PUBLISHING
Articles designed for optimal readership across devices

FOLLOW US
@frontiersin

IMPACT METRICS
Advanced article metrics track visibility across digital media

EXTENSIVE PROMOTION
Marketing and promotion of impactful research

LOOP RESEARCH NETWORK
Our network increases your article's readership